

10 项代表性学术成果

序号	第一作者	所属单位	论文题目	发表刊物/论文集	收录情况 (IF=**)
1	曾燕妮	财贸学院	Cultural similarity of non-local independent directors and financial	International Review of Financial Analysis	SSCI (IF=8.2)
2	李洁	财贸学院	A smart energy IoT model based on the Itsuku PoW technology	Results in Engineering	SCI (IF=5.0)
3	王国华	食品与生物技术学院	Deleting specific residues from the HNH linkers creates a CRISPR-SpCas9 variant with high fidelity and efficiency	Journal of Biotechnology	SCI (IF=4.1)
4	姜全德	公共课教学部	Asymptotically Almost Automorphic Solutions for Impulsive Quaternion-Valued Neural Networks with Mixed Delays	Neural Processing Letters	SCIE (IF=3.1)
5	陈大华	轻化工技术学院	Effect of roll temperature on the structure and properties of oriented polypropylene cast film and stretched microporous membrane	journal of applied polymer science	SCI (IF=3.0)
6	冯爱娟	食品与生物技术学院	A new chromone derivative from an endophytic <i>Aspergillus</i> sp. GXNU-B1	Natural Product Research	SCI (IF=2.2)
7	梅文兵	艺术设计学院	Research on the weighting values of community aging-friendly construction indexes with different expert groups	INQUIRY: The Journal of Health Care Organization, Provision, and Financing	SSCI (IF=2.099)
8	陈大华	轻化工技术学院	Effect of molecular weight distribution on the structure and properties of polypropylene cast film and stretched microporous membrane.	J Polym Eng	SCI (IF=2.0)

9	杨红玲	管理学院	Trait mindfulness and cell phone addiction in adolescents: A moderated mediation model	social behavior and personality	SSCI (IF=1.183)
10	赖金志	信息技术学院	A congestion-aware hybrid SRAM and STT-RAM buffer design for network-on-chip router	IEICE Electronics Express	SSCI(IF=0.709)

论文收录引用
检索报告

委托人：张浩

委托人单位：广东外语外贸大学

检索要求：张浩发表的论文被 SSCI 收录

检索时段：2023 年至 2023 年

检索结果

数据库	论文收录
Social Sciences Citation Index (SSCI)	1 篇

声明：本次检索根据张浩提供的论文目录，并按其提出的要求进行检索，详情见附件，若有不实，由委托人承担全部责任。

广东外语外贸大学图书馆

检索人：张爱优

2023年12月11日

检索证明专用章

《社会科学引文索引》(SSCI)收录 1 篇

第 1 条, 共 1 条

标题: Cultural similarity of non-local independent directors and financial reporting quality

作者: Zeng, YN (Zeng, Yanni) [1];Liu, MN (Liu, Mengna) [2];Ding, AS (Ding, Ashley) [3];Xu, R (Xu, Rui) [4,5];Zhang, H (Zhang, Hao) [2,6,7,8]

来源出版物: INTERNATIONAL REVIEW OF FINANCIAL ANALYSIS 卷:90 文献号:102918 出版年:NOV 2023

DOI: 10.1016/j.irfa.2023.102918

入藏号: WOS:001080232900001

文献类型: Article

地址: [1]Sch Finance & Trade, Guangdong Ind Polytech, Gaungzhou, Peoples R China [2]Guangdong Univ Foreign Studies, Sch Finance, Gaungzhou, Peoples R China [3]Macquarie Univ, Ctr Corp Sustainabil & Environm Finance, Sydney, Australia [4]Guangdong Univ Foreign Studies, Sch Accounting, Gaungzhou, Peoples R China [5]Res Ctr Accounting & Econ Dev, Guangdong Hong Kong, Hong Kong, Peoples R China [6]Guangdong Univ Foreign Studies, Inst Financial Openness & Asset Management, Gaungzhou, Peoples R China [7]Inst Fortune Management Res, Gaungzhou, Peoples R China [8]Guangdong Univ Foreign Studies, Sch Finance, Gaungzhou 510006, Guangdong, Peoples R China

通讯作者地址: Zhang, Hao(通讯作者)Guangdong Univ Foreign Studies, Sch Finance, Gaungzhou 510006, Guangdong, Peoples R China.

电子邮件地址: haozhang@gdufs.edu.cn;

IDS 号: T8DM7

ISSN: 1057-5219

Web of Science 核心合集中的“被引频次”: 0

委托人贡献: 通讯作者

期刊《INTERNATIONAL REVIEW OF FINANCIAL ANALYSIS》2022 年的影响因子为 8.200

期刊《INTERNATIONAL REVIEW OF FINANCIAL ANALYSIS》2022 年的 JCR 分区情况为:

JCR®类别	类别中的排序	JCR 分区
BUSINESS, FINANCE	4/111	Q1

期刊《INTERNATIONAL REVIEW OF FINANCIAL ANALYSIS》2022 年的中科院升级版分区情况为:

分类	学科名称	分区	Top 期刊
小类	BUSINESS, FINANCE 商业: 财政与金融	2	-
大类	经济学	2	否



Cultural similarity of non-local independent directors and financial reporting quality

Yanni Zeng^a, Mengna Liu^b, Ashley Ding^c, Rui Xu^{d,e}, Hao Zhang^{b,f,g,*}

^a School of Finance and Trade, Guangdong Industry Polytechnic, Gaungzhou, China

^b School of Finance, Guangdong University of Foreign Studies, Gaungzhou, China

^c Centre for Corporate Sustainability and Environmental Finance, Macquarie University, Sydney, Australia

^d School of Accounting, Guangdong University of Foreign Studies, Gaungzhou, China

^e Research Center for Accounting and Economic Development of Guangdong-Hong Kong-Macao Greater Bay Area, Gaungzhou, China

^f Institute of Financial Openness and Asset Management, Guangdong University of Foreign Studies, Gaungzhou, China

^g Institute of Fortune Management Research, Gaungzhou, China

ARTICLE INFO

JEL codes:

G34

M12

M41

Keywords:

Cultural similarity

Non-local independent directors

Financial reporting quality

Dialect

ABSTRACT

By manually collecting data on the birthplaces of independent directors of Chinese A-share listed companies from 2005 to 2019, we construct a cultural similarity index for non-local independent directors according to the dialect data and empirically test its impact on the financial reporting quality of listed companies. The results show that an increase in the cultural similarity of non-local independent directors is conducive to improving the financial reporting quality of the listed companies in which they serve. The mechanism analysis shows that cultural similarity can improve financial reporting quality by improving internal control quality and information disclosure quality. Our heterogeneity analysis shows that this effect is more pronounced when the listed company has a better external monitoring environment, the company is a non-state-owned enterprise, and the company is located in a region with a high degree of marketization. In addition, the robustness test results show that our conclusion is robust.

1. Introduction

The intersection and integration of “culture and corporate behavior” have gained attention in recent years as a hot topic in corporate finance research. Studies have shown that cultural factors significantly influence individual behavior and corporate decision-making (Bereskin, Byun, Officer, & Oh, 2018; Du, 2019; Pham, Pham, & Truong, 2022). Although the formal institutional constraints in different regions of China are similar, the cultural and other informal institutions vary widely between regions. Culture is an essential supplement to formal institutional arrangements in economics research (Zingales, 2011), and its differences are the underlying reasons that affect economic activities. As a multi-ethnic country, China boasts multiculturalism, and one manifestation of this is the coexistence of Mandarin and dialects.

Dialect, as a perspective for studying cultural issues, has unique adaptability in the Chinese context (Bian, Ji, & Zhang, 2019; Huang, He, Meng, & Ma, 2022). Firstly, the formation of Chinese civilization is the result of the assimilation and integration of many nations in history.

China's vast territory and the large span between the north and south have resulted in completely different local cultures, providing a natural foundation for studying cultural and economic development. As an important carrier, language comprehensively embodies the result of cultural horizontal transmission, and cultural differences can be reflected in the characteristics of dialects to a large extent. Secondly, although China has a unified script, it has many dialects, which provides an important research scenario for studying the impact of language on economic activities in the same political, economic, and legal environment. This overcomes the challenge of institutional differences that are difficult to eliminate in comparative studies between countries. Language is a vital tool for communication and a significant symbol of culture (Meng et al., 2023). It profoundly affects the cognition, communication, and decision-making choices of economic subjects, providing a feasible scenario for this paper to examine the impact of cultural differences on corporate behavior from the micro-individual level.

China's capital market is currently in a phase of high-quality

* Corresponding author at: School of Finance, Guangdong University of Foreign Studies, Guangdong 510006, China.

E-mail address: haozhang@gdufs.edu.cn (H. Zhang).

<https://doi.org/10.1016/j.irfa.2023.102918>

Received 25 February 2023; Received in revised form 20 August 2023; Accepted 6 September 2023

Available online 9 September 2023

1057-5219/© 2023 Elsevier Inc. All rights reserved.

development, and the enhancement of the quality of listed companies has become an essential prerequisite for promoting the healthy growth of the capital market. However, the issue of financial report disclosure violations and information distortion in Chinese listed companies has drawn criticism, as it not only increases the information asymmetry between investors and enterprises, but also damages investors' rights and interests and hinders the effective allocation of resources. Such violations and distortions provide false information to investors, which can harm their economic decision-making, as well as cause losses to other stakeholders and undermine the healthy economic order of the market. High-quality financial reports are critical in the effective disclosure of information by listed companies. Prior studies have shown that high-quality financial information can effectively reduce agency costs and capital costs for financial statement users (Herath & Albarqi, 2017; Lambert, Leuz, & Verrecchia, 2007; Ying, 2016). Various corporate governance mechanisms, including the external audit system, independent director system, and analyst attention, are designed to strengthen and supervise information disclosure to enhance the quality of financial reporting. On 1 March 2020, the Securities Law of the People's Republic of China was officially implemented, providing a legal basis for the protection of investors' rights and the stable development of the capital market. In the wake of this enactment, regulators and academia have shown considerable interest in financial reporting disclosure and governance. Therefore, improving the financial reporting quality of listed companies in an effective manner has become a critical issue to address.

In listed companies, the board of directors is one of the core mechanisms of internal corporate governance and has an important and direct impact on the quality of financial reporting. Independent directors have important functions on the board, such as monitoring and consultation, to mitigate agency problems. In recent years, it has become common for listed companies to appoint non-local independent directors (i.e., people from other provinces or cities). Currently, over 60% of listed companies employ non-local independent directors in Chinese listed companies. However, research shows that the monitoring effectiveness of non-local independent directors in corporate governance is poor (Masulis, Wang, & Xie, 2012; Quan & Zhang, 2021). For example, Quan and Zhang (2021) find that firms with non-local independent directors tend to have more tunneling activities and earnings management, lower CEO pay-performance sensitivity and lower investment sensitivity than other firms.

From a cultural perspective, this study aims to address the following questions: Does the cultural similarity of non-local independent directors impact the financial reporting quality of listed companies? What are the underlying mechanisms? And are there any differences in the impact on various types of listed companies? Considering that non-local independent directors originate from diverse dialect regions and dialects symbolize a significant cultural dimension, we employ dialect similarity and dialect concentration as proxies for cultural similarity. This approach allows us to investigate whether the cultural affinity among non-local independent directors impacts the financial reporting quality of listed companies.

Using a sample of Chinese A-share listed companies from 2005 to 2019, we identify non-local independent directors by manually collecting information on their birthplaces¹ and the registered headquarters of the listed companies in which they serve. We manually match data on dialect areas with data on birthplaces and the registered headquarters of the listed companies and construct our indicators of dialect similarity and dialect concentration. The results show that the greater the cultural similarity of non-local independent directors, the higher the financial reporting quality of listed companies. Our results also shed

light on the underlying mechanism by which cultural similarity improves financial reporting quality. We find that the internal control system and information disclosure system are key channels through which non-local independent directors can constrain earnings management and improve financial reporting quality.

We also investigate whether the cultural similarity of non-local independent directors has different effects on the financial reporting quality of different types of listed companies. We find that the effect of cultural similarity on financial reporting quality is more pronounced when the listed company has a better external monitoring environment, when the company is a non-state-owned enterprise (non-SOEs), and the company is located in a region with a high degree of marketization. To address endogeneity issues, we use a two-stage least squares (2SLS) regression in which the instrumental variables are topographic differences and genetic distance, and the results show that the cultural similarity of non-local independent directors reduces the earnings management of listed companies and improves the financial reporting quality. Our baseline regression and endogeneity test results support the governance role of the cultural similarity of non-local independent directors in improving financial reporting quality.

We contribute to the literature in several ways. First, studies on the effectiveness of non-local independent directors typically focus on the effect of geographical distance on the monitoring role of independent directors (Deng, Kanagaretnam, & Zhou, 2020; Quan & Zhang, 2021). In contrast, we take into consideration the cultural similarity of non-local independent directors and provide a more comprehensive understanding of the impact of cultural similarity on financial reporting quality based on dialect similarity and dialect concentration. Second, we identify the mechanism through which the cultural similarity of non-local independent directors affects the financial reporting quality of listed companies. Thirdly, we collected information on the birthplaces of non-local independent directors and the locations of incorporation (registered headquarters) of the listed companies in which they serve from the resumes of independent directors. We then constructed a dialect similarity index, which serves as a more precise proxy. By using this more accurate method, we are able to provide a more nuanced understanding of the role that cultural similarity plays in the effectiveness of non-local independent directors.

2. Literature review

Studies show that corporate financial reporting is an important tool for mitigating information asymmetry and agency problems (Benkraiem, Bensaad, & Lakhali, 2022; Fu, Kraft, & Zhang, 2012; Habib, Ranasinghe, & Huang, 2018; Suharsono, Nirwanto, & Zuhroh, 2020; Han, Ding and Zhang, 2022). Therefore, improving the financial reporting quality has certain economic implications; for example, high-quality financial reporting can improve investment efficiency by alleviating information asymmetry (Biddle, Hilary, & Verdi, 2009; Chen, Hope, Li, & Wang, 2011). In addition, previous literature mainly studies the factors that affect the financial reporting quality of listed companies from the perspective of internal governance and external monitoring. For example, effective internal control can reduce information asymmetry and improve the company's financial reporting quality (Herath & Albarqi, 2017). Moreover, the personal characteristics of members of the executive team (i.e., age, gender, education level and financial work experience) are significantly associated with financial reporting quality (Qi, Lin, Tian, & Lewis, 2018). Studies show also that CEOs with academic or financial experience engage less in earnings management and thus provide higher quality financial statements than CEOs without such experience (Jiang, Zhu, & Huang, 2013; Ma, Novoselov, Zhou, & Zhou, 2019). Moreover, the quality of financial reporting is higher if members of the audit committee have a mixed background of legal, accounting and financial and regulatory expertise than otherwise (Krishnan, Wen, & Zhao, 2011; Kusnadi, Leong, Suwardy, & Wang, 2016). In terms of external monitoring, improvements in the legal environment (Filip,

¹ we conducted extensive data collection efforts, incorporating sources like Baidu, Google, the annual reports of listed company, and information regarding the organizations of the non-local independent director works.

Labelle, & Rousseau, 2015; Zhang, Luo, Han, & Liu, 2021), media scrutiny (Cahan, Chen, & Wang, 2021) and the effectiveness of institutional investors as regulators (Pucheta-Martínez & García-Meca, 2014) all contribute to the financial reporting quality of listed companies.

With the rise of geographical economics in recent years, geographical distance has gradually received attention in corporate finance and corporate governance research (Deng et al., 2020). The literature on non-local independent directors mainly focuses on the motivations of companies to hire non-local independent directors and the role played by non-local independent directors. For instance, studies find that the existence of non-local independent directors is the product of the company actively weakening supervision and strengthening consultation (Masulis et al., 2012; Quan & Zhang, 2021). Studies also show that the motivation of companies to appoint non-local independent directors is to build political connections (Quan, Lim, & Liang, 2017), and it provides the possibility for major shareholder tunneling behavior (Lin & Cao, 2019).

Non-local independent directors' supervisory role depends on their independence and supervisory ability. Various factors affect the effectiveness of independent directors in fulfilling their supervisory responsibilities, and among these factors is the location where they work. According to studies, the appointment of non-local independent directors has a negative impact on corporate governance (Fei, 2022; Lin & Cao, 2019). The reason for this is that non-local independent directors may not be familiar with the company's operating environment, making it difficult for them to acquire soft information, which is critical for effectively monitoring the company's performance. Moreover, the high cost of information acquisition and the information disadvantage of non-local independent directors limit their ability to supervise. However, independent directors who work farther from the company headquarters may have fewer personal connections with company executives, thus making them more independent and effective in their supervisory role (Quan & Zhang, 2021). In contrast, local independent directors may have more information advantages, but their frequent contacts with company management may shorten their personal relationships with them, affecting their independence in performing their duties. Hence, non-local independent directors' greater independence makes them more effective supervisors.

Masulis et al. (2012) find that the presence of non-local independent directors limits their ability and motivation to gather information to closely monitor management due to geographical distance and high monitoring costs. In this case, the presence of non-local independent directors weakens the effectiveness of board oversight, leading to more serious agency problems between managers and shareholders and poorer corporate performance. Fei (2022) also finds that non-local independent directors have a negative impact on corporate environmental disclosure. In addition, Deng et al. (2020) explore the impact of the geographical distance of independent directors on fraud and irregularities in Chinese listed companies and conclude that local independent directors at the provincial and municipal levels reduce the frequency and extent of misconduct in listed companies. Similarly, local independent directors with accounting expertise are more likely to inhibit surplus management than their non-local counterparts (Zhou, Hao, & Yang, 2019).

Regarding the consulting role of non-local independent directors, some studies have shown that non-local independent directors have the information advantage of being related to different places, which will have a positive impact on the company. Non-local independent directors are conducive to the development of non-local resource relationship networks, providing valuable advice and assistance to the company, and improving the advisory capabilities of the board of directors, mainly in terms of improving the efficiency of non-local mergers and acquisitions (M&A) and non-local operations (Masulis et al., 2012; Quan & Zhang, 2021). These directors can provide region-specific expertise that is valuable to M&A parties in assessing M&A targets and assessing the value of the M&A value (Masulis et al., 2012). At the same time, the

appropriate use of the consulting function of non-local independent directors can help companies break through the regional segmentation of commodity markets and improve the efficiency of non-local operations (Deng, 2019; Quan & Zhang, 2021).

As a type of informal institution, culture is an important complement to formal institutions in economic research (Zingales, 2011). Studies show that culture has a significant impact on corporate governance systems (Hashim, 2012). For example, culture can influence corporate disclosure quality (Braguinsky & Mityakov, 2015) and financial reporting quality (Bhandari, Mammadov, Thevenot, & Vakilzadeh, 2022; Herath & Albarqi, 2017). Relationship culture (*guanxi*-based business practices) can also reduce transaction costs through effective communication and negotiation (Standifird & Marshall, 2000), thereby generating competitive advantages in market expansion and thus improving firm performance (Park & Luo, 2001). Cultural similarity facilitates communication and coordination and promotes the development of interpersonal identity, which has positive implications for corporate governance. Indeed, studies show that cultural proximity between auditors and CFOs is related to audit quality (Pham et al., 2022). That is, when audited business partners are culturally close to client executives, they are more likely to share a common philosophy and way of doing things, and this commonality reduces the cost of communication and coordination between them by increasing the effectiveness of accounting negotiations, thus improving audit quality. In addition, cultural similarity helps to form social networks and private information communication channels for the analysts (Du, Yu, & Yu, 2017). Bereskin et al. (2018) examine the impact of firms' cultural similarity on M&A decisions and outcomes and find that firms with similar cultures are more likely to merge than those with different cultures. Moreover, these mergers are associated with greater synergies and superior long-term business performance. Hence, culture can have a significant impact on the economic behavior of microeconomic individuals and on corporate governance.

3. Hypothesis development

The cultural similarity of non-local independent directors, as part of the core mechanism of corporate governance, can have an impact on their communication decisions and, ultimately, on the overall decision-making and governance of the board. In this study, we use language as a proxy for culture to emphasise cultural characteristics at the individual level. Language, as a form of cultural representation, reflects the results of the horizontal transmission of culture in many ways; the less linguistic variability there is between regions, the more similar cultural perceptions will be (Chen, 2013). Piekkari, Oxelheim, and Randøy (2015) explore and explain how increased linguistic diversity affects the decision-making and work processes of boards of directors. They find that the excessive variety of languages causes some board members to interact less with other board members, resulting in some members feeling marginalised and therefore unable to participate fully in board discussions. This feeling of marginalisation has a negative impact on their access to information and may reduce the quality of the decisions taken at board meetings. Based on principal-agent theory, in the absence of formal institutions, the ability of independent directors to access information is inevitably affected by the information barriers erected by management with an incentive to act opportunistically. Some studies show that greater cultural distance induces higher communication costs for the company (e.g., Du et al., 2017), reducing the efficiency of decision-making.

The cultural similarity of non-local independent directors plays a crucial role in not only obtaining public information related to the company but also obtaining micro information related to company operations. When the cultural similarity between non-local independent directors and the listed companies they serve is high, it promotes interpersonal communication and cooperation, reduces information friction, and facilitates information exchange (Portes, 2001). As dialect

is an integral part of culture (Jiang & Zhang, 2010), it inherently affects group behavior. Cultural similarity can influence mutual trust through cultural identity (Bian et al., 2019), thereby reducing the possibility of mutual concealment of information. Non-local independent directors born from the same dialect area possess information and resource advantages, which reduce the degree of information asymmetry, communication costs, and efficiency losses (Lang, 1986). This positively impacts board participation in corporate governance. The cultural similarity of non-local independent directors helps reduce communication costs, alleviate information asymmetry, and improve supervision efficiency, which, in turn, can effectively monitor managers' manipulation of financial statements. Therefore, we propose **Hypothesis 1** as follows:

Hypothesis 1. The increase in cultural similarity of the non-local independent directors can improve the financial reporting quality of listed companies.

Various studies have demonstrated that internal controls play a significant role in enhancing the financial reporting quality of listed companies (Chen, 2016; Herath & Albarqi, 2017). The internal control system comprises five key elements: internal environment, risk assessment, control activities, information communication, and internal supervision. Among these, information communication encourages listed companies to establish effective communication channels both internally and externally to reduce information asymmetry. On the other hand, internal supervision helps companies to identify and rectify significant deficiencies in their operations and investments promptly. As the overseer of a company, the increased cultural similarity of independent directors can strengthen the role of internal supervision, enhance the quality of internal controls, and ultimately improve the financial reporting quality of listed companies.

Furthermore, information disclosure by listed companies can mitigate information asymmetry and have a positive impact on the financial reporting quality (Suharsono et al., 2020). A company with a well-established information collection system and an efficient information processing and transmission system can facilitate communication and feedback across different levels, departments, and business processes. The improvement of cultural similarity among non-local independent directors can also foster information disclosure, thereby reducing the degree of information asymmetry in the company. Previous studies have shown a significant correlation between information disclosure and financial reporting quality, as evidenced by the value relevance of the information disclosed (Pavlopoulos, Magnis, & Iatridis, 2019; Suharsono et al., 2020). With increased cultural similarity among non-local independent directors, information disclosure can be enhanced, thus further improving the financial reporting quality of listed companies by reducing information asymmetry. Therefore, we propose **Hypothesis 2** as follows:

Hypothesis 2. The cultural similarity of the non-local independent directors will enhance the information disclosure quality and internal control quality of listed companies, then improve the financial reporting quality.

4. Research design

4.1. Sample and data

In 2001, the China Securities Regulatory Commission (CSRC) issued its *Guiding Opinions for the Establishment of an Independent Director System in Listed Companies* (hereinafter referred to as the 'Opinions') to formally regulate internal corporate governance through the system of independent directors. In accordance with the requirements of the *Opinions*, by the end of June 2003 at least one third of a listed company's board members had to be independent directors. Moreover, the 2005 revisions to *China's Company Law* require listed companies to have independent

directors. Hence, we include all A-shared listed companies in China between 2005 and 2019 as a sample in this study. We obtain financial data on Chinese listed companies from the Corporate Governance Structure file of the China Securities Market and Accounting Research (CSMAR) database. We obtain data on the registered headquarters of the listed companies from the Wind database. We exclude (1) all financial firms due to their special disclosure standards and (2) all special treatment² firms due to their abnormal financial conditions. We also remove all observations with missing data for the dependent and independent variables. Our final sample consists of 28,209 firm-year observations. To minimise the influence of outliers, we winsorise all continuous variables at the 1% and 99% levels. The main variables used in the study are defined in Appendix A.

4.2. Discretionary accruals

Following Guo and Ma (2015), we use earnings quality as a measure of financial reporting quality. And, we also use the modified Jones model (Dechow, Sloan, & Sweeney, 1995) to compute discretionary accruals of listed companies. Specifically, we identify the discretionary portion of accruals for a given firm by estimating the following model using ordinary least squares at time t and controlling for performance:

$$\frac{TACC_t}{TA_{t-1}} = \alpha_1 \frac{1}{TA_{t-1}} + \alpha_2 \frac{\Delta REV_t - \Delta REC_t}{TA_{t-1}} + \alpha_3 \frac{PPE}{TA_{t-1}} + \varepsilon_t \quad (1)$$

where $TACC_t$ is total accruals in year t , measured as the difference between net income and cash flow from operations (i.e., $TACC_t = NI_t - CFO_t$). ΔREV_t is the change in revenue in year t . ΔREC_t is the change in accounts receivable in year t . Finally, PPE_t is the level of gross property, plant and equipment in year t .

Each variable in the model is deflated by the lagged book value of total assets (TA_{t-1}) to avoid heteroscedasticity in the error term. The residual (ε_t) from the regression is the level of opportunistic earnings management and the intercept is constrained to 0. To minimise the influence of outliers, we winsorise discretionary accruals from the residuals at the 1% and 99% levels. We then take the absolute value of discretionary accruals (DA) as a proxy for earnings management, as our hypotheses focus on the level of accruals rather than on the direction of accrual management. DA is an inverse indicator, with a higher value of DA suggesting that firms are more likely to engage in earnings management, resulting in lower financial reporting quality.

4.3. Cultural similarity of non-local independent directors

To identify the prefecture-level cities where the majority of non-local independent directors work, we obtain the resumes of 122,335 independent directors of A-shared listed companies between 2005 and 2019 from the CSMAR database. For missing resumes, we search annual reports, Sina Finance, Phoenix Finance, and Google to locate the city where a given independent director works. Information on the registered headquarters of all A-share listed companies is obtained from the Wind database. From the information on the registered headquarters of the listed companies and the city where the companies' given independent director works, we can get that if the independent director is the non-local independent director or not. Then we search annual reports, Independent Directors Research Database (IDRD) of Chinese Research Data Services Platform (CNRDS), Baidu, and Google as well as the information regarding the organizations of the non-local independent director works, to locate the birthplace of these non-local independent director hand-collected.

² special treatment (ST) refers to the special treatment of stocks traded by listed companies with abnormal financial or other conditions by the Shanghai and Shenzhen Stock Exchanges. If a stock is marked with * ST, it indicates a risk of delisting.

The dialect data used in this study was collected, sorted and released publicly by the team of Professor Xianxiang Xu from Lingnan College of Sun Yat-sen University. This data set is systematically compiled according to the *Dictionary of Chinese Dialects*. According to the classification of the *Language Atlas of China*, there are 10 supergroups, 25 groups, and 108 subgroups of Chinese dialects. Based on the dialect tree diagram, the study takes prefecture-level cities as the analysis unit of dialect similarity and dialect concentration (Spolaore & Wacziarg, 2009).

The method for constructing and computing the dialect similarity variable is as follows (Bian et al., 2019). First, we determine the dialect similarity between the prefecture-level city where a firm is registered and the prefecture-level city where a non-local independent director born. The specific classification rules are as follows: The main independent variable of interest is *CSimilar*, which is an ordered variable to measure the degree of dialect similarity. It takes the value of 3 if the dialects of the two places belong to the same subgroups; it takes the value of 2 if the dialects of the two places belong to different subgroups under the same groups; it takes the value of 1 if the dialects of the two places belong to different groups under the same supergroups; it takes the value of 0 if the dialects of the two places belong to different supergroups. We then calculate the average *CSimilar* of non-local independent directors by firm and year. We also compute dialect concentration (*Dia*) as the proportion of non-local independent directors from the same dialect groups to the total number of non-local independent directors. It is the ratio of the number of non-local independent directors from the same dialect group divided by the total number of non-local independent directors in a company, the higher the ratio, the more non-local independent directors from the same dialect group in the company, indicating that the dialect is more concentrated.³

4.4. Control variables

We draw on the literature to identify and control for a wide range of firm and industry characteristics that may influence earnings management practices and financial reporting quality (e.g., Quan & Zhang, 2021; Zhang, Tan, Chen, & Chan, 2021). Specifically, we control for the following variables: proportion of shares held by the largest shareholder (*TOP1*), board size (*Bsize*), proportion of independent directors (*IDP*), proportion of shares held by management (*Mshare*), CEO–chairman duality⁴ (*Dual*), firm type (*SOE*), firm size (*Size*), leverage ratio (*Lev*), proportion of fixed assets (*Tangible*), sales growth (*Growth*), return on assets (*ROA*) and education level (*Edu*).

We also include industry dummy variables to control for the difference in accrual properties across industries, and year dummy variables to control for time-specific effects. Specifically, we use the 2012 *Guidelines for the Industry Classification of Listed Companies* (hereinafter referred to as the ‘*Guidelines*’) issued by the CSRC to classify industries. As most listed companies belong to the manufacturing industry, the *Guidelines* add an auxiliary grade between Category and Type (i.e., Subcategory). Hence, we classify all industries in our sample based on Subcategory codes for firms in the manufacturing industry and on Category codes for firms in other industries. As a result, we identify 19 industries in our sample and therefore include 18 industry dummy variables in the regression. In addition, based on our sample period

³ Indeed, as the reviewer suggested, it would be more appropriate to use the dialect differences between the birthplace of independent directors and the location of the listed company as a measure of cultural distance. Thanks for the reviewer's suggestions!

⁴ CEO–chairman duality is a unique leadership structure in which a company's CEO also serves as the chairman of the board of directors. This structure is characterized by a unity of power at the highest level of decision-making. If the CEO and chairman positions are held by the same individual, then the duality value is 1; otherwise, it is 0.

(2005–2019), 14 year dummy variables are included. We winsorise all of the continuous variables at the 1% and 99% levels to minimise the impact of extreme values. Detailed definitions of all variables can be found in Appendix A.

4.5. Descriptive statistics

Table 1 presents the descriptive statistics of the key variables for the full sample. The mean *DA* is 7.9% of total assets, with a standard deviation of 0.089. The average *CSimilar* is 2.052. *Dia* is 0.682. *TOP1* is 35.3% on average, indicating a relatively high level of control by controlling shareholders. The average proportion of independent directors (*IDP*) is 37.1%, meeting the requirement of the *Opinions*. The average board size (*Bsize*) in the sample is 8.775, which is consistent with previous studies. The distribution of other control variables, such as firm size, industry, and ownership structure, is also largely consistent with previous relevant research.

5. Empirical results

5.1. Baseline regressions

We begin our investigation of the relationship between the cultural similarity of non-local independent directors and financial reporting quality by estimating the following regression models to test Hypothesis 1:

$$DA_{i,t} = \alpha_0 + \alpha_1 CSimilar_{i,t} + \sum \alpha_j Control_{i,t} + Industry + Year + \varepsilon_{i,t} \quad (2)$$

All of the variables are defined in Appendix A. Model (2) for the full sample is used to investigate the influence of dialect similarity on earnings management by Chinese listed companies. We also use dialect concentration (*Dia*) as an alternative dependent variable.

Table 2 presents the results of Models (2). In column (1), we report the results without controlling for firm characteristics, while in column (2) we report the results after controlling for firm characteristics, using *DA* as the measure of financial reporting quality. The results in columns (1) and (2) of Table 2 show that the coefficient on *CSimilar* is negative and significant at 1% level, indicating that the greater the dialect similarity between non-local independent directors and listed companies, the lower the level of earnings management and the better the financial reporting quality of listed companies.

The results in columns (3) and (4) show that the coefficients on *Dia* are also negative and significant, which suggests that the higher the cultural concentration of non-local independent directors, the lower the level of earnings management and thus the better the financial reporting quality of listed companies. Overall, these results support Hypothesis 1, which posits that the cultural similarity of non-local independent directors has a positive effect on the financial reporting quality of Chinese

Table 1
Descriptive statistics.

Variable	N	Mean	Median	Std.	Min	Max
<i>DA</i>	28,209	0.079	0.050	0.089	0.001	0.772
<i>CSimilar</i>	28,209	2.052	2	0.836	0	3
<i>Dia</i>	28,209	0.682	0.671	0.401	0	1
<i>Size</i>	28,209	21.840	21.70	1.190	18.740	25.740
<i>ROA</i>	28,209	0.037	0.033	0.070	−0.754	0.285
<i>Growth</i>	28,209	0.211	0.108	0.656	−0.737	9.560
<i>TOP1</i>	28,209	0.353	0.333	0.150	0.081	0.759
<i>Lev</i>	28,209	0.442	0.436	0.217	0.021	2.555
<i>Tangible</i>	28,209	0.215	0.179	0.169	0.001	0.807
<i>Dual</i>	28,209	0.235	0	0.424	0	1
<i>Bsize</i>	28,209	8.775	9	1.768	5	15
<i>IDP</i>	28,209	0.371	0.333	0.053	0.300	0.600
<i>EDU</i>	28,209	1.537	1	0.574	0	2
<i>Mshare</i>	28,209	0.108	0.001	0.186	0	0.699
<i>SOE</i>	28,209	0.447	0	0.497	0	1

Table 2
Baseline Regressions.

Variable	(1)	(2)	(3)	(4)
	DA	DA	DA	DA
<i>CSimilar</i>	-0.004*** (-3.958)	-0.003*** (-3.246)		
<i>Dia</i>			-0.006*** (-4.375)	-0.004*** (-3.745)
<i>Size</i>		-0.007*** (-10.456)		-0.008*** (-10.138)
<i>ROA</i>		-0.149*** (-9.475)		-0.142*** (-10.689)
<i>Growth</i>		0.016*** (9.046)		0.018*** (8.936)
<i>TOP1</i>		0.011*** (3.565)		0.013*** (3.265)
<i>Lev</i>		0.044*** (10.965)		0.041*** (9.856)
<i>Tangible</i>		0.011** (2.378)		0.007* (1.857)
<i>Dual</i>		0.000 (0.645)		0.001 (0.947)
<i>Bsize</i>		-0.001** (-2.057)		-0.002*** (-2.963)
<i>IDP</i>		0.016 (1.406)		0.011 (1.068)
<i>Mshare</i>		-0.006** (-2.387)		-0.005** (-2.057)
<i>EDU</i>		-0.002 (-1.146)		-0.002 (-1.146)
<i>SOE</i>		-0.009*** (-7.035)		-0.007*** (-6.756)
Constant	0.081*** (46.735)	0.203*** (16.463)	0.092*** (71.406)	0.219*** (14.467)
Obs.	28,209	28,209	28,209	28,209
R-squared	0.101	0.185	0.099	0.175
Year FE	Yes	Yes	Yes	Yes
Industry FE	Yes	Yes	Yes	Yes

Robust t-statistics are reported in parentheses. *, **, and *** denote significance at the 10%, 5% and 1% levels, respectively.

listed companies.

5.2. Mechanism analysis

Based on the Hypothesis 2, we conduct the mechanism analysis by referring to the method used by Zhang (2020) to explore whether the cultural similarity of non-local independent directors can enhance financial reporting quality through improved information disclosure and internal control of listed companies.

Following Chen (2016), the Internal Control Index (ICQ) is used as a proxy for internal control quality. To ensure the uniformity of the results, the value of ICQ is divided by 100. To identify the relationship between cultural similarity and internal control quality, we first model internal control quality as a function of dialect similarity or concentration as follows:

$$ICQ_{i,t} = \omega_0 + \omega_1 CSimilar_{i,t} + \sum \varphi Controls_{i,t} + Industry + Year + \varepsilon_{i,t} \quad (3)$$

where a significant and positive ω_1 suggests that non-local independent directors with greater cultural similarity can promote the internal control quality of the firms in which they serve.

Following Kim and Verrecchia (2001), we use the trading volume fluctuation dependency method (KV measurement method) to measure the quality of information disclosure. Determine the quality of company information disclosure based on the degree of dependence of investors on trading volume information. The basic principle is that the more sufficient information disclosure is, the less dependent investors' stock returns on their stock trading volume information, and the greater their dependence on company information disclosure. If the quality of company information disclosure is poor, investors cannot use information

disclosure to judge the investment value of the company, thus relying heavily on its stock trading volume. The advantage of KV measurement method lies in its dynamic comprehensive analysis of voluntary and mandatory disclosure of information, which can reflect the actual effect of company information disclosure and is a variable that can comprehensively measure the quality of company information disclosure. We use the following model to construct the KV index:

$$\ln|(P_t - P_{t-1})/P_{t-1}| = \lambda_0 + \lambda(Vol_t/Vol_0 - 1) + \varepsilon \quad (4)$$

where P_t and Vol_t are the closing prices and trading volumes of stocks on day t , while Vol_0 is the average daily trading volume on trading days during the study period. The influence coefficient of transaction volume on returns is KV index, which is obtained by regression of each company with ordinary least squares method λ Value. It reflects the degree of information disclosure of a company through the dependence of the market on trading volume information. When information disclosure is more sufficient, the impact of stock trading volume on returns is relatively small (i.e. λ It's smaller). Therefore, the higher the KV value, the lower the quality of information disclosure. To identify the relationship between cultural similarity and the quality of information disclosure, we model the quality of information disclosure as a function of dialect similarity or concentration as follows:

$$KV_{i,t} = \mu_0 + \mu_1 CSimilar_{i,t}(Dia_{i,t}) + \sum \varphi Controls_{i,t} + Industry + Year + \varepsilon_{i,t} \quad (5)$$

where a significant and negative μ_1 suggests that non-local independent directors with greater cultural similarity can promote the quality of information disclosure of the firms.

Table 3
Mechanism analysis.

Variable	(1)	(2)	(3)	(4)
	ICQ	ICQ	KV	KV
<i>CSimilar</i>	0.047*** (4.754)		-0.003** (-2.302)	
<i>Dia</i>		0.135*** (4.339)		-0.007** (-1.996)
<i>Size</i>	0.331*** (31.245)	0.329*** (32.574)	0.026*** (19.475)	0.031*** (15.953)
<i>ROA</i>	5.745*** (27.424)	5.784*** (26.441)	0.371*** (21.343)	0.370*** (20.945)
<i>Growth</i>	0.060*** (3.944)	0.061*** (3.418)	0.004** (2.301)	0.004** (2.279)
<i>TOP1</i>	0.398*** (5.334)	0.393*** (5.075)	-0.014** (-1.998)	-0.014** (-2.042)
<i>Lev</i>	-0.942*** (-12.595)	-0.940*** (-13.473)	-0.028*** (-5.736)	-0.027*** (-5.684)
<i>Tangible</i>	-0.553*** (-9.776)	-0.543*** (-9.843)	-0.028*** (-4.734)	-0.028*** (-4.525)
<i>Dual</i>	0.032* (1.735)	0.032* (1.702)	0.003 (1.056)	0.002 (1.175)
<i>Bsize</i>	0.011** (2.224)	0.011** (2.216)	-0.000 (-0.653)	-0.000 (-0.668)
<i>IDP</i>	0.290* (1.799)	0.292* (1.803)	0.040* (1.832)	0.041* (1.783)
<i>Mshare</i>	0.528*** (10.323)	0.530*** (11.374)	-0.006 (-1.056)	-0.006 (-1.196)
<i>EDU</i>	0.002 (1.353)	0.003 (1.496)	-0.001 (-1.162)	-0.001 (-1.076)
<i>SOE</i>	0.039** (2.146)	0.038** (1.998)	0.002 (0.735)	0.002 (0.686)
Constant	-0.991*** (-5.132)	-0.990*** (-5.146)	-0.148*** (-5.634)	-0.151*** (-5.944)
Obs.	28,209	28,209	28,209	28,209
R-squared	0.239	0.241	0.231	0.232
Year FE	Yes	Yes	Yes	Yes
Industry FE	Yes	Yes	Yes	Yes

Robust t-statistics are reported in parentheses. *, **, and *** denote significance at the 10%, 5% and 1% levels, respectively.

Table 3 presents the results of the mechanism analysis. The (1) and (2) columns show the impact of cultural similarity on the internal control quality. The coefficients of *CSimilar* and *Dia* are significant and positive at the 1% level respectively, indicating that non-local independent directors with greater cultural similarity can improve the internal control quality of listed companies. Meanwhile, relevant studies have shown that high-quality internal control can significantly improve the financial reporting quality of listed companies (Chen, 2016; Herath & Albarqi, 2017). Therefore, the cultural similarity of non-local independent directors can improve the financial reporting quality of listed companies by improving their internal control quality.

The (3) and (4) columns of Table 3 show the impact of cultural similarity on the quality of information disclosure. The coefficients of *CSimilar* and *Dia* are significant and negative. Since a lower KV value indicates a higher quality of information disclosure, the results of negative coefficients indicate that non-local independent directors with greater cultural similarity can improve the quality of information disclosure of listed companies. Previous studies have shown a significant relationship between information disclosure and financial reporting quality (Pavlopoulos et al., 2019; Suharsono et al., 2020). Therefore, the cultural similarity of non-local independent directors is beneficial for alleviating information asymmetry and has a positive impact on the financial reporting quality of listed companies by improving the quality of information disclosure. Overall, these results support Hypothesis 2.

6. Additional analysis

6.1. Heterogeneity analysis

Given that there are significant differences among listed companies in China, the effect of the cultural similarity of non-local independent directors may vary across firms. Therefore, we further investigate whether the cultural similarity of non-local independent directors affects financial reporting quality differently across different types of firms.

(1) External monitoring status of the firm

The first measure we use in this analysis is institutional ownership. Higher institutional ownership in a firm means stronger external monitoring (Desai & Dharmapala, 2009; Kim, Li, & Zhang, 2011). Indeed, institutional investors have more information resources than individual investors and can therefore better monitor a company's unreasonable and illegal behaviours (Xu, Li, Yuan, & Chan, 2014). Therefore, based on the median of the institutional ownership ratio, we divide the sample into a high institutional ownership group (institutional ownership ratio greater than or equal to the median) and a low institutional ownership group (institutional ownership ratio less than the median).

Columns (1) and (2) of Table 4 present the regression results, showing that the coefficient on *CSimilar* in the high institutional ownership group is -0.003 , significant at the 1% level, and the coefficient for the low institutional ownership group is -0.001 , insignificant at the 10% level. We use a Chow test to test the coefficient difference between the groups. We obtain an empirical p -value of 0.004, significant at the 1% level. That is, the influence of the cultural similarity of non-local independent directors on financial reporting quality is stronger when institutional ownership is high rather than low. This suggests that institutional ownership, as an external monitoring mechanism, creates a good monitoring environment for non-local independent directors to play their monitoring role.

The second measure we use is the level of attention received from analysts. Analysts collect and transmit information about firms in the capital market and predict future business operations; therefore, they play the role of information intermediary and external monitor (Dyck, Morse, & Zingales, 2010). When a firm receives a high level of attention

Table 4
Heterogeneity analysis.

Variable	(1)	(2)	(3)	(4)
	DA	DA	DA	DA
	High InstOwn	Low InstOwn	High Attention	Low Attention
<i>CSimilar</i>	-0.003*** (-4.007)	-0.001 (-0.588)	-0.004*** (-3.995)	-0.001 (-1.227)
<i>Size</i>	-0.006*** (-6.865)	-0.010*** (-9.854)	-0.012*** (-7.657)	-0.005*** (-6.443)
<i>ROA</i>	-0.091*** (-5.631)	-0.193*** (-8.538)	-0.221*** (-10.075)	-0.042** (-2.254)
<i>Growth</i>	0.017*** (7.506)	0.011*** (5.836)	0.017*** (6.735)	0.019*** (7.056)
<i>TOP1</i>	0.014*** (3.341)	0.001 (0.965)	0.018*** (3.950)	0.003 (1.056)
<i>Lev</i>	0.062*** (5.527)	0.028*** (7.685)	0.048*** (7.946)	0.037*** (6.957)
<i>Tangible</i>	0.016*** (3.846)	-0.002 (-0.537)	0.003 (0.807)	0.016** (2.057)
<i>Dual</i>	-0.000 (-0.510)	0.001 (0.357)	-0.001 (-0.372)	0.001 (0.573)
<i>Bsize</i>	-0.001*** (-3.247)	-0.001 (-0.845)	-0.000 (-0.794)	-0.001** (-2.156)
<i>IDP</i>	0.019 (1.106)	0.006 (0.745)	0.026 (0.568)	0.007 (0.647)
<i>Mshare</i>	-0.007* (-1.749)	-0.006 (-1.546)	-0.010*** (-2.946)	-0.003* (1.832)
<i>EDU</i>	-0.003 (-1.212)	-0.002 (-1.056)	-0.002 (-1.052)	-0.001 (-1.173)
<i>SOE</i>	-0.008*** (-4.335)	-0.010*** (-4.657)	-0.011*** (-6.065)	-0.005*** (-3.946)
Constant	0.200*** (10.572)	0.253*** (10.113)	0.273*** (10.468)	0.187*** (9.957)
Obs.	14,105	14,104	13,858	14,351
R-squared	0.174	0.177	0.181	0.143
Year FE	Yes	Yes	Yes	Yes
Industry FE	Yes	Yes	Yes	Yes
t-test (p-value)	0.004***		0.037**	

Variable	(5)	(6)	(7)	(8)
	DA	DA	DA	DA
	SOE	Non-SOE	High marketization	Low marketization
<i>CSimilar</i>	-0.001* (-1.706)	-0.004*** (-4.995)	-0.002*** (-3.964)	-0.002 (-1.256)
<i>Size</i>	-0.007*** (-8.457)	-0.008*** (-8.056)	-0.009*** (-9.354)	-0.008*** (-8.957)
<i>ROA</i>	-0.085*** (-4.105)	-0.183*** (-7.335)	-0.176*** (-9.336)	-0.113*** (-4.484)
<i>Growth</i>	0.015*** (5.835)	0.018*** (6.373)	0.016*** (7.553)	0.023*** (4.946)
<i>TOP1</i>	0.014*** (3.835)	0.009** (1.969)	0.015*** (4.949)	0.003 (1.529)
<i>Lev</i>	0.034*** (6.624)	0.052*** (7.954)	0.036*** (8.573)	0.050*** (4.843)
<i>Tangible</i>	0.023*** (4.694)	0.004* (1.752)	0.009** (1.986)	0.018* (1.748)
<i>Dual</i>	-0.001 (-0.405)	0.001 (0.845)	0.001 (0.634)	-0.002 (-0.853)
<i>Bsize</i>	-0.001** (-2.271)	-0.001 (-1.124)	-0.001* (-1.784)	-0.001 (-0.884)
<i>IDP</i>	0.010 (0.894)	0.021* (1.694)	0.013 (1.124)	0.008 (0.946)
<i>Mshare</i>	-0.014* (1.794)	-0.004* (-1.665)	-0.005** (-2.262)	-0.004* (-1.824)
<i>EDU</i>	-0.002 (-1.335)	-0.001 (-0.883)	-0.002 (-1.495)	-0.002 (-1.384)
<i>SOE</i>			-0.008*** (-5.356)	-0.004*** (-3.846)
Constant	0.206*** (11.533)	0.242*** (10.946)	0.221*** (13.344)	0.232*** (7.957)
Obs.	12,607	15,602	23,876	4333

(continued on next page)

Table 4 (continued)

Variable	(5)	(6)	(7)	(8)
	DA	DA	DA	DA
	SOE	Non-SOE	High marketization	Low marketization
R-squared	0.138	0.194	0.199	0.205
Year FE	Yes	Yes	Yes	Yes
Industry FE	Yes	Yes	Yes	Yes
t-test (p-value)	0.008***		0.010**	

Robust t-statistics are reported in parentheses. *, **, and *** denote significance at the 10%, 5% and 1% levels, respectively.

from analysts, it can alleviate information asymmetry. Specifically, analysts can accurately analyse public and private firm information such as financial reports through their expertise, thus improving the transparency of firm information. This increased transparency creates a good monitoring environment for non-local independent directors to facilitate their monitoring role. Therefore, when a firm receives a high level of analyst attention, the cultural similarity of non-local independent directors should have a stronger impact on the financial reporting quality of listed companies than when analyst attention is low.

To test this conjecture, we use analyst attention to measure the level of analyst monitoring in companies. Specifically, we measure analyst attention by the number of analysts (teams) following a firm in a year. The firms in the sample are then divided into two subsamples based on the median of analyst attention, high analyst attention (analyst attention greater than or equal to the median) and low analyst attention (analyst attention less than the median). Columns (3) and (4) of Table 4 present the regression results. The results show that the coefficient on the *CSimilar* for the low analyst attention subsample (Low Attention) is not significant, while that for the high analyst attention subsample is negative and significant at the 1% level. This suggests that the cultural similarity of non-local independent directors has a stronger effect on the financial reporting quality of firms when analyst attention is high rather than low. This indicates that analyst attention, as an external supervision mechanism, plays an information intermediary role and improves the information transparency of listed companies, thereby creating a good supervision environment for independent directors to play a supervisory role.

(2) The nature of property rights in listed companies

Studies show that SOEs and non-SOEs differ in terms of social status, business objectives and social responsibilities (Zhang, Ma, Su, & Zhang, 2014). As SOEs typically have different regulatory environments and management philosophies from non-SOEs, they have different incentives to engage in surplus management (Wang, Braam, Reimsbach, & Wang, 2020). Hence, we examine whether the effect of the cultural similarity of non-local independent directors on financial reporting quality varies between SOEs and non-SOEs. We divide the firms in our sample into SOEs and non-SOEs based on the nature of their property rights, and report the results in columns (5) and (6) of Table 4. In the SOE subsample, the coefficient on *CSimilar* is -0.001 , significant at the 10% level. In comparison, in the non-SOE subsample, the impact on *CSimilar* is higher (-0.004) and significant at the 1% level. In addition, we test the coefficient difference between the groups and obtain an empirical *p*-value of 0.008, significant at the 1% level. This indicates that the cultural similarity of non-local independent directors has a strong effect on financial reporting quality when listed companies are non-SOEs, while the effect in SOEs is limited.

(3) The degree of marketization

The degree of marketization refers to the level and extent of market

development in a region. Studies have shown that in regions with a high degree of marketization, a well-developed system of legal protection and regulation provides institutional safeguards for the quality of financial information (Herath & Albarqi, 2017). To measure the degree of marketization, we draw on the provincial marketization index database of China, which is available at <https://cmi.ssap.com.cn/>. We use the marketization index of each provincial administrative region from 2005 to 2019 as a proxy for the degree of marketization, and match this index with the place of incorporation of each company in our sample.

Drawing on the provincial marketization index database of China,⁵ we use the marketization index of each provincial administrative region from 2005 to 2019 as a measure of the degree of marketization, and match this index with the registered headquarters of each company in our sample. We divide the firms in our sample into a high marketization group and a low marketization group based on whether the marketization index of a company's registered headquarter is higher than the national average degree of marketization in a year, and conduct regression analyses. The results in columns (7) and (8) of Table 4 show that the coefficients of *CSimilar* are negative and significant at the 1% level in the high marketization group, but not significant in the low marketization group. One potential explanation is that companies operating in a good external governance environment generally have higher information quality and internal communication efficiency (Jacoby, Liu, Wang, Wu, & Zhang, 2019), thus creating a better external regulatory environment for non-local independent directors' cultural similarity to play a significant role in monitoring the financial reporting quality of listed firms. Therefore, in regions with a high degree of marketization, the cultural similarity of non-local independent directors can have a greater impact on the financial reporting quality.

6.2. Robustness tests

(1) Instrumental variable test

To overcome possible endogeneity problems, we use the raster-scale Chinese topographic slope indicator based on the terrain difference calculation of Feng, Tang, and Yang (2007) as an instrumental variable (*DIFF_Podu*, measured as the absolute value of the difference between the topography of a company's registered headquarter and the average topography of an independent director's birthplace) to re-examine the impact of the cultural similarity of non-local independent directors on the financial reporting quality of listed companies. We choose this indicator as an instrumental variable because topography is an important natural condition in a region, and the historical formation of dialects is usually closely linked to topography. The more complex the topography, the steeper the slope, and the more mountains and rivers there are, the more likely the region was historically divided into different small, relatively enclosed areas. The population of a region was divided accordingly, resulting in the formation of multiple dialects in that region and, therefore, the formation of distinct local cultures in each dialect area. Therefore, the steeper the topographic slope of a region, the more likely the region will develop a different culture (i.e., the cultural similarity of a region is negatively related to its topographic variance value).

However, the financial reporting quality of listed companies does not influence the natural topography, especially in modern society in which topographic differences have little effect on corporate behavior as accessibility continues to increase. Therefore, terrain differences have no direct effect on corporate governance behavior.

Following Gorodnichenko and Roland (2021), we also use genetic distance (*Gene*) as an instrumental variable of cultural similarity. To measure *Gene*, we use immunoglobulin Gm haplotype frequency data, a widely used genetic marker due to its stability and ethnic heterogeneity. Genetic genes are highly exogenous because they are constructed from

⁵ The database is available at <https://cmi.ssap.com.cn/>.

neutral genes that are not subject to natural selection and vary randomly (Spolaore & Wacziarg, 2009). They are also not influenced by institutional or economic factors and are randomly divergent. Hence, reverse causality is unlikely to be an issue.

The results of our instrumental variable tests are presented in columns (1) to (4) of Table 5. Columns (1) and (3) report the results of the first-stage regression. The results show that *DIFF_Podu* and *Gene* are all significantly and negatively correlated with *CSimilar*, indicating that these variables are valid instrumental variables of cultural similarity. Moreover, the greater the magnitude of these variables, the lower the dialect similarity. The F-statistics for the weak instrumental variable test indicates that these instrumental variables are not weak.

Columns (2) and (4) show the results of the second-stage regression. All of the instrumental variables remain negative and significant, which again confirms the main findings of this study that the cultural similarity of non-local independent directors does indeed reduce earnings management by listed companies and improve their financial reporting quality. Therefore, our main results are robust.

(2) Substitution of explanatory variables

We use the reliability of financial statements (*Weak*) as a proxy for financial reporting quality. If a firm issues a financial restatement, it may indicate that its financial report is of low quality and unreliable. In this case, *Weak* takes a value of 1 and 0 otherwise. Columns (1) of Table 6 show the empirical results.

Table 5 Instrument variable regression.

Variable	(1) <i>CSimilar</i>	(2) <i>DA</i>	(3) <i>CSimilar</i>	(4) <i>DA</i>
<i>DIFF_Podu</i>	-0.684*** (-34.643)			
<i>Gene</i>			-4.896*** (-63.754)	
<i>CSimilar</i>		-0.007** (-2.064)		-0.009*** (-2.953)
<i>Size</i>	-0.065*** (-9.332)	-0.007*** (-10.283)	-0.030*** (-6.524)	-0.008*** (-9.868)
<i>ROA</i>	0.109 (1.275)	-0.152*** (-10.950)	-0.180** (-2.018)	-0.151*** (-10.464)
<i>Growth</i>	-0.014* (-1.862)	0.017*** (9.484)	-0.014** (-2.134)	0.018*** (8.575)
<i>TOP1</i>	0.241*** (6.074)	0.012*** (3.436)	0.185*** (5.847)	0.014*** (3.743)
<i>Lev</i>	-0.033 (-1.154)	0.043*** (10.235)	-0.097*** (-3.857)	0.044*** (11.452)
<i>Tangible</i>	-0.120*** (-3.064)	0.009** (2.274)	-0.299*** (-8.458)	0.009** (2.295)
<i>Dual</i>	-0.003 (-0.430)	0.000 (0.573)	0.024** (2.250)	0.000 (0.462)
<i>Bsize</i>	-0.018*** (-4.352)	-0.001** (-2.232)	-0.011*** (-3.953)	-0.001** (-2.254)
<i>IDP</i>	-0.278** (-2.356)	0.013 (1.054)	-0.045 (-0.705)	0.012 (1.242)
<i>Mshare</i>	0.285*** (7.377)	-0.006* (-1.753)	0.354*** (9.964)	-0.006** (-1.992)
<i>EDU</i>	0.001* (1.685)	-0.003 (-1.221)	0.003* (1.894)	-0.002 (-1.057)
<i>SOE</i>	0.185*** (11.883)	-0.009*** (-5.734)	0.166*** (11.663)	-0.008*** (-4.956)
Constant	3.751*** (27.984)	0.208*** (12.551)	2.930*** (24.454)	0.201*** (12.647)
Obs.	28,209	28,209	28,209	28,209
R-squared	0.190	0.172	0.321	0.170
Year FE	Yes	Yes	Yes	Yes
Industry FE	Yes	Yes	Yes	Yes
F value in the first stage	165.2		527.6	

Robust t-statistics are reported in parentheses. *, **, and *** denote significance at the 10%, 5% and 1% levels, respectively.

Table 6 Other robustness tests.

Variable	(1) <i>Weak</i>	(2) <i>DA2</i>	(3) <i>DA</i>	(4) <i>DA</i>
<i>CSimilar</i>	-0.008*** (-4.046)	-0.002*** (-3.143)	-0.004** (-2.053)	-0.005*** (-3.884)
<i>Size</i>	-0.032*** (-12.431)	-0.003*** (-9.865)	-0.007*** (-4.745)	-0.009*** (-10.223)
<i>ROA</i>	-0.443*** (-10.623)	0.043*** (8.371)	-0.156*** (-10.422)	-0.151*** (-11.204)
<i>Growth</i>	0.010** (2.354)	0.006*** (7.785)	0.012*** (7.006)	0.013*** (6.156)
<i>TOP1</i>	-0.065*** (-3.785)	0.006** (2.285)	0.022** (2.117)	0.013*** (3.984)
<i>Lev</i>	0.194*** (10.551)	0.028*** (11.174)	0.031*** (4.424)	0.045*** (8.843)
<i>Tangible</i>	-0.012 (-0.834)	-0.028*** (-13.485)	-0.001 (-0.328)	0.008** (2.074)
<i>Dual</i>	0.005 (0.745)	0.000 (1.075)	0.000 (0.201)	-0.000 (-0.095)
<i>Bsize</i>	-0.000 (-0.181)	-0.001* (-1.758)	-0.000 (-0.751)	-0.001* (-1.732)
<i>IDP</i>	0.021 (0.643)	-0.001 (-0.358)	0.019 (0.435)	0.015 (1.364)
<i>Mshare</i>	-0.028*** (-4.754)	-0.001 (-0.964)	-0.002 (-0.574)	-0.006* (-1.748)
<i>EDU</i>	-0.001 (-1.064)	-0.002 (-1.081)	-0.000 (-0.556)	-0.002 (-1.495)
<i>SOE</i>	-0.027*** (-4.095)	-0.004*** (-3.842)	-0.010*** (-2.865)	-0.009*** (-6.094)
Constant	1.008*** (14.965)	0.123*** (13.708)	0.091*** (6.853)	0.211*** (15.339)
Obs.	28,209	28,209	28,209	25,643
R-squared	0.179	0.096	0.240	0.158
Year FE	Yes	Yes	Yes	Yes
Industry FE	Yes	Yes	No	Yes
Firm FE	No	No	Yes	No

Robust t-statistics are reported in parentheses. *, **, and *** denote significance at the 10%, 5% and 1% levels, respectively.

We also use other DA2 as alternative measures of financial reporting quality. Following Kothari, Leone, and Wasley (2005), We control for the impact of performance on estimated discretionary accruals using a performance-matched firm's discretionary accrual. Then we use the modified Jones model with performance adjustment to calculate the absolute value of discretionary accruals, which is DA2.

$$\frac{TACC_{i,t}}{ASSET_{i,t-1}} = \alpha_1 \frac{1}{ASSET_{i,t-1}} + \alpha_2 \frac{\Delta REV_{i,t}}{ASSET_{i,t-1}} + \alpha_3 \frac{PPE_{i,t}}{ASSET_{i,t-1}} + \alpha_4 ROA_{i,t} + \epsilon_{i,t} \tag{6}$$

where $TACC_{i,t}$ is total accruals in year t . $ASSET_{i,t-1}$ is total assets in year $t-1$. $\Delta REV_{i,t}$ is the change in operating income. $PPE_{i,t}$ is the original value of fixed assets, and $ROA_{i,t}$ is return on assets. The residual (ϵ_t) from the regression is the level of discretionary accruals. The regression results reported in columns (2) of Table 6.

The results show that the coefficients on *CSimilar* is negative and significant, indicating that an increase in the cultural similarity of non-local independent directors will significantly improve the financial reporting quality of listed companies. This finding confirms the robustness of our results.

(3) Controlling for firm fixed effects

We also control for firm fixed effects, taking into account unobserved characteristics of firms. The regression results reported in columns (3) of Table 6 show that the direction and significance of the coefficients on *CSimilar* are consistent with our previous results after controlling for firm fixed effects, indicating the robustness of our results.

(4) Deleting certain observations

We further process the sample by excluding all observations with a value of 0 for *CSimilar*. The results reported in columns (4) of Table 6 show that the coefficients on *CSimilar* is still negative and significant, indicating the robustness of our results.

7. Conclusion

In this study, we empirically test the impact of the cultural similarity of non-local independent directors on the financial reporting quality of listed companies using data from China over the 2005–2019 period. We manually identify the birthplaces of non-local independent directors, match them with their respective dialect supergroups, dialect groups and dialect subgroups and measure dialect similarity to collate a unique dataset. The results show that the cultural similarity of non-local independent directors significantly improves the financial reporting quality of Chinese listed companies, and these results are robust to different tests such as endogeneity tests, controlling for firm fixed effects and replacement of explanatory variables. In the mechanism analysis, we show that the cultural similarity of non-local independent directors improves financial reporting quality by improving the internal control quality and information disclosure quality of listed companies. In our heterogeneity analysis, this effect is more pronounced when the listed company has a better external monitoring environment, for a non-state-owned enterprise (non-SOEs) and for the company is located in a region with a high degree of marketization.

Based on our research findings, relevant suggestions are proposed as follows. First, Regulators have a crucial role to play in improving the effectiveness of independent directors in listed firms. To achieve this, they should focus on strengthening the supervisory and advisory role of independent directors, reflecting their functional value. The selection process for independent directors should take into account the specific needs of the company, such as companies with high consulting or supervision requirements. A reasonable selection of independent directors

is essential for the development of corporate governance. The supervisory and advisory functions of different independent directors should be combined to maximize the overall governance effectiveness of the board of directors. By supervising the selection process and emphasizing the importance of independent directors' roles, regulators can promote greater transparency and accountability in corporate decision-making.

Secondly, companies should consider implementing measures to optimize the appointment mechanism for independent directors in different locations. For instance, non-local independent directors could be encouraged to conduct on-site research, and more information should be shared between listed companies and their non-local independent directors. This will enable independent directors to participate more effectively in the company's development and play their monitoring role, thereby promoting the overall improvement of the corporate governance environment.

Lastly, in addition to the mandatory regulatory function of formal (or explicit) governance mechanisms, more attention should be given to the role of informal institutional factors, such as traditional customs, moral ethics, and cultural norms, in economic and social development. As a complete formal governance mechanism is being constructed, informal institutional factors can be directed to play a positive role in economic and social development, further complementing the formal system.

Data availability

Data will be made available on request.

Acknowledgements

National Natural Science Foundation of China (72373022), Statistics Science Research Fundation of China (2021LY089), Guangdong Provincial Natural Science Foundation (2022A1515010998).

Appendix A. Variable definitions

Variable	Definition
<i>DA</i>	Absolute value of discretionary accruals
<i>CSimilar</i>	Dialect similarity (the average dialect similarity degree of the annual non-local independent directors of the company)
<i>Dia</i>	Proportion of non-local independent directors from the same dialect groups to the total number of non-local independent directors
<i>Size</i>	Firm size (natural log of total assets)
<i>ROA</i>	Return on assets (ratio of net profit to total assets)
<i>Growth</i>	Revenue growth rate
<i>TOP1</i>	Percentage of shares held by the largest shareholder at the end of the year
<i>Lev</i>	Leverage ratio (ratio of total ending liabilities to total ending assets)
<i>Tangible</i>	Proportion of fixed assets (ratio of net fixed assets to total assets)
<i>Dual</i>	Coded as 1 if there is a dual CEO-chairman role at a firm, and 0 otherwise
<i>Bsize</i>	Board size (number of directors)
<i>IDP</i>	Proportion of independent directors
<i>EDU</i>	Education level of non-local independent directors
<i>Mshare</i>	Proportion of shares held by management
<i>SOE</i>	Coded as 1 if the firm is a state-owned enterprise, and 0 otherwise

References

Benkraiem, R., Bensaad, I., & Lakhali, F. (2022). How do International financial reporting standards affect information asymmetry? The importance of the earnings quality channel. *Journal of International Accounting, Auditing and Taxation*, 46, Article 100445.

Bereskin, F., Byun, S. K., Officer, M. S., & Oh, J. M. (2018). The effect of cultural similarity on mergers and acquisitions: Evidence from corporate social responsibility. *Journal of Financial and Quantitative Analysis*, 53(5), 1995–2039.

Bhandari, A., Mammadov, B., Thevenot, M., & Vakilzadeh, H. (2022). Corporate culture and financial reporting quality. *Accounting Horizons*, 36(1), 1–24.

Bian, W., Ji, Y., & Zhang, H. (2019). Does dialect similarity add value to banks? Evidence from China. *Journal of Banking & Finance*, 101, 226–241.

Biddle, G. C., Hilary, G., & Verdi, R. S. (2009). How does financial reporting quality relate to investment efficiency? *Journal of Accounting and Economics*, 48(2–3), 112–131.

Braguinsky, S., & Mityakov, S. (2015). Foreign corporations and the culture of transparency: Evidence from Russian administrative data. *Journal of Financial Economics*, 117(1), 139–164.

Cahan, S. F., Chen, C., & Wang, R. (2021). Does media exposure affect financial reporting quality through auditors? *Journal of Accounting, Auditing and Finance*, 36(4), 750–775.

Chen, F., Hope, O. K., Li, Q., & Wang, X. (2011). Financial reporting quality and investment efficiency of private firms in emerging markets. *The Accounting Review*, 86(4), 1255–1288.

- Chen, M. K. (2013). The effect of language on economic behavior: Evidence from savings rates, health behaviors, and retirement assets. *American Economic Review*, 103(2), 690–731.
- Chen, T. (2016). Internal control, life cycle and earnings quality—An empirical analysis from Chinese market. *Open Journal of Business and Management*, 4(2), 301–311.
- Dechow, P. M., Sloan, R. G., & Sweeney, A. P. (1995). Detecting earnings management. *The Accounting Review*, 70(2), 193–225.
- Deng, C., Kanagaretnam, K., & Zhou, Z. (2020). Do locally based independent directors reduce corporate misconduct? Evidence from Chinese listed firms. *Journal of International Accounting Research*, 19(3), 61–90.
- Deng, T. (2019). Literature review on the Independence and effectiveness of independent directors. *Open Journal of Business and Management*, 7(2), 1063–1071.
- Desai, M. A., & Dharmapala, D. (2009). Corporate tax avoidance and firm value. *The Review of Economics and Statistics*, 91(3), 537–546.
- Du, Q., Yu, F., & Yu, X. (2017). Cultural proximity and the processing of financial information. *Journal of Financial and Quantitative Analysis*, 52(6), 2703–2726.
- Du, X. (2019). Does CEO-auditor dialect sharing impair pre-IPO audit quality? Evidence from China. *Journal of Business Ethics*, 156, 699–735.
- Dyck, A., Morse, A., & Zingales, L. (2010). Who blows the whistle on corporate fraud? *The Journal of Finance*, 65(6), 2213–2253.
- Fei, Q. (2022). Opposite effects of returnee and non-local independent directors on firm's environmental disclosure and performance. *Applied Economics*, 54(11), 1257–1277.
- Feng, Z. M., Tang, Y., & Yang, Y. Z. (2007). Topographic relief and its correlation with population distribution in China. *Acta Geographica Sinica*, 62(10), 1073–1082.
- Filip, A., Labelle, R., & Rousseau, S. (2015). Legal regime and financial reporting quality. *Contemporary Accounting Research*, 32(1), 280–307.
- Fu, R., Kraft, A., & Zhang, H. (2012). Financial reporting frequency, information asymmetry, and the cost of equity. *Journal of Accounting and Economics*, 54(2–3), 132–149.
- Gorodnichenko, Y., & Roland, G. (2021). Culture, institutions and democratization. *Public Choice*, 187(1), 165–195.
- Guo, F., & Ma, S. (2015). Ownership characteristics and earnings management in China. *The Chinese Economy*, 48(5), 372–395.
- Habib, A., Ranasinghe, D., & Huang, H. J. (2018). A literature survey of financial reporting in private firms. *Research in Accounting Regulation*, 30(1), 31–37.
- Han, M., Ding, A., & Zhang, H. (2022). Foreign ownership and earnings management. *International Review of Economics and Finance*, 80, 114–133.
- Hashim, H. A. (2012). The influence of culture on financial reporting quality in Malaysia. *Asian Social Science*, 8(13), 192.
- Herath, S. K., & Albarqi, N. (2017). Financial reporting quality: A literature review. *International Journal of Business Management and Commerce*, 2(2), 1–14.
- Huang, G., He, D., Meng, C., & Ma, D. (2022). Cultural proximity, venture capital and firm performance. *Borsa Istanbul Review*, 22(5), 975–984.
- Jacoby, G., Liu, M., Wang, Y., Wu, Z., & Zhang, Y. (2019). Corporate governance, external control, and environmental information transparency: Evidence from emerging markets. *Journal of International Financial Markets Institutions and Money*, 58, 269–283.
- Jiang, F., Zhu, B., & Huang, J. (2013). CEO's financial experience and earnings management. *Journal of Multinational Financial Management*, 23(3), 134–145.
- Jiang, Y., & Zhang, H. (2010). The structure of fellow-townsmen concepts and the development of questionnaire. *Psychological Research*, 3(4), 63–69.
- Kim, J. B., Li, Y., & Zhang, L. (2011). Corporate tax avoidance and stock price crash risk: Firm-level analysis. *Journal of Financial Economics*, 100(3), 639–662.
- Kim, O., & Verrecchia, R. E. (2001). The relation among disclosure, returns, and trading volume information. *The Accounting Review*, 76(4), 633–654.
- Kothari, S. P., Leone, A. J., & Wasley, C. E. (2005). Performance matched discretionary accrual measures. *Journal of Accounting and Economics*, 39(1), 163–197.
- Krishnan, J., Wen, Y., & Zhao, W. (2011). Legal expertise on corporate audit committees and financial reporting quality. *The Accounting Review*, 86(6), 2099–2130.
- Kusnadi, Y., Leong, K. S., Suwardy, T., & Wang, J. (2016). Audit committees and financial reporting quality in Singapore. *Journal of Business Ethics*, 139(1), 197–214.
- Lambert, R., Leuz, C., & Verrecchia, R. E. (2007). Accounting information, disclosure, and the cost of capital. *Journal of Accounting Research*, 45(2), 385–420.
- Lang, K. (1986). A language theory of discrimination. *The Quarterly Journal of Economics*, 101(2), 363–382.
- Lin, Y., & Cao, C. F. (2019). The appointment of non-local independent directors in the circumstance where control is separated from ownership. *Management Review*, 31(3), 211.
- Ma, Z., Novoselov, K. E., Zhou, K., & Zhou, Y. (2019). Managerial academic experience, external monitoring and financial reporting quality. *Journal of Business Finance & Accounting*, 46(7–8), 843–878.
- Masulis, R. W., Wang, C., & Xie, F. (2012). Globalizing the boardroom—The effects of foreign directors on corporate governance and firm performance. *Journal of Accounting and Economics*, 53(3), 527–554.
- Meng, H., Huang, X., Mao, X., Xia, Y., Lin, B., & Zhou, Y. (2023). The formation and proximity mechanism of population flow networks under multiple traffic in China. *Cities*, 136, Article 104211.
- Park, S. H., & Luo, Y. (2001). Guan xi and organizational dynamics: Organizational networking in Chinese firms. *Strategic Management Journal*, 22(5), 455–477.
- Pavlopoulos, A., Magnis, C., & Iatridis, G. E. (2019). Integrated reporting: An accounting disclosure tool for high quality financial reporting. *Research in International Business and Finance*, 49, 13–40.
- Pham, A. V., Pham, M. H., & Truong, C. (2022). Audit quality: An analysis of audit partner cultural proximity to client executives. *The European Accounting Review*, 1–33.
- Piekkari, R., Oxelheim, L., & Randøy, T. (2015). The silent board: How language diversity may influence the work processes of corporate boards. *Corporate Governance: An International Review*, 23(1), 25–41.
- Portes, A. (2001). Introduction: The debates and significance of immigrant transnationalism. *Global Networks*, 1(3), 181–194.
- Pucheta-Martínez, M. C., & García-Meca, E. (2014). Institutional investors on boards and audit committees and their effects on financial reporting quality. *Corporate Governance: An International Review*, 22(4), 347–363.
- Qi, B., Lin, J. W., Tian, G., & Lewis, H. C. X. (2018). The impact of top management team characteristics on the choice of earnings management strategies: Evidence from China. *Accounting Horizons*, 32(1), 143–164.
- Quan, Y., Lim, S., & Liang, S. (2017). Chasing political resources by listed companies: A perspective on hiring non-local independent directors from Beijing. *China Journal of Accounting Studies*, 5(3), 361–378.
- Quan, Y., & Zhang, W. (2021). Geographic distance and board monitoring: Evidence from the relocation of independent directors. *Journal of Corporate Finance*, 2021(66), Article 101802.
- Spolaore, E., & Wacziarg, R. (2009). The diffusion of development. *The Quarterly Journal of Economics*, 124(2), 469–529.
- Standifird, S. S., & Marshall, R. S. (2000). The transaction cost advantage of guanxi-based business practices. *Journal of World Business*, 35(1), 21–42.
- Suharsono, R. S., Nirwanto, N., & Zuhroh, D. (2020). Voluntary disclosure, financial reporting quality and asymmetry information. *The Journal of Asian Finance, Economics and Business*, 7(12), 1185–1194.
- Wang, Z., Braam, G., Reimsbach, D., & Wang, J. (2020). Political embeddedness and firms' choices of earnings management strategies in China. *Accounting and Finance*, 60(5), 4723–4755.
- Xu, N., Li, X., Yuan, Q., & Chan, K. C. (2014). Excess perks and stock price crash risk: Evidence from China. *Journal of Corporate Finance*, 25, 419–434.
- Ying, Y. (2016). Internal control information disclosure quality, agency cost and earnings management—Based on the empirical data from 2011 to 2013. *Modern Economy*, 7(1), 64–70.
- Zhang, C. (2020). Clans, entrepreneurship, and development of the private sector in China. *Journal of Comparative Economics*, 48(1), 100–123.
- Zhang, H., Luo, X., Han, M., & Liu, X. (2021). Cultural diversity in ownership and stock liquidity commonality: Evidence from China. *Finance Research Letters*, 40, Article 101856.
- Zhang, M., Ma, L., Su, J., & Zhang, W. (2014). Do suppliers applaud corporate social performance? *Journal of Business Ethics*, 121(4), 543–557.
- Zhang, X., Tan, J., Chen, Y., & Chan, K. C. (2021). Does environmental law enforcement matter for financial reporting quality? *The North American Journal of Economics and Finance*, 57, Article 101445.
- Zhou, J., Hao, L., & Yang, M. (2019). Earnings quality and travel convenience in China for non-local independent directors with accounting expertise. *China Journal of Accounting Studies*, 6(3), 295–320.
- Zingales, L. (2011). The "cultural revolution" in finance. Causes and consequences of corporate culture. *Journal of Financial Economics*, 117(1), 1–4.

检索证明

根据委托方提供的论文目录, 经 SCI 网络数据库和《期刊引用报告》JCR 网络数据库 (2023) 检索, 李洁 (Li Jie) 发表的论文被《科学引文索引》SCI 网络版收录, 为第一作者, 题录如下:

1. 标题: **A smart energy IoT model based on the Itsuku PoW technology**

作者: Li, J (Li, Jie); Chen, YS[✉] (Chen, Yansheng); Chen, YL (Chen, YanLing); Zhang, WP (Zhang, Weiping); Liu, ZH (Liu, Zhonghao)

来源出版物: RESULTS IN ENGINEERING 卷: 18

文献号: 101147 DOI: 10.1016/j.rineng.2023.101147 出版年: JUN 2023

人藏号: WOS:001001793100001

语言: English

文献类型: Article

地址: [Li, J (Li, Jie)] Guangdong Ind Polytech, Sch Finance & Trade, Guangzhou 510300, Peoples R China

[Chen, YS (Chen, Yansheng)][✉] Guangdong Ind Polytech Guangzhou, Dept Inst Big Data & Artificial Intelligence Appli, Guangzhou 510300, Peoples R China

[Chen, YL (Chen, YanLing)] Guangdong Ind Polytech, Sch Art & Design, Guangzhou 510300, Peoples R China

[Zhang, WP (Zhang, Weiping)] Guangdong Ind Polytech, Dept Acad Affairs, Guangzhou 510300, Peoples R China

[Liu, ZH (Liu, Zhonghao)] Hong Kong Polytech Univ, Dept Comp, Hong Kong 999077, Peoples R China

通讯作者地址: Chen, YS (通讯作者), Guangdong Ind Polytech Guangzhou, Dept Inst Big Data & Artificial Intelligence Appli, Guangzhou 510300, Peoples R China

电子邮件地址: yschenchina@qq.com

期刊信息:

期刊影响因子™

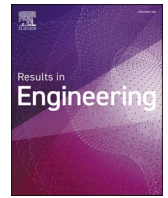
5 4.8

2022 5年

JCR 学科类别	类别排序	JCR 分区
ENGINEERING, MULTIDISCIPLINARY	19/178	Q1

特此证明





A smart energy IoT model based on the Itsuku PoW technology[☆]

Jie Li^a, Yansheng Chen^{b,*}, YanLing Chen^c, Weiping Zhang^d, Zhonghao Liu^e

^a School of Finance and Trade, Guangdong Industry Polytechnic, Guangzhou, 510300, China

^b Dept. of Institute of Big Data and Artificial Intelligence Applications, Guangdong Industry Polytechnic Guangzhou, 510300, China

^c School of Art and Design, Guangdong Industry Polytechnic, Guangzhou, 510300, China

^d Dept. of Academic Affairs, Guangdong Industry Polytechnic, Guangzhou, 510300, China

^e Dept. of Computing, Hong Kong Polytechnic University, Hong Kong, 999077, China

ARTICLE INFO

Keywords:

Blockchain
The proof of work (PoW)
Smart energy networks
Internet of Things(IoT)
Software defined network(SDN)

ABSTRACT

Based on the blockchain + software defined network(SDN) technology, we explore and research a new smart energy networks IoT architecture model of distributed trust to solve the “stuck neck” problems such as bandwidth constraints and trust obstruction of the current centralized network architecture of smart energy networks. In order to achieve efficient data flow and sharing and co-governance. Based on the MTP-Argon2 hash function algorithm in the Itsuku PoW technical solution, we add computing power optimization and correction multi-objective optimization operations, and use the network control right separation technology of the FS-Open Security SDN model to establish local database access policies and storage credentials. The traditional hardware devices are separated from the centralized network architecture of the smart energy network into a hybrid network architecture model of distributed trust. The results show that the distributed trust hybrid network architecture model achieves low latency and circumvents network bandwidth limitations, reflecting the energy efficiency gain and security stability of the model, as well as network load robustness.

1. Introduction

Major countries in the world are accelerating the development of blockchain technology. The integrated application of blockchain technology plays an important role in new technological innovation and industrial transformation. Blockchain is an important breakthrough for independent innovation technology. China attaches great importance to the integration and application of blockchain technology, strives to promote the underlying technical services of blockchain, focuses on the integration with the construction of new smart energy networks, explores the construction of information infrastructure, and uses blockchain technology to promote smart energy networks. Large-scale interconnection to ensure the orderly and efficient flow of production factors within the region. The above discussion clarifies the importance of combining the core technology of blockchain with the construction of intelligent energy network information infrastructure in my country in the future, as well as the response strategy to ensure the orderly and efficient flow of production factors in energy. Based on the above main directions, we strive to overcome the bottlenecks and limitations of the current network architecture of smart cities, and combine the core

technology of blockchain with the construction of smart energy networks information infrastructure to solve the key to the orderly and efficient flow of production factors in urban areas. Scientific and technological issues are of theoretical significance in line with the national development strategy of network power and the development of the digital economy.

The Internet of Things (IoT) has given vitality to traditional devices, and its intelligent and autonomous vision is being quietly realized by the commercialization of technologies such as 5G, NB-IoT and eMTC. The “Smarter Planet” concept was proposed by IBM in 2008. Today, with the technological innovation and diffusion of the Internet, big data and artificial intelligence, IoT technology that “everything can be linked” has made the smart energy network a reality. The centralized IT infrastructure of smart energy networks originates from exponentially growing intelligent information processing devices controlled by heterogeneous network systems [1,2], as well as ubiquitous sources of sensor information on the order of millions; however, in the “everything can be linked” of IoT, the massive unstructured data formed by the network connection exceeds the traditional data by several orders of magnitude, and the real-time management, exchange, storage, and

[☆] Co-first author: Jie Li, Yansheng Chen, Zhonghao Liu.

* Corresponding author.

E-mail address: yschenchina@qq.com (Y. Chen).

mining processing processes of streaming data make the traditional smart energy network architecture still inevitable. Latency, bandwidth bottlenecks, data reliability, privacy and security, and scalability issues. The proliferation of emerging technology innovations will drive the iterative development of future smart energy networks and IoT [3]. It is necessary to rethink the design of an efficient, safe and scalable distributed network architecture based on network energy efficiency and storage resource terminals to solve the current centralized network architecture of smart energy networks. The constraints of data security and the limitations of data security are explored, and the integrated application to realize the transformation of the smart energy Internet of Things to a self-regulating and self-managing distributed network architecture model is explored.

Based on blockchain + SDN technology, we build a prototype of a new smart energy network operation model, which is the main innovation of this paper. We conducted systematic literature mining on the IoT scalability network efficiency and security requirements on which smart energy networks rely, as well as the energy efficiency of IoT by blockchain technology. Looking forward to discovering the use of blockchain to solve IoT technology security issues? And how to achieve a self-regulating, self-managing distributed model transformation of smart energy IoT operations through SDN? We use these two themes as clues to carry out a comprehensive literature study. However, from the existing literature retrieval research, it is found that the research work of smart energy network architecture based on blockchain and SDN is rare. This may also confirm the novelty of the research idea of building a smart energy hybrid network model with blockchain and SDN technologies. Therefore, we find the current research significance from the two aspects of blockchain consensus mechanism technology (BCM) and SDN, and expand the theoretical significance and application value of applied basic research based on the above technologies.

2. Related work

In this section, we summarize the traditional approaches related to blockchain technology resolution services, and provide some background about the blockchain and its latest applications for achieving distributed trusted resolution services.

2.1. Traditional approaches

We found from the research of existing high-cited literature [4] on the theme of blockchain technology, one of which is the focus of financial technology research. Pilkington (2016) outlined the evolutionary technologies of blockchain, such as Ethereum, Ripple, Gridcoin, and blockchain related research based on Markov Chain theory, put forward the practical basis for the non-financial application of blockchain [5]. Tschorsch and Scheuermann (2015) studied robust models based on digital currency technology, discussed the characteristic properties of Bitcoin, and described the consensus mechanism in detail. Second, focus on general applications of blockchain and home IoT [6]. Dorri, Kanhere, & Jurdak (2017) propose a lightweight smart home IoT architecture, focusing on the limitations of blockchain, while proposing solutions to avoid Bitcoin's computationally intensive, TX confirmation delay, and scalability issues [7]. Huh, Cho, & Kim (2017) use blockchain smart contracts to configure and manage IoT devices to circumvent the security and synchronization issues of traditional C/S server architectures [8]. Buterin, Reijdsbergen, Leonardos and Piliouras(2020) leverage the trust distributed architecture of blockchain to build Ethereum smart contract configuration and home IoT devices. Third, pay attention to the security technical issues highlighted by digital currency and transactions [9]. Conoscenti, Vetrò and De Martin (2016) different from the blockchain application of the encryption mechanism, a literature review was conducted on the applicability of digital currency transaction security technology to find the Bitcoin such as integrity attacks, de-anonymization and other related vulnerabilities [10]. Dagher, Bünz,

Bonneau, Clark, and Boneh (2015) conducted an in-depth analysis of Bitcoin forks based on many Bitcoin security properties, summarized and proposed alternatives to Bitcoin consensus mechanism, user anonymity or privacy technology [11]. Fourth, the operation mechanism of blockchain and smart contracts, and the application of Industry 4.0 have become new topics in the industry. Christidis, and Devetsikiotis (2016) [12]delved into the operational mechanisms of blockchain and smart contracts, such as shared services and resource pooling mechanisms among IoT devices, as well as P2P markets and supply chain management (SCM) mechanisms for renewable sources, expanding A practical case of blockchain and IoT. the paper also focuses on testing the application of blockchain in IoT with low TX throughput, high latency of blockchain based on Proof of work (PoW), user and TX content privacy, as well as the performance characteristics and expectations of smart contracts related legal and transformational issues. In addition, research on the promotion and application of blockchain technology in the manufacturing industry has also become a new topic, such as the strategic route to Industry 4.0 [13] and the prospect of smart factories implementing Industry 4.0 [14].Most of the previous literature focuses on the foundation and theory of independent blockchain technology or SDN [15], or discussions of exploration and verification applications [16], and research on the application of blockchain and IoT in specific scenarios [17]. At present, the most familiar research accumulation with this paper is the subject research on Chain-network Integration between Blockchain and Enterprise Network [18,19], but It is still in the stage of theoretical research and has not been further extended.

The above literature mainly focuses on blockchain-related research based on Markov Chain theory, smart contracts, future manufacturing application exploration, industry 4.0 strategic route support, blockchain privacy protection and efficient aggregation, blockchain and The promotion and application of digital currency technology, DDoS attacks and 51% attacks highlighted by Bitcoin and Bitcoin transactions, as well as problems such as Ethereum mining, energy efficiency and applicability. However, from the perspective of smart energy and the Internet of Things, the related research that explores blockchain technology to solve problems such as the scalability of smart energy networks, data transmission delay, network bandwidth congestion, data privacy and security, etc., has not received extensive attention. , the thematic research has its theoretical contribution to seize the dominance of the new generation of information technology, showing the urgent need of thematic research.

2.2. Blockchain and relevant nonrepudiation applications

Under the background of the national development strategy of building a network power country and developing a digital economy with blockchain technology, it combines the concept of a hybrid network architecture with blockchain and SDN technologies, combining the core technology of blockchain with information infrastructure. Building a scalable smart energy IoT to overcome the bottlenecks and limitations of the current architecture. That will help to enhance access control security, data privacy, network storage and scalability, circumvention of bandwidth limitations, etc., to achieve a transition from an expensive, cumbersome and over-centralized centralized smart energy network architecture to a self-regulating, self-management The transformation of the distributed network architecture model to solve the "stuck neck" problems such as "bandwidth constraints" and "trust obstruction" of the current centralized network architecture, so as to achieve efficient energy flow and resource sharing and co-governance. It is a trend to focus on the integrated application of blockchain technology in smart energy networks and to promote the research and development of blockchain underlying technology services.

First, the shared value system of the blockchain gradually forms a consensus. Traditional industries and emerging industries rely on shared value systems to develop decentralized applications (Dapps) in order to build decentralized trust autonomous organizations and decentralized

autonomous society, (DAS) in central cities around the world. In response to current and future challenges, smart energy may be able to take advantage of SDN and blockchain technology to design solutions specifically to address the challenges of network scalability, data transmission delay, network bandwidth congestion, data privacy and security, etc. A new architectural model shift for self-regulating, self-managing distributed networks to address the limitations of a centralized network architecture for smart energy.

Second, the original intention of the “six ones” planning and design of smart energy makes the construction of smart energy network architecture tend to be centralized IT infrastructure. On the basis of traditional data center network architecture (such as Fat-tree, Portland, VL2, Dcell, Bcube, etc.), combined with the dynamic monitoring characteristics of smart energy construction, a perception layer represented by MEMS, GPS, smart sensors and other technologies is built [1]. The network layer with multiple wireless communication methods as the core and the application layer with multiple specialized capabilities [20]. In the future of highly intelligent cities, smart energy networks can provide all organizations or individuals with a high-quality transaction experience through smart transportation, smart living, smart mobility, smart energy, and smart business models. However, the exponentially growing intelligent information processing infrastructure controlled by heterogeneous network systems, as well as the ubiquitous millions of information source sensors, and the massive data formed by them, give the intelligent energy network framework of the centralized IT infrastructure, bringing increasing pressure. These include network scalability, data transmission delay, network bandwidth congestion, data privacy and security issues.

3. Preliminary

This section provides the necessary background knowledge of the consensus mechanism and Software Defined Network(SDN) used in this paper.

3.1. Understanding and discovery of the applicability of consensus mechanism technology

The blockchain shared value system is applied by cryptocurrencies, and with the proposal of the blockchain ecosystem, it has evolved and developed, such as Ethereum, smart contracts and asset tokenization (ICO), etc. The sharing economy, and even the blockchain country. Privacy and security of the blockchain ecosystem, and properties such as immutability. It is guaranteed by consensus mechanisms such as Proof of Work (PoW), Proof of Stake (PoS) and Delegated Proof of Stake (DPoS), as well as distributed ledger consistency. In cryptocurrency and blockchain technology, PoW is the core content that supports large-scale distributed public ledgers. This mechanism makes any block data tampering or attacking behavior, the block must be recalculated and All subsequent blocks form a SHA-256 puzzle. Proof-of-work is powered by the output of a hash function, originally proposed to mitigate spam problems, and later as the Bitcoin protocol. Proof of work is usually iteratively computed based on the double encryption function SHA-256, which is easy to check but difficult to compute [21]. As the core algorithm of cryptographic functions, Argon2 was developed in 2010, became the optimal algorithm in the hash cryptography competition in 2015, and was later fully applied [22]. Biryukov et al. (2016) proposed a proof-of-work scheme using Merkle hash trees on the Argon2 hash chain. It consists of storage encryption and parameter calculation examples for cryptocurrency applications, a proof-of-work model is used to construct a Merkle tree, and a leaf set is selected based on the pseudo-random hash of the root of the Merkle tree as a basis for calculation. In the Argon2 chain, it is difficult for an attacker to find the correct content of the Argon2 chain block through the Merkle tree path. Therefore, if an attacker tries to deceive and store only part of the Argon2 chain, it will be quickly discovered. Currently, the algorithm is

considered to be superior to Bcrypt, the most widely used cryptographic hash function today, both in terms of security and cost-effectiveness. In addition to being a cryptographic hash function, the algorithm is also suitable for data privacy and security operations based on consensus mechanisms such as blockchain of PoW.

3.2. Understanding and discovery of the applicability of SDN technology

SDN originated from the Clean Slate research project of Stanford University in 2006. It is a new network architecture model that can define and control the network in the form of software programming. It has the characteristics of separation of control plane and forwarding plane, and open source programmability. Structural research provides a new approach and greatly promotes the development of the next-generation Internet. SDN has the characteristics of openness, standardization, and programmability through the hierarchical distribution settings of the network architecture, replacing the traditional expensive, complicated and excessively centralized network architecture. From the previous literature research, it can be found that there are different network architecture models existing on the SDN architecture. Monshizadeh, Khatri, & Kantola (2017) proposed a multi-layer IDS model [23], which uses programmable SDN control switches to detect and prevent future failures. Authorized attack network, clustered SDN application and control, and detection-as-a-service (DaaS) algorithm functions, highlighting the combination of load balancing technology and clustering of sampled traffic, reducing the computing power cost and network delay in the SDN controller. Machado et al. (2017) propose an ANSwer architecture with network functions virtualization (NFV) and SDN capabilities [16] that can create scalable network policies and feedback control loops to identify and analyze abnormal behavior of network infrastructure. Ammar et al. (2016) propose an enhanced SDN data center security network architecture [24]. The architecture combines the programmability of SDN and detects threats through persistent search and analysis of abnormal behavior of network traffic, and uses security agents to collect and analyze security logs to block attacks. As well as improving data center security performance at the physical network security layer by integrating applications at the adaptive layer. In addition, Sharma et al. (2017) proposed a blockchain-based distributed in-vehicle network architecture in smart cities, which provides ideas for building a safe and reliable distributed network architecture model for transmission management systems [20], and that proposed the DistBlockNet model, a distributed mesh network model for IoT using SDN and blockchain, which defines an update scheme of data flow rules to update and verify the mesh securely of data flow rules in the network. However, due to the lack of standardization of smart energy IoT products, countries around the world have not agreed on a single smart energy network architecture model standard. The layered architectures and their tasks, functions or purposes discussed in different literatures vary according to the scenarios and application practices.

4. Approach

The IoT of a smart energy network system usually consists of three elements: sensor nodes, IoT gateways, and access points. Since sensor nodes in smart energy networks are usually limited in computing and storage resources, when the IoT of SDN is combined with a blockchain system, these sensor nodes are usually divided into transaction nodes in the blockchain system, at each boundary the miner nodes of the network use MiniNET to build SDN support controller nodes. The blockchain system through SDN allows border transaction nodes to only send transactions without mining and storing complete ledger information. The smart energy IoT gateway can be used as the full node (FNs) of the blockchain system SDN, which has abundant computing and storage resources. We use the network control separation technology of the FS-Open Security SDN model to establish local database access policies and storage credentials, so the blockchain system requires full nodes to

perform hash operations to access the ledger and store new blocks. In the SDN model network, we define the access point to determine whether it is the node of the gateway's block transmission by sending an ACK frame, and the access point does not participate in mining, as a backup for the download of the new block gateway, which can be used for blocks sent by the storage gateway.

4.1. Test environment

We use the go-Ethereum experimental platform to build a private blockchain network according to the experimental parameters and performance requirements, and test the distributed properties of the hybrid network architecture through the Mist browser simulation experiment. We use the Argon2 hash function algorithm to define the generated block, and use MiniNET to build the SDN support controller node on the miner node of each border network. The random concurrent big data is generated through the computing power simulation of the combination of distributed computer server groups, and it is defined as the hash transaction of the blockchain. We assume that there are N gateways in IoT, and the computing power of the gateways is constant. The minimum contention window W_{min} on the node is set to 1, the maximum contention window W_{max} is set to 2048, the maximum backoff stage m is set to 8, the packet header H is set to 256 bits, the size of the ACK frame is set to 512 bits, and the channel bit rate is set to 1Mbit/s, the transmission delay is set to $2\mu s$, the time slot size is set to $64\mu s$, the short inter-frame interval SIFS is set to $16\mu s$, the distributed inter-frame interval DIFS is set to $128\mu s$, the size of the block header D_h is set to 512 bits, and the size of the transaction D_t is set to 1 M bits.

4.2. Test process

We adopt the IEEE 802.11 distributed coordination function to transmit blocks, and define Proof of Work (PoW) as the output of the Hash function of the Argon2 hash function algorithm. Essentially, PoW has the characteristics of being difficult to tamper with and verify, which is equivalent to finding a hard solution to the random process of Hash Collision (HC) to reduce the occurrence of block collisions. The PoW algorithm needs to go through the following steps to reach a consensus in the IoT of the smart energy network system: First, the sensor node acts as a transaction node to generate a new transaction and broadcast it to all nodes through a broadcast channel. Second, full nodes collect new transactions and continuously perform hash operations (mining) to compete for the priority of producing legitimate blocks. Third, the gateway that generates the legal block competes for the channel based on the distributed coordination function and obtains the block broadcasting right. Fourth, after the sensor node and the full node accept and verify the new block, the new block is stored in the ledger of the transaction node in the divided blockchain system, and an ACK frame is returned to the full node that sent the block. Fifth, when a new block is stored in the transaction node ledger in the blockchain system, the block has reached a preliminary consensus. Sixth, with the continuous accumulation of subsequent blocks, the probability of the block storage transaction being tampered with will decay exponentially, that is, the more blocks accumulated, the higher the degree of consensus.

5. Results analysis and discussion

5.1. Results analysis

On the premise that the forked block is not broadcast, the PoW algorithm can increase the block generation rate by reducing the difficulty value of the hash operation, so as to achieve the purpose of improving the transaction throughput. In order to verify the performance of the PoW algorithm using the block access control scheme in the hybrid network architecture IoT, we deduced the transaction throughput, block loss rate, block utilization and mining pause time to derive expressions for performance metrics.

● Transaction Throughput

Transaction Throughput is the maximum number of transactions per second that a block can successfully transmit on a network channel. We believe that transaction throughput is equal to the number of blocks successfully transmitted per second on the channel multiplied by the maximum number of transactions a block can hold. In order to reduce the probability of forks and improve the consensus efficiency, consider that the gateway can transmit a whole block after each block rollback, including the block header and all transactions in the block. In this case, a single packet average (bits) can be identified as the size of a block. We deduce the transaction throughput formula with reference to the Markov chain model network throughput calculation formula:

$$V_w = p_1 d_p / (p_0 t + p_1 T_s + (1 - p_0 - p_1) T_b) \quad (1)$$

$$T_s = H_d + d_p + 2\lambda + SIFS + ACK + DIFS \quad (2)$$

$$T_b = H_d + d_p + DIFS + \lambda \quad (3)$$

Among them, λ is the block generation rate, $SIFS$ is the short inter-frame space, $DIFS$ is the distribution coordination function inter-frame space, and ACK is the response inter-frame space. Use T_s to represent the size of the block header, T_b to represent the size of a transaction, and d_p to represent the maximum number of transactions that a block can accommodate. Since each successful transmission of a block can accommodate up to d_p transactions, the transaction throughput V_w can be obtained.

● Block discard rate

The block discard rate V_d is defined as the number of forked blocks discarded by the gateways of the entire network per second. This performance indicator can reflect the wasted computing resources of the PoW consensus process from the side. Blocks are discarded in two cases: First, when a successful block transfer occurs in the channel, one or more gateways are in block rollback state V_{d1} . Second, when a block collision occurs in the channel, one or more gateways are in block transfer state V_{d2} . Through integration, the total block discard rate $V_d = V_{d1} + V_{d2}$ can be obtained. According to the transaction throughput formula, the expandable formula is:

$$V_-(d) = \left(\sum_{d_p=0}^{d_p-1} d_p \times P\{V_{d1}\} + \sum_{d_p=0}^{d_p-1} d_p \times P\{V_{d2}\} \right) / (p_1 d_p + (p_0 t + p_1 T_s + (1 - p_0 - p_1) T_b)) \quad (4)$$

● Block utilization and mining suspension probability

In order to study what proportion of blocks can become effective blocks to protect the security of the ledger, the block utilization rate is represented by V_u , which is defined as the steady-state proportion of the number of successfully transmitted blocks to the total number of generated blocks. To get V_u , we first analyze how many blocks the entire IoT can successfully transmit in T time. Let V_{us} be the successful block transmission rate, which means the number of blocks successfully transmitted per second in the entire network, and V_{ud} be the number of blocks discarded by the entire IoT within T time. The block utilization rate can be expressed as:

$$v_u = \lim_{T \rightarrow \infty} (v_u / (v_u + v_{us})) \tag{5}$$

We analyze the steady-state probability p_v of mining suspension, and its physical meaning is the long-range proportion of the entire network mining suspension time to the total system time. We can understand it this way, the average number of blocks generated by a gateway per second is λ , and its value is the quotient of the gateway hash rate and the hash operation difficulty value. When the mining strategy is not used to suspend mining, the entire network will generate d_p blocks on average in T time. When affected by the mining strategy, the entire network will only generate d_{ps} blocks on average in T time. From this, we can get:

$$p_v = \lim_{T \rightarrow \infty} ((\lambda d_p - (v_u + v_{us})T) / \lambda d_p) \tag{6}$$

5.2. Results discussion

Considering that the actual block size is determined by the number of transactions contained in the block, we use the above formula to calculate the change curve of transaction throughput, block discard rate and mining suspension probability according to the parameter settings. At the same time, we set the number of gateways d_p and the block generation rate λ to $2^3, 2^4, 2^5$ and 2^6 for comparative calculation to reflect the impact of the number of gateways on various performance indicators.

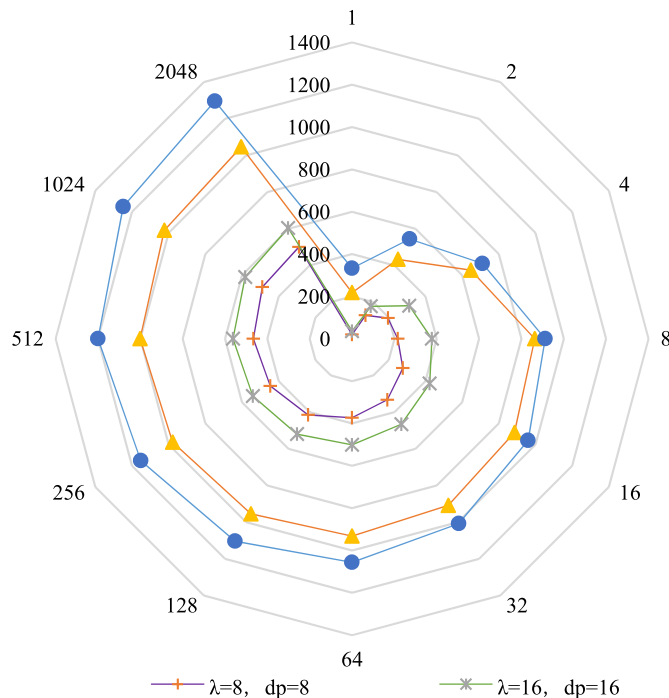


Fig. 1. Evaluation of the impact of the maximum number of transactions throughput.

● The impact of the maximum number of transactions on performance

The results in Fig. 1 show that transaction throughput increases as d_p increases. At the same time, the growth rate of transaction throughput will gradually decrease with the increase of d_p , and eventually become stable. Even when $d_p = 2^{20}$, the four curves have no downward trend. This is because when d_p increases, each time block rollback ends, a block sent by the gateway can accommodate more transactions. Statistically speaking, the smaller the average backoff latency experienced by a single exchange, the more transactions per second are transferred. On the other hand, the larger the block generation rate λ and d_p , the faster the transaction throughput grows, but the lower the maximum transaction throughput when it reaches a plateau. When $d_p = 2^{20}$, the transaction throughput of λ and d_p equal to 2^3 is 501tps, the transaction throughput of λ and d_p equal to 2^4 is 604tps, the transaction throughput of λ and d_p equal to 2^5 is 1047tps, and the transaction throughput of λ and d_p equal to 2^6 is 1296 tps. This is because when d_p is small, the block transmission delay is small. In this case, the larger λ and d_p , the higher the channel resource utilization, the more transactions per second are transmitted. When the d_p is large, the block transmission delay is large. In this case, the larger λ and d_p , the more congested the channel, and the overload phenomenon occurs. The frequent collision of blocks reduces the maximum transaction throughput when it is stable.

The results in Fig. 2 show that the block discard rate decreases as d_p increases. This is because when d_p increases, the block transmission delay increases, making the mining pause time longer. The mining suspension will slow down the block generation rate of the gateway, at the same time, reducing the probability of blocks appearing in the rollback state, and ultimately reducing the block discard rate. When d_p is constant, the larger the λ and d_p , the greater the probability of fork will be generated, and the more blocks will be discarded. According to the block utilization formula, we know that the block utilization does not change with the change of d_p . That is, as d_p increases, the ratio of the successful block transfer rate to the block discard rate is constant. Combining the results in Fig. 1, we can see that with the increase of d_p , the successful block transmission rate and the block discard rate will decrease at the same rate, so that the block utilization rate can be kept constant. The reason for the decrease in the successful block transmission rate is that the channel resources are limited. The longer the transmission time of a single block, the fewer blocks that can be successfully transmitted per second. Since the premise of the test is that the gateway computing power and PoW difficulty value are constant, the decrease in the successful block transmission rate will lead to less

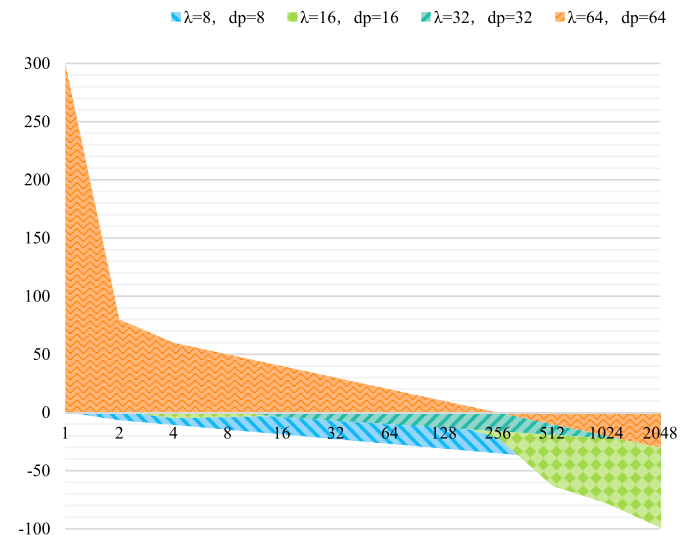


Fig. 2. Evaluation of the impact of the maximum number of transactions on the block discard rate.

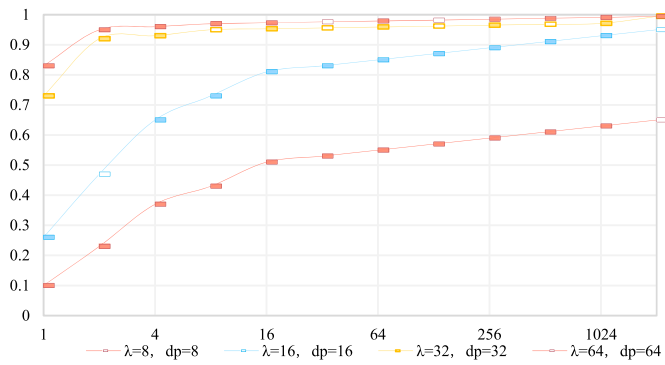


Fig. 3. Evaluation of the impact of the maximum number of transactions on the probability of mining suspension.

● Block Generation Rate and Performance Analysis

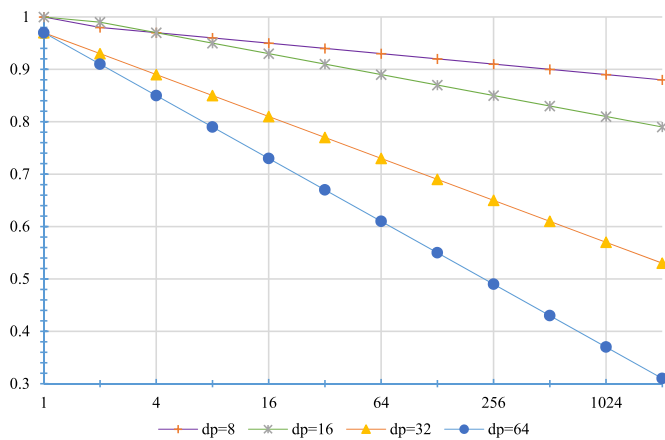


Fig. 4. Comparison and evaluation of block utilization and block generation rate.

cumulative computing power per unit time of the ledger. That is, an increase in d_p reduces security.

The results in Fig. 3 show that the mining suspension probability increases as d_p increases. This is because when the d_p increases, the block occupies the channel for a longer time, so the mining strategy will suspend the mining of the gateway more frequently to reduce the generation of forks and keep the block utilization constant. On the contrary, if the mining suspension strategy is not used, when blocks are transmitted in the channel, forked blocks will be generated, which will reduce the block utilization rate. We can find that the larger the d_p setting, the higher the transaction throughput of the consensus process, but the block utilization will not be affected while the throughput increases. On the other hand, the increase of d_p will increase the block transmission delay, resulting in fewer accumulated blocks per unit time of the ledger, which affects security. Therefore, in actual scenarios, d_p can be set according to specific requirements to achieve a balance between performance and security.

It can be found from Fig. 4 that the block discard rate increases monotonically as λ increases, which is opposite to the effect of d_p on the block discard rate in Fig. 3. This is because when λ becomes larger, more blocks will enter the rollback state at the same time, and only one of these blocks will be successfully transmitted in the end, and the rest will be discarded due to forks. In contrast, when the d_p becomes larger, the probability of the pause time increases, and at the same time, there are fewer blocks entering the rollback state. In addition, we also found that the increase of the number of gateways d_p and the block generation rate λ has a similar effect on the block discard rate, that is, the block discard rate increases. The results in Fig. 4 show that with the increase of λ , the

block utilization rate will decrease, that is, the proportion of successfully broadcast blocks in the total generated blocks will become smaller. When the block utilization is less than 0.3, most of the blocks will be discarded due to forks. The reason for this phenomenon is that the increase in the block generation rate increases the number of blocks that enter the rollback state at the same time, and the proportion of forked blocks increases. Since the computing power for generating forked blocks cannot be accumulated on the main chain of the ledger, under the condition that the computing power of the gateway is constant, the increase in the proportion of forked blocks will “dilute” the computing power of the gateway and affect the security.

6. Conclusion and limitations

6.1. Conclusion

Considering that the PoW consensus algorithm has the problems of limited transaction throughput and large consumption of computing resources, we propose a block access control scheme to deal with the fork problem of the PoW algorithm in the smart energy IoT scenario. We speed up the block generation rate while improving the effectiveness of computing resources to achieve the purpose of improving transaction throughput. Next, we established a Markov chain model [25] to analyze the performance of PoW algorithm with block access control scheme in smart energy IoT, including: transaction throughput, block discard rate, block utilization, and mining pause probability.

The analysis results show that the PoW algorithm using the block access control scheme can achieve high transaction throughput in the smart energy IoT. Under ideal channel conditions, transaction throughput can reach up to 1296 tps. In the consensus process, the more transactions a single block contains, the higher the transaction throughput, but this also increases the block transmission delay, which reduces the cumulative blocks per unit time of the ledger, which affects security. When the computing power of the gateway is constant, the system can increase the block generation rate by reducing the PoW difficulty value to achieve the purpose of improving the transaction throughput, but at the same time, the block utilization and security will be reduced. Therefore, in actual scenarios, the block size and difficulty value can be set according to specific requirements to achieve a balanced load among transaction throughput, block utilization, and security. In general, the block access control scheme improves the transaction throughput and block utilization of the PoW algorithm in the smart energy IoT environment, but its resource consumption is still greater than the DAG consensus, and its advantages lie in energy efficiency and security stability, Not easily affected by network load.

6.2. Limitations

Based on the challenges and dilemmas faced by the current smart energy centralized network architecture, we conceive a conceptual model of distributed trust network operation to realize the smart energy IoT network security architecture and sustainable development, but there are still the following limitations:

- Avoid the bottleneck problem of network bandwidth limitation. For the business practices and application scenarios of smart energy, the current centralized network architecture solutions are not suitable for circumventing network bandwidth limitations. Centralized network architectures have to send the massive data collected by sensors to the core network, which consumes a lot of network bandwidth, addresses bandwidth constraints and reduces bandwidth usage. We need to design a network architecture that allows distributed autonomous regulation and management of local data processing and analytical operations.
- Avoid the single point of failure problem. Due to the massive data eruption of heterogeneous networks, the network architecture of

smart energy may be overloaded, resulting in a large number of single points of failure and reducing the quality of service envisaged by smart energy. We need to design a trust network architecture that provides network fault tolerance and tamper resistance.

Declaration of competing interest

The authors declare that they have no known competing financial interests or personal relationships that could have appeared to influence the work reported in this paper.

Data availability

Data will be made available on request.

Acknowledgements

This research was funded by Guangdong Province Philosophy and Social Sciences Planning 2020 Disciplinary Co-construction Foundation (Project#GD20XGL49), 2021 Annual Project of Guangdong Social Science Planning Foundation (Project#GD21CGL13), Guangzhou 2021 Basic and Applied Basic Research Foundation (Project#202102080475), and 2022 Provincial Key Platform Scientific Research Innovation Team (Natural Science) Project of Guangdong Provincial Department of Education (Project#2022KCXTD042).

References

- [1] Salem Al-Naemi, Awani Al-Otoom, Smart sustainable greenhouses utilizing microcontroller and IOT in the GCC countries; energy requirements & economical analyses study for a concept model in the state of Qatar, *Results in Engineering* 17 (2023), 100889, <https://doi.org/10.1016/j.rineng.2023.100889>.
- [2] H.S. Shrishya, Boregowda Uma, An energy efficient and scalable endpoint linked green content caching for Named Data Network based Internet of Things, *Results in Engineering* 13 (2022), 100345, <https://doi.org/10.1016/j.rineng.2022.100345>.
- [3] Giral-Ramírez, Diego Armando, César Augusto Hernández-Suárez, César Augusto García-Ubaque, Spectral decision analysis and evaluation in an experimental environment for cognitive wireless networks, *Results in Engineering* 12 (2021), 100309, <https://doi.org/10.1016/j.rineng.2021.100309>.
- [4] Chen, Lin, Business intelligence capabilities and firm performance: a study in China, *Int. J. Inf. Manag.* (2020), 102232, <https://doi.org/10.1016/j.ijinfomgt.2020.102232>.
- [5] Pilkington, Does the fintech industry need a new risk management philosophy?, *Digital Currencies and e-money Services in Luxembourg* (March 8, 2016) (2016), doi:10.2139/ssrn.2744899.
- [6] Tschorsch, Scheuermann, Bitcoin and beyond: a technical survey on decentralized digital currencies, *IEEE Communications Surveys & Tutorials* (2016) (2016) 2084–2123, <https://doi.org/10.1109/COMST.2016.2535718>.
- [7] Kanhere Dorri, Jurdak, Towards an optimized Blockchain for IoT, *The second IEEE/ACM conference on Internet of Things Design and Implementation* (2017) 173–178, <https://doi.org/10.1145/3054977.3055003>, 2017.
- [8] Cho Huh, Kim, Managing IoT devices using blockchain platform." 2017 19th international conference on advanced communication technology (ICACT), IEEE (2017) (2017) 464–467, <https://doi.org/10.23919/ICACT.2017.7890132>.
- [9] V. Buterin, D. Reijnders, S. Leonardos, G. Piliouras, Incentives in Ethereum's hybrid Casper protocol, *Int. J. Netw. Manag.* 30 (5) (2020), e2098, <https://doi.org/10.1002/nem.2098>.
- [10] Vetrò Conoscenti, De Martin, Blockchain for the Internet of Things: a systematic literature review, 2016 IEEE/ACIS 13th International Conference of Computer Systems and Applications (AICCSA) (2016) 1–6, <https://doi.org/10.1109/AICCSA.2016.7945805>, 2016.
- [11] Gaby Dagher, Benedikt Bünz, Bonneau Joseph, Jeremy Clark, Dan Boneh, Provisions: privacy-preserving proofs of solvency for Bitcoin exchanges, in: *Proceedings of the 22nd ACM SIGSAC Conference on Computer and Communications Security (CCS '15)*, Association for Computing Machinery, 2015, pp. 720–731, <https://doi.org/10.1145/2810103.2813674>, 2015.
- [12] Christidis, Devetsikiotis, Blockchains and smart contracts for the internet of things, *IEEE Access* 4 (2016) 2292–2303, <https://doi.org/10.1109/ACCESS.2016.2566339>, 2016.
- [13] M. Ghobakhloo, The future of manufacturing industry: a strategic roadmap toward Industry 4.0, *J. Manuf. Technol. Manag.* 29 (6) (2018) 910–936, <https://doi.org/10.1108/JMTM-02-2018-0057>.
- [14] Wan Wang, Li Zhang, Zhang, Towards smart factory for industry 4.0: a self-organized multi-agent system with big data based feedback and coordination, *Comput. Network.* 101 (4) (2016) 158–168, <https://doi.org/10.1016/j.comnet.2015.12.017>, 2016.
- [15] Kumar, Tripathi, Implementation of distributed file storage and access framework using IPFS and blockchain." *2019 fifth international conference on image information processing, ICIP* (2019) (2019) 246–251, <https://doi.org/10.1109/ICIP47207.2019.8985677>.
- [16] Machado, Wickboldt, Granville, Schaeffer-Filho, Arkham: an advanced refinement toolkit for handling service level agreements in software-defined networking, *J. Netw. Comput. Appl.* 90 (JUL) (2017) 1–16, <https://doi.org/10.1016/j.jnca.2017.04.009>, 2017.
- [17] Guizani Al-Fuqaha, Aledhari Mohammadi, Ayyash, Internet of things: a survey on enabling technologies, protocols, and applications, *IEEE Commun. Surv. Tutor* 17 (4) (2015) 2347–2376, <https://doi.org/10.1109/COMST.2015.2444095>, 2015.
- [18] Li Chen, Hu Liu, Wang, A study of the theory of chain-network integration between blockchain and Enterprise network, *Proc. SPIE* (2021), 1207909, <https://doi.org/10.1117/12.2622717>, 2021.
- [19] Liu Chen, Li, Zhang, The integration of blockchain and Enterprise network: a distributed operation solution, *IEEE Computer Society* (2021) (2021) 965–976, <https://doi.org/10.1109/CISAI54367.2021.00194>.
- [20] Singh Sharma, Jeong, Park, DistBlockNet: a distributed blockchains-based secure SDN architecture for IoT networks, *IEEE Commun. Mag.* 55 (9) (2017) 78–85, <https://doi.org/10.1109/MCOM.2017.1700041>, 2017.
- [21] Feige Dwork, Naor Kilian, Safra, Low Communication 2-prover Zero-Knowledge Proofs for NP, *springer*, 1992, 1992, https://link.springer.com/content/pdf/10.1007%2F3-540-48071-4_15.pdf.
- [22] Dinu Biryukov, Khovratovich, Argon2: new generation of memory-hard functions for password hashing and other applications, 2016 IEEE European Symposium on Security and Privacy (EuroS&P) (2016) 292–302, <https://doi.org/10.1109/EuroSP.2016.31>, 2016.
- [23] Khatri Monshizadeh, Kantola, An adaptive detection and prevention architecture for unsafe traffic in SDN enabled mobile networks, *Integrated Network & Service Management* (2017) (2017) 883–884, <https://doi.org/10.23919/INM.2017.7987395>.
- [24] Rizk Ammar, Abdel-Hamid, Aboul-Seoud, A framework for security enhancement in SDN-based datacenters, *Ifip International Conference on New Technologies* (2016) (2016) 1–4, <https://doi.org/10.1109/NTMS.2016.7792427>.
- [25] Richardson, Domingos, *Markov Logic Networks*, vol. 62, Kluwer Academic Publishers, 2006, pp. 107–136, <https://doi.org/10.1007/s10994-006-5833-1>, 2006.

ID号: 50764

报告编号: Y0120237818-1

文献收录/引用情况

检索报告

委托内容: 李娟 发表文献被 SCI-E 收录情况

委托人: 李娟

委托单位: 南方医科大学

检索单位: 南方医科大学图书馆

委托日期: 2023年12月25日

完成日期: 2023年12月25日

南方医科大学图书馆

二〇二三年



(盖章)

人

2023年12月25日

时间

检索要求与检索条件	<p>李娟 发表文献 SCI-E 收录情况 数据库 《科学引文索引》 (SCI-E) 网络版 检索年限 1900-present 检索式 文献的题名+作者姓名</p>		
检索结果	<p>根据委托人提供的文献线索及检索要求，经检索上述数据库后发现： 李娟 发表的 1 篇文献被 SCI-E 收录。 标题: Deleting specific residues from the HNH linkers creates a CRISPR-SpCas9 variant with high fidelity and efficiency Author-作者: Wang, GH (Wang, Guohua); Wang, CM (Wang, Canmao); Chu, T (Chu, Teng); Wu, XJ (Wu, Xinjun); Anderson, CM (Anderson, Christopher M.); Huang, DW (Huang, Dongwei); Li, J (Li, Juan) 来源出版物: JOURNAL OF BIOTECHNOLOGY 卷: 368 页码范围: 42-52 DOI: 10.1016/j.jbiotec.2023.04.008 出版年: MAY 20 2023 提前访问日期: APR 2023 Web of Science 核心合集中的”被引频次”:0 所有数据库中的被引频次合计:0 入藏号:WOS:000989817000001 文献类型: Article 地址: [Wang, Guohua] Guangdong Ind Polytech, Sch Food & Biotechnol, Guangzhou 510300, Peoples R China [Wang, Canmao] Southern Med Univ, Nanfang Hosp, Dept Pharm, Guangzhou 510515, Peoples R China [Wang, Canmao] Southern Univ Sci & Technol Hosp SUS Tech Hosp, Dept Pharm, Shenzhen 518000, Peoples R China [Chu, Teng] Sangon Biotech Shanghai Co Ltd, Shanghai 201611, Peoples R China [Wu, Xinjun] Univ N Carolina, Lineberger Comprehens Canc Ctr, Chapel Hill, NC 27517 USA [Anderson, Christopher M.] East Carolina Univ, Dept Biol, Greenville, NC 27517 USA [Huang, Dongwei] Jinhua Polytech, Pharmaceut & Mat Engn Sch, Jinhua 321007, Peoples R China [Li, Juan] Southern Med Univ, Sch Basic Med Sci, Dept Histol & Embryol, Guangzhou 510515, Peoples R China 通讯作者地址: [Li, Juan] (corresponding author), Southern Med Univ, Sch Basic Med Sci, Dept Histol & Embryol, Guangzhou 510515, Peoples R China 电子邮件地址: lijuan860103@163.com ISSN:0168-1656 EISSN:1873-4863 IF2022=4.1 JCR (中科院 2021 年发布) 分区: 学科名称 大类: 工程技术 3 小类: BIOTECHNOLOGY & APPLIED MICROBIOLOGY 生物工程与应用微生物 3 JCR (中科院 2022 年发布) 升级版分区: 学科名称 大类: 工程技术 3 小类: BIOTECHNOLOGY & APPLIED MICROBIOLOGY 生物工程与应用微生物 3 特此证明!</p> <div style="text-align: right;">  南方医科大学图书馆 (盖章) </div>		
检索时间	2023 年 12 月 25 日	检索人	(签字) 



Deleting specific residues from the HNH linkers creates a CRISPR-SpCas9 variant with high fidelity and efficiency

Guohua Wang^{a,1}, Canmao Wang^{b,c,1}, Teng Chu^d, Xinjun Wu^e, Christopher M. Anderson^f, Dongwei Huang^g, Juan Li^{h,*}

^a School of Food and Biotechnology, Guangdong Industry Polytechnic, Guangzhou 510300, China

^b Department of Pharmacy, Nanfang Hospital, Southern Medical University, Guangzhou 510515, China

^c Department of Pharmacy, Southern University of Science and Technology Hospital (SUS Tech Hospital), Shenzhen 518000, China

^d Sangon Biotech (Shanghai) Co., Ltd., Shanghai 201611, China

^e Lineberger Comprehensive Cancer Center, the University of North Carolina at Chapel Hill, Chapel Hill, NC 27517, USA

^f Department of Biology, East Carolina University, Greenville, NC 27517, USA

^g Pharmaceutical and Material Engineering School, Jinhua Polytechnic, Jinhua 321007, China

^h Department of Histology and Embryology, School of Basic Medical Sciences, Southern Medical University, Guangzhou 510515, China

ARTICLE INFO

Keywords:

CRISPR
SpCas9
High fidelity
Efficiency
HNH linkers
Design

ABSTRACT

Clustered Regularly Interspaced Short Palindromic Repeats (CRISPR) and CRISPR-associated (Cas) systems are immunological defenses used in archaea and bacteria to recognize and destroy DNA from external invaders. The CRISPR-SpCas9 system harnessed from *Streptococcus pyogenes* (SpCas9) has become the most widely utilized genome editing tool and shows promise for clinical application. However, the off-target effect is still the major challenge for the genome editing of CRISPR-SpCas9. Based on analysis of the structure and cleavage procedures, we proposed two strategies to modify the SpCas9 structure and reduce off-target effects. Shortening the HNH or REC3 linkers (Strategy #1) aimed to move the primary position of HNH or REC3 far away from the single-guide RNA (sgRNA)/DNA hybrid (hybrid), while elongating the helix around the sgRNA (Strategy #2) aimed to strengthen the contacts between SpCas9 and the sgRNA/DNA. We designed 11 SpCas9 variants (variant No.1–variant No.11) and verified their efficiencies on the classic genome site *EMX1-1*, *EMX1-1-OT1*, and *EMX1-1-OT2*. The top three effective SpCas9 variants, variant No.1, variant No.2, and variant No.5, were additionally validated on other genome sites. The further selected variant No.1 was compared with two previous SpCas9 variants, HypaCas9 (a hyper-accurate Cas9 variant released in 2017) and eSpCas9 (1.1) (an “enhanced specificity” SpCas9 variant released in 2016), on two genome sites, *EMX1-1* and *FANCF-1*. The results revealed that the deletion of Thr769 and Gly906 could substantially decrease off-target effects, while maintaining robust on-target efficiency in most of the selected genome sites.

1. Introduction

The clustered regularly interspaced short palindromic repeats (CRISPR) loci were first discovered in 1987 (Ishino et al., 1987). The characteristics of CRISPR loci are that the repeats are interspaced by a similarly sized nonrepetitive sequence (spacer) and were clustered in one or several loci of the chromosome (Jansen et al., 2002). The spacer of CRISPR was derived from “invaders” (Bolotin et al., 2005). CRISPR and CRISPR-associated (Cas) systems were harnessed by archaea and bacteria to provide acquired heritable immunity against viruses,

plasmids, and other mobile genetic elements (Barrangou et al., 2007; Sorek et al., 2008). The CRISPR-SpCas9 system is one of the most thoroughly studied genome editing tools (Jinek et al., 2012; Akram et al., 2020; Sternberg et al., 2014). While the SpCas9 system has been widely utilized, off-target effects and the large size (1368 amino-acid residues) of SpCas9 have hindered potential clinical usage (Jinek et al., 2012; Doudna, 2020; Li et al., 2020; Zatloukalová et al., 2019; Kim et al., 2019; Gemberling et al., 2021). Many strategies have been developed to decrease off-target effect, including using truncated guide RNAs, fusion of catalytically inactive Cas9 to *FokI* nuclease,

* Corresponding author.

E-mail address: lijuan860103@163.com (J. Li).

¹ Contribute equally to this work.

neutralization of positive charges in the non-target DNA strand groove, reduce the nonspecific contacts, and prime editing (Wright et al., 2015; Fu et al., 2014; Guiling et al., 2014; Anzalone et al., 2019; Slaymaker et al., 2016; Kleinstiver et al., 2016; Chen et al., 2017). In addition, some prominent Cas9 variants have been developed, such as eSpCas9 (1.1) (Slaymaker et al., 2016), SpCas9 HF1 (Kleinstiver et al., 2016) (a High-Fidelity variant #1, which was released in 2016), HypaCas9 (Chen et al., 2017), Cas9_R63A/Q768A (Bratović et al., 2020) (a SpCas9 variant, which was released in 2020), LZ3 Cas9 (Schmid-Burgk et al., 2020) (a high specificity variant with a unique +1 insertion profile, which was released in 2020), and HiFi Cas9 (Vakulskas et al., 2018; Kulcsár et al., 2020) (a high fidelity Cas9, which was released in 2018), nearly all which employ strategies aimed at decreasing the interaction between the SpCas9 protein and the sgRNA/DNA. These strategies could effectively decrease off-target effects, but would lead to decreases in on-target cleavage efficiency at the same time (Slaymaker et al., 2016; Kleinstiver et al., 2016; Chen et al., 2017; Bratović et al., 2020; Schmid-Burgk et al., 2020; Vakulskas et al., 2018; Kulcsár et al., 2020). In this study, we tried two strategies to adjust the physical structure of SpCas9 so as to decrease the off-target effects while maintaining on-target cleavage efficiency.

2. Materials and methods

2.1. Plasmids

Variant No.1– variant No.10 were mutated from the wild-type (WT) SpCas9 (VB191031–1069mad, Vector Builder), which was designed to have two nuclear localization sequences and constructed by Vector Builder. WT1-SpCas9 and variant No.11 was mutated from BPK4410²⁰. BPK4410- human expression plasmid for SpCas9 Cluster 1 (HypaCas9) was a gift from Jennifer Doudna & Keith Joung (Addgene plasmid #101178; <http://n2t.net/addgene:101178>; RRID: Addgene_101178); eSpCas9(1.1) was a gift from Feng Zhang (Addgene plasmid # 71814; <http://n2t.net/addgene:71814>; RRID: Addgene_71814). SgRNAs were generated from VB191120–4142cbb (Vector Builder). Plasmid DNA sequences of WT-SpCas9, variant No.1, and sgRNA-EMX1–1 are listed in the supplementary sequences.

2.2. SpCas9 structure analysis

SpCas9 structures were analyzed using Pymol 2.4 (Schrödinger). All 3D structure figures were generated using Pymol 2.4 (Schrödinger).

2.3. Cell culture and transfection

HEK293T cells were used to validate the designed variants. HEK293T cells were maintained in Dulbecco's Modified Eagle's medium with 10% fetal bovine serum at 37 °C in an atmosphere of 5% CO₂. Cells were seeded in 24-well plates (1.5 × 10⁵ cells/well, 1 mL) on day 0 and transfected with 1 µg plasmids (750 ng of nuclease and 250 ng of gRNA) using Lipofectamine 3000 reagent (Invitrogen, 1.5 µL of lipo3000, 2 µL of p3000) according to the standard recommended procedures when they reached 70–80% confluence on day 1. After transfection for 24 h, cells were selected with 4 µg mL⁻¹ puromycin (Solarbio Life Sciences, China) for 3 days. Cells were collected on day 6, and genomic DNA was processed from these cells for ddPCR and the T7E1 assay.

2.4. DdPCR

DdPCR could quantitate initial targets in limited dilution and precisely quantify specific double-strand DNA breaks (Dibitto et al., 2018; Sykes et al., 1992; Miyaoka et al., 2018; Rose et al., 2017; Carballar-Lejarazú et al., 2021). DdPCR has been widely used for detection and quantification of NHEJ induced by genome editing at the endogenous gene loci induced by CRISPR-Cas9 (Carballar-Lejarazú et al., 2021,

2020; Hussain et al., 2021). A ddPCR drop-off assay using two probes (one drop-off TaqMan-MGB probe and one reference probe) was employed to detect the indel in the present study. The ddPCR drop-off assay was performed using Bio-Rad QX200 Droplet Digital system (BioRad Laboratories). Briefly, the drop-off probe labeled with a fluorophore uniquely binds to the nuclease target site in the WT sequence, while the cleavage-induced non-homologous end joining (NHEJ) indels block the binding of the probe to the edited sites. Meanwhile, the reference probe labeled with another fluorophore is designed to bind the reference sequence adjacent to, but not overlapping the cleavage site. In the case of the unedited WT sequence, both probes could bind to their complementary regions and produce a double-positive population. In the case of the cleavage-induced NHEJ indel sequence, the drop-off probe could not bind to its target due to the indel, yielding a single-positive reference probe population. Based on the above principle, the indel frequency was calculated as: (drop-off-, reference+)/[(drop-off-, reference+) + (drop-off+, reference+)]. A total of 16.5 ng genome DNA was used.

2.5. T7E1 assay

The T7E1 assay is one of the classic methods for measuring the cleavage efficiency (Singh et al., 2018; Hu et al., 2018; Helfer-Hungerbuehler et al., 2021). In the present study, T7E1 assay was used to quantify on-target loci mutagenesis induced by the different Cas9 variants. T7E1 assays were performed as previously described (Kleinstiver et al., 2016; Sentmanat et al., 2018). Briefly, ~700nt amplicons (Table S1) including on-target sites were amplified from ~100 ng of genomic DNA. PCR reactions were carried out in a 50 µL system by Q5® Hot Start High-Fidelity 2X Master Mix (NEB) according to the manufacturer's instructions. The primers and specific conditions utilized are listed in Table S1. PCR products were denatured, annealed, and then co-incubated with T7 Endonuclease 1. Digestion was then visualized using 1.5% agarose gel. The staining quantification of the acquired pictures was performed using the ImageJ program (Helfer-Hungerbuehler et al., 2021; Sentmanat et al., 2018; Zulijani and Dekanić, 2021). The cleavage efficiency (NHEJ) was calculated with the following formula (Helfer-Hungerbuehler et al., 2021; Sentmanat et al., 2018; Guschin et al., 2010): Cleavage % = 100 × [1 – (1 – (density of digested-product bands)/(density of digested-product bands + density of undigested-parental band))^{1/2}].

3. Results

3.1. Shortening the HNH or REC3 linkers to design variant No.1 to variant No.6 (Strategy #1)

CRISPR-SpCas9-induced DNA cleavage is initiated by interaction between the REC3 and sgRNA/DNA hybrid, with one key cleaving action being the movement of the HNH domain (Wang and Li, 2021; Nishimasu et al., 2014; Zhu et al., 2019). The energy launching HNH domain movement is initiated by hybrid formation and extrusion (Wang and Li, 2021). While a hybrid mismatch would decrease this energy, mismatched hybrids can still initiate cleavage (Sternberg et al., 2014; Slaymaker et al., 2016). Therefore, the perfect hybrid is one that provides more energy than is necessary. We hypothesized that a different amount of energy could move the HNH domain to a different distance - the larger the energy, the farther the distance (we named it energy-distance hypothesis, ED hypothesis). Therefore, we further hypothesized that shortening the HNH linkers or REC3 linkers to make the HNH or REC3 away from the hybrid could decrease the off-target effect (Strategy #1).

We attempted to shorten the linkers of the HNH domain, allowing only the perfect complementary hybrid to make the HNH domain move to the right position to cleave. In 2019, three consecutive conformations

(600Z, 600Y, 600X) of active Cas9-sgRNA-DNA complex were released (Zhu et al., 2019). 600Z conformation (checkpoint conformation) is a proofreading state of SpCas9 that assesses whether sufficient sgRNA/DNA compensation has been formed to initiate the cleavage. 600Y conformation (postcatalytic conformation) is a state of SpCas9 that HNH domain is catalytically competent (Wang and Li, 2021; Zhu et al., 2019). We implemented the design based on the 600Y conformation (Zhu et al., 2019).

There are two linkers that bind to HNH: residues 763–770 (MAR-ENQTT, the first linker), and residues 906–916 (GGLSELDKAGF, the second linker) (Fig. 1A). There are two continuous threonine residues (769–770) in the first linker, and two continuous glycine residues (906–907) in the second linker. We hypothesized that the deletion of one of the two consecutive residues would cause less of an effect than other residues. In order to affect the conformation as little as possible, we deleted Thr769 and Gly906 to yield variant No.1: SpCas9 (Δ Thr769, Δ Gly906) (Fig. 1A) (Δ : deletion) (Table 1).

After merging “the checkpoint conformation” (600Z) and “post-catalytic conformation” (600Y), we found that the second linker may have moved a greater distance than the first linker. Therefore, we tried to delete two residues in the second linker as well (Fig. 1A-B). In the second linker, the Lys902 and Arg905 residues are positively charged, and the Glu904 residue is negatively charged. To affect the primary structure as little as possible, Leu908 was deleted after being randomly selected from Ala903, Gly906, Gly907, Leu908, and Ser909 to yield variant No. 2: SpCas9 (Δ Thr769, Δ Gly906, Δ Leu908) (Table 1).

Next, we tried to shorten the two linkers that bind to REC3. For REC3, one linker is residues 497–512 (NFDKKNLPNEKVLPKHS, the first linker), and the other is residues 711–719 (AQVSGQGDS, the second linker). Considering the length, the structure of the two linkers and the properties of the residues of the two linkers, we designed variant No.3: SpCas9 (Δ Pro509; Δ Gln712), variant No.4: SpCas9 (Δ Leu508-Lys510; Δ Gln712), variant No.5: SpCas9 (Δ Phe498-Asn504; Δ Gln712-Val713) (Fig. S1) and variant No. 6: SpCas9 (Δ Phe498-Asn504; Δ Pro509; Δ Ala711-Val713) (Table 1).

3.2. Elongating the helix around the sgRNA to design variant No.7 to variant No.10 (Strategy #2)

According to previous studies, N-methyl substituted bridged nucleic acids and locked nucleic acids (LNA) in the guide region of sgRNA could significantly decrease the off-target effects by impairing the formation of the stable “zipped” conformation hybrid during hybridization to off-target sequences (Cromwell et al., 2018; Soler-Bistué et al., 2019). Because hybrid formation is one of the key steps during cleavage initiation (Jiang et al., 2016), we hypothesized that strengthening the interaction between the Cas9 protein and sgRNA could prevent the hybrid formation when mismatch occurs (Strategy #2).

We tried to elongate the helix around the sgRNA to increase the interaction between the sgRNA and the SpCas9 protein, finally enhanced the rigidity of sgRNA. We tripled helix residues 721–727 (HEHIANL) and doubled helix residues 729–732 (GSPA) to yield variant No. 7: SpCas9 (\blacktriangle 727–728, HEHIANLHEHIANL; \blacktriangle 732–733, GSPA) (Fig. 1C) (\blacktriangle : insert). We tripled helix residues 921–926: LVETRQ, and doubled helix residues 925–937 (RQITKHVAQILDSD) to yield variant No. 8: SpCas9 (\blacktriangle 926–927, LVETRQLVETRQ; \blacktriangle 937–938, RQITKHVAQILDSD). We doubled helix residues 920–925: QLVETR and helix residues 927–933: ITKHVAQ to yield variant No. 9: SpCas9 (\blacktriangle 925–926, QLVETR; \blacktriangle 933–934, ITKHVAQ). We tripled part of the helix residues 921–926: LVETRQ to yield variant No. 10: SpCas9 (\blacktriangle 926–927, LVETRQLVETRQ) (Table 1).

3.3. Variant No.1, variant No.2, and variant No.5 could dramatically reduce off-target effects while maintaining robust on-target activity in EMX1-1

EMX1-1 and its two corresponding off-target sites *EMX1-1-OT1*, *EMX1-1-OT2* were classic genome sites usually used for primary screening of the SpCas9 variants (Slaymaker et al., 2016; Kleinstiver et al., 2016; Bratović et al., 2020). Using *EMX1-1*, *EMX1-1-OT1* and *EMX1-1-OT2*, we verified the efficiency and off-target effects of variant No.1 - variant No.10 variants. The results revealed that on *EMX1-1-OT1*, compared with the WT-SpCas9 (10.86%), variant No.1 (0.13%), variant No.2 (0.54%), and variant No.5 (0.13%) could dramatically decrease the off-target effect by at least 20-fold; on *EMX1-1-OT2*, compared with the WT-SpCas9 (6.67%), variant No.1 (0.27%), variant No.2 (0.81%), and variant No.5(0.15%) could decrease the off-target effect by at least 8-fold; on *EMX1-1*, compared with the WT-SpCas9 (85.30%), variant No.1 (81.38%) and variant No.2 (74.20%) maintained robust on-target cleavage efficiency (Fig. 2, Fig. S2). Variant No.1 reduced the off-target effect on both *EMX1-1-OT1* and *EMX1-1-OT2* by at least 24.7-fold, while maintaining 95.4% on-target cleavage efficiency on *EMX1-1*, as compared to WT-SpCas9 (Fig. 2, Fig. S2).

Variant No.3, variant No.4, variant No.6 (from strategy #1) variant No.8, and variant No.9 (from strategy #2) SpCas9 variants showed substantially decreased off-target cleavage (Fig. 2E). However, their on-target cleavage efficiency was also dramatically damaged and nearly inactivated. This means that shortening the HNH domain linkers was amino acid selective. Some deletions/insertions of the amino residues may be lethal to SpCas9 (Fig. 2E). In particular, the insertion of the residues to elongate the helix around the sgRNA (Strategy #2) almost thoroughly inactivated the variants. For Strategy #2 guided variants, only variant No.7 and variant No.10 were not inactivated, which indicates that elongating the helix around the sgRNA is futile (Fig. 2E).

To further confirm our results, we carried out the T7E1 assay to analyze the on-target cleavage efficiency of WT-SpCas9, variant No.1, variant No.2, and variant No.5. Compared to the WT-SpCas9 (43.46%), variant No.1 (43.32%), variant No.2 (42.92%), and variant No.5 (31.22%) could maintain robust on-target cleavage efficiency on *EMX1-1*, which was consistent with the ddPCR results (Figs. 2F, 3J).

3.4. Variant No.1 shows dramatically reduced off-target cleavage while maintaining robust on-target cleavage on alternate genome sites

To assess whether variant No.1, variant No.2, and variant No.5 have a broadly efficient nuclease activity, we expanded the assay to six other genome target sites (*EMX1-2*, *FANCF-1*, *FANCF-3*, *VEGFA-1*, *VEGFA-2*, and *VEGFA-5*) spanning three genomic loci (Fig. 3, Fig. S3.1–3.5). On-target and off-target cleavage efficiency for *EMX1-2*, *FANCF-1*, *FANCF-3*, and *VEGFA-5* were verified by ddPCR. On *EMX1-2*, *FANCF-1*, *FANCF-3*, and *VEGFA-5*, compared with the WT-SpCas9 (59.90%, 55.04%, 70.79%, 18.21%), variant No.1 (55.84%, 49.73%, 45.18%, 18.24%) and variant No.2 (42.84%, 42.38%, 33.86%, 9.48%), but not the variant No.5 (21.89%, 32.54%, 22.37%, 0.67%) yielded robust on-target cleavage efficiency (Fig. 3, Fig. S3.1–3.5). On *EMX1-2-OT2*, *FANCF-1-OT3*, *FANCF-3-OT2*, compared with the WT-SpCas9 (0.58%, 27.20%, 2.44%), variant No.1 (0.00%, 0.06%, 0.07%) and variant No.2 (0.00%, 4.40%, 0.04%) substantially decreased the off-target effects (Fig. 3E-G, Fig. S3.1–3.3). On *FANCF-1-OT1*, compared with the WT-SpCas9 (46.04%), variant No.1 (30.80%) and variant No.2 (22.95%) could decrease the off-target effects at a larger scale (Fig. 3F, Fig. S3.2).

To further confirm the results, the T7E1 assay was carried out to verify the on-target cleavage efficiency. *VEGFA-1* and *VEGFA-2* were only tested for on-target cleavage efficiency by T7E1 assay for lack of proper ddPCR probes. T7E1 assay results revealed that: on *EMX1-1*, *EMX1-2*, *FANCF-1*, *FANCF-3*, *VEGFA-1*, *VEGFA-2*, and *VEGFA-5*, compared with the WT-SpCas9 (43.46%, 41.44%, 39.07%, 53.92%, 49.53%, 38.35%, 21.15%), variant No.1 (43.32%, 41.75%, 37.56%,

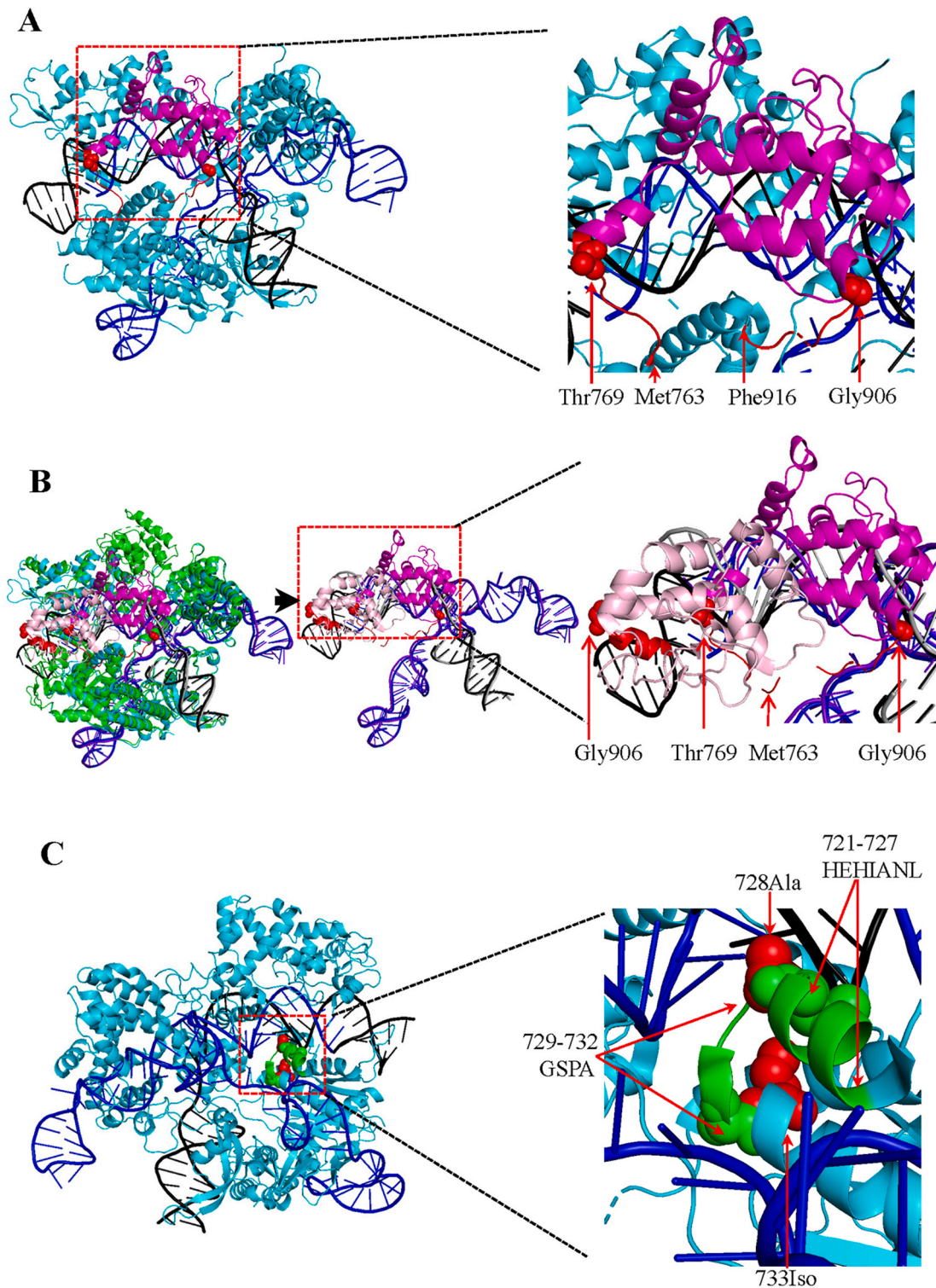


Fig. 1. Structure-guided design of SpCas9 variants. **A.** The selected residues Thr769 and Gly906 are both marked with red spheres. The two linkers: M763 - A764 - R765 - E766 - N767 - Q768 - T769 - T770, and G906 - G907 - L908 - S909 - E910 - L911 - D912 - K913 - A914 - G915 - F916 are marked with red. PDB ID: 6O0Y. HNH domain is marked with magenta, other domains are marked with cyan, sgRNA is marked with blue, and DNA is marked with black. **B.** The second linker may move a longer distance than the first linker. The merged conformation of the checkpoint conformation and postcatalytic conformation. The HNH domain is marked with pink (6O0Z) and magenta (6O0Y), respectively. The two linkers are marked with red. Gly906 and Thr769 are marked with a red sphere. Thr769 was disordered in checking conformation. In checking conformation (6O0Z), the sgRNA is marked with purpleblue, the DNA is marked with gray, the Cas9 is marked with green; in postcatalytic conformation (6O0Y), the sgRNA is marked with blue, the DNA is marked with black, the Cas9 is marked with cyan. **C.** The selected residues 729–732 (GSPA, marked with green) were inserted between 732Ala (marked with green sphere) and 733Ile (marked with red sphere); residues 721–727 (HEHIANL, marked with green) were inserted between 727Leu (marked with green sphere) and 728Ala (marked with red sphere). PDB ID: 6O0Y. SgRNA is marked with blue, and DNA is marked with black, other domains are marked with cyan.

Table 1
Variants, corresponding mutations, and strategy.

Variant	Mutation (Δ : delete; \blacktriangle : insert.)	Strategy
No.1	Δ Thr769, Δ Gly906	Shortening the HNH linkers
No.2	Δ Thr769, Δ Gly906; Δ Leu908	Shortening the HNH linkers
No.3	Δ Pro509, Δ Gln712	Shortening the REC3 linkers
No.4	Δ Leu508-Lys510, Δ Gln712	Shortening the REC3 linkers
No.5	Δ Phe498-Asn504, Δ Gln712-Val713	Shortening the REC3 linkers
No.6	Δ Phe498-Asn504, Δ Pro509, Δ Ala711-Val713	Shortening the REC3 linkers
No.7	\blacktriangle 727–728 (HEHIANLHEHIANL), \blacktriangle 732–733 (GSPA)	Elongating the helix around sgRNA
No.8	\blacktriangle 926–927 (LVETRLQVETRQ), \blacktriangle 937–938 (RQITKHVAQILDS)	Elongating the helix around sgRNA
No.9	\blacktriangle 925–926 (QLVETR), \blacktriangle 933–934 (ITKHVAQ)	Elongating the helix around sgRNA
No.10	\blacktriangle 926–927 (LVETRLQVETRQ)	Elongating the helix around sgRNA
No.11	Δ Ala764, Δ Ala914	Shortening the HNH linkers

44.40%, 43.11%, 15.84%, 21.28%) and variant No.2 (42.92%, 33.07%, 40.49%, 33.71%, 34.50%, 15.60%, 17.65%) but not variant No.5 (31.22%, 21.53%, 26.02%, 21.73%, 21.04%, 11.29%, 8.13%) yielded robust on-target cleavage efficiency (Fig. 3I–J).

Together, these results revealed that variant No.1 and variant No.2 could dramatically reduce off-target cleavage efficiency on *EMX1–2-OT2*, *FANCF-1-OT3*, and *FANCF-3-OT2*, while maintaining robust on-target cleavage efficiency on nearly all of the selected genome sites. Variant No.1 had the highest on-target efficiency and lowest off-target effects.

3.5. Variant No.11 was almost dumber

After the verification of the variant No.1 - variant No.10, we further designed SpCas9 variant No. 11 based on the successful designing of variant No.1 (Δ Thr769; Δ Gly906). We wondered whether other deletions on the first and second linkers of HNH could also produce promising variant. There is an alanine residue in both the first linker and the second linker. Considering that there is an alanine residue in both the linkers of HNH, and the alanine residue is usually used as the mutation result, we designed variant No.11 (Δ Ala764, Δ Ala914) (Table 1). As *EMX1–1* was usually used in primary verification of the variant, we verified the cleavage efficiency of the variant No.11 on *EMX1–1* by ddPCR. The results revealed that compared to the WT-SpCas9 (55.11%), the SpCas9 variant No.11 (1.02%) was nearly inactivated (Fig. 4, Fig. S4).

3.6. Variant No.1 showed similar or higher efficiency than HypaCas9 and eSpCas9 (1.1)

To verify the efficiency of our SpCas9 variants, we carried out side-by-side comparisons of variant No.1 with two other high fidelity SpCas9 variants: HypaCas9 (Plasmid #101178) and eSpCas9 (1.1) (Plasmid #71814) (Fig. 5, Fig. S5.1–5.2). We used *EMX1–1* and *FANCF-1* as our target sites and chose *EMX1–1-OT1*, *EMX1–1-OT2*, *FANCF-1-OT1* and *FANCF-1-OT3* as their corresponding off-target sites. On *EMX1–1*, the on-target cleavage efficiency of variant No.1 (70.32%) was much higher than HypaCas9 (11.87%) and eSpCas9 (1.1) (27.61%), and just similar to the WT-SpCas9 (79.69%) (Fig. 5A–D, I; Fig. S5.1). The off-target effects on *EMX1–1-OT1* and *EMX1–1-OT2* were substantially decreased by variant No.1 (0.08%, 0.06%), HypaCas9 (0.11%, 0.15%) and eSpCas9 (1.1) (0.07%, 0.09%) compared with the WT-SpCas9 (6.08%, 3.90%) (Fig. 5E–H, I; Fig. S5.1). On *FANCF-1*, the on-target cleavage efficiency of variant No.1 (67.99%) was much higher than HypaCas9 (35.82%), and was similar to eSpCas9 (1.1) (71.90%) and WT-SpCas9 (70.09%) (Fig. 5J, Fig. S5.2). The off-target effects on *FANCF-1-OT1* were decreased by variant No.1 (27.38%), HypaCas9

(2.42%) and eSpCas9 (1.1) (17.33%) compared with the WT-SpCas9 (43.55%) (Fig. 5J, Fig. S5.2). The off-target effects on *FANCF-1-OT3* were dramatically decreased by variant No.1 (0.18%), HypaCas9 (0.08%) and eSpCas9 (1.1) (0.10%) compared with the WT-SpCas9 (43.55%) (Fig. 5J, Fig. S5.2).

4. Discussion

In this study, we proposed two strategies to develop effective SpCas9 variants, and revealed that deletion of the specific residues to shorten the HNH linkers was efficient in designing high fidelity SpCas9 variants. Variant No.1 (Δ Thr769, Δ Gly906) performs best, with variant No. 2 (Δ Thr769, Δ Gly906, Δ Leu908) working slightly worse than variant No.1. However, the same strategy induced similar variant No. 11 (Δ Ala764, Δ Ala914) had almost no on-target activities. The comparison of the mutation sites of variant No.1, variant No. 2 and variant No. 11 revealed that: 1. all of the mutation sites (Thr769, Gly906, Leu908, Ala764 and Ala914) didn't form hydrogen bond with the sgRNA/DNA (Fig. 4D); 2. Thr769 and Ala764 are on the first linker, while Gly906, Leu908, and Ala914 are on the second linker (Fig. 4E), and their positions are different; 3. the next adjacent residue of Thr769 is also a threonine residue Thr770, and the next adjacent residue of Gly906 is also a glycine residue Gly907; 4. the side chain hydrophobicity's of the threonine (0.26), glycine (0.00), leucine (1.70), alanine (0.31) are different from each other (Fauchère et al., 1988); 5. the isoelectric points of them are similar. It seemed that there are at least two possibilities for the underlying mechanism of successful variant No.1. The first possibility is that the ED hypothesis is right, and the deletion of the Thr769 and Gly906 adjust the HNH domain to the proper position that only the perfect compensation of the sgRNA/DNA hybrid could offer enough energy to move the HNH to the cleavage site. Though the deletion of the Ala764 and Ala914 shortened the linker of HNH, it did not adjust the HNH to the proper position; the reason may be that the deletion of one of the two consecutive residues makes less conformation effect than the deletion of other residues. Many studies have proved that the proper decrease of the interaction between the SpCas9 protein and the sgRNA/DNA hybrid is helpful for the decreasing of the off-target effect. Therefore, the second possibility is that the deletion of Thr769 and Gly906 adjusts the hydrophobic interaction between the variant No.1 (Δ Thr769, Δ Gly906) protein and the sgRNA/DNA hybrid to the proper level that only the perfect sgRNA/DNA could initiate the cleavage. The deletion of Ala764 and Ala914 also decreased the hydrophobicity of the SpCas9 protein, however, the position of the Ala764 and Ala914 made the variant No.11 (Δ Ala764, Δ Ala914) protein can't afford enough hydrophobic interaction with the sgRNA/DNA hybrid even the sgRNA perfectly compensated with the DNA.

Compared to other released variants, the most notable advantage of variant No.1 was the high on-target cleavage efficiency. If the first possibility was true, it indicated that adjusting the physical structure of SpCas9 could maintain higher efficiency than decreasing the contacts between SpCas9 and sgRNA/DNA hybrid.

variant No.1 and variant No.2 were targeting the linkers of HNH domain, while variant No.3, variant No.4, variant No.5, and variant No.6 were targeting the linkers of REC3 domain. variant No.1 and variant No.2 performed much better than variant No.3, variant No.4, variant No.5, and variant No.6. Therefore, targeting the linkers of HNH domain worked better than targeting the linkers of REC3 domain. The deleted amino acid residues in variant No.3 (Δ Pro509; Δ Gln712), variant No.4 (Δ Leu508-Lys510; Δ Gln712), and variant No.6 (Δ Phe498-Asn504; Δ Pro509; Δ Ala711-Val713) were evidently crucial for proper functioning, as their deletion seriously damaged the normal cleavage activity of SpCas9. None of the variants based on elongating the helix around the sgRNA worked, which may indicate that elongating the helix around the sgRNA dramatically disrupted the proper conformation which is crucial the normal cleavage.

In most of the selected genome sites (*EMX1–1*, *EMX1–1-OT1*,

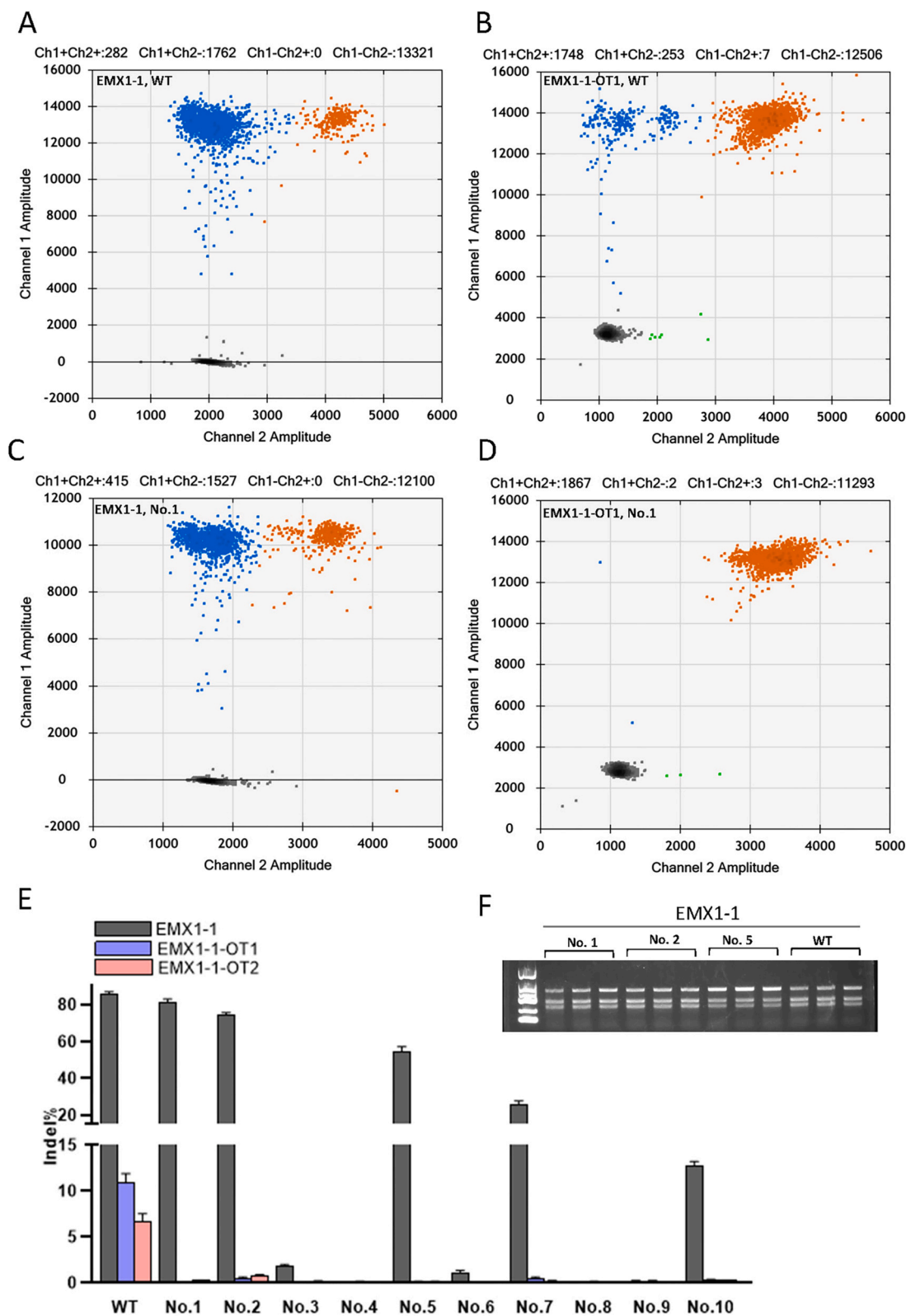


Fig. 2. Variant No.1, variant No.2, and variant No.5 improved specificity while maintaining robust on-target activity in *EMX1-1*. A-B. DdPCR 2D amplitude results of WT-SpCas9 on *EMX1-1* (A) and *EMX1-1-OT1* (B). Channel 1 amplitude is the FAM amplitude, which shows blue fluorescence; Channel 2 amplitude is the VIC amplitude, which shows green fluorescence. The blue dots indicate mutation events while the brown (blue+ & green+) dots indicate wild-type events. C-D. DdPCR 2D amplitude results of variant No.1 on *EMX1-1* (C) and *EMX1-1-OT1* (D). Channel 1 amplitude is the FAM amplitude, which shows blue fluorescence; Channel 2 amplitude is the VIC amplitude, which shows green fluorescence. The blue dots indicate mutation events while the brown (blue+ & green+) dots indicate wild-type events. E. Screen of variants for improvement in specificity and corresponding on-target cleavage efficiency by ddPCR on *EMX1-1*, *EMX1-1-OT1* and *EMX1-1-OT2*. Error bars represent S.E.M. for n = 3. F. The on-target cleavage efficiency of WT-SpCas9, SpCas9 variant No.1, variant No.2 and variant No.5 on *EMX1-1* were further verified by T7E1 assay.

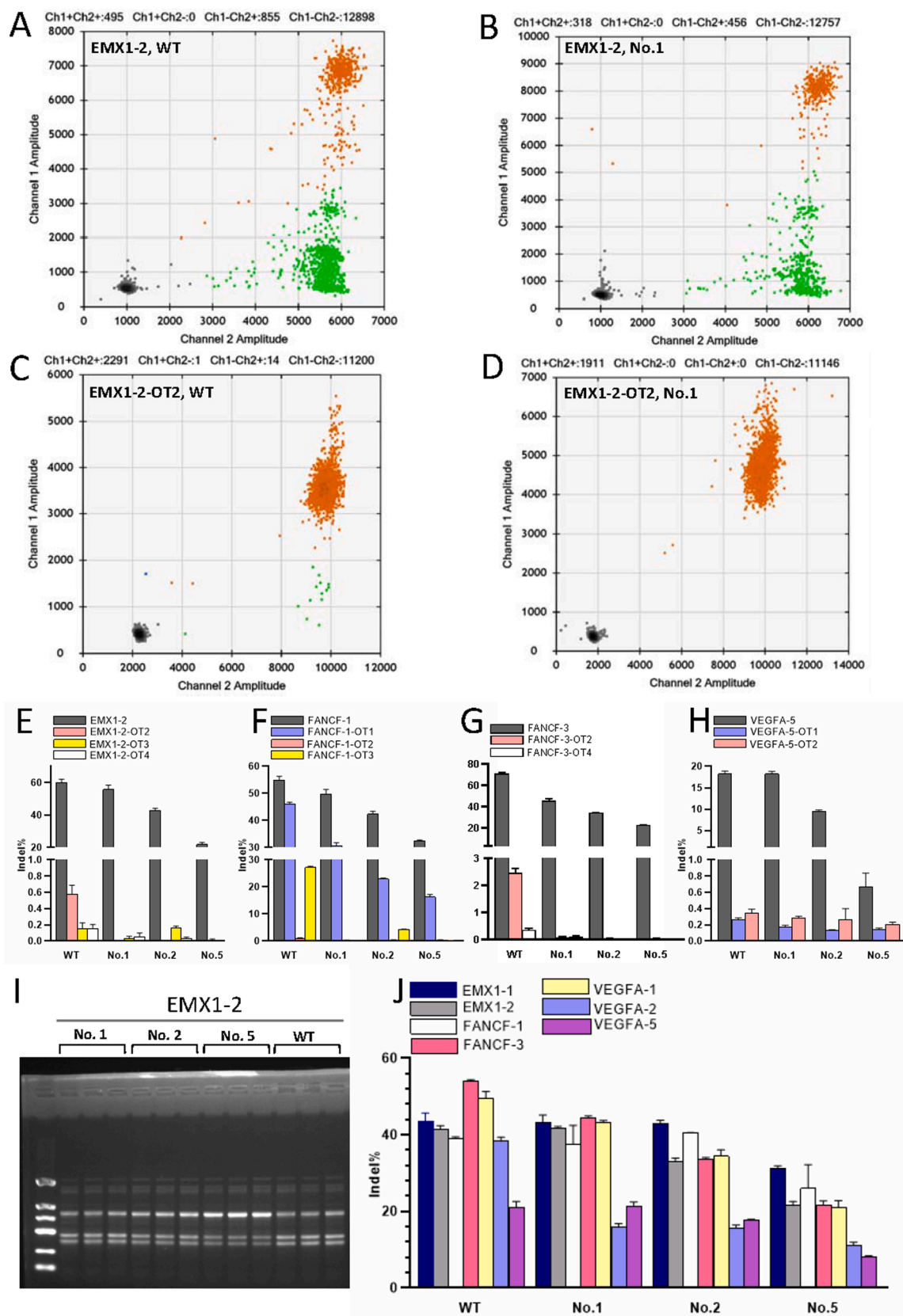


Fig. 3. Variant No.1 could always show robust efficiency and high fidelity on alternate gene sites. A-D. DdPCR 2D amplitude results of WT-SpCas9 (A) and variant No.1 (B) on *EMX1-2* and *EMX1-2-OT2*. Channel 1 amplitude is the FAM amplitude, which shows blue fluorescence; Channel 2 amplitude is the VIC amplitude, which shows green fluorescence. The green dots indicate mutation events, and the brown (blue+ & green+) dots indicate wild-type events. E-H. The on-target and off-target cleavage effect of variant No.1, variant No.2, and variant No.5 were further verified on genome sites *EMX1-2*(E), *FANCF-1*(F), *FANCF-3* (G), and *VEGFA-5* (H) in HEK293T cells by ddPCR. Error bars represent S.E.M. for $n = 3$. I. Uncropped gel images from PAGE experiments for T7E1 of *EMX1-1*. J. On-target cleavage efficiency of variant No.1, variant No.2, and variant No.5 was further verified by T7E1 in HEK293T cells. Error bars represent S.E.M. for $n = 3$.

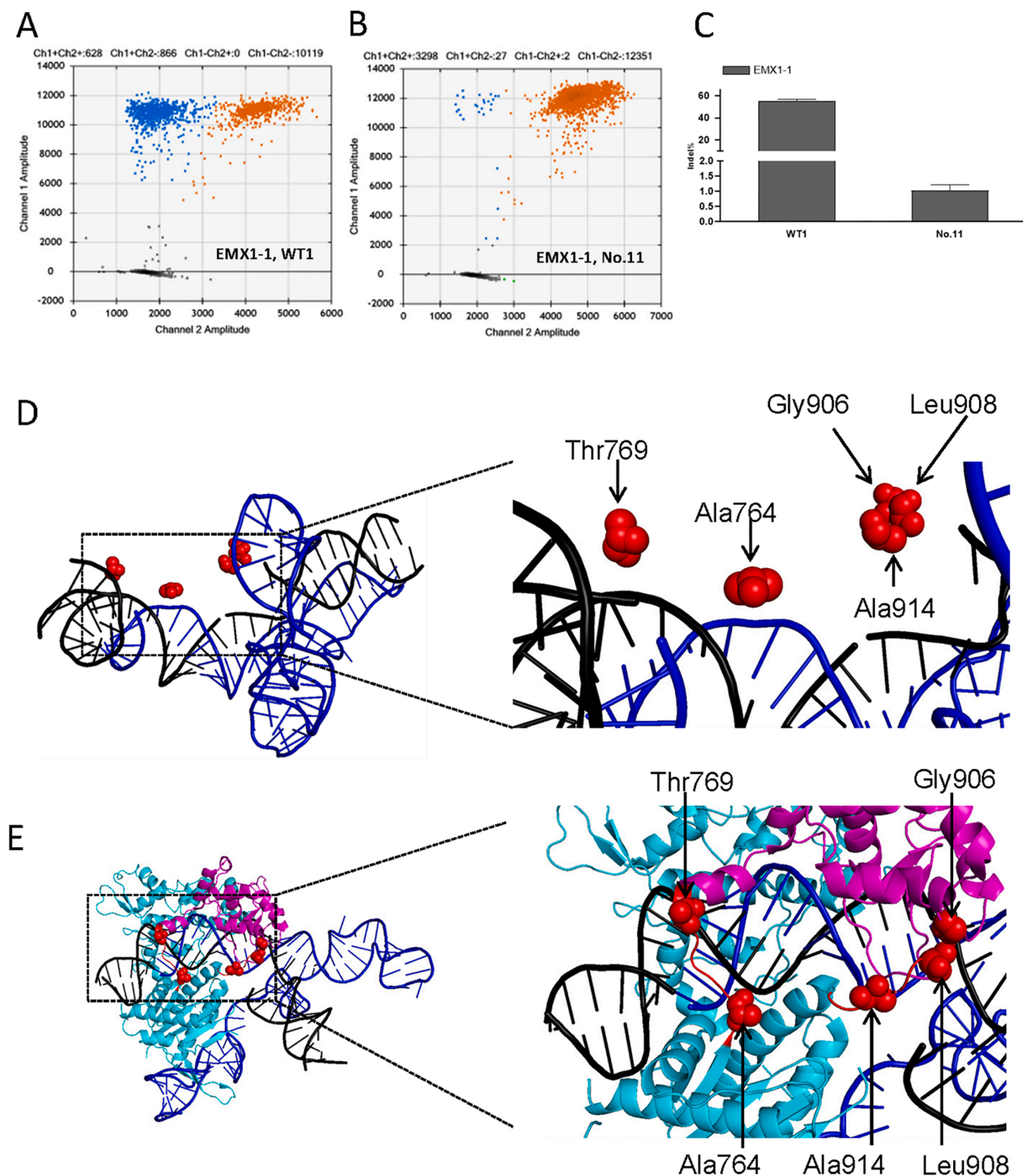


Fig. 4. Variant No. 11 was nearly dumber, and the mutation sites of variant No.1, variant No.2 and variant No.5. **A-B.** DdPCR 2D amplitude results of WT-SpCas9 (A) and variant No.11 (B) cleavage of *EMX1-1*. Channel 1 amplitude is the FAM amplitude, which shows blue fluorescence; Channel 2 amplitude is the VIC amplitude, which shows green fluorescence. The blue dots indicate mutation events and the brown (blue+ & green+) dots indicate wild-type events. **C.** The on-target cleavage efficiency of variant No.11 on *EMX1-1* was dramatically damaged. Error bars represent S.E.M. for $n = 3$. **D.** Thr769, Gly906, Leu908, Ala764 and Ala914 didn't form hydrogen bonds with the sgRNA/DNA. SgRNA is marked with blue, DNA is marked with black. The mutant sites are noted with red spheres. HNH domain is marked with magenta cartoon, while RuvC domain is marked with cyan cartoon. The first linker and the second linker of HNH domain are marked with red. **E.** Ala764 and Thr769 are both on the first linker; Gly906, Leu908, and Ala914 are all on the second linker. SgRNA is marked with blue, DNA is marked with black. The mutant sites are noted with red spheres. HNH domain is marked with magenta cartoon, while RuvC domain is marked with cyan cartoon. The first linker and the second linker of HNH domain are marked with red.

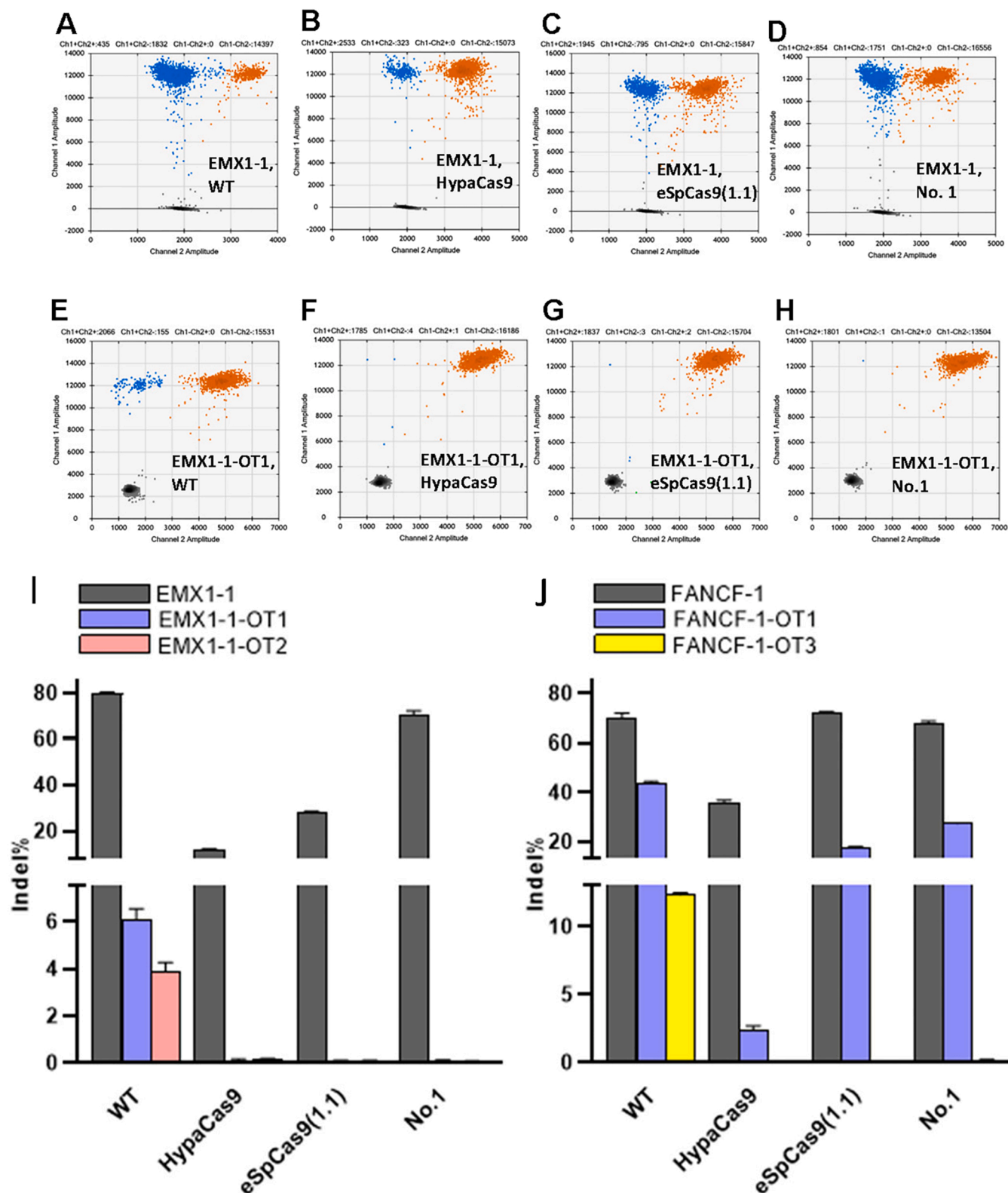


Fig. 5. Comparisons between variant No.1 and previous SpCas9 variants. A-H. DdPCR 2D amplitude results of WT-SpCas9 (A, E), HypaCas9 (B, F), eSpCas9 (1.1) (C, G), and variant No.1 (D, H) on *EMX1-1* and *EMX1-1-OT1*. Channel 1 amplitude is the FAM amplitude, which shows blue fluorescence; Channel 2 amplitude is the VIC amplitude, which shows green fluorescence. The blue dots indicate mutation events while the brown (blue + & green +) dots indicate wild-type events. I. Cleavage efficiencies of variant No.1, HypaCas9 and eSpCas9 (1.1) on *EMX1-1*, *EMX1-1-OT1* and *EMX1-1-OT2* in HEK293T cells. Error bars represent S.E.M. for n = 3. J. Cleavage efficiencies of variant No.1, HypaCas9 and eSpCas9 (1.1) on *FANCF-1*, *FANCF-1-OT1*, and *FANCF-1-OT3* in HEK293T cells. Error bars represent S.E.M. for n = 3.

EMX1-1-OT2, *FANCF-1-OT3*), variant No.1 performed better than eSp-Cas9(1.1) and hypaCas9. However, on *FANCF-1-OT1*, variant No.1, HypaCas9 and eSpCas9(1.1) all show serious off-target effects (>2%), and variant No.1 show higher off-target editing efficiency than Hypa-Cas9 and eSpCas9(1.1). This means that variant No.1 was not always better than HypaCas9 and eSpCas9(1.1), and a pre-test should be carried out before the selection of the SpCas9 variant.

This study mainly focused on proposing and verifying our hypothesis which could be used to develop high fidelity variants of CRISPR-SpCas9 system. Therefore, we carried out the assays on some already known genome sites used to screen the potential high fidelity variants. Unbiased detection of off-target mutations and the tolerance of mismatched bases at different positions along the hybrid should be continued before the active usage.

In conclusion, our study revealed that deleting the specific residues of HNH linkers induced variant No.1 (Δ Thr769, Δ Gly906) was a high fidelity SpCas9 variant with high efficiency. Variant No.1 may be a valuable option for applications requiring high-precision genome editing.

CRedit authorship contribution statement

Guohua Wang: Conceptualization, Methodology, Formal analysis, Investigation, Data curation, Visualization, Writing - original draft, Writing - review & editing, Funding acquisition. **Canmao Wang:** Methodology, Conceptualization, Investigation, Writing - review & editing, Funding acquisition. **Teng Chu:** Methodology, Writing - review & editing. **Xinjun Wu:** Methodology, Writing - review & editing, Discussion. **Dongwei Huang:** Writing - review & editing. **Christopher M. Anderson:** Writing - review & editing, Data analysis. **Juan Li:** Conceptualization, Methodology, Investigation, Supervision, Writing - original draft, Writing - review & editing, Funding acquisition.

Declaration of Competing Interest

The authors declare that they have no known competing financial interests or personal relationships that could have appeared to influence the work reported in this paper.

Data availability

Data will be made available on request.

Acknowledgments

This work was supported by the Characteristic Innovation Project in General Colleges and Universities of Guangdong Province (2022KTSCX230), National Natural Science Foundation of China (Grant No. 81601654), Natural Science Foundation of Guangdong Province, China (Grant No. 2014A030310090 and 2016A030313578), Medical Scientific Research Foundation of Guangdong Province, China (Grant No. A2015207), and Pearl River S&T Nova Program of Guangzhou (201806010037), Medical Science and Technology Research Foundation of Guangdong Province (No. A2023283) Nanshan District Science and Technology Plan Project (No. NS2022077).

Disclosure

All authors report no biomedical financial interests or potential conflicts of interest.

Appendix A. Supporting information

Supplementary data associated with this article can be found in the online version at [doi:10.1016/j.jbiotec.2023.04.008](https://doi.org/10.1016/j.jbiotec.2023.04.008).

References

- Akram, F., Ikram Ul, H., Ahmed, Z., Khan, H., Ali, M.S., 2020. CRISPR-Cas9 a promising therapeutic tool for cancer therapy: a review. *Protein Pept. Lett.* <https://doi.org/10.2174/0929866527666200407112432>.
- Anzalone, A.V., et al., 2019. Search-and-replace genome editing without double-strand breaks or donor DNA. *Nature* 576, 149–157. <https://doi.org/10.1038/s41586-019-1711-4>.
- Barrangou, R., et al., 2007. CRISPR provides acquired resistance against viruses in prokaryotes. *Science* 315, 1709–1712. <https://doi.org/10.1126/science.1138140>.
- Bolotin, A., Quinquis, B., Sorokin, A., Ehrlich, S.D., 2005. Clustered regularly interspaced short palindrome repeats (CRISPRs) have spacers of extrachromosomal origin. *Microbiology* 151, 2551–2561. <https://doi.org/10.1099/mic.0.28048-0>.
- Bratović, M., et al., 2020. Bridge helix arginines play a critical role in Cas9 sensitivity to mismatches. *Nat. Chem. Biol.* 16, 587–595. <https://doi.org/10.1038/s41589-020-0490-4>.
- Carballar-Lejarazú, R., Kelsey, A., Pham, T.B., Bennett, E.P., James, A.A., 2020. Digital droplet PCR and IDAA for the detection of CRISPR indel edits in the malaria species *Anopheles stephensi*. *BioTechniques* 68, 172–179. <https://doi.org/10.2144/btn-2019-0103>.
- Carballar-Lejarazú, R., Pham, T.B., Kelsey, A., Tushar, T., James, A.A., 2021. Digital-droplet PCR to detect indels mutations in genetically modified anopheline mosquito populations. *J. Vis. Exp. JoVE.* <https://doi.org/10.3791/62607>.
- Chen, J.S., et al., 2017. Enhanced proofreading governs CRISPR-Cas9 targeting accuracy. *Nature* 550, 407–410. <https://doi.org/10.1038/nature24268>.
- Cromwell, C.R., et al., 2018. Incorporation of bridged nucleic acids into CRISPR RNAs improves Cas9 endonuclease specificity. *Nat. Commun.* 9, 1448. <https://doi.org/10.1038/s41467-018-03927-0>.
- Dibitetto, D., La Monica, M., Ferrari, M., Marini, F., Pelliccioli, A., 2018. Formation and nucleolytic processing of Cas9-induced DNA breaks in human cells quantified by droplet digital PCR. *DNA Repair* 68, 68–74. <https://doi.org/10.1016/j.dnarep.2018.06.005>.
- Doudna, J.A., 2020. The promise and challenge of therapeutic genome editing. *Nature* 578, 229–236. <https://doi.org/10.1038/s41586-020-1978-5>.
- Fauchère, J.L., Charton, M., Kier, L.B., Verloop, A., Pliska, V., 1988. Amino acid side chain parameters for correlation studies in biology and pharmacology. *Int. J. Pept. Protein Res.* 32, 269–278. <https://doi.org/10.1111/j.1399-3011.1988.tb01261.x>.
- Fu, Y., Sander, J.D., Reyon, D., Cascio, V.M., Joung, J.K., 2014. Improving CRISPR-Cas9 nuclease specificity using truncated guide RNAs. *Nat. Biotechnol.* 32, 279–284. <https://doi.org/10.1038/nbt.2808>.
- Gemberling, M.P., Siklenka, K., Rodriguez, E., 2021. Transgenic mice for in vivo epigenome editing with CRISPR-based systems, 18, 965–974. <https://doi.org/10.1038/s41592-021-01207-2>.
- Guillinger, J.P., Thompson, D.B., Liu, D.R., 2014. Fusion of catalytically inactive Cas9 to FokI nuclease improves the specificity of genome modification. *Nat. Biotechnol.* 32, 577–582. <https://doi.org/10.1038/nbt.2909>.
- Guschin, D.Y., et al., 2010. A rapid and general assay for monitoring endogenous gene modification. *Methods Mol. Biol.* 649, 247–256. https://doi.org/10.1007/978-1-60761-753-2_15.
- Helfer-Hungerbuehler, A.K., et al., 2021. Adeno-associated vector-delivered CRISPR. SaCas9 Syst. Reduces Feline Leuk. *Virus Prod. Vitr.* 13 <https://doi.org/10.3390/v13081636>.
- Hu, P., Zhao, X., Zhang, Q., Li, W., Zu, Y., 2018. Comparison of various nuclear localization signal-fused Cas9 proteins and Cas9 mRNA for genome editing in zebrafish. *G3 Bethesda Md.* 8, 823–831. <https://doi.org/10.1534/g3.117.300359>.
- Hussain, S.S., et al., 2021. Meas. nonhomologous End. Join. Homol. Recomb. Altern. End. Join. simultaneously Endog. locus any transfectable Hum. Cell 49, e74. <https://doi.org/10.1093/nar/gkab262>.
- Ishino, Y., Shinagawa, H., Makino, K., Amemura, M., Nakata, A., 1987. Nucleotide sequence of the *iap* gene responsible for alkaline phosphatase isozyme conversion in *Escherichia coli* and identification of the gene product. *J. Bacteriol.* 169, 5429–5433. <https://doi.org/10.1128/jb.169.12.5429-5433.1987>.
- Jansen, R., Embden, J.D., Gastra, W., Schouls, L.M., 2002. Identification of genes that are associated with DNA repeats in prokaryotes. *Mol. Microbiol.* 43, 1565–1575. <https://doi.org/10.1046/j.1365-2958.2002.02839.x>.
- Jiang, F., et al., 2016. Structures of a CRISPR-Cas9 R-loop complex primed for DNA cleavage. *Science* 351, 867–871. <https://doi.org/10.1126/science.aad8282>.
- Jinek, M., et al., 2012. A programmable dual-RNA-guided DNA endonuclease in adaptive bacterial immunity. *Science* 337, 816–821. <https://doi.org/10.1126/science.1225829>.
- Kim, D., Luk, K., Wolfe, S.A., Kim, J.S., 2019. Evaluating and enhancing target specificity of gene-editing nucleases and deaminases. *Annu. Rev. Biochem.* 88, 191–220. <https://doi.org/10.1146/annurev-biochem-013118-111730>.
- Kleinstiver, B.P., et al., 2016. High-fidelity CRISPR-Cas9 nucleases with no detectable genome-wide off-target effects. *Nature* 529, 490–495. <https://doi.org/10.1038/nature16526>.
- Kulcsár, P.I., et al., 2020. Blackjack Mutat. Improv. Target Act. Increase Fidel. Var. SpCas9 5'G-Ext. sgRNAs 11, 1223. <https://doi.org/10.1038/s41467-020-15021-5>.
- Li, H., et al., 2020. Applications of genome editing technology in the targeted therapy of human diseases: mechanisms advances and prospects. *Signal Transduct. Target. Ther.* 5, 1. <https://doi.org/10.1038/s41392-019-0089-y>.
- Miyaoka, Y., Mayerl, S.J., Chan, A.H., Conklin, B.R., 2018. Detection and quantification of HDR and NHEJ Induced by genome editing at endogenous gene loci using droplet digital PCR. *Methods Mol. Biol.* 1768, 349–362. https://doi.org/10.1007/978-1-4939-7778-9_20.

- Nishimasu, H., et al., 2014. Crystal structure of Cas9 in complex with guide RNA and target DNA. *Cell* 156, 935–949. <https://doi.org/10.1016/j.cell.2014.02.001>.
- Rose, J.C., et al., 2017. Rapidly inducible Cas9 and DSB-ddPCR to probe editing kinetics. *Nat. Methods* 14, 891–896. <https://doi.org/10.1038/nmeth.4368>.
- Schmid-Burgk, J.L., et al., 2020. Highly parallel profiling of Cas9 variant specificity. *Mol. Cell* 78 (794–800), e798. <https://doi.org/10.1016/j.molcel.2020.02.023>.
- Sentmanat, M.F., Peters, S.T., Florian, C.P., Connelly, J.P., Pruett-Miller, S.M., 2018. A survey of validation strategies for CRISPR-Cas9 editing. *Sci. Rep.* 8, 888. <https://doi.org/10.1038/s41598-018-19441-8>.
- Singh, K., et al., 2018. Efficient in vivo liver-directed gene editing using CRISPR/Cas9. *Mol. Ther. J. Am. Soc. Gene Ther.* 26, 1241–1254. <https://doi.org/10.1016/j.ymthe.2018.02.023>.
- Slaymaker, I.M., et al., 2016. Rationally engineered Cas9 nucleases with improved specificity. *Science* 351, 84–88. <https://doi.org/10.1126/science.aad5227>.
- Soler-Bistué, A., Zorreguieta, A., Tolmasky, M.E., 2019. Bridged nucleic acids reloaded. [doi:10.3390/molecules24122297](https://doi.org/10.3390/molecules24122297) *Molecules* 24. [doi:10.3390/molecules24122297](https://doi.org/10.3390/molecules24122297).
- Sorek, R., Kunin, V., Hugenholtz, P., 2008. CRISPR—a widespread system that provides acquired resistance against phages in bacteria and archaea. *Nat. Rev. Microbiol.* 6, 181–186. <https://doi.org/10.1038/nrmicro1793>.
- Sternberg, S.H., Redding, S., Jinek, M., Greene, E.C., Doudna, J.A., 2014. DNA interrogation by the CRISPR RNA-guided endonuclease Cas9. *Nature* 507, 62–67. <https://doi.org/10.1038/nature13011>.
- Sykes, P.J., et al., 1992. Quantitation of targets for PCR by use of limiting dilution. *BioTechniques* 13, 444–449.
- Vakulskas, C.A., Dever, D.P., Rettig, G.R., 2018. A High-Fidelity Cas9 Mutant Deliv. A ribonucleoprotein Complex enables Effic. gene Ed. *Hum. Hematop. stem Progenit. Cells* 24, 1216–1224. <https://doi.org/10.1038/s41591-018-0137-0>.
- Wang, G., Li, J., 2021. Review, analysis, and optimization of the CRISPR Streptococcus pyogenes Cas9 system. *Med. Drug Discov.* 9, 100080 <https://doi.org/10.1016/j.medidd.2021.100080>.
- Wright, A.V., et al., 2015. Rational design of a split-Cas9 enzyme complex. *Proc. Natl. Acad. Sci. USA* 112, 2984–2989. <https://doi.org/10.1073/pnas.1501698112>.
- Zatloukalová, P., Krejčí, R., Valík, D., Vojtěšek, B., 2019. CRISPR-Cas9 as a Tool in Cancer Therapy. *Klin. Onkol.: Cas. Ceske a Slov. Onkol. Spol.* 32, 13–18. <https://doi.org/10.14735/amko20193S>.
- Zhu, X., et al., 2019. Cryo-EM Struct. Reveal Coord. Domain Motions that Gov. DNA cleavage Cas9 26, 679–685. <https://doi.org/10.1038/s41594-019-0258-2>.
- Zulijani, A., Dekanić, A., 2021. Met. Megal. Expr. Profil. Premalig. Malig. Oral. Squamous Epithel. Lesions 13. <https://doi.org/10.3390/cancers13184530>.



检索报告

编号：20231475Z

作者：姜全德

作者单位：广东轻工职业技术学院

检索工具：Science Citation Index Expanded (SCI E)

检索报告

经查证，在姜全德提供的文献清单中，共有 1 篇论文（发表年限 2023 年 1-12 月）分别被以下数据库收录，详见附件。

数据库	数量
SCI E (收)	1 篇

论文：不含传记、书目、书评、摘要、勘误、撤稿、会议录等文献类型。

中国科学技术信息研究所

2023年12月18日



附件

SCIE 收录:

编号: 20231475Z

第 1 条, 共 1 条

标题: Asymptotically Almost Automorphic Solutions for Impulsive Quaternion-Valued Neural Networks with Mixed Delays

作者: Jiang, QD (Jiang, Quande); Wang, QR (Wang, Qiru)

来源出版物: NEURAL PROCESSING LETTERS DOI: 10.1007/s11063-023-11434-7 提前访问日期: NOV 2023

入藏号: WOS:001101259600001

语言: English

文献类型: Article; Early Access

地址: [Jiang, Quande] Guangdong Ind Polytech, Math Teaching & Res Dept, 152, Xingang Xi Rd, Guangzhou 510300, Guangdong, Peoples R China.

[Wang, Qiru] Sun Yat sen Univ, Sch Math, 135, Xingang Xi Rd, Guangzhou 510275, Guangdong, Peoples R China.

通讯作者地址: Jiang, QD (通讯作者), Guangdong Ind Polytech, Math Teaching & Res Dept, 152, Xingang Xi Rd, Guangzhou 510300, Guangdong, Peoples R China.

电子邮件地址: 2015109047@gdip.edu.cn; mcswqr@mail.sysu.edu.cn

Affiliations: Guangdong Industry Polytechnic; Sun Yat Sen University

Web of Science 类别: Computer Science, Artificial Intelligence

IDS 号: X8ZC4

ISSN: 1370-4621

eISSN: 1573-773X

基金资助致谢:

基金资助机构 授权号

This work is supported by the National Natural Science Foundation of China (Grant No. 12071491) and by the Scientific Research Project of Guangdong Industry Polytechnic (Grant No. KJ2019-029).
12071491

National Natural Science Foundation of China

KJ2019-029

Scientific Research Project of Guangdong Industry Polytechnic

This work is supported by the National Natural Science Foundation of China (Grant No. 12071491) and by the Scientific Research Project of Guangdong Industry Polytechnic (Grant No. KJ2019-029).

附件

JCR:

编号: 20231475Z

Rank	Full Journal Title	Year	Journal Impact Factor	JCR Category	Category Quartile
1	NEURAL PROCESSING LETTERS	2022	3.1	COMPUTER SCIENCE, ARTIFICIAL INTELLIGENCE - SCIE	Q3



Asymptotically Almost Automorphic Solutions for Impulsive Quaternion-Valued Neural Networks with Mixed Delays

Quande Jiang¹ · Qiru Wang²

Accepted: 1 October 2023

© The Author(s), under exclusive licence to Springer Science+Business Media, LLC, part of Springer Nature 2023

Abstract

In this paper, we consider a class of impulsive quaternion-valued neural networks with mixed delays. By using the General Lipschitz condition, the contraction mapping principle, the exponential dichotomy of linear dynamic equations and the generalized Gronwall–Bellman inequality technique, we obtain the conditions for the existence, uniqueness and global exponential stability of asymptotically almost automorphic solutions of the system. Finally, two examples are given to illustrate the efficiency of our theoretical results.

Keywords Impulsive quaternion-valued neural networks with mixed delays · Asymptotically almost automorphic solutions · Existence uniqueness and global exponential stability · Generalized Gronwall–Bellman inequality technique

1 Introduction

Neural networks have gained more and more attention since they are widely applied in many fields (see [1–7]). In addition to this, there are many impulsive phenomena and time delay phenomena in nature. So, in recent years, the existence and stability of solutions for impulsive neural networks with time delays have been extensively studied (see [8–13]). On the other hand, the study of asymptotically almost automorphic solutions for neural networks has been extensively studied (see [14, 15]).

In 1843, the quaternion group was discovered by Hamilton (see [16]), after that quaternion algebra was developed (see [17]). In 1978, Sudbery proposed quaternion analysis (see [18]). The quaternion group includes one real and three imaginary parts. The three imaginary units

✉ Quande Jiang
2015109047@gdip.edu.cn

Qiru Wang
mcswqr@mail.sysu.edu.cn

¹ Mathematics Teaching and Research Department, Guangdong Industry Polytechnic, No. 152, Xingang Xi Road, Guangzhou 510300, Guangdong, People's Republic of China

² School of Mathematics, Sun Yat-sen University, No. 135, Xingang Xi Road, Guangzhou 510275, Guangdong, People's Republic of China

i, j and k obey the Hamilton's multiplication rules:

$$ij = -ji = k, jk = -kj = i, ki = -ik = j, i^2 = j^2 = k^2 = ijk = -1.$$

We denote $\mathbb{H} := \{q : q = q^R + iq^I + jq^J + kq^K\}$, where q^R, q^I, q^J, q^K are real numbers. The quaternion-valued neural networks (QVNNs), which are a generalization of the real-valued and complex-valued neural networks, can be widely applied in the fields such as satellite tracking, aerospace, image processing and processing of polarized waves.

One of the benefits of using quaternion is that the three-dimensional geometrical affine transformation can be represented efficiently and compactly based on quaternion-variable neural networks (QVNNs) especially spatial rotation (see [19]). Compared with complex-valued neural networks (CVNNs) and the real-valued neural networks (RVNNs), the QVNNs can take more the inner relationship. Therefore, the study of QVNNs has received much attention of many scholars and some good results have been obtained for the stability, periodicity and pseudo almost periodicity of QVNNs (see [7, 17, 20–25]). For example, the accuracy of the classification of prostate Cancer Gleason Grading can achieve 98.87% in QVNNs (see [26]) which outperforms other published automatic Gleason grading systems like RVNNs and CVNNs. The quaternion field can also carry more information, that is, it has a large storage capacity, the results of (see [27]) show that the n -neuron QVNNs can have 16^n stable equilibrium points more than the CVNNs and RVNNs, and the designed QVNNs work efficiently on storing and retrieving true-color images, the QVNNs perform much better when it comes. Since many stimulated neural networks, optimal control models in economics, evolution processes, etc. are characterized by impulsive dynamical behavior, impulsive system is playing an important role. For QVNNs, impulsive effects should also be considered to resist the disturbance of some abrupt phenomena or stabilize them. Recently, some authors have studied impulsive QVNNs (IQVNNs) and obtained some excellent results. The authors in [15] discussed the exponential stability of the discrete-time IQVNNs by Lyapunov methods and quaternion-modulus inequality technique.

In 2007, Xia, Cao and Huang in [28] studied the impulsive SICNN neural network with almost periodic coefficients

$$\begin{cases} x'_{ij}(t) = -a_{ij}(t)x_{ij}(t) + \sum_{C_{hl} \in N_r(ij)} C_{ij}^{hl}(t)f_{ij}(x_{hl}(t))x_{ij}(t) + L_{ij}(t), & t \neq t_k, \\ \Delta(x_{ij}(t_k)) = \alpha_{ij}^k x_{ij}(t_k) + I_{ij}^k(x_{ij}(t_k)) + L_{ij}^k, & t = t_k, i = 1, 2, \dots, m, j = 1, 2, \dots, n, \end{cases}$$

where $\Delta(x_{ij}(t_k)) = x_{ij}(t_k^+) - x_{ij}(t_k^-)$ are impulses at moment t_k , and $t_1 < t_2 < \dots$ is a strictly increasing sequence such that $\lim_{k \rightarrow \infty} t_k = +\infty$.

In 2018, Chaouki and Farah in [15] considered the impulsive non-autonomous high-order Hopfield neural networks with mixed delays

$$\begin{cases} x'_i(t) = \sum_{j=1}^n c_{ij}(t)x_j(t) + \sum_{j=1}^n a_{ij}(t)f_j(x_j(t - \zeta_j)) \\ \quad + \sum_{j=1}^n \sum_{l=1}^n b_{ijl}(t)g_j(x_j(t - \sigma_j))g_l(x_l(t - \nu_l)) \\ \quad + \sum_{j=1}^n d_{ij}(t) \int_{-\infty}^t K_{ij}(t - s)h_j(x_j(s))ds \\ \quad + \sum_{j=1}^n \sum_{l=1}^n r_{ijl}(t) \int_{-\infty}^t P_{ijl}(t - s)k_j(x_j(s))ds \\ \quad \times \int_{-\infty}^t Q_{ijl}(t - s)k_l(x_l(s))ds + \gamma_i(t), & t \neq t_k, \\ \Delta(x(t_k)) = \alpha_k x(t_k) + I_k(x(t_k)) + \omega_k, & k \in \mathbb{Z}, t \in \mathbb{R}, t = t_k. \end{cases}$$

Under proper conditions, they studied the existence, uniqueness and global exponential stability of the above systems.

In 2018, Meng and Li in [7] studied pseudo almost periodic solutions for the following quaternion-valued cellular neural networks

$$x'_p(t) = -c_p(t)x_p(t) + \sum_{q=1}^n a_{pq}(t)f_q(x_q(t - \tau_{pq}(t))) + \sum_{q=1}^n b_{pq}(t) \int_0^{+\infty} K_{pq}(u)g_q(x_q(t - u))du + u_p(t).$$

Motivated by the above works, in this paper, we consider parallel neural networks to above three networks of the following form

$$\begin{cases} x'_p(t) = -c_p(t)x_p(t) + \sum_{q=1}^n a_{pq}(t)f_q(x_q(t - \tau_{pq}(t))) \\ \quad + \sum_{q=1}^n b_{pq}(t) \int_0^{+\infty} k_{pq}(u)g_q(x_q(t - u))du + u_p(t), \quad t \in \mathbb{R}, t \neq t_k, \\ \Delta(x(t_k)) = \alpha_k x(t_k) + I_k(x(t_k)) + \omega_k, \quad k \in \mathbb{Z}, \end{cases} \tag{1.1}$$

where $p \in \{1, 2, \dots, n\} := \Lambda$, n corresponds to the number of units in the neural network; $x_p(t) \in \mathbb{H}$, corresponds to the activation of the p th neuron at time t ; \mathbb{H} represents the set of all quaternion functions; $c_p : \mathbb{R} \rightarrow \mathbb{R}^+$ represents the rate with which the p th unit will reset its potential to the resting state in isolation when disconnected from the network and external inputs at time t ; $a_{pq}(t), b_{pq}(t) \in \mathbb{H}$ are the synaptic weights of delayed feedback between cell p and q at time t respectively; $f_q, g_q \in \mathbb{H}$ denote the activation functions of signal transmission; $u_p(t) \in \mathbb{H}$ is an external input on the p th unit at time t ; τ_{pq} are transmission delays at time t ; the kernel function $k_{pq} : \mathbb{R} \rightarrow \mathbb{R}^+$ satisfies that $\int_0^{+\infty} k_{pq}(s)ds = 1; t \in \mathbb{R}, p, q \in \Lambda. \alpha_k \in \mathbb{R}^n$ is connection weight of impulse at moment $t_k; I_k : \mathbb{R}^n \rightarrow \mathbb{R}^n$ is a continuous function; $\omega_k \in \mathbb{R}^n$ is the external inputs of impulses at moment $t_k; \Delta(x(t_k)) = (\Delta(x_1(t_k)), \Delta(x_2(t_k)), \dots, \Delta(x_n(t_k)))^T, x(t) = (x_1(t), x_2(t), \dots, x_n(t))^T, \Delta(x_i(t_k)) = x_i(t_k^+) - x_i(t_k^-)$ is the impulse at moments $t_k; x_i(t_k^-) = x_i(t_k)$ and $x_i(t_k^+)$ are the activations of the i th neuron before and after impulsive perturbation, respectively; $t_1 < t_2 < \dots$ is a strictly increasing sequence such that $\lim_{k \rightarrow \infty} t_k = +\infty$.

The initial conditions with system (1.1) are of the following form

$$x_p(s) = \phi_p(s), p \in \Lambda, s \in (-\infty, 0], \tag{1.2}$$

where $\phi_p = \phi_p^R + i\phi_p^I + j\phi_p^J + k\phi_p^K$ is the quaternion-valued bounded continuous function defined on $(-\infty, 0]$.

Motivated by above analyses, this paper focuses on the exponential stability conditions of the IQVNNs by utilizing generalized Gronwall–Bellman inequality technique. Comparing with the existing results, this paper has the following main extend contributions: (1) A general IQVNN model is constructed by the impulsive differential system and QVNNs. In the cause of overcoming the noncommutativity of quaternion multiplication, it is decomposed into impulsive disturbed delayed systems. (2) Based on the definition the norm of $\|x\| = \max\{\sup_{p \in \Lambda} \sup_{t \in \mathbb{T}} |x_p^l(t)|, l \in E\}$, a novel stability definition is introduced to investigate the stability criteria of IQVNNs. (3) According to the norm of $\|x\| = \max\{\sup_{p \in \Lambda} \sup_{t \in \mathbb{T}} |x_p^l(t)|, l \in E\}$

and QVDNNs, special are constructed to prove the stability of IQVNNs. The obtained results show that the stable system of this paper has certain capacity under some special conditions.

The rest of this paper is as follows. In Sect. 2, we will give some definitions and some useful lemmas for the later sections. In Sect. 3, we obtain the existence and uniqueness of asymptotically almost automorphic solutions of system (1.1) by exploiting general Lipschitz condition, contraction mapping principal and exponential dichotomy of linear dynamic equations. In Sect. 4, by utilizing generalized Gronwall–Bellman inequality technique, we discuss the global exponential stability of the unique asymptotically almost automorphic solution. In Sect. 5, we will give two examples to illustrate the application of the abstract results.

2 Preliminaries

In this section, we introduce some denotes and basic definitions and also some preliminary assumptions which are useful throughout this paper (see [1, 9, 12, 15]).

- ◇ $C(\mathbb{R}, \mathbb{H}^n)$ denotes the set whose functions are continuous from \mathbb{R} to \mathbb{H}^n .
- ◇ $BC(\mathbb{R}, \mathbb{H}^n)$ is the set whose functions are bounded continuous from \mathbb{R} to \mathbb{H}^n .
- ◇ $B(\mathbb{R}, \mathbb{H}^n, \|\cdot\|_\infty)$ denotes a Banach space, where $\|\cdot\|_\infty$ is the sup norm $\|f\| := \max_{1 \leq i \leq n} \sup_{t \in \mathbb{R}} |f_i(t)|$.
- ◇ $PC(\mathbb{I}, \mathbb{H}^n) = \{f : \mathbb{I} \rightarrow \mathbb{H}^n, f \text{ is a piecewise continuous function from } \mathbb{I} \subset \mathbb{R} \text{ to } \mathbb{H}^n \text{ with points of discontinuity of the first kind } t_k, k = 1, 2, \dots; \text{ That is, at } t_k \text{ that } f(t_k^+) \text{ and } f(t_k^-) \text{ exist, and left continuous } f(t_k^-) = f(t_k)\}$.
- ◇ $PC_0(\mathbb{R} : \mathbb{H}^n) = \{\phi \in PC(\mathbb{R}, \mathbb{H}^n), \lim_{t \rightarrow \infty} \|\phi(t, x)\| = 0 \text{ at } t \text{ uniformly in } x \in \mathbb{H}^n\}$.
- ◇ $B = \{(t_k)_{k=-\infty}^\infty : t_k \in \mathbb{R}, t_k < t_{k+1}, \lim_{k \rightarrow \pm\infty} t_k = \pm\infty\}$ is the set of all sequences which are unbounded and strictly increasing.

Definition 1 ([15]) Let $f : \mathbb{R} \rightarrow \mathbb{X}$ be a bounded continuous function. We say that f is almost automorphic if for every sequence of real numbers $(s_n)_{n \in \mathbb{N}}$, there exists a subsequence $(\tau_n)_{n \in \mathbb{N}}$ such that $g(t) = \lim_{n \rightarrow \infty} f(t + \tau_n)$ is well-defined for each $t \in \mathbb{R}$ and $\lim_{n \rightarrow \infty} g(t - \tau_n) = f(t)$ for each $t \in \mathbb{R}$. Denote by $AA(\mathbb{R}, \mathbb{X})$ the set of all such functions.

Definition 2 ([29]) A bounded continuous function $f : \mathbb{R} \times \mathbb{X} \rightarrow \mathbb{X}$ is called almost automorphic in t uniformly for x in compact subsets of \mathbb{X} , if for every compact subset \mathbb{K} of \mathbb{X} and every real sequence $(s_n)_{n \in \mathbb{N}}$, there exists a subsequence $(\tau_n)_{n \in \mathbb{N}}$ such that $g(t, x) = \lim_{n \rightarrow \infty} f(t + \tau_n, x)$ is well-defined for each $t \in \mathbb{R}, x \in \mathbb{K}$ and $\lim_{n \rightarrow \infty} g(t - \tau_n, x) = f(t, x)$ for each $t \in \mathbb{R}, x \in \mathbb{K}$. Denote $AA(\mathbb{R}, \mathbb{X})$ as the set of all such functions.

Definition 3 ([30]) A bounded continuous function $f : \mathbb{R} \rightarrow \mathbb{H}^n$ is called asymptotically almost automorphic if and only if it can be written as $f = g + \varphi$, where $g \in AA(\mathbb{R}, \mathbb{H}^n)$ and $\varphi \in PC_0(\mathbb{R}, \mathbb{H}^n)$. This kind of functions is denoted by $AAA(\mathbb{R}, \mathbb{H}^n)$.

Lemma 1 [31] Let X, Y be Banach spaces, and if $f, f_1, f_2 \in AA(\mathbb{R}, X)$, then

- (i) $f_1 + f_2 \in AA(\mathbb{R}, X)$;
- (ii) $\alpha f \in AA(\mathbb{R}, X)$ for any constant $\alpha \in \mathbb{R}$;
- (iii) if $\varphi : X \rightarrow Y$ is a continuous function, then the composite function $f \circ \varphi : \mathbb{R} \rightarrow Y$ is almost automorphic.

Lemma 2 (Generalized Gronwall–Bellman inequality, see [15]) *Let a nonnegative function $x(\cdot) \in PC(\mathbb{R}, \mathbb{R}^n)$ satisfy for $t \geq t_0$*

$$x(t) \leq C(t) + \int_{t_0}^t u(s)x(s)ds + \sum_{t_0 < t_k < t} \beta_i x(t_i),$$

with $C(t)$ a positive non-decreasing function for $t \geq t_0$, $\beta_i \geq 0$, $u(t) \geq 0$ and t_i are the first kind discontinuity points of the function $x(\cdot)$. Then the following estimate holds for the function $x(\cdot)$:

$$x(t) \leq C(t) \prod_{t_0 < t_k < t} (1 + \beta_i) e^{\int_{t_0}^t u(s)ds}.$$

In order to decompose the quaternion neural network into four real value systems, we need the following assumption:

(H0) [[7]] Let $x_p = x_p^R + ix_p^I + jx_p^J + kx_p^K \in BC(\mathbb{R}, \mathbb{H}^n)$, then f_q, g_q can be expressed as follows

$$\begin{aligned} f_q(x_q) &= f_q^R(x_q^R, x_q^I, x_q^J, x_q^K) + if_q^I(x_q^R, x_q^I, x_q^J, x_q^K) \\ &\quad + jf_q^J(x_q^R, x_q^I, x_q^J, x_q^K) + kf_q^K(x_q^R, x_q^I, x_q^J, x_q^K), \\ g_q(x_q) &= g_q^R(x_q^R, x_q^I, x_q^J, x_q^K) + ig_q^I(x_q^R, x_q^I, x_q^J, x_q^K) \\ &\quad + jg_q^J(x_q^R, x_q^I, x_q^J, x_q^K) + kg_q^K(x_q^R, x_q^I, x_q^J, x_q^K), \end{aligned}$$

where $f_q^l, g_q^l : \mathbb{R}^4 \rightarrow \mathbb{R}$, $p \in \Lambda, l \in E := \{R, I, J, K\}$.

Then by Hamilton multiplication rules, (1.1) and (1.2) can be decomposed into four real systems as follows

$$\left\{ \begin{aligned} (x_p^R(t))' &= -c_p(t)x_p^R(t) + \sum_{q=1}^n (a_{pq}^R(t)f_q^R(t, \tau, x) - a_{pq}^I(t)f_q^I[t, \tau, x] \\ &\quad - a_{pq}^J(t)f_q^J[t, \tau, x] - a_{pq}^K(t)f_q^K[t, \tau, x]) \\ &\quad + \sum_{q=1}^n (b_{pq}^R(t) \int_0^{+\infty} k_{pq}(u)g_q^R[t, u, x]\Delta u \\ &\quad - b_{pq}^I(t) \int_0^{+\infty} k_{pq}(u)g_q^I[t, u, x]\Delta u \\ &\quad - b_{pq}^J(t) \int_0^{+\infty} k_{pq}(u)g_q^J[t, u, x]\Delta u \\ &\quad - b_{pq}^K(t) \int_0^{+\infty} k_{pq}(u)g_q^K[t, u, x]\Delta u) + u_p^R(t) \\ &\triangleq -c_p(t)x_p^R(t) + G_p^R(t, x(t)) + u_p^R(t), \quad p \in \Lambda, t > 0, t \neq t_k, \\ \Delta(x^R(t_k)) &= \alpha_k x^R(t_k) + I_k^R(x^R(t_k)) + \omega_k^R, \quad k \in \mathbb{Z}, \\ x_p^R(s) &= \phi_p^R(s), \quad s \in (-\infty, 0]; \end{aligned} \right.$$

$$\left\{ \begin{aligned} (x_p^I(t))' &= -c_p(t)x_p^I(t) + \sum_{q=1}^n (a_{pq}^R(t)f_q^I(t, \tau, x) + a_{pq}^I(t)f_q^R[t, \tau, x] \\ &\quad + a_{pq}^J(t)f_q^K[t, \tau, x] - a_{pq}^K(t)f_q^J[t, \tau, x]) \\ &\quad + \sum_{q=1}^n (b_{pq}^R(t) \int_0^{+\infty} k_{pq}(u)g_q^I[t, u, x]\Delta u \\ &\quad + b_{pq}^I(t) \int_0^{+\infty} k_{pq}(u)g_q^R[t, u, x]\Delta u \\ &\quad + b_{pq}^J(t) \int_0^{+\infty} k_{pq}(u)g_q^K[t, u, x]\Delta u \\ &\quad - b_{pq}^K(t) \int_0^{+\infty} k_{pq}(u)g_q^J[t, u, x]\Delta u) + u_p^I(t) \\ &\triangleq -c_p(t)x_p^I(t) + G_p^I(t, x(t)) + u_p^I(t), \quad p \in \Lambda, t > 0, t \neq t_k, \\ \Delta(x^I(t_k)) &= \alpha_k x^I(t_k) + I_k^I(x^I(t_k)) + \omega_k^I, \quad k \in \mathbb{Z}, \\ x_p^I(s) &= \phi_p^I(s), \quad s \in (-\infty, 0]; \end{aligned} \right.$$

$$\left\{ \begin{aligned} (x_p^J(t))' &= -c_p(t)x_p^J(t) + \sum_{q=1}^n (a_{pq}^R(t)f_q^J(t, \tau, x) + a_{pq}^J(t)f_q^R[t, \tau, x] \\ &\quad - a_{pq}^I(t)f_q^K[t, \tau, x] + a_{pq}^K(t)f_q^I[t, \tau, x]) \\ &\quad + \sum_{q=1}^n (b_{pq}^R(t) \int_0^{+\infty} k_{pq}(u)g_q^J[t, u, x]\Delta u \\ &\quad + b_{pq}^I(t) \int_0^{+\infty} k_{pq}(u)g_q^R[t, u, x]\Delta u \\ &\quad - b_{pq}^J(t) \int_0^{+\infty} k_{pq}(u)g_q^K[t, u, x]\Delta u \\ &\quad + b_{pq}^K(t) \int_0^{+\infty} k_{pq}(u)g_q^J[t, u, x]\Delta u) + u_p^J(t) \\ &\triangleq -c_p(t)x_p^J(t) + G_p^J(t, x(t)) + u_p^J(t), \quad p \in \Lambda, t > 0, t \neq t_k, \\ \Delta(x^J(t_k)) &= \alpha_k x^J(t_k) + I_k^J(x^J(t_k)) + \omega_k^J, \quad k \in \mathbb{Z}, \\ x_p^J(s) &= \phi_p^J(s), \quad s \in (-\infty, 0]; \end{aligned} \right.$$

$$\left\{ \begin{aligned} (x_p^K(t))' &= -c_p(t)x_p^K(t) + \sum_{q=1}^n (a_{pq}^R(t)f_q^K(t, \tau, x) + a_{pq}^K(t)f_q^R[t, \tau, x] \\ &\quad + a_{pq}^I(t)f_q^J[t, \tau, x] - a_{pq}^J(t)f_q^I[t, \tau, x]) \\ &\quad + \sum_{q=1}^n (b_{pq}^R(t) \int_0^{+\infty} k_{pq}(u)g_q^K[t, u, x]\Delta u \\ &\quad + b_{pq}^I(t) \int_0^{+\infty} k_{pq}(u)g_q^R[t, u, x]\Delta u \\ &\quad + b_{pq}^J(t) \int_0^{+\infty} k_{pq}(u)g_q^J[t, u, x]\Delta u \\ &\quad - b_{pq}^K(t) \int_0^{+\infty} k_{pq}(u)g_q^K[t, u, x]\Delta u) + u_p^K(t) \\ &\triangleq -c_p(t)x_p^K(t) + G_p^K(t, x(t)) + u_p^K(t), \quad p \in \Lambda, t > 0, t \neq t_k, \\ \Delta(x^K(t_k)) &= \alpha_k x^K(t_k) + I_k^K(x^K(t_k)) + \omega_k^K, \quad k \in \mathbb{Z}, \\ x_p^K(s) &= \phi_p^K(s), \quad s \in (-\infty, 0]; \end{aligned} \right.$$

where for $p \in \Lambda, l \in E, f_q^l[t, \tau, x] \triangleq f_q^l(x_q^R(t - \tau_{pq}(t)), x_q^I(t - \tau_{pq}(t)), x_q^J(t - \tau_{pq}(t)), x_q^K(t - \tau_{pq}(t))), g_q^l[t, u, x] \triangleq g_q^l(x_q^R(t - u), x_q^I(t - u), x_q^J(t - u), x_q^K(t - u))$. That is, system (1.1) can be decomposed into the following equivalent real system

$$\begin{cases} (x_p^l(t))' &= -c_p(t)x_p^l(t) + G_p^l(t, x(t)) + u_p^l(t), \quad p \in \Lambda, l \in E, t > 0, t \neq t_k, \\ \Delta(x^l(t_k)) &= \alpha_k x^l(t_k) + I_k^l(x^l(t_k)) + \omega_k^l, \quad k \in \mathbb{Z}, \\ x_p^l(s) &= \phi_p^l(s), \quad s \in (-\infty, 0]. \end{cases} \tag{2.1}$$

Firstly, let us consider the following system

$$\begin{cases} (x_p^l(t))' &= -c_p(t)x_p^l(t), \quad p \in \Lambda, l \in E, t > 0, t \neq t_k, \\ \Delta(x^l(t_k)) &= \alpha_k x^l(t_k), \quad k \in \mathbb{Z}. \end{cases} \tag{2.2}$$

If $U_k(t, s)$ is the Cauchy matrix for the following system

$$(x_p^I(t))' = -c_p(t)x_p^I(t), \quad t \in [t_{k-1}, t_k], \quad \{t_k\} \in B,$$

and if $\det(I + \alpha_k) \neq 0$, α_k and $\{t_k\}$ also are asymptotically almost automorphic, I is the Identity matrix of the same order with α_k , then according to [32, 33] the Cauchy matrix $W(t, s)$ for the system (2.2) is as follows

$$W(t, s) = \begin{cases} U_k(t, s), & t_{k-1} < s \leq t \leq t_k, \\ U_{k+1}(t, t_k^+) (I + \alpha_k) U_k(t_k, s), & t_{k-1} < s \leq t_k < t \leq t_{k+1}, \\ U_{k+1}(t, t_k^+) \prod_{j=k}^{i+1} [(I + \alpha_j) U_j(t_j, t_{j-1}^+)] (I + \alpha_i) U_i(t_i, s), & t_{i-1} < s \leq t_i < t_k < t \leq t_{k+1}. \end{cases}$$

By simple calculation, we have

$$\begin{aligned} W(t, t) &= I, \quad W(t_k^-, t_k) = W(t_k, t_k^-) = I, \\ W(t_k^+, s) &= (I + \alpha_k) W(t_k, s), \quad W(s, t_k^+) = W(s, t_k) (I + \alpha_k)^{-1}, \\ \frac{\partial W(t, s)}{\partial t} &= -c_p(t) W(t, s), \quad t \neq t_k, \\ \frac{\partial W(t, s)}{\partial s} &= W(t, s) c_p(s), \quad s \neq t_k. \end{aligned}$$

By further calculation, we can choose

$$W(t, s) = \begin{cases} \text{diag}(e^{-\int_s^t c_1(m)dm}, e^{-\int_s^t c_2(m)dm}, \dots, e^{-\int_s^t c_n(m)dm}), & t_{k-1} < s \leq t \leq t_k, \\ \text{diag}(e^{-\int_{t_k^+}^t c_1(m)dm}, e^{-\int_{t_k^+}^t c_2(m)dm}, \dots, e^{-\int_{t_k^+}^t c_n(m)dm}) \\ \times (I + \alpha_k) \text{diag}(e^{-\int_s^{t_k} c_1(m)dm}, e^{-\int_s^{t_k} c_2(m)dm}, \dots, e^{-\int_s^{t_k} c_n(m)dm}), & t_{k-1} < s \leq t_k < t \leq t_{k+1}, \\ \text{diag}(e^{-\int_{t_k^+}^t c_1(m)dm}, e^{-\int_{t_k^+}^t c_2(m)dm}, \dots, e^{-\int_{t_k^+}^t c_n(m)dm}) \\ \times \prod_{j=k}^{i+1} [(I + \alpha_j) \text{diag}(e^{-\int_{t_{j-1}^+}^{t_j} c_1(m)dm}, e^{-\int_{t_{j-1}^+}^{t_j} c_2(m)dm}, \dots, e^{-\int_{t_{j-1}^+}^{t_j} c_n(m)dm})] \\ (I + \alpha_i) \text{diag}(e^{-\int_s^{t_i} c_1(m)dm}, e^{-\int_s^{t_i} c_2(m)dm}, \dots, e^{-\int_s^{t_i} c_n(m)dm}), & t_{i-1} < t \leq t_i < t_k < s \leq t_{k+1}. \end{cases}$$

3 Existence and Uniqueness

In this section, by using general Lipschitz condition, contraction mapping principal and exponential dichotomy of linear dynamic equations, we obtain the existence and uniqueness of asymptotically almost automorphic solutions of system (1.1). We set

$\mathbb{X} = \{x \mid x = (x_1^R, x_1^I, x_1^J, x_1^K, \dots, x_n^R, x_n^I, x_n^J, x_n^K) \in C(\mathbb{R}, \mathbb{H}^{4n}) : x_p^I \text{ are asymptotically almost automorphic functions, } l \in E, p \in \Lambda\}$

and equip it with the norm $\|x\| = \max\{\sup_{p \in \Lambda} \sup_{t \in \mathbb{T}} |x_p^I(t)|, l \in E\}$, so \mathbb{X} is a Banach space.

For convenience, for any asymptotically almost automorphic function $f(t)$, we denote $f^- = \inf_{t \geq 0} |f(t)|$ and $f^+ = \sup_{t \leq 0} |f(t)|$.

Throughout this paper, we assume that the following conditions hold:

- (H₁) [32] $\det(I + \alpha_k) \neq 0$, the sequence α_k , and t_k are asymptotically almost automorphic;
- (H₂) [15] $c_p(t) > 0$ is asymptotically almost automorphic;
- (H₃) [7] $f_q(t), g_q(t), a_{pq}(t), b_{pq}(t), u_p(t), \tau_{pq}(t)$ are asymptotically almost automorphic functions, $p, q \in \Lambda$;
- (H₄) [32] The sequence I_k is asymptotic almost automorphic and there exists a positive constant L such that $|I_k^l(u) - I_k^l(v)| \leq L|u - v|$, $p, q \in \Lambda, k \in \mathbb{Z}, u, v \in \mathbb{R}$;
- (H₅) [7] For $q \in \Lambda, l \in E, f_q^l(0, 0, 0, 0) = g_q^l(0, 0, 0, 0) = 0$ and there exist positive constants α_q^l, β_q^l such that

$$\begin{aligned} & |f_q^l(x_p^R, x_p^I, x_p^J, x_p^K) - f_q^l(y_p^R, y_p^I, y_p^J, y_p^K)| \\ & \leq \alpha_q^R |x_p^R - y_p^R| + \alpha_q^I |x_p^I - y_p^I| + \alpha_q^J |x_p^J - y_p^J| + \alpha_q^K |x_p^K - y_p^K|, \\ & |g_q^l(x_q^R, x_q^I, x_q^J, x_q^K) - g_q^l(y_q^R, y_q^I, y_q^J, y_q^K)| \\ & \leq \beta_q^R |x_q^R - y_q^R| + \beta_q^I |x_q^I - y_q^I| + \beta_q^J |x_q^J - y_q^J| + \beta_q^K |x_q^K - y_q^K|; \end{aligned}$$

- (H₆) [15] There is a positive constants \tilde{K} for the delay kernel $k_{pq} : [0, +\infty) \rightarrow \mathbb{R}$, such that $\int_0^{+\infty} |k_{pq}(u)| du \leq \tilde{K}$.

Lemma 3 [15] Assume that assumptions (H₅) and (H₆) hold. For all $1 \leq i, j \leq n$, if $\phi(\cdot) \in AAA(\mathbb{R}, \mathbb{R}^n)$, then the function $\Phi_{ij} : t \mapsto \int_{-\infty}^t k_{ij}(t - s)h_j(\phi_j(s))ds$ belongs to $AAA(\mathbb{R}, \mathbb{R}^n)$.

Lemma 4 [33] If the conditions (H₀) – (H₂), (H₅) and (H₆) hold, then we have

- (1) For the Cauchy matrix $W(t, s)$ of the system (2.2) there exist positive constants K^* and ζ such that

$$|W(t, s)| \leq K^* e^{-\zeta(t-s)}, t \geq s, t, s \in \mathbb{T};$$

- (2) For any $\varepsilon > 0, t, s \in \mathbb{T}, t \geq s, |t - t_k| > \varepsilon > 0, |s - t_k| > 0, k \in \mathbb{Z}$ there exists a relatively dense set of \tilde{T} of asymptotically almost automorphic $c_i(t)$ and a positive constant \hat{K} such that for $\tau \in \tilde{T}$, it follows

$$|W(t + \tau, s + \tau) - W(t, s)| \leq \varepsilon \hat{K} e^{-\frac{\zeta}{2}(t-s)}.$$

Lemma 5 If the hypothesis (H₅) and (H₆) hold, $\tilde{\phi}_j(\cdot)$ belongs to $AAA(\mathbb{R}, \mathbb{X})$, for all $1 \leq i, j \leq n$, then the function $\Phi_{ij}(t) = \int_0^{+\infty} T_{ij}(s)f_j(\tilde{\phi}_j(t - s))ds$ belongs to $AAA(\mathbb{R}, \mathbb{X})$.

Proof Since

$$\begin{aligned} \int_0^{+\infty} T_{ij}(s)f_j(\tilde{\phi}_j(t - s))ds &= \int_t^{-\infty} T_{ij}(t - u)f_j(\tilde{\phi}_j(u))(-du) \\ &= \int_{-\infty}^t T_{ij}(t - u)f_j(\tilde{\phi}_j(u))du, \end{aligned} \tag{3.1}$$

by Lemma 3 we have $\int_{-\infty}^t T_{ij}(t - u)f_j(\tilde{\phi}_j(u))du \in AAA(\mathbb{R}, \mathbb{X})$. Then, $\int_0^{+\infty} T_{ij}(s)f_j(\tilde{\phi}_j(t - s))ds \in AAA(\mathbb{R}, \mathbb{X})$. This complete the proof.

For any $\varphi = (\varphi_1^R, \varphi_1^I, \varphi_1^J, \varphi_1^K, \dots, \varphi_n^R, \varphi_n^I, \varphi_n^J, \varphi_n^K)^T \in AAA(\mathbb{R}, \mathbb{R}^{4n})$, define the non-linear operator $(\Xi_\varphi)_p^l$ as follows

$$(\Xi_\varphi)_p^l(t) = \int_{-\infty}^t W(t, s)(U_\varphi)_p^l(s)ds + \sum_{t_k < t} W(t, t_k)(I_k^l(\varphi(t_k)) + \omega_k^l), \quad p \in \Lambda, l \in E, \tag{3.2}$$

where

$$\begin{aligned} (U_\varphi)_p^R(s) &= \sum_{q=1}^n \left(a_{pq}^R(s) f_q^R[s, \tau, \varphi] - a_{pq}^I(s) f_q^I[s, \tau, \varphi] \right. \\ &\quad \left. - a_{pq}^J(s) f_q^J[s, \tau, \varphi] - a_{pq}^K(s) f_q^K[s, \tau, \varphi] \right) \\ &\quad + \sum_{q=1}^n \left(b_{pq}^R(s) \int_0^{+\infty} k_{pq}(m) g_q^R[s, m, \varphi] dm \right. \\ &\quad \left. - b_{pq}^I(s) \int_0^{+\infty} k_{pq}(m) g_q^I[s, m, \varphi] dm \right. \\ &\quad \left. - b_{pq}^J(s) \int_0^{+\infty} k_{pq}(m) g_q^J[s, m, \varphi] dm \right. \\ &\quad \left. - b_{pq}^K(s) \int_0^{+\infty} k_{pq}(m) g_q^K[s, m, \varphi] dm \right) + u_p^R(s); \\ (U_\varphi)_p^I(s) &= \sum_{q=1}^n \left(a_{pq}^R(s) f_q^I[s, \tau, \varphi] + a_{pq}^I(s) f_q^R[s, \tau, \varphi] \right. \\ &\quad \left. + a_{pq}^J(s) f_q^K[s, \tau, \varphi] - a_{pq}^K(s) f_q^J[s, \tau, \varphi] \right) \\ &\quad + \sum_{q=1}^n \left(b_{pq}^R(s) \int_0^{+\infty} k_{pq}(m) g_q^I[s, m, \varphi] dm \right. \\ &\quad \left. + b_{pq}^I(s) \int_0^{+\infty} k_{pq}(m) g_q^R[s, m, \varphi] dm \right. \\ &\quad \left. + b_{pq}^J(s) \int_0^{+\infty} k_{pq}(m) g_q^K[s, m, \varphi] dm \right. \\ &\quad \left. - b_{pq}^K(s) \int_0^{+\infty} k_{pq}(m) g_q^J[s, m, \varphi] dm \right) + u_p^I(s); \\ (U_\varphi)_p^J(s) &= \sum_{q=1}^n \left(a_{pq}^R(s) f_q^J[s, \tau, \varphi] + a_{pq}^J(s) f_q^R[s, \tau, \varphi] \right. \\ &\quad \left. - a_{pq}^I(s) f_q^K[s, \tau, \varphi] + a_{pq}^K(s) f_q^I[s, \tau, \varphi] \right) \\ &\quad + \sum_{q=1}^n \left(b_{pq}^R(s) \int_0^{+\infty} k_{pq}(m) g_q^J[s, m, \varphi] dm \right. \\ &\quad \left. + b_{pq}^J(s) \int_0^{+\infty} k_{pq}(m) g_q^R[s, m, \varphi] dm \right. \end{aligned}$$

$$\begin{aligned}
 & - b_{pq}^I(s) \int_0^{+\infty} k_{pq}(m) g_q^K[s, m, \varphi] dm \\
 & + b_{pq}^K(s) \int_0^{+\infty} k_{pq}(m) g_q^I[s, m, \varphi] dm \Big) + u_p^J(s); \\
 (U_\varphi)_p^K(s) = & \sum_{q=1}^n \left(a_{pq}^R(s) f_q^K[s, \tau, \varphi] + a_{pq}^K(s) f_q^R[s, \tau, \varphi] \right. \\
 & \left. + a_{pq}^I(s) f_q^J[s, \tau, \varphi] - a_{pq}^J(s) f_q^I[s, \tau, \varphi] \right) \\
 & + \sum_{q=1}^n \left(b_{pq}^R(s) \int_0^{+\infty} k_{pq}(m) g_q^K[s, m, \varphi] dm \right. \\
 & + b_{pq}^K(s) \int_0^{+\infty} k_{pq}(m) g_q^R[s, m, \varphi] dm \\
 & + b_{pq}^I(s) \int_0^{+\infty} k_{pq}(m) g_q^J[s, m, \varphi] dm \\
 & \left. - b_{pq}^J(s) \int_0^{+\infty} k_{pq}(m) g_q^I[s, m, \varphi] dm \right) + u_p^K(s),
 \end{aligned}$$

where for $p \in \Lambda, l \in E, f_q^l[s, \tau, \varphi] \triangleq f_q^l(\varphi_q^R(s - \tau_{pq}(s)), \varphi_q^I(s - \tau_{pq}(s)), \varphi_q^J(s - \tau_{pq}(s)), \varphi_q^K(s - \tau_{pq}(s)))$, $g_q^l[s, m, \varphi] \triangleq g_q^l(\varphi_q^R(s - m), \varphi_q^I(s - m), \varphi_q^J(s - m), \varphi_q^K(s - m))$.

Now, we present our first theorem.

Theorem 1 Suppose that $(H_0) - (H_6)$ hold, then $(\Xi_\varphi)_p^l(t)$ maps $AAA(\mathbb{R}, \mathbb{H}^n)$ into itself, $p \in \Lambda, l \in E$.

Proof Step 1: we prove $\Theta_p^l(t) := \int_{-\infty}^t W(t, s)(U_\varphi)_p^l(s) ds$ maps $AAA(\mathbb{R}, \mathbb{H}^n)$ into itself, $p \in \Lambda, l \in E$.

First, by Lemmas 1–5, $(U_\varphi)_p^R$ belongs to $AAA(\mathbb{R}, \mathbb{H}^n)$. Then $(U_\varphi)_p^R(t) \in BC(\mathbb{R}, \mathbb{H}^n)$ and

$$\begin{aligned}
 | \Theta_p^R(t) | & \leq \int_{-\infty}^t | W(t, s)(U_\varphi)_p^R(s) | ds \\
 & \leq \| (U_\varphi)_p^R \| \int_{-\infty}^t K^* e^{-\zeta(t-s)} ds \leq \| (U_\varphi)_p^R \| \frac{K^*}{\zeta}.
 \end{aligned}$$

We see that $\int_{-\infty}^t W(t, s)(U_\varphi)_p^R(s) ds$ is continuous, absolutely convergent and bounded. As $(U_\varphi)_p^R(t)$ belongs to $AAA(\mathbb{R}, \mathbb{H}^n)$, there exist two functions $(\Lambda_p^R)(\cdot) \in AA(\mathbb{R}, \mathbb{H}^n)$ and $(\Omega_p^R)(\cdot) \in PC_0(\mathbb{R}, \mathbb{H}^n)$ such that $(U_\varphi)_p^R(\cdot) = (\Lambda_p^R)(\cdot) + (\Omega_p^R)(\cdot)$. So, we can rewrite Θ_p^R as

$$\Theta_p^R(t) = \int_{-\infty}^t W(t, s)(\Lambda_p^R)(s) ds + \int_{-\infty}^t W(t, s)(\Omega_p^R)(s) ds.$$

Let us consider the almost automorphy of

$$\Theta_{p1}^R : t \rightarrow \int_{-\infty}^t W(t, s)(\Lambda_p^R)(s) ds.$$

For every real numbers sequence $(s_n)_{n \in \mathbb{N}}$, by Definitions 2.2 and 2.3, we can extract a subsequence $(s_n)_{n \in \mathbb{N}}$ of $(s'_n)_{n \in \mathbb{N}}$ such that

$$\lim_{n \rightarrow +\infty} (\Lambda_p^R)(t + s_n) = (\Lambda_p^R)^1(t), \forall t \in \mathbb{R},$$

and

$$\lim_{n \rightarrow +\infty} (\Lambda_p^R)^1(t - s_n) = (\Lambda_p^R)(t), \forall t \in \mathbb{R}.$$

Let

$$\Theta_{p1}^{R1}(t) = \int_{-\infty}^t W(t, s)(\Lambda_p^R)^1(s)ds.$$

When $n \rightarrow +\infty$, we have

$$\begin{aligned} & | \Theta_{p1}^R(t + s_n) - \Theta_{p1}^{R1}(t) | \\ &= | \int_{-\infty}^{t+s_n} W(t + s_n, s)(\Lambda_p^R)(s)ds - \int_{-\infty}^t W(t, s)(\Lambda_p^R)^1(s)ds | \\ &= | \int_{-\infty}^t W(t + s_n, s + s_n)(\Lambda_p^R)(t + s_n)ds - \int_{-\infty}^t W(t + s_n, s + s_n)(\Lambda_p^R)^1(s)ds \\ &\quad + \int_{-\infty}^t W(t + s_n, s + s_n)(\Lambda_p^R)^1(s)ds - \int_{-\infty}^t W(t, s)(\Lambda_p^R)^1(s)ds | \\ &\leq | \int_{-\infty}^t W(t + s_n, s + s_n)(\Lambda_p^R)(t + s_n)ds - \int_{-\infty}^t W(t + s_n, s + s_n)(\Lambda_p^R)^1(s)ds | \\ &\quad + | \int_{-\infty}^t W(t + s_n, s + s_n)(\Lambda_p^R)^1(s)ds - \int_{-\infty}^t W(t, s)(\Lambda_p^R)^1(s)ds | \tag{3.3} \\ &\leq \int_{-\infty}^t | W(t + s_n, s + s_n) | | (\Lambda_p^R)(t + s_n) - (\Lambda_p^R)^1(s) | ds \\ &\quad + \int_{-\infty}^t | W(t + s_n, s + s_n) - W(t, s) | | (\Lambda_p^R)^1(s) | ds \\ &\leq \int_{-\infty}^t K^* e^{-\zeta(t-s)} | (\Lambda_p^R)(t + s_n) - (\Lambda_p^R)^1(s) | ds \\ &\quad + \int_{-\infty}^t \hat{K} \varepsilon e^{-\frac{\zeta}{2}(t-s)} | (\Lambda_p^R)^1(s) | ds \\ &\leq \int_{-\infty}^t K^* e^{-\zeta(t-s)} \varepsilon ds + \int_{-\infty}^t \hat{K} \varepsilon e^{-\frac{\zeta}{2}(t-s)} | (\Lambda_p^R)^1(s) | ds. \end{aligned}$$

By the Lebesgue-dominated convergence theorem, we get that for all $t \in \mathbb{R}$

$$\lim_{n \rightarrow +\infty} \Theta_{p1}^R(t + s_n) = \Theta_{p1}^{R1}(t).$$

Also, we can get that

$$\lim_{n \rightarrow +\infty} \Theta_{p1}^{R1}(t - s_n) = \Theta_{p1}^R(t),$$

which implies that $\Theta_{p1}^R \in AA(\mathbb{R}, \mathbb{H}^n)$.

Similarly, we can get that $\Theta_{p1}^l \in AA(\mathbb{R}, \mathbb{H}^n), l \in \{I, J, K\}$.

Second, we now turn to prove $\Theta_{p2}^l : t \rightarrow \int_{-\infty}^t W(t, s)(\Omega_p^l(s))ds \in PC_0(\mathbb{R}, \mathbb{H}^n), l \in \{R, I, J, K\}$. Since $(\Omega_p^l) \in PC_0(\mathbb{R}, \mathbb{H}^n)$, by Lemma 3 we have $\Theta_{p2}^l \in PC(\mathbb{R}, \mathbb{H}^n)$ and $\lim_{t \rightarrow +\infty} |\int_{-\infty}^t W(t, s)(\Omega_p^l(s))ds| = 0$.

Based on the Lebesgue-dominated convergence theorem, we can get

$$\lim_{t \rightarrow +\infty} \int_{-\infty}^t W(t, s)(\Omega_p^l(s))ds = 0,$$

which implies that $\Theta_{p2}^l \in PC_0(\mathbb{R}, \mathbb{H}^n)$. Then, $\Theta_p^l(t) := \int_{-\infty}^t W(t, s)(U_\varphi)_p^l(s)ds$ maps $AAA(\mathbb{R}, \mathbb{H}^n)$ into itself.

Step 2: we prove $\sum_{t_k < t} W(t, t_k)(I_k^l(\varphi(t_k)) + \omega_k^l) \in AAA(\mathbb{R}, \mathbb{H}^n)$.

From (H_1) , (H_4) and Lemma 3, we have $(I_k^l(\varphi(t_k)) + \omega_k^l) \in AAA(\mathbb{R}, \mathbb{H}^n)$ and then $(I_k^l(\varphi(t_k)) + \omega_k^l) \in BC(\mathbb{R}, \mathbb{H}^n)$. For $\varpi = \inf_{k \in \mathbb{Z}} (t_{k+1} - t_k) > 0$, we have

$$\begin{aligned} |\sum_{t_k < t} W(t, t_k)(I_k^l(\varphi(t_k)) + \omega_k^l)| &\leq \|I_k^l(\varphi(t_k)) + \omega_k^l\| \sum_{t_k < t} K^* e^{-\zeta(t-t_k)} \\ &\leq \|I_k^l(\varphi(t_k)) + \omega_k^l\| \frac{K^*}{1 - e^{-\zeta\varpi}}. \end{aligned} \tag{3.4}$$

Then, $\sum_{t_k < t} W(t, t_k)(I_k^l(\varphi(t_k)) + \omega_k^l)$ is continuous, bounded and absolutely convergent.

From assumption (H_4) , for $I_k^l(\varphi(t_k)) \in AAA(\mathbb{R}, \mathbb{R}^n)$, by the definition, it can be rewritten as

$$I_k^l(\varphi(t_k)) = I_{k1}^l(\varphi(t_k)) + I_{k2}^l(\varphi(t_k)),$$

where

$$I_{k1}^l(\varphi(t_k)) \in AA(\mathbb{R}, \mathbb{H}^n), \quad I_{k2}^l(\varphi(t_k)) \in PC_0(\mathbb{R}, \mathbb{H}^n).$$

Then

$$\begin{aligned} \sum_{t_k < t} W(t, t_k)(I_k^l(\varphi(t_k)) + \omega_k^l) &= \sum_{t_k < t} W(t, t_k)(I_{k1}^l(\varphi(t_k)) + \omega_k^l) \\ &\quad + \sum_{t_k < t} W(t, t_k)(I_{k2}^l(\varphi(t_k))). \end{aligned}$$

For every real sequence $(t_n)_{n \in \mathbb{N}}$, by Definitions 2.2 and 2.3, we can extract a subsequence $(t_{n_k})_{n_k \in \mathbb{N}}$ of $(t_k)_{k \in \mathbb{N}}$ such that

$$\begin{aligned} \lim_{n_k \rightarrow +\infty} I_{k1}^l(\varphi(t_k + t_{n_k})) &= \tilde{I}_{k1}^l(\varphi(t_k)) \quad \forall t \in \mathbb{R}, \\ \lim_{n_k \rightarrow +\infty} \tilde{I}_{k1}^l(\varphi(t_k - t_{n_k})) &= I_{k1}^l(\varphi(t_k)), \quad \forall t \in \mathbb{R}. \end{aligned}$$

Note that

$$\begin{aligned} & \left| \sum_{t_k < t + t_{n_k}} W(t + t_{n_k}, t_k)(I_{k1}^l(\varphi(t_k)) + \omega_k^l) \right. \\ & \left. - \sum_{t_k < t} W(t, t_k)(\tilde{I}_{k1}^l(\varphi(t_k)) + \omega_k^l) \right| \\ &= \left| \sum_{t_k < t} W(t + t_{n_k}, t_k + t_{n_k})(I_{k1}^l(\varphi(t_k + t_{n_k})) + \omega_k^l) \right. \\ & \left. - \sum_{t_k < t} W(t, t_k)(\tilde{I}_{k1}^l(\varphi(t_k)) + \omega_k^l) \right| \\ &= \left| \sum_{t_k < t} W(t + t_{n_k}, t_k + t_{n_k})(I_{k1}^l(\varphi(t_k + t_{n_k})) + \omega_k^l) \right. \\ & \left. - \sum_{t_k < t} W(t + t_{n_k}, t_k + t_{n_k})(\tilde{I}_{k1}^l(\varphi(t_k)) + \omega_k^l) \right. \\ & \left. + \sum_{t_k < t} W(t + t_{n_k}, t_k + t_{n_k})(\tilde{I}_{k1}^l(\varphi(t_k)) + \omega_k^l) \right. \\ & \left. - \sum_{t_k < t} W(t, t_k)(\tilde{I}_{k1}^l(\varphi(t_k)) + \omega_k^l) \right| \\ &\leq \left| \sum_{t_k < t} W(t + t_{n_k}, t_k + t_{n_k})(I_{k1}^l(\varphi(t_k + t_{n_k})) + \omega_k^l) \right. \\ & \left. - \sum_{t_k < t} W(t + t_{n_k}, t_k + t_{n_k})(\tilde{I}_{k1}^l(\varphi(t_k)) + \omega_k^l) \right| \\ & \left. + \left| \sum_{t_k < t} W(t + t_{n_k}, t_k + t_{n_k})(\tilde{I}_{k1}^l(\varphi(t_k)) + \omega_k^l) \right. \right. \\ & \left. \left. - \sum_{t_k < t} W(t, t_k)(\tilde{I}_{k1}^l(\varphi(t_k)) + \omega_k^l) \right| \right. \\ &\leq \sum_{t_k < t} |W(t + t_{n_k}, t_k + t_{n_k})| |I_{k1}^l(\varphi(t_k + t_{n_k})) + \omega_k^l - (\tilde{I}_{k1}^l(\varphi(t_k)) + \omega_k^l)| \\ & \quad + \sum_{t_k < t} |W(t + t_{n_k}, t_k + t_{n_k}) - W(t, t_k)| |(\tilde{I}_{k1}^l(\varphi(t_k)) + \omega_k^l)| \\ &\leq \sum_{t_k < t} K^* e^{-\zeta(t-t_k)} |I_{k1}^l(\varphi(t_k + t_{n_k})) - \tilde{I}_{k1}^l(\varphi(t_k))| \\ & \quad + \sum_{t_k < t} \hat{K} \varepsilon e^{-\frac{\zeta}{2}(t-t_k)} | \tilde{I}_{k1}^l(\varphi(t_k)) + \omega_k^l | \\ &\leq \sum_{t_k < t} K^* e^{-\zeta(t-t_k)} \varepsilon + \sum_{t_k < t} \hat{K} \varepsilon e^{-\frac{\zeta}{2}(t-t_k)} | \tilde{I}_{k1}^l(\varphi(t_k)) + \omega_k^l |. \end{aligned} \tag{3.5}$$

Since $|\tilde{I}_{k1}^l(\varphi(t_k)) + \omega_k^l|$ is bounded, we have

$$\lim_{n_k \rightarrow +\infty} \sum_{t_k < t + t_{n_k}} W(t + t_{n_k}, t_k)(I_{k1}^l(\varphi(t_k)) + \omega_k^l) = \sum_{t_k < t} W(t, t_k)(\tilde{I}_{k1}^l(\varphi(t_k)) + \omega_k^l),$$

and

$$\lim_{n_k \rightarrow +\infty} \sum_{t_k < t} W(t + t_{n_k}, t_k + t_{n_k})(I_{k1}^l(\varphi(t_k + t_{n_k})) + \omega_k^l) = \sum_{t_k < t} W(t, t_k)(\tilde{I}_{k1}^l(\varphi(t_k)) + \omega_k^l).$$

Similarly, we have

$$\sum_{t_k < t - t_{n_k}} W(t - t_{n_k}, t_k)(\tilde{I}_{k1}^l(\varphi(t_k)) + \omega_k^l) = \sum_{t_k < t} W(t - t_{n_k}, t_k - t_{n_k})(I_{k1}^l(\varphi(t_k - t_{n_k})) + \omega_k^l),$$

and

$$\lim_{n_k \rightarrow +\infty} \sum_{t_k < t} W(t - t_{n_k}, t_k - t_{n_k})(\tilde{I}_{k1}^l(\varphi(t_k - t_{n_k})) + \omega_k^l) = \sum_{t_k < t} W(t, t_k)(I_{k1}^l(\varphi(t_k)) + \omega_k^l).$$

So, $\sum_{t_k < t} W(t, t_k)(I_{k1}^l(\varphi(t_k)) + \omega_k^l) \in AA(\mathbb{R}, \mathbb{H}^n)$.

On the other hand, as $\sum_{t_k < t} |W(t, t_k)| < \infty$ and $I_{k2}^l(\varphi(t_k)) \in PC_0(\mathbb{R}, \mathbb{H}^n)$, we have

$$\lim_{t_k \rightarrow +\infty} \sum_{t_k < t} |W(t, t_k)I_{k2}^l(\varphi(t_k))| = 0,$$

which implies that $\sum_{t_k < t} W(t, t_k)(I_{k2}^l(\varphi(t_k))) \in PC_0(\mathbb{R}, \mathbb{R}^n)$. Hence, $\sum_{t_k < t} W(t, t_k)(I_k^l(\varphi(t_k)) + \omega_k^l) \in AAA(\mathbb{R}, \mathbb{H}^n)$.

From Steps 1 and 2, we have that $(\Xi_\varphi)_p^l(t)$ maps $AAA(\mathbb{R}, \mathbb{H}^n)$ into itself. The proof is complete.

Theorem 2 Assume that $(H_0) - (H_6)$ hold and

(H_7)

$$\eta = \sup_{t \in \mathbb{R}} \left\{ \frac{K^*}{\zeta} \max_{1 \leq p \leq n} \Gamma_p + \frac{K^*L}{1 - e^{-\zeta\varpi}} \right\} < 1,$$

$$\varrho - \zeta = \frac{\ln(1 + K^*L)}{\varpi} + K^* \sum_{p=1}^n \Gamma_p - \zeta < 0,$$

where K^* defined as in Lemma 3, $\varpi = \inf_{k \in \mathbb{Z}} (t_{k+1} - t_k) > 0$, $\Gamma_p = A_p^* + B_p^*$, $p \in \Lambda$,

$$A_p^* = \sum_{q=1}^n (a_{pq}^{R+} + a_{pq}^{I+} + a_{pq}^{J+} + a_{pq}^{K+})(\alpha_q^R + \alpha_q^I + \alpha_q^J + \alpha_q^K), p \in \Lambda,$$

$$B_p^* = \sum_{q=1}^n \tilde{K}(b_{pq}^{R+} + b_{pq}^{I+} + b_{pq}^{J+} + b_{pq}^{K+})(\beta_q^R + \beta_q^I + \beta_q^J + \beta_q^K), p \in \Lambda.$$

Then, there exists a unique asymptotic almost automorphic solution

$$\varphi = (\varphi_1^R, \varphi_1^I, \varphi_1^J, \varphi_1^K, \dots, \varphi_n^R, \varphi_n^I, \varphi_n^J, \varphi_n^K)^T \in AAA(\mathbb{R}, (\mathbb{R})^{4n})$$

of system (1.1) in the region

$$S^*(\varphi_0, \eta) = \{ \varphi \in AAA(\mathbb{R}, \mathbb{R}^{4n}); \|\varphi_p^l - (\varphi_0)_p^l\| \leq \frac{\eta}{1-\eta} \bar{R}, \quad l \in \{R, I, J, K\}, p \in \Lambda \},$$

where

$$\bar{R} = K^* \eta^* \left(\frac{1}{\zeta} + \frac{1}{1-e^{-\zeta}} \right), \quad \eta^* = \max \left\{ \max_{1 \leq i \leq n} |u_p^l(s)|, \max_{t_k < t} |\omega_k^l| \right\},$$

$$\varphi_0(t) = \begin{pmatrix} \int_{-\infty}^t W(t, s) u_1^l(s) ds + \sum_{t_k < t} W(t, t_k) \omega_1^l \\ \int_{-\infty}^t W(t, s) u_2^l(s) ds + \sum_{t_k < t} W(t, t_k) \omega_2^l \\ \vdots \\ \int_{-\infty}^t W(t, s) u_n^l(s) ds + \sum_{t_k < t} W(t, t_k) \omega_n^l \end{pmatrix}_{n \times 1},$$

$$(\varphi_0)_p^l(t) = \int_{-\infty}^t W(t, s) u_p^l(s) ds + \sum_{t_k < t} W(t, t_k) \omega_p^l, \quad p \in \Lambda, \quad l \in \{R, I, J, K\}.$$

Proof First, we calculate the norm of $(\varphi_0)_p^l$,

$$\begin{aligned} \|(\varphi_0)_p^l(t)\| &= \sup_{t \in \mathbb{R}} \left\{ \max_{1 \leq p \leq n} \left\{ \int_{-\infty}^t |W(t, s)| |u_p^l(s)| ds + \sum_{t_k < t} |W(t, t_k)| |\omega_k^l| \right\} \right\} \\ &\leq \sup_{t \in \mathbb{R}} \left\{ \max_{1 \leq p \leq n} \left\{ \int_{-\infty}^t K^* e^{-\zeta(t-s)} |u_p^l(s)| ds + \sum_{t_k < t} K e^{-\zeta(t-t_k)} |\omega_k^l| \right\} \right\} \quad (3.6) \\ &\leq K^* \eta^* \left(\frac{1}{\zeta} + \frac{1}{1-e^{-\zeta}} \right) = \bar{R}. \end{aligned}$$

For $\varphi^l \in S^*(\varphi_0, \eta)$, we have

$$\|(\varphi)_p^l(t)\|_\infty \leq \|(\varphi)_p^l(t) - (\varphi_0)_p^l(t)\| + \|(\varphi_0)_p^l(t)\| \leq \frac{\eta}{1-\eta} \bar{R} + \bar{R} = \frac{\bar{R}}{1-\eta}.$$

Obviously, $S^*(\varphi_0, \eta)$ is a closed convex subset of $AAA(\mathbb{R}, \mathbb{H}^n)$.

For $\varphi(t) \in S^*(\varphi_0, \eta)$ and $(U_\varphi)_p^l(s)$ defined as (3.2), by the above estimate and (H_7) we have

$$\begin{aligned} &\|(\Xi_\varphi)_p^R(t) - (\varphi_0)_p^R(t)\| \\ &\leq \sup_{t \in \mathbb{R}} \left\{ \max_{1 \leq p \leq n} \left\{ \int_{-\infty}^t |W(t, s)| \left| \sum_{q=1}^n (a_{pq}^R(s) f_q^R[s, \tau, \varphi] - a_{pq}^I(s) f_q^I[s, \tau, \varphi] \right. \right. \right. \\ &\quad \left. \left. - a_{pq}^J(s) f_q^J[s, \tau, \varphi] - a_{pq}^K(s) f_q^K[s, \tau, \varphi] \right) \right. \\ &\quad \left. + \sum_{q=1}^n (b_{pq}^R(s) \int_0^{+\infty} k_{pq}(m) g_q^R[s, m, \varphi] dm - b_{pq}^I(s) \int_0^{+\infty} k_{pq}(m) g_q^I[s, m, \varphi] dm \right. \\ &\quad \left. - b_{pq}^J(s) \int_0^{+\infty} k_{pq}(m) g_q^J[s, m, \varphi] dm - b_{pq}^K(s) \int_0^{+\infty} k_{pq}(m) g_q^K[s, m, \varphi] dm) \right\} ds \end{aligned}$$

$$\begin{aligned}
 & + \sum_{t_k < t} \left\{ |W(t, t_k)| |I_k^R(\varphi(t_k))| \right\} \\
 \leq & \sup_{t \in R} \left\{ \max_{1 \leq p \leq n} \left\{ \int_{-\infty}^t K^* e^{-\zeta(t-s)} \left| \sum_{q=1}^n [|a_{pq}^R(s)| |f_q^R[s, \tau, \varphi]| + |a_{pq}^I(s)| |f_q^I[s, \tau, \varphi]| \right. \right. \right. \\
 & + |a_{pq}^J(s)| |f_q^J[s, \tau, \varphi]| + |a_{pq}^K(s)| |f_q^K[s, \tau, \varphi]| \left. \left. \left. \right. \right. \\
 & + \sum_{q=1}^n [|b_{pq}^R(s)| \int_0^{+\infty} |k_{pq}(m)| |g_q^R[s, m, \varphi]| dm \\
 & + |b_{pq}^I(s)| \int_0^{+\infty} |k_{pq}(m)| |g_q^I[s, m, \varphi]| dm \\
 & + |b_{pq}^J(s)| \int_0^{+\infty} |k_{pq}(m)| |g_q^J[s, m, \varphi]| dm \\
 & + |b_{pq}^K(s)| \int_0^{+\infty} |k_{pq}(m)| |g_q^K[s, m, \varphi]| dm \left. \right] ds \\
 & + \sum_{t_k < t} K^* e^{-\zeta(t-t_k)} |I_k^R(\varphi(t_k))| \left. \right\} \\
 \leq & \sup_{t \in R} \left\{ \max_{1 \leq p \leq N} \left\{ \int_{-\infty}^t K^* e^{-\zeta(t-s)} \left| \sum_{q=1}^n (a_{pq}^{R+} + a_{pq}^{I+} + a_{pq}^{J+} + a_{pq}^{K+}) (\alpha_q^R | \varphi_q^R(s - \tau_{pq}(s)) | \right. \right. \right. \\
 & + \alpha_q^I | \varphi_q^I(s - \tau_{pq}(s)) | + \alpha_q^J | \varphi_q^J(s - \tau_{pq}(s)) | + \alpha_q^K | \varphi_q^K(s - \tau_{pq}(s)) | \left. \left. \right. \right. \\
 & + \sum_{q=1}^n \int_0^{+\infty} |k_{pq}(m)| (b_{pq}^{R+} + b_{pq}^{I+} + b_{pq}^{J+} + b_{pq}^{K+}) (\beta_q^R | \varphi_q^R(s - m) | \\
 & + \beta_q^I | \varphi_q^I(s - m) | + \beta_q^J | \varphi_q^J(s - m) | + \beta_q^K | \varphi_q^K(s - m) |) dm \left. \right. \left. \right. ds \\
 & + \sum_{t_k < t} K^* e^{-\zeta(t-t_k)} |I_k^R(\varphi(t_k))| \left. \right\} \\
 \leq & \sup_{t \in R} \left\{ \max_{1 \leq p \leq N} \left\{ \int_{-\infty}^t K^* e^{-\zeta(t-s)} \left| \sum_{q=1}^n \right. \right. \right. \\
 & \times (a_{pq}^{R+} + a_{pq}^{I+} + a_{pq}^{J+} + a_{pq}^{K+}) (\alpha_q^R + \alpha_q^I + \alpha_q^J + \alpha_q^K) \|\varphi\| \\
 & + \sum_{q=1}^n \tilde{K} (b_{pq}^{R+} + b_{pq}^{I+} + b_{pq}^{J+} + b_{pq}^{K+}) (\beta_q^R + \beta_q^I + \beta_q^J + \beta_q^K) \|\varphi\| \left. \right. \left. \right. ds \\
 & + \sum_{t_k < t} K^* e^{-\zeta(t-t_k)} L | \varphi(t_k) | \left. \right\} \\
 \leq & \sup_{t \in R} \left\{ \frac{K^*}{\zeta} \max_{1 \leq q \leq N} \left\{ \left[\sum_{q=1}^n (a_{pq}^{R+} + a_{pq}^{I+} + a_{pq}^{J+} + a_{pq}^{K+}) (\alpha_q^R + \alpha_q^I + \alpha_q^J + \alpha_q^K) \|\varphi\| \right. \right. \right. \\
 & + \sum_{q=1}^n \tilde{K} (b_{pq}^{R+} + b_{pq}^{I+} + b_{pq}^{J+} + b_{pq}^{K+}) (\beta_q^R + \beta_q^I + \beta_q^J + \beta_q^K) \|\varphi\| + \frac{K^* L}{1 - e^{-\zeta \varpi}} \|\varphi\| \left. \left. \right. \right\}
 \end{aligned}$$

$$\begin{aligned} &\leq \sup_{t \in \mathbb{R}} \left\{ \frac{K^*}{\zeta} \max_{1 \leq p \leq n} \Gamma_p + \frac{K^* L}{1 - e^{-\zeta}} \right\} \|\varphi\| \\ &= \eta \|\varphi\| \leq \eta \frac{\tilde{R}}{1 - \eta}. \end{aligned}$$

Thus, $(\Xi_\varphi)_p^R \in S^*(\varphi_0, \eta)$.

Next, we prove that $(\Xi_\varphi)_p^R$ is a contraction map. For any

$$\varphi = (\varphi_1^R, \varphi_1^I, \varphi_1^J, \varphi_1^K, \dots, \varphi_n^R, \varphi_n^I, \varphi_n^J, \varphi_n^K)$$

and

$$\varphi_* = (\varphi_{*1}^R, \varphi_{*1}^I, \varphi_{*1}^J, \varphi_{*1}^K, \dots, \varphi_{*n}^R, \varphi_{*n}^I, \varphi_{*n}^J, \varphi_{*n}^K)$$

in the region $S^*(\varphi_0, \eta)$ ($l \in \{R, I, J, K\}$), we have

$$\begin{aligned} &\|(\Xi_\varphi)_p^R - (\Xi_{\varphi_*})_p^R\| \\ &\leq \sup_{t \in \mathbb{R}} \left\{ \max_{1 \leq i \leq n} \left\{ \int_{-\infty}^t |W(t, s)| \|(U_\varphi)_p^R(s) - (U_{\varphi_*})_p^R(s)\| ds \right. \right. \\ &\quad \left. \left. + \sum_{t_k < t} |W(t, t_k)| \|(I_k^R(\varphi(t_k)) + \omega_k^R) - (I_k^R(\varphi_*(t_k)) + \omega_k^R)\| \right\} \right\} \\ &\leq \sup_{t \in \mathbb{R}} \left\{ \max_{1 \leq p \leq n} \left\{ \int_{-\infty}^t K^* e^{-\zeta(t-s)} \left[\sum_{q=1}^n [|a_{pq}^R(s)| |f_q^R[s, \tau, \varphi] - f_q^R[s, \tau, \varphi_*]| \right. \right. \right. \\ &\quad \left. \left. + |a_{pq}^I(s)| |f_q^I[s, \tau, \varphi] - f_q^I[s, \tau, \varphi_*]| + |a_{pq}^J(s)| |f_q^J[s, \tau, \varphi] - f_q^J[s, \tau, \varphi_*]| \right. \right. \\ &\quad \left. \left. + |a_{pq}^K(s)| |f_q^K[s, \tau, \varphi] - f_q^K[s, \tau, \varphi_*]| \right] \right. \\ &\quad \left. + \sum_{q=1}^n [|b_{pq}^R(s)| \int_0^{+\infty} |k_{pq}(m)| |g_q^R[s, m, \varphi] - g_q^R[s, m, \varphi_*]| dm \right. \\ &\quad \left. + |b_{pq}^I(s)| \int_0^{+\infty} |k_{pq}(m)| |g_q^I[s, m, \varphi] - g_q^I[s, m, \varphi_*]| dm \right. \\ &\quad \left. + |b_{pq}^J(s)| \int_0^{+\infty} |k_{pq}(m)| |g_q^J[s, m, \varphi] - g_q^J[s, m, \varphi_*]| dm \right. \\ &\quad \left. + |b_{pq}^K(s)| \int_0^{+\infty} |k_{pq}(m)| |g_q^K[s, m, \varphi] - g_q^K[s, m, \varphi_*]| dm \right] ds \\ &\quad \left. + \sum_{t_k < t} K^* e^{-\zeta(t-t_k)} |I_k^R(\varphi(t_k)) - I_k^R(\varphi_*(t_k))| \right\} \\ &\leq \sup_{t \in \mathbb{R}} \left\{ \max_{1 \leq p \leq n} \left\{ \int_{-\infty}^t K^* e^{-\zeta(t-s)} \left[\sum_{q=1}^n (a_{pq}^{R+} + a_{pq}^{I+} + a_{pq}^{J+} + a_{pq}^{K+}) (\alpha_q^R + \alpha_q^I + \alpha_q^J + \alpha_q^K) \right. \right. \right. \\ &\quad \left. \left. + \sum_{q=1}^n \tilde{K} (b_{pq}^{R+} + b_{pq}^{I+} + b_{pq}^{J+} + b_{pq}^{K+}) (\beta_q^R + \beta_q^I + \beta_q^J + \beta_q^K) \right] ds \right. \\ &\quad \left. + \sum_{t_k < t} K^* e^{-\zeta(t-t_k)} L \|\varphi - \varphi_*\| \right\} \end{aligned}$$

$$\begin{aligned} &\leq \sup_{t \in \mathbb{R}} \left\{ \frac{K^*}{\zeta} \max_{1 \leq p \leq n} \left[\sum_{q=1}^n (a_{pq}^{R+} + a_{pq}^{I+} + a_{pq}^{J+} + a_{pq}^{K+})(\alpha_q^R + \alpha_q^I + \alpha_q^J + \alpha_q^K) \right. \right. \\ &\quad + \sum_{q=1}^n \tilde{K} (b_{pq}^{R+} + b_{pq}^{I+} + b_{pq}^{J+} + b_{pq}^{K+})(\beta_q^R + \beta_q^I + \beta_q^J + \beta_q^K) \\ &\quad \left. \left. + \frac{K^*L}{1 - e^{-\zeta}} \right\} \|\varphi - \varphi_*\| \\ &= \eta \|\varphi - \varphi_*\|. \end{aligned}$$

By (H7), $\eta < 1$ and then $(\Xi_\varphi)_p^R$ is a contraction map.

According to the Banach fixed point theorem, $(\Xi_\varphi)_p^R$ has a unique fixed point.

Similarly, for $l \in \{I, J, K\}$, we can prove that $(\Xi_\varphi)_p^l \in S^*(\varphi_0, \eta)$ and $(\Xi_\varphi)_p^l$ is a contraction map and has a unique fixed point. Then there exists a unique asymptotic almost automorphic solution of system (1.1) in $S^*(\varphi_0, \eta)$. This completes the proof. \square

4 Global exponential stability

In this section, by utilizing generalized Gronwall–Bellman inequality technique, we shall discuss the global exponential stability of the unique asymptotically almost automorphic solution.

Definition 4 Let $x(t) = (x_1^R, x_1^I, x_1^J, x_1^K, \dots, x_n^R, x_n^I, x_n^J, x_n^K)$ be a solution of (1.1) with the initial value $\varphi = (\varphi_1^R, \varphi_1^I, \varphi_1^J, \varphi_1^K, \dots, \varphi_n^R, \varphi_n^I, \varphi_n^J, \varphi_n^K) \in C((-\infty, 0], \mathbb{R}^{4n})$ and $y(t) = (y_1^R, y_1^I, y_1^J, y_1^K, \dots, y_n^R, y_n^I, y_n^J, y_n^K)$ be an arbitrary solution of system (1.1) with the initial value $\psi = (\psi_1^R, \psi_1^I, \psi_1^J, \psi_1^K, \dots, \psi_n^R, \psi_n^I, \psi_n^J, \psi_n^K) \in C((-\infty, 0], \mathbb{R}^{4n})$. If there exist positive constants k and M such that

$$\|x(t) - y(t)\| \leq M \|\varphi - \psi\| e^{-kt}, \quad t > 0,$$

where

$$\|x(t) - y(t)\| = \max_{p \in \Lambda, t \in \mathbb{R}} \{|x_p^l(t) - y_p^l(t)|, l \in E\}.$$

Then the solution $x(t)$ of system (1.1) is said to be globally exponentially stable.

Theorem 3 *If (H0) – (H7) hold, then the unique asymptotic almost automorphic solution of system (1.1) is globally exponentially stable.*

Proof By Theorem 2, $(\Xi_\varphi)_p^l$ has a fixed point φ . Then, for all $t \in \mathbb{R}$, the fixed point φ satisfies the following integral system

$$\varphi(t) = \int_{-\infty}^t W(t, s)(U_\varphi)_p^l(s)ds + \sum_{t_k < t} W(t, t_k)(I_k^l(\varphi(t_k)) + \omega_k^l), \quad p \in \Lambda, l \in E.$$

Fixed $t = a, a \neq t_k, k \in \mathbb{Z}$, we have

$$\varphi(a) = \int_{-\infty}^a W(a, s)(U_\varphi)_p^l(s)ds + \sum_{t_k < a} W(a, t_k)(I_k^l(\varphi(t_k)) + \omega_k^l)$$

and

$$\begin{aligned} \varphi(t) &= \int_{-\infty}^a W(t, s)(U_\varphi)_p^l(s)ds + \sum_{t_k < a} W(t, t_k)(I_k^l(\varphi(t_k)) + \omega_k^l) \\ &\quad + \int_a^t W(t, s)(U_\varphi)_p^l(s)ds + \sum_{a < t_k < t} W(t, t_k)(I_k^l(\varphi(t_k)) + \omega_k^l) \\ &= W(t, a)\varphi(a) + \int_a^t W(t, s)(U_\varphi)_p^l(s)ds + \sum_{a < t_k < t} W(t, t_k)(I_k^l(\varphi(t_k)) + \omega_k^l). \end{aligned} \tag{4.1}$$

Second, by Theorem 2, we know that system (1.1) has an asymptotically almost automorphic solution $u(t)$. By using the integral form of system (1.1), if $t > \sigma, \sigma \neq t_k, k \in \mathbb{Z}$, then

$$u(t) = W(t, \sigma)u(\sigma) + \int_\sigma^t W(t, s)(U_u)_p^l(s)ds + \sum_{\sigma < t_k < t} W(t, t_k)(I_k^l(u(t_k)) + \omega_k^l). \tag{4.2}$$

Let $u(t) = u(t; \sigma, \varphi)$ and $v(t) = v(t; \sigma, \psi)$ be two solutions of system (1.1), then

$$\begin{aligned} u(t) &= W(t, \sigma)u(\sigma) + \int_\sigma^t W(t, s)(U_u)_p^l(s)ds + \sum_{\sigma < t_k < t} W(t, t_k)(I_k^l(u(t_k)) + \omega_k^l), \\ v(t) &= W(t, \sigma)v(\sigma) + \int_\sigma^t W(t, s)(U_v)_p^l(s)ds + \sum_{\sigma < t_k < t} W(t, t_k)(I_k^l(v(t_k)) + \omega_k^l). \end{aligned} \tag{4.3}$$

Therefore,

$$\begin{aligned} \|u(t) - v(t)\| &\leq \|W(t, \sigma)(\varphi(t) - \psi(t))\| + \left\| \int_\sigma^t W(t, s)((U_u)_p^l(s) - (U_v)_p^l(s))ds \right\| \\ &\quad + \left\| \sum_{\sigma < t_k < t} W(t, t_k)[I_k^l(u(t_k)) - I_k^l(v(t_k))] \right\| \\ &\leq \|W(t, \sigma)\|\|\varphi - \psi\| + \int_\sigma^t \|W(t, s)\| \|((U_u)_p^l(s) - (U_v)_p^l(s))\| ds \\ &\quad + \sum_{\sigma < t_k < t} \|W(t, t_k)\| \| [I_k^l(u(t_k)) - I_k^l(v(t_k))] \| \\ &\leq K^* e^{-\zeta(t-\sigma)} \|\varphi - \psi\| + \int_\sigma^t K^* e^{-\zeta(t-\sigma)} \sum_{p=1}^n \Gamma_p \|u(s) - v(s)\| ds \\ &\quad + \sum_{\sigma < t_k < t} K^* e^{-\zeta(t-t_k)} L \|u(t_k) - v(t_k)\|, \end{aligned} \tag{4.4}$$

then

$$\begin{aligned} e^{\zeta t} \|u(t) - v(t)\| &\leq K^* e^{\zeta \sigma} \|\varphi - \psi\| + \int_\sigma^t K^* \sum_{p=1}^n \Gamma_p e^{\zeta s} \|u(s) - v(s)\| ds \\ &\quad + \sum_{\sigma < t_k < t} K^* e^{\zeta t_k} L \|u(t_k) - v(t_k)\|. \end{aligned} \tag{4.5}$$

Let $\mu(t) = e^{\zeta t} \|u(t) - v(t)\|$, Eq. (4.5) can be rewritten in the following form:

$$\mu(t) \leq K^* \mu(\sigma) + \int_{\sigma}^t K^* \sum_{p=1}^n \Gamma_p \mu(s) ds + \sum_{0 < t_k < t} K^* L \mu(t_k). \tag{4.6}$$

By the generalized Gronwall–Bellman inequality, we have

$$\begin{aligned} \mu(t) &\leq K^* \mu(\sigma) \prod_{\sigma < t_k < t} (1 + K^* L) e^{\int_{\sigma}^t K^* \sum_{p=1}^n \Gamma_p ds} \\ &= K^* \mu(\sigma) \prod_{\sigma < t_k < t} (1 + K^* L) e^{K^* \sum_{p=1}^n \Gamma_p (t - \sigma)}. \end{aligned} \tag{4.7}$$

Since $\varpi = \inf_{k \in Z} (t_{k+1} - t_k) > 0$, we have

$$\mu(t) \leq K^* \mu(\sigma) (1 + K^* L)^{\frac{t - \sigma}{\varpi}} e^{K^* \sum_{p=1}^n \Gamma_p (t - \sigma)} = K^* \|\varphi - \psi\| e^{\varrho(t - \sigma)},$$

where

$$\varrho = \frac{\ln(1 + K^* L)}{\varpi} + K^* \sum_{p=1}^n \Gamma_p.$$

That is

$$\|u(t) - v(t)\| \leq K^* \|\varphi - \psi\| e^{(\varrho - \zeta)(t - \sigma)}.$$

Since (H_7) , $\varrho - \zeta < 0$, then system (1.1) has an exponential stable asymptotically almost automorphic solutions. This completes the proof. \square

Remark 1 • The condition H_5, H_7 are wild conditions for the above three theorems. And the condition $H_0, H_1, H_2, H_3, H_4, H_5, H_6, H_7$ are practical conditions for the above three theorems.

- The condition that the activation function in the paper is bounded, as well as being easily decomposable, looks like a little conservative. The future work we can consider the condition that the activation function in the paper whether or not can be more relax.
- Since the multiplication of quaternions does not satisfy the commutative law, the methods for dealing with real-valued networks and complex-valued networks cannot be used to deal directly with quaternion numerical neural networks. In order to overcome the difficulty that quaternion multiplication is not commutative, the quaternion system can be decomposed into four real-valued systems or two complex-valued systems by using Hamilton multiplication law of quaternion or complex decomposition method of quaternion.
- The future work we can consider if the existence and uniqueness and the global exponential stability of almost periodic solutions of QVNNs can be gained by direct method not by decomposing the functions into four real systems.

5 Examples

In this section, we present two numerical examples to illustrate the results given in this paper.

Example 1 Consider the system (1.1), when $n = 2$,

$$\begin{cases} x'_p(t) = -c_p(t)x_p(t) + \sum_{q=1}^n a_{pq}(t)f_q(x_q(t - \tau_{pq}(t))) \\ \quad + \sum_{q=1}^n b_{pq}(t) \int_0^\infty K_{pq}(u)g_q(x_q(t - u))du + u_p(t), \quad t \neq t_k, \\ \Delta(x(t_k)) = \alpha_k x(t_k) + I_k(x(t_k)) + \omega_k, \quad k \in \mathbb{Z}, t \in \mathbb{R}, t = t_k = 2k. \\ x'_p(s) = \varphi'_p(s) = 1, \quad s \in (-\infty, 0]. \end{cases} \quad (5.1)$$

For $p, q = 1, 2$, the coefficients are as follows:

$$\begin{aligned} c_1(t) &= 4 + \sin(t), \quad c_2(t) = 3 + \cos(t), \quad f_q(x_q) = 0.2 \sin(x_q^R) + \cos(|x_q^I + x_q^J|) \\ &+ 0.3 \cos(x_q^J)j + 0.5 \tanh(x_q^K)k, \quad g_q(x_q) = 0.3 \sin(\sqrt{2}x_q^R) + 0.2 \sin^2(x_q^R + x_q^I)i \\ &+ 0.8 \sin(x_q^J)j + 0.2 \cos(\sqrt{5}x_q^K)k, \quad a_{11}(t) = a_{12}(t) = 0.02 \sin(\frac{\pi}{2+\sin(\sqrt{3}t)}) + 0.05 \sin(t)i \\ &+ 0.03 \cos(\sqrt{2}t)j + 0.03 \cos(\frac{\pi}{2+\sin(\sqrt{5}t)})k, \quad a_{21}(t) = a_{22}(t) = 0.03 \sin(\frac{2\pi}{2+\sin(\sqrt{3}t)}) \\ &+ 0.02 \cos(\sqrt{3}t)i + 0.02e^{-t^2}j + 0.02 \cos(\frac{2\pi}{2+\sin(\sqrt{5}t)})k, \quad b_{11}(t) = b_{12}(t) = 0.02e^{-t^2} + \\ &0.02 \cos(\sqrt{2}t)i + 0.05 \sin(\sqrt{2}t)j + 0.03 \cos(\sqrt{2}t)k, \quad b_{21}(t) = b_{22}(t) = 0.03 \cos(\sqrt{3}t) + \\ &0.01 \cos(\frac{2\pi}{2+\sin(\sqrt{5}t)})i + 0.01e^{-t^2}j + 0.02 \sin(t)k, \quad u_1(t) = (0.2 + \frac{1}{1+t^2}) + 0.01e^{-t^2}i + \\ &0.2 \sin(2t)j + 0.02 \frac{1}{1+2t^2}k, \quad u_2(t) = (0.2 + \frac{1}{1+0.5t^2}) + 0.01e^{-0.5t^2}i + 0.5 \sin(1.5t)j + \\ &0.4 \frac{1}{3+\sin(2t)}k, \quad \tau_{1q}^R(t) = 0.2, \tau_{1q}^I(t) = 0.1, \tau_{1q}^J(t) = 0.6t, \tau_{1q}^K(t) = 0.2t, \quad k_{pq}(s) = \\ &e^{-s}, \quad \Delta x_1(2k) = \frac{1}{40}x_1(2k) + \frac{1}{80} \cos(x_1(2k)) + \frac{1}{40}, \quad \Delta x_2(2k) = \frac{1}{40}x_2(2k) + \frac{1}{80} \sin(x_1(2k)) + \\ &\frac{1}{80}. \end{aligned}$$

By calculations, we have $c_1^- = 3, \quad c_1^+ = 5, \quad c_2^- = 2, \quad c_2^+ = 4, \quad a_{11}^{R+} = a_{12}^{R+} = 0.02, \quad a_{11}^{I+} = a_{12}^{I+} = 0.05, \quad a_{11}^{J+} = a_{12}^{J+} = 0.03, \quad a_{11}^{K+} = a_{12}^{K+} = 0.03, \quad a_{21}^{R+} = a_{22}^{R+} = 0.03, \quad a_{21}^{I+} = a_{22}^{I+} = 0.02, \quad a_{21}^{J+} = a_{22}^{J+} = 0.02, \quad a_{21}^{K+} = a_{22}^{K+} = 0.02, \quad b_{11}^{R+} = b_{12}^{R+} = 0.02, \quad b_{11}^{I+} = b_{12}^{I+} = 0.02, \quad b_{11}^{J+} = b_{12}^{J+} = 0.05, \quad b_{11}^{K+} = b_{12}^{K+} = 0.03, \quad b_{21}^{R+} = b_{22}^{R+} = 0.03, \quad b_{21}^{I+} = b_{22}^{I+} = 0.5, \quad b_{21}^{J+} = b_{22}^{J+} = 0.01, \quad b_{21}^{K+} = b_{22}^{K+} = 0.02, \quad u_1^{R+} = 1.2, \quad u_1^{I+} = 0.01, \quad u_1^{J+} = 0.2, \quad u_1^{K+} = 0.02, \quad u_2^{R+} = 1.2, \quad u_2^{I+} = 0.01, \quad u_2^{J+} = 0.5, \quad u_2^{K+} = 0.2, \quad \int_0^{+\infty} |k_{pq}(u)| du \leq 1, \quad L = \frac{1}{80}, \quad A_1^* = 0.52, \quad B_1^* = 0.36, \quad \Gamma_1 = 0.88, \quad A_2^* = 0.36, \quad B_2^* = 1.68, \quad \Gamma_2 = 2.04.$

Also, after calculation we have

$$W(t, s) = \begin{cases} \text{diag} \left(e^{-\int_s^t [4+\sin(m)]dm}, e^{-\int_s^t [3+\cos(m)]dm} \right), \\ \quad t, s \in (t_{k-1}, t_k], \\ \text{diag} \left(e^{-\int_k^t [4+\sin(m)]dm}, e^{-\int_k^t [3+\cos(m)]dm} \right) \\ \quad \times (I + \text{diag}(\frac{1}{40}, \frac{1}{40})) \text{diag} \left(e^{-\int_s^k [4+\sin(m)]dm}, e^{-\int_s^k [3+\cos(m)]dm} \right), \\ \quad t_{k-1} < s \leq t_k < t \leq t_{k+1}, \\ \text{diag} \left(e^{-\int_k^t [4+\sin(m)]dm}, e^{-\int_k^t [3+\cos(m)]dm} \right) \\ \quad \times \prod_{j=k}^{i+1} \left[(I + \text{diag}(-\frac{1}{40}, -\frac{1}{40})) \text{diag} \left(e^{-\int_{j-1}^t [4+\sin(m)]dm}, e^{-\int_{j-1}^t [3+\cos(m)]dm} \right) \right] \\ \quad \times (I + \text{diag}(-\frac{1}{40}, -\frac{1}{40})) \text{diag} \left(e^{-\int_s^t [4+\sin(m)]dm}, e^{-\int_s^t [3+\cos(m)]dm} \right), \\ \quad t_{i-1} < s \leq t_i < t \leq t_{k+1}, \end{cases}$$

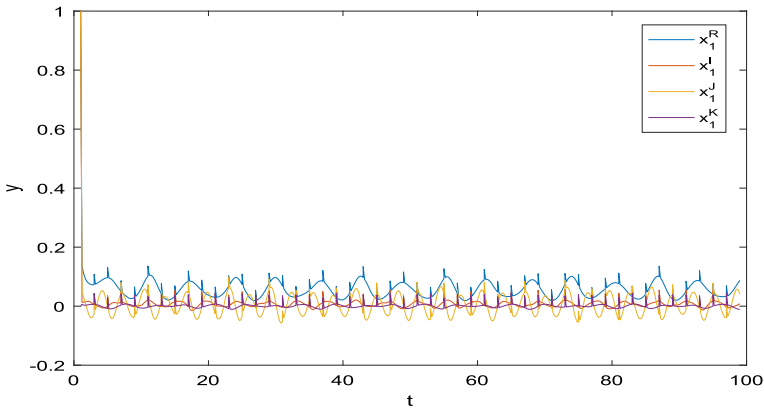


Fig. 1 Transient response of state variables $x_1^R, x_1^I, x_1^J, x_1^K$ for system (5.1) when $t \in [0, 100]$

and

$$\begin{aligned}
 |W(t, s)| &\leq \left(1 + \frac{1}{40}\right)^4 e^{(-4-3)(t-s)} e^{-(\cos(t-s)+\sin(t-s))} \\
 &\leq 1.1038 e^{(-7+\sqrt{2})(t-s)}.
 \end{aligned}$$

So, we can let $K^* \simeq 1.1038, \zeta = -(-7 + \sqrt{2}) = 5.586,$

$$\begin{aligned}
 \eta &= \frac{K^*}{\zeta} \max_{1 \leq i \leq 2} \left[\sum_{j=1}^2 (a_{pq}^{R+} + a_{pq}^{I+} + a_{pq}^{J+} + a_{pq}^{K+})(\alpha_q^R + \alpha_q^I + \alpha_q^J + \alpha_q^K) \right. \\
 &\quad \left. + \sum_{j=1}^2 \tilde{K} (b_{pq}^{R+} + b_{pq}^{I+} + b_{pq}^{J+} + b_{pq}^{K+})(\beta_q^R + \beta_q^I + \beta_q^J + \beta_q^K) \right] + \frac{K^*L}{1 - e^{-\zeta\omega^*}} \\
 &= \frac{1.1038}{5.586} [0.36 + 1.68] + \frac{1.1038 \times \frac{1}{80}}{1 - e^{-5.586 \times 2}} = 0.4161 < 1, \\
 \varrho &= \frac{\ln(1 + K^*L)}{\omega} + K^* \sum_{p=1}^2 \Gamma_p \\
 &= \frac{\ln(1 + 1.1038 \times \frac{1}{80})}{2} + 1.1038 \times (0.36 + 1.68) \approx 2.3329, \\
 \varrho - \zeta &= 2.3329 - 5.586 < 0.
 \end{aligned}$$

Obviously, $(H_0) - (H_7)$ hold. By Theorem 3.1, system (5.1) has a unique asymptotic almost automorphic solution in the region $S^*(\varphi_0, \eta)$. By Theorem 3, this asymptotic almost automorphic solution of system (5.1) is globally exponentially stable (see Figs. 1, 2, 3, 4).

Example 2 Consider the following system of Example 1 without impulses, when $n = 2,$

$$\begin{cases}
 x'_p(t) = -c_p(t)x_p(t) + \sum_{q=1}^n a_{pq}(t)f_q(x_q(t - \tau_{pq}(t))) \\
 \quad + \sum_{q=1}^n b_{pq}(t) \int_0^{+\infty} K_{pq}(u)g_q(x_q(t - u))du + u_p(t) \\
 x'_p(s) = \varphi'_p(s) = 1, \quad s \in (-\infty, 0].
 \end{cases} \tag{5.2}$$

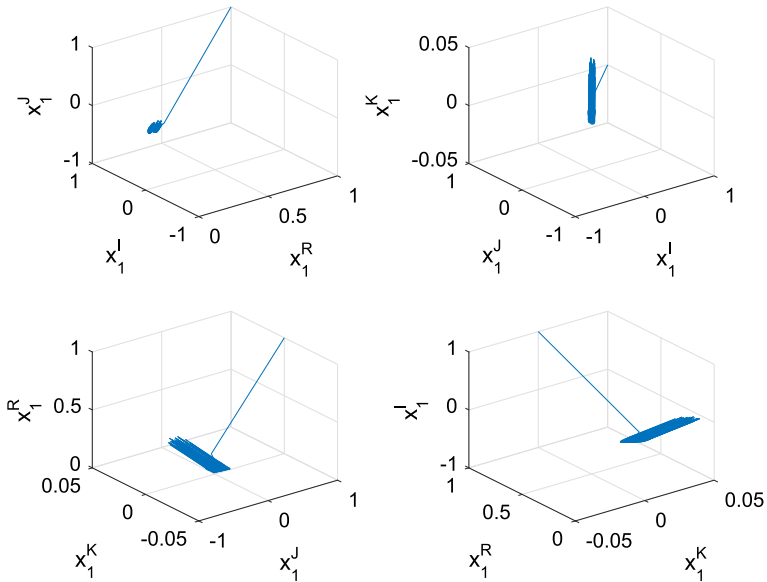


Fig. 2 Orbit of two of $x_1^R, x_1^I, x_1^J, x_1^K$ for system (5.1) in 3-dimensional space when $t \in [0, 100]$

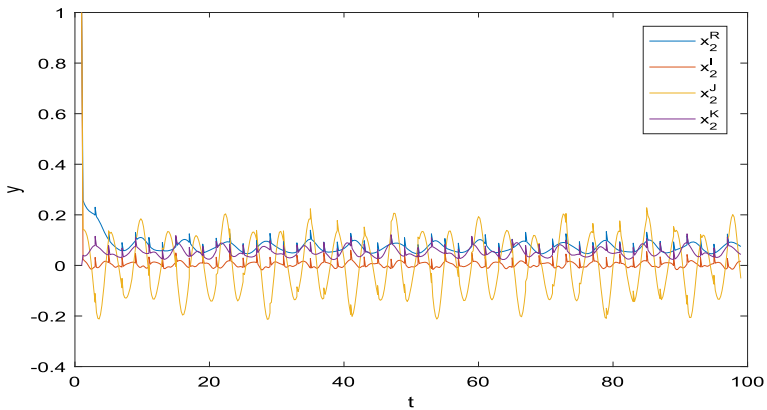


Fig. 3 Transient response of state variables $x_2^R, x_2^I, x_2^J, x_2^K$ for system (5.1) when $t \in [0, 100]$

For $p, q = 1, 2$ and the coefficients of Example 2 are the same as Example 1.

System (5.2) has a unique asymptotic almost automorphic solution, which is globally exponentially stable. The results are verified by the numerical simulations in the Figs. 5, 6, 7, 8.

Remarks

- If we do not take into account the impulsive effects, then system (5.1) can be reduced to system (5.2).
- Underlining a very remarkable difference between the figures of the system (5.1) and the figures of the system (5.2), the effects of the impulsion are quite profound.

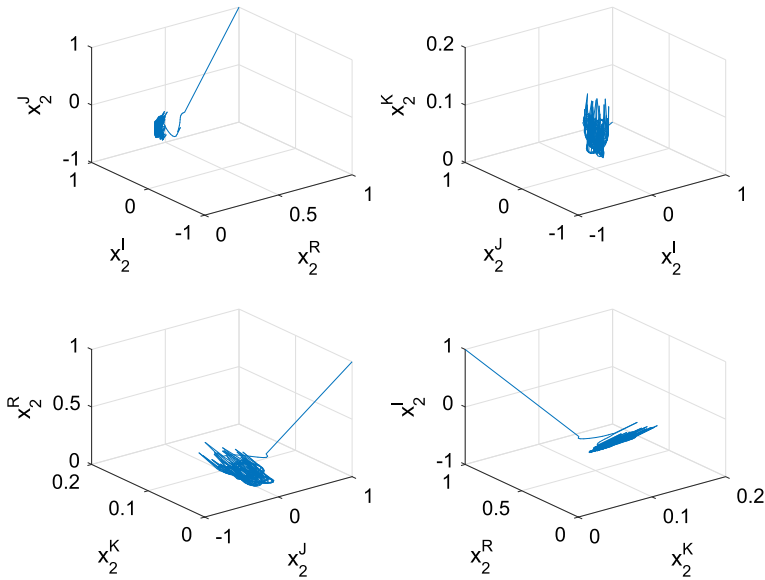


Fig. 4 Orbit of three of x_2^R, x_2^J, x_2^K for system (5.1) in 3-dimensional space when $t \in [0, 100]$

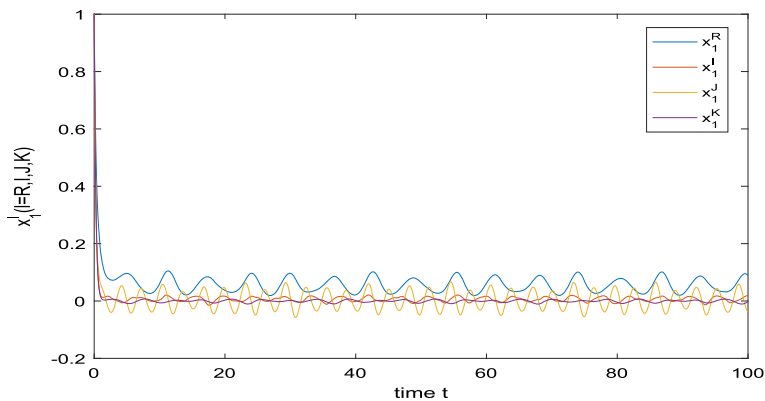


Fig. 5 Transient response of state variables $x_1^R, x_1^I, x_1^J, x_1^K$ for system (5.2) when $t \in [0, 100]$

- Figs. 1, 2, 3, 4 of system (5.1) depict the numerical simulations of state variables of $x_p^l, p = 1, 2, l \in E$ and show that the existence, uniqueness and stability of asymptotic almost automorphic solutions of system (5.1) are subject to instantaneous perturbations and change of the state abruptly due to the effects of the impulse.
- In Figs. 5, 6, 7, 8 of system (5.2), the orbits in three-dimensional spaces, we can see the dynamic behavior of the asymptotic almost automorphic solutions of the system (5.2) without impulse.
- From the comparison of Fig. 1 with Fig. 5 and from the comparison of Fig. 3 with Fig. 7, it can be seen that the impulses have local effect on the original function.
- From the comparison of Fig. 2 and Fig. 6 and from the comparison of Fig. 4 with Fig. 8, it can be seen that the graph of solutions of neural network with impulse is larger than

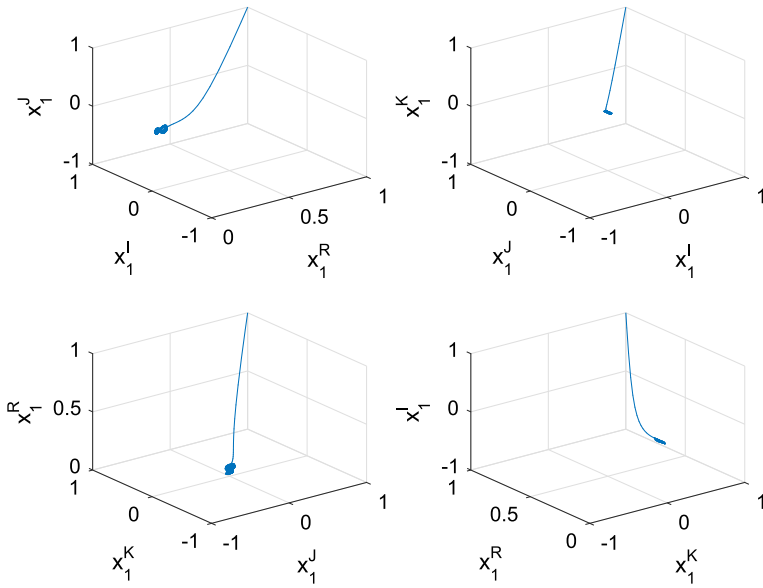


Fig. 6 Orbit of two of $x_1^R, x_1^I, x_1^J, x_1^K$ for system (5.2) in 3-dimensional space when $t \in [0, 100]$

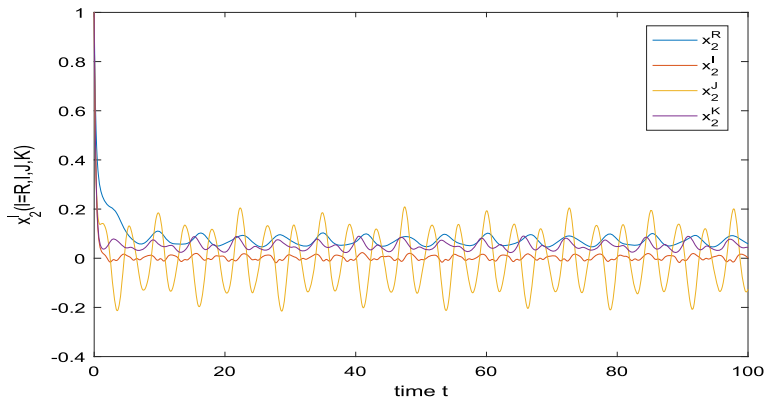


Fig. 7 Transient response of state variables $x_2^R, x_2^I, x_2^J, x_2^K$ for system (5.2) when $t \in [0, 100]$

that of neural network without impulse. It means that the range of solutions for impulsive neural networks wider than the solutions for neural networks.

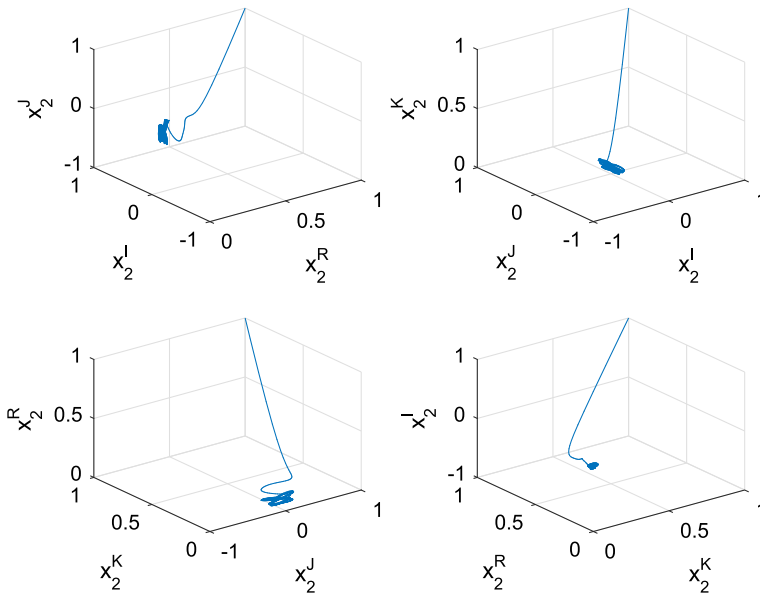


Fig. 8 Orbit of three of $x_2^R, x_2^J, x_2^I, x_2^K$ for system (5.2) in 3-dimensional space when $t \in [0, 100]$

Acknowledgements This work is supported by the National Natural Science Foundation of China (Grant No. 12071491) and by the Scientific Research Project of Guangdong Industry Polytechnic (Grant No. KJ2019-029).

Author Contributions QJ: Writing-original draft. QW: Writing-review and editing.

Declarations

Conflicts of interest The authors declare that they have no conflict of interest.

References

- Jiang Q, Wang Q (2021) Almost periodic solutions for quaternion-valued neural networks with mixed delays on time scales. *Neurocomputing* 439:363–373. <https://doi.org/10.1016/j.neucom.2020.09.063>
- Luo D, Jiang Q, Wang Q (2022) Anti-periodic solutions on Clifford-valued high-order Hopfield neural networks with multi-proportional delays. *Neurocomputing* 472:1–11. <https://doi.org/10.1016/j.neucom.2021.11.001>
- Gao J, Wang Q, Zhang L (2014) Existence and stability of almost-periodic solutions for cellular neural networks with time-varying delays in leakage terms on time scales. *Appl Math Comput* 237:639–649. <https://doi.org/10.1002/ama.3574>
- Xiao B, Meng H (2009) Existence and exponential stability of positive almost periodic solutions for high-order hopfield neural networks. *Math Comput Model* 33(1):532–542. <https://doi.org/10.1016/j.apm.2007.11.027>
- Li Y, Yang L (2014) Almost automorphic solution for neutral type high-order hopfield neural networks with delays in leakage terms on time scales. *Appl Math Comput* 242:679–693. <https://doi.org/10.1016/j.amc.2014.06.052>
- Wang P, Li Y, Ye Y (2016) Almost periodic solutions for neutral-type neural networks with the delays in the leakage term on time scales. *Math Methods Appl Sci* 39(15):4297–4310. <https://doi.org/10.1002/mma.3857>

7. Meng X, Li Y (2018) Pseudo almost periodic solutions for quaternion-valued cellular neural networks with discrete and distributed delays. *J Inequal Appl* 245:1–17. <https://doi.org/10.1186/s13660-018-1837-1>
8. Ren Y, Cheng X, Sakthivel R (2014) Impulsive neutral stochastic functional integro-differential equations with infinite delay driven by fbm. *Appl Math Comput* 247:205–212. <https://doi.org/10.1016/j.amc.2014.08.095>
9. Qiu B, Li L, Peng H, Yang Y (2018) Asymptotic and finite-time synchronization of memristor-based switching networks with multi-links and impulsive perturbation. *Neural Comput Appl* 31:4031–4047. <https://doi.org/10.1007/s00521-017-3312-1>
10. Maharajan C, Raja R, Cao J et al (2018) Global exponential stability of Markovian jumping stochastic impulsive uncertain bam neural networks with leakage mixed time delays and α -inverse Holder activation functions. *Adv Diff Equ* 113:1–31. <https://doi.org/10.1186/s13662-018-1553-7>
11. Zhao K (2018) Existence of positive periodic solutions for the impulsive lotka-volterra cooperative population model with time-delay and harvesting control on time scales. *Adv Differ Equ* 228:1–17. <https://doi.org/10.1186/s13662-018-1686-8>
12. Yu X, Wang Q, Bai Y (2018) Permanence and almost periodic solutions for n-species nonautonomous lotka-volterra competitive systems with delays and impulsive perturbations on time scales. *Complexity*. <https://doi.org/10.1155/2018/2658745>
13. Yu X, Wang Q (2019) Weighted pseudo-almost periodic solutions for shunting inhibitory cellular neural networks on time scales. *Bull Malays Math Sci Soc* 42(5):2055–2074. <https://doi.org/10.1007/s40840-017-0595-4>
14. Diagana T (2010) Existence of almost automorphic solutions to some classes of nonautonomous higher order differential equations. *Electron J Differ Equ* 22:1–26. <https://doi.org/10.14232/ejqtde.2010.1.22>
15. Chaouki A, Dridi F (2019) Piecewise asymptotically almost automorphic solutions for impulsive non-autonomous high-order hopfield neural networks with mixed delays. *Neural Comput Appl* 31:5527–5545. <https://doi.org/10.1007/s00521-018-3378-4>
16. Girard PR (2007) Quaternions. Clifford algebras and relativistic physics, Springer
17. Li Y, Wang H, Meng X (2019) Almost automorphic synchronization of quaternion-valued high-order hopfield neural networks with time-varying and distributed delays. *IMA J Math Control I* 36(3):983–1013. <https://doi.org/10.1093/imamci/dny015>
18. Sudbery A (1979) Quaternionic analysis. In: *Math Proc Cambridge*. Cambridge University Press 85:199–225
19. Matsui N, Isokawa T, Kusamichi H et al (2004) Quaternion neural network with geometrical operators. *J Intell Fuzzy Syst* 15((3,4)):149–164
20. Liu X, Li Z (2019) Global μ -stability of quaternion-valued neural networks with unbounded and asynchronous time-varying delays. *IEEE Access* 7:9128–9141. <https://doi.org/10.1109/ACCESS.2019.2891721>
21. Xiang J, Li Y (2019) Pseudo almost automorphic solutions of quaternion-valued neural networks with infinitely distributed delays via a non-decomposing method. *Adv Differ Equ* 356:1–17. <https://doi.org/10.1186/s13662-019-2295-x>
22. Xia Y, Huang L, Huang L et al (2019) Two matrix-type projection neural networks for matrix-valued optimization with application to image restoration. *Neural Process Lett* 53(3):1–23. <https://doi.org/10.1007/s11063-019-10086-w>
23. Xinqi L, Jun W, Sam K (2021) Hash bit selection via collaborative neurodynamic optimization with discrete hopfield networks. *IEEE Trans Neural Netw Learn Syst* 33:5116–5124
24. Qingshan L, Jun W (2013) A one-layer projection neural network for nonsmooth optimization subject to linear equalities and bound constraints. *IEEE Trans Neural Netw Learn Syst* 24:812–824
25. Zicong X, Yang L, Jianquan L et al (2020) Penalty method for constrained distributed quaternion-variable optimization. *IEEE Trans Cybern* 51:5631–5636
26. Greenblatt A, Mosquera-Lopez C, Aгаian S (2013) Quaternion neural networks applied to prostate cancer gleason grading. *Proc IEEE Int Conf Syst Man Cybern* 24(5):1144c1149
27. Song Q, Chen X (2018) Multistability analysis of quaternion-valued neural networks with time delays. *IEEE Trans Neural Netw Learn Syst* 29:5430–5440. <https://doi.org/10.1109/TNNLS.2018.2801297>
28. Xia Y, Cao J, Huang Z (2007) Existence and exponential stability of almost periodic solution for shunting inhibitory cellular neural networks with impulses. *Chaos Soliton Fract* 34(5):1599–1607. <https://doi.org/10.1016/j.chaos.2006.05.003>
29. Santos J, Cuevas C (2010) Asymptotically almost automorphic solutions of abstract fractional integro-differential neutral equations. *Appl Math Lett* 23(9):960–965. <https://doi.org/10.1016/j.aml.2010.04.016>
30. Hsia C, Shiue M (2013) On the asymptotic stability analysis and the existence of time-periodic solutions of the primitive equations. *Indiana U Math J* 62(2):403–441. <https://doi.org/10.1512/iumj.2013.62.4902>

31. Diagana T (2013) Almost automorphic type and almost periodic type functions in abstract spaces. Springer International Publishing, New York
32. Stamov G (2012) Almost periodic solutions of impulsive differential equations. Springer International Publishing, New York
33. Wang C (2016) Piecewise pseudo-almost periodic solution for impulsive non-autonomous high-order Hopfield neural networks with variable delays. Neurocomputing 171(1):1291–1301. <https://doi.org/10.1016/j.neucom.2015.07.054>

Publisher's Note Springer Nature remains neutral with regard to jurisdictional claims in published maps and institutional affiliations.

Springer Nature or its licensor (e.g. a society or other partner) holds exclusive rights to this article under a publishing agreement with the author(s) or other rightsholder(s); author self-archiving of the accepted manuscript version of this article is solely governed by the terms of such publishing agreement and applicable law.

暨南大学 文献收录证明

检索课题：广东轻工职业技术学院陈大华发表的文献在 SCIE 数据库中的收录情况。

检索工具及年限：

Science Citation Index Expanded (SCI-EXPANDED) 2000-2023 年

检索结果：根据委托方提供的文献目录，经上述数据库及年限范围内检索，共计 1 篇论文被 SCIE 收录，结果如下：

序号	文献信息	作者顺序	影响因子	中科院 大类 分区
1	标题:Effect of roll temperature on the structure and properties of oriented polypropylene cast film and stretched microporous membrane 作者:Chen, Dahua;Chen, Xiande;Yin, Liangdong;Xie, Jiayi;Xu, Ruijie;Lei, Caihong; 来源出版物:JOURNAL OF APPLIED POLYMER SCIENCE 卷:140 期:30 页 DOI:10.1002/app.54080 出版年:AUG 10 2023 Web of Science 核心合集集中的 被引频次:0 入藏号:WOS:000985672000001 文献类型:Article ISSN:0021-8995	第一作者	3.0	3 区

声明：本证明的文献信息由委托人提供，检索结果已由委托人核实确认无误。如果由于委托人提供信息不实而造成任何后果，本查新站概不负责。

委托人（签名）：

检索员：大汤华清
教育部科技查新工作站(Z15)
暨南大学图书馆学科服务与咨询部
2023年10月13日

Effect of roll temperature on the structure and properties of oriented polypropylene cast film and stretched microporous membrane

Dahua Chen¹ | Xiande Chen² | Liangdong Yin² | Jiayi Xie³ | Ruijie Xu² | Caihong Lei² 

¹School of Chemical Engineering and Technology, Guangdong Industry Polytechnic, Guangzhou, People's Republic of China

²School of Materials and Energy, Guangdong University of Technology, Guangzhou, People's Republic of China

³School of Chemistry and Civil Engineering, Shaoguan University, Shaoguan, People's Republic of China

Correspondence

Jiayi Xie, School of Chemistry and Civil Engineering, Shaoguan University, Shaoguan 512005, People's Republic of China.

Email: xiejy710@163.com

Caihong Lei, School of Materials and Energy, Guangdong University of Technology, Guangzhou 510006, People's Republic of China.

Email: lch528@gdut.edu.cn

Funding information

Foshan Science and Technology Innovation Project, Grant/Award Number: FS0AA-KJ919-4402-0145; Guangzhou Science and Technology Plan Project, Grant/Award Number: 202102020952; Project of National Science Foundation of China, Grant/Award Number: 52173033; Project of Science Foundation of Guangdong Province, Grant/Award Number: 2021A1515011914; The Youth Fund Project of Regional Joint Foundation- Fundamental and Applied Basic Research Foundation of Guangdong Province, Grant/Award Number: 2021A1515110648

Abstract

The effect of roll temperature from 60 to 120°C on the crystalline structure and properties of oriented polypropylene (PP) cast films and the stretched microporous membrane was studied. It was found that the long period, the thickness of the crystalline and amorphous phase increase with the increasing roll temperature. And the regularity of the lamellar structure also improves with the increasing roll temperature. In comparison, the lamellae lateral dimension is nearly unchanged at 50 nm. The orientation of the lamellar structure slightly decreases from 0.81 to 0.76 with increasing roll temperature. The increase of the long period and the improvement of the regularity of the lamellar structure lead to the increase of the elastic recovery value of PP cast film. The corresponding microporous membrane also shows a smaller thickness of lamellar clusters, larger pores, better air permeability and better thermal shrinkage resistance. The higher roll temperature is beneficial to the perfection of the lamellar structure, obtaining the higher-performance microporous membrane.

KEYWORDS

crystallization, membranes

1 | INTRODUCTION

Microporous membranes have been extensively used in many separation applications, such as electronic vehicles, rechargeable electronics, water filtration and medical applications.¹ The microporous membrane as a separator is one of the critical components in Li-ion

batteries, allowing the transportation of ionic charge carriers and preventing electrical short circuits between a cathode and an anode.² Currently, the main preparation methods of commercial microporous membranes include the dry method (melt-stretching) and the wet method.^{3,4} Among them, polypropylene (PP) microporous membranes prepared by the melt-stretching

method are one of the most widely used separators in industry.⁵ Studying the polypropylene microporous membrane preparation by the melt-stretching method helps guide the production of high-performance microporous membranes.

Preparing polypropylene microporous membranes by melt-stretching is generally divided into the following four steps: (1) the extruded melt forms highly oriented lamellar structures under stress and temperature fields; (2) annealing to improve the lamellar structure, increase the thickness of the lamellae and improve the orientation⁶; (3) stretching at low temperature and high temperature to form a regular pore structure⁷; (4) heat-setting to stabilize the pore structure.^{8,9} During the melt-stretching process, the polymer melt would be stretched and oriented under high-speed stretching force when it flows out of the die. At the same time, the oriented molecule chains would be rapidly cooled by the air knife and start to form the initial oriented lamellar structures. Then, the oriented lamellar structures further grow up on the hot casting roller. It is generally accepted that both the raw material and processing parameters are key factors for forming highly oriented lamellar structures.^{10–13} Much research has focused on the processing parameters such as extruding temperature, melt-stretching ratio, and cooling air.^{14–18} Although researchers generally believe that higher roll temperature is beneficial to the formation of oriented lamellar structures and the improvement of the performance of the stretched microporous membranes, little attention has been paid to the effect of roll temperature. Ajji et al.¹⁹ suggested that the roll temperature has a crucial role in the orientation of the crystalline as well as the amorphous phases. Liu et al.²⁰ found that the roll temperature of 90°C is suitable for polyethylene to form the oriented lamellae structure with the largest lamellae orientation degree, the thinnest lamellae thickness, further obtaining the best uniform microporous membrane with the larger pore size and better pore distribution. However, the relationship between roll temperature and lamellar structure parameters and the properties of cast films and stretched microporous membranes has not yet been established.

This paper intends to study the effect of the roll temperature on the microstructure parameters and the properties of PP cast films and stretched microporous membranes. The crystalline parameters were characterized using two-dimensional small-angle x-ray scattering (2D-SAXS), DSC, SEM and FTIR. The relationships between the roll temperature, lamellar structure parameters and the properties of PP cast film and stretched microporous membranes were determined.

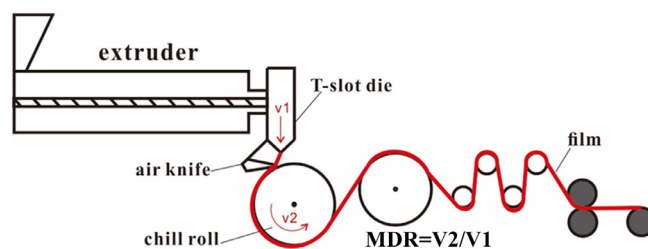


FIGURE 1 Schematic diagram for the melt-stretching process. [Color figure can be viewed at [wileyonlinelibrary.com](https://onlinelibrary.wiley.com/doi/10.1002/app.54080)]

2 | MATERIALS AND EXPERIMENTS

2.1 | Material

A polypropylene resin (F401) with a melt flow rate value of 2.0 g/10 min (230°C, 2.16 kg) from Yangzi Petrochemical Company, China, was used.

2.2 | The PP cast film preparation

The PP cast film was prepared by cast extrusion through a T-slot die, followed by stretching and cooling (Figure 1). During extrusion, the uniaxial stretching (machine direction, MD) was applied to PP melt, which resulted in the oriented lamellar structures. The die temperature was set at 210°C, and a melt draw ratio of 125 was applied. The melt-draw ratio is a specific ratio between the line speed of the casting roll and the extruding velocity of the PP melt. The thickness of the cast film is 25 μm. Since the roll temperature during melt stretching process was generally set between the relaxation temperature of the crystalline region (60–70°C for PP) and the maximum crystallization temperature (120–130°C for PP), the cast roll temperature was set at 60, 80, 100 and 120°C, respectively.

2.3 | Annealed and stretched microporous membrane preparation

The prepared PP cast film was first annealed for 30 min at 145°C in a hot oven to improve the crystalline structure. Then, the PP annealed film was stretched by the H&P Inspekt table blue machine equipped with a heating chamber. The detailed procedures were shown as follows: the PP annealed films were first stretched to 30% with a drawing speed of 100%/min at room temperature and then stretched to 120% with a drawing speed of 100%/min at 130°C; the stretched membrane was further heat-set for 5 min at 145°C.

2.4 | Tensile test and the elastic recovery value

The tensile test used an H&P Inspekt table blue machine. As the deformation was homogeneous in the tensile test, the sample was cut into long strips 80 mm long and 15 mm wide. The gage length was 50 mm. The grip had standard plate jaws used for flat and thin specimens. The stretching speed in the tensile test was 50 mm/min. The elastic recovery value (ER %) was also tested using an H&P Inspekt table blue machine at a 50 mm/min deformation rate. It was determined along the stretching direction of the film. The ER (%) was calculated by the following equation:

$$\text{ER}(\%) = (L - L') / (L - L_0) \times 100\%, \quad (1)$$

where, L_0 was the initial length of the film before the extension, L was the length when strained to 100%, and L' was the length at the end of the extension.

2.5 | Scanning electron microscopy

The surface morphology was characterized by scanning electron microscopy (SEM; S3400N, Hitachi, Japan). All the samples were sputtered with a platinum ion beam for 100 s before the test. To clearly observe the lamellar clusters of the cast films, an etching method was used to remove the amorphous part. The films were dissolved in a 0.7% solution of potassium permanganate in a mixture of 35 vol% of orthophosphoric and 65 vol% of sulfuric acid. The SEM images were analyzed with Nano Measurer software to get information on the structural units in the microporous membrane. The calculation process selected more than 200 research units to obtain a final average result by manual measure and further calculate the standard deviation.

2.6 | Differential scanning calorimetry

Differential scanning calorimetry measurements were performed with a Mettler-Toledo DSC3. The temperature and heat flow were calibrated with indium. Samples weighing approximately 8 mg were encapsulated in hermetic aluminum pans, and heated with a temperature ramp of 10 K/min from 25 to 140°C under a nitrogen flow of 50 mL/min. The crystallinity (X_c) was calculated as follows²¹:

$$X_c(\%) = \Delta H_m / \Delta H_m^0 \times 100\%, \quad (2)$$

where, ΔH_m was the endothermic heat of melting, ΔH_m^0 was the endothermic heat for perfectly crystalline PP (290 J g⁻¹).²¹

The lamellae thickness corresponding to the melting peaks in the DSC curves was calculated according to the Thomson–Gibbs Equation:

$$L = \frac{2\sigma_e}{\Delta h_m} \frac{T_m^0}{T_m^0 - T_m} \times 10^9, \quad (3)$$

where, L was the lamellae thickness, nm, σ_e was fold surface free energy of α form PP crystal, 49.6×10^{-3} J/m², T_m^0 was the equilibrium melting temperature, 457 K, T_m was the melting temperature, Δh_m was the enthalpy of fusion per unit volume, 1.34×10^8 J/m³.

2.7 | Small-angle x-ray scattering

The PP cast films prepared under different roll temperatures were tracked using the beamline 1W2A, Beijing Synchrotron Radiation Facility (China). SX165-CCD was set at 4880 mm sample-detector distance. The exposure time was 15 s. The scattering intensities were integrated within $\pm 5^\circ$ along the vertical direction of 2D SAXS patterns.

The average thicknesses of the crystalline phase layers (L_c) and the amorphous phase layers (L_a) were calculated from the integrated curve by the one-dimensional electron density correlation function $K(r)$ as shown²²:

$$K(z) = \frac{\int_0^\infty I(q) \cos(qz) dq}{\int_0^\infty I(q) dq}, \quad (4)$$

where, z was parallel to the drawing direction. $I(q)$ was the integrated intensity along the vertical direction.

2.8 | Fourier transform infrared spectroscopy

FTIR spectroscopy spectra were obtained using a Nicolet IS50 FTIR instrument from Thermo Electron Corp. (DTGS detector, resolution 4 per cm, accumulation of 128 scans). The beam was polarized via a Spectra-Tech zinc selenide wire grid polarizer from Thermo Electron Corp. The dichroic ratio (R) was calculated by the ratio of the absorbance from beams polarized parallel ($A_{//}$) and perpendicular (A_{\perp}) to the melt extrusion direction. Then the data were evaluated in the degree of orientation, f :

$$R = \frac{A_{//}}{A_{\perp}}, \quad (5)$$

$$f = \frac{R-1}{R+2} \times \frac{R_0+1}{R_0-2}. \quad (6)$$

R_0 was given by:

$$R_0 = 2 \cot^2 \Psi, \quad (7)$$

where, Ψ was the angle between the polymer chain axis and the transition moment of the investigated absorption band.²³

2.9 | Air permeability and porosity

The air permeability of stretched microporous membranes was characterized by Gurley Densometer model No. 4150 (Gurley Precision Instruments, New York, USA) according to ASTM D726. The Gurley value was defined as the time required for a specific amount of air (100 mL) to pass through a specific area of the microporous membrane under a specific pressure (20 kgf/cm²). The porosity was measured using the density method described in the previous work.²⁴

2.10 | Heat resistance property

The thermal shrinkage data, reported as accelerated shrinkage in percent, represented the decrease in length of the dimension along the stretching direction after exposing the membrane under 130°C for 1 h. The percent was reported as the percent based on the original length of the membrane prior to its exposure to 130°C for 1 h.

3 | RESULTS AND DISCUSSION

3.1 | The effect of roll temperature on the mechanical properties of PP cast films

Figure 2a shows the stress–strain curves of PP cast films prepared under different roll temperatures. When the roll temperature is 60°C, the stress–strain curve has a weak yield point but no obvious yield stress drop, indicating that highly oriented lamellar structures are formed.¹² When the roll temperature increases from 60 to 100°C, the yield stress decreases slightly with the increasing roll temperature. And the strain-hardening phenomenon becomes more apparent with the increasing roll temperature, implying the formation of more perfect oriented

lamellar structures under higher roll temperatures.²⁵ The change in mechanical properties may come from the difference in the microstructure of PP cast film prepared under different roll temperatures.

Figure 2b shows the elastic recovery of PP cast films prepared under different roll temperatures. When the roll temperature increases from 60 to 120°C, the elastic recovery value of the cast film significantly increases from 82% to 88%. This result is mainly related to the improvement of lamellar structure.²⁶ The microstructure of PP cast film prepared under different roll temperatures should be further investigated.

3.2 | The effect of roll temperature on the microstructure of PP cast films

Usually, the melt-stretching process could prepare the cast film with row-nucleated lamellar structures, and the roll temperature is a key factor in determining the growth of crystalline structure. To characterize the effect of roll temperature on lamellar structures, the SEM images of the etched PP cast films prepared under different roll temperatures were tested and shown in Figure 3. The lamellar clusters can be clearly observed from the surface morphology of the etched PP cast films. With the roll temperature set at 60°C, the thickness of the lamellar clusters is small, and the arrangement of lamellar clusters is also irregular. Besides, there are some defects shown in the SEM image. When the roll temperature is increased to 80°C, the thickness and the arrangement regularity of the lamellae clusters increase apparently. When the roll temperature is further increased to 100 and 120°C, the thickness of the lamellar clusters becomes larger, and the arrangement of lamellae clusters becomes more regular. And the defects of lamellae clusters also become less. It is apparent that increasing the roll temperature is beneficial to improve the thickness and arrangement of the lamellae clusters and eliminate the defects of lamellae clusters.

To further explore the effect of roll temperature on the crystallization of PP cast films, the thermal behavior of PP cast films prepared under different roll temperatures was analyzed by the DSC test. It can be seen from Figure 4 and Table 1 that the crystallinity and melting point of the cast film are 56.3% and 158.9°C when the roll temperature is 60°C. As the roll temperature increases, the crystallinity and melting point increase slightly. When the roll temperature is increased to 120°C, the crystallinity and melting point of the cast film show the maximum values of 58.8% and 160.1°C, respectively. The average lamellar thickness of the PP cast film calculated by the Gibbs–Thomson equation is also shown in Table 1. The lamellar thickness

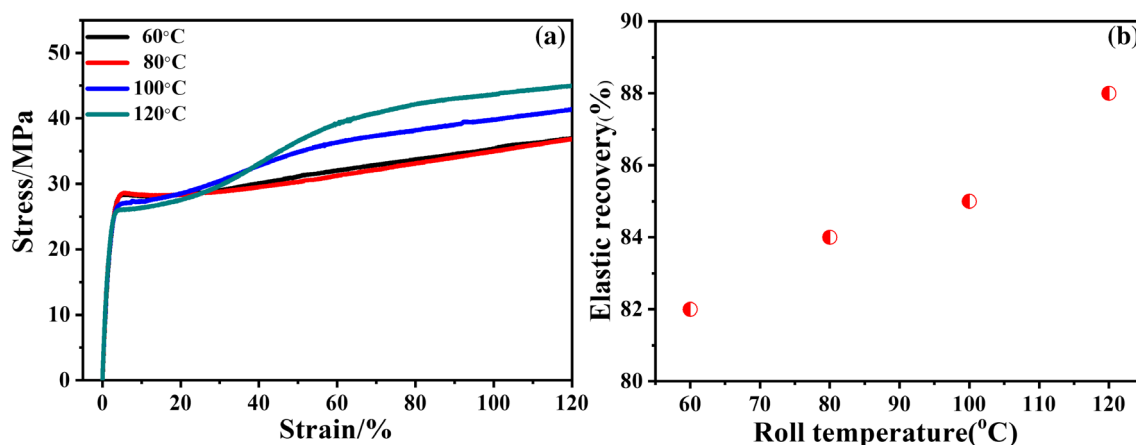
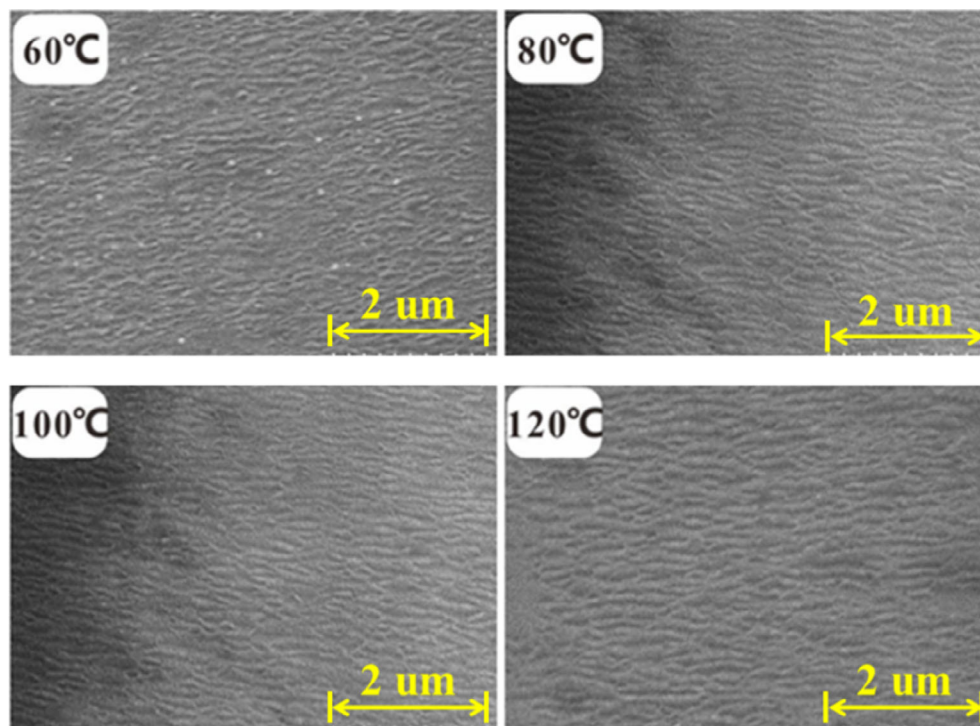


FIGURE 2 Stress-strain curves (a), elastic recovery value (b) of cast films prepared under different roll temperatures. [Color figure can be viewed at wileyonlinelibrary.com]

FIGURE 3 The surface morphology of PP cast films prepared under different roll temperatures. [Color figure can be viewed at wileyonlinelibrary.com]



increases from 13.6 to 14.3 nm with the increasing roll temperature, which is consistent with the SEM results.

To further describe the effect of roll temperature on the lamellar structure, the SAXS experiment was used to track the scattering signals of PP cast films prepared under different roll temperatures, as shown in Figure 5. It can be seen that there are two symmetrical scattering spots in the meridian direction of all the scattering patterns, indicating that the highly oriented lamellae structures were formed during the melt-stretching process.^{17,27} With the increase of the roll temperature, the scattering

pattern gradually changes from a long teardrop shape to a short ellipsoid spindle shape, indicating that the regularity of lamellae increases with roll temperature. At the same time, the scattering pattern gradually moves to the beam center, which means that the lamellae size increases with roll temperature. Compared with the scattering pattern of the annealed film, secondary scattering signals are not found in the cast films with different roll temperatures.^{15,28–30} Highly oriented lamellar structures typically exhibit high-order scattering spots in the scattering pattern. Hence, we could infer that increasing roll

temperature could not improve the regularity of the lamellar structure to a level similar to that of annealed film. Although the cast film prepared under higher roll temperature has a larger lamellar thickness and better structural integrity, the annealing process is still necessary.

Figure 6 shows the one-dimensional integrated curve along the vertical direction. When the roll temperature increases from 60 to 120°C, the peak value q of the scattering vector decreases gradually, and the peak value q of the scattering vector reaches the minimum value at the roller temperature of 120°C, indicating the long period of lamellar structure increase with the roll temperature. The full width at half maximum (FWHM) for the intensity

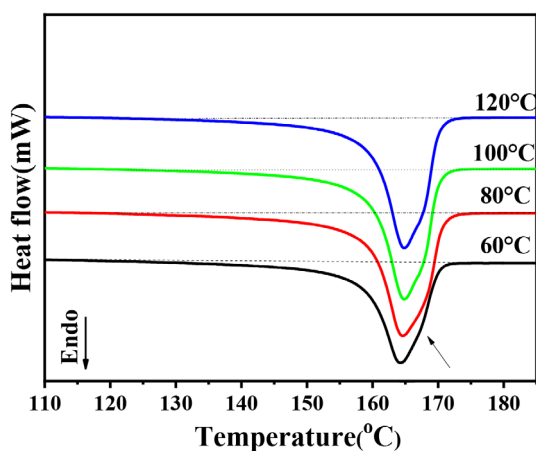


FIGURE 4 DSC curves of PP cast films prepared under different roll temperatures. [Color figure can be viewed at [wileyonlinelibrary.com](https://onlinelibrary.wiley.com/doi/10.1002/app.54080)]

TABLE 1 The crystallinity and melting point of PP cast films prepared under different roll temperatures.

Roll temperature (°C)	Crystallinity (%)	Melting point (°C)	Lamellar thickness (nm)
60	56.3	158.9	13.6
80	57.3	159.5	13.9
100	57.9	159.8	14.1
120	58.8	160.1	14.3

peak was also calculated and shown in Figure 6b. The value of FWHM markedly decreases from 0.3 to 0.22 with increasing roll temperature, which means that roll temperature effectively improves the regularity of the lamellar structure and reduces weak lamellae, further leading to the apparent strain-hardening behavior in the stress–strain curve. The detailed parameters of lamellar structures were further calculated by the one-dimensional correlation function and shown in Table 2.²² When the roll temperature increases from 60 to 120°C, the long period increases slightly from 11.51 to 12.13 nm, and the thickness of the crystalline region and the amorphous region also increases with roll temperature. However, the long period at a roll temperature of 120°C is only 5.4% higher than that at a roll temperature of 60°C. The effect of roll temperature on the lamellar size is limited. This limited effect may be due to the short residence time of the cast film on the heating cast roll. During the melt-stretching process, a high melt drawing ratio is necessary to obtain the highly oriented lamellar structures; the high stretching speed makes the film only stays a short time on the heating casting roll. There is not enough time for the cast film to grow up the crystalline structure at a suitable temperature. The limited thickening of lamellar structures is consistent with the previous DSC results.

The lamellar lateral size was further calculated from the width of the peaks at half-height along the horizontal direction.^{31,32} Figure 6d shows that the lateral size of the PP lamellar structure decreases slightly from 52 to 50 nm with the roll temperature. Apparently, the effect of roll temperature on the lamellar lateral size is also limited as cast film only grows up the crystalline structure within the short staying time on the heating cast roll.

The orientation of the lamella was further calculated from intensity curves along the azimuthal direction.³³ Figure 7a presents that the orientation degree of the lamellar structures slightly decreases from 0.81 to 0.76 with increasing roll temperature. The orientation degree of the chain segment was also characterized by FTIR. The characteristic bands at 998 cm^{-1} are related to the crystalline regions.³⁴ Figure 7b shows that the orientation of the molecular chains slightly decreases from 0.58 at a roll temperature of 60°C to 0.565 at a roll temperature of 120°C. These two similar orientation results indicate that the higher roll temperature does not benefit the formation of oriented

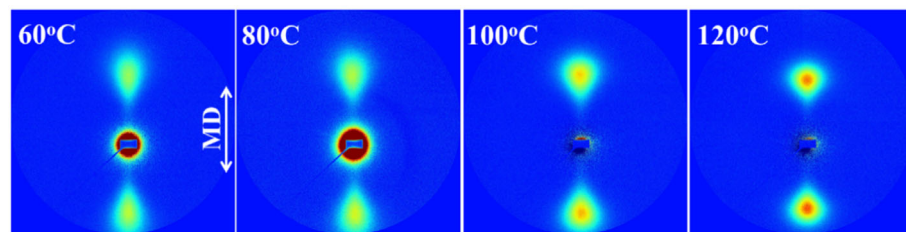


FIGURE 5 2D SAXS patterns of PP cast films prepared under different roll temperatures; the machine direction (MD) is the meridional direction. [Color figure can be viewed at [wileyonlinelibrary.com](https://onlinelibrary.wiley.com/doi/10.1002/app.54080)]

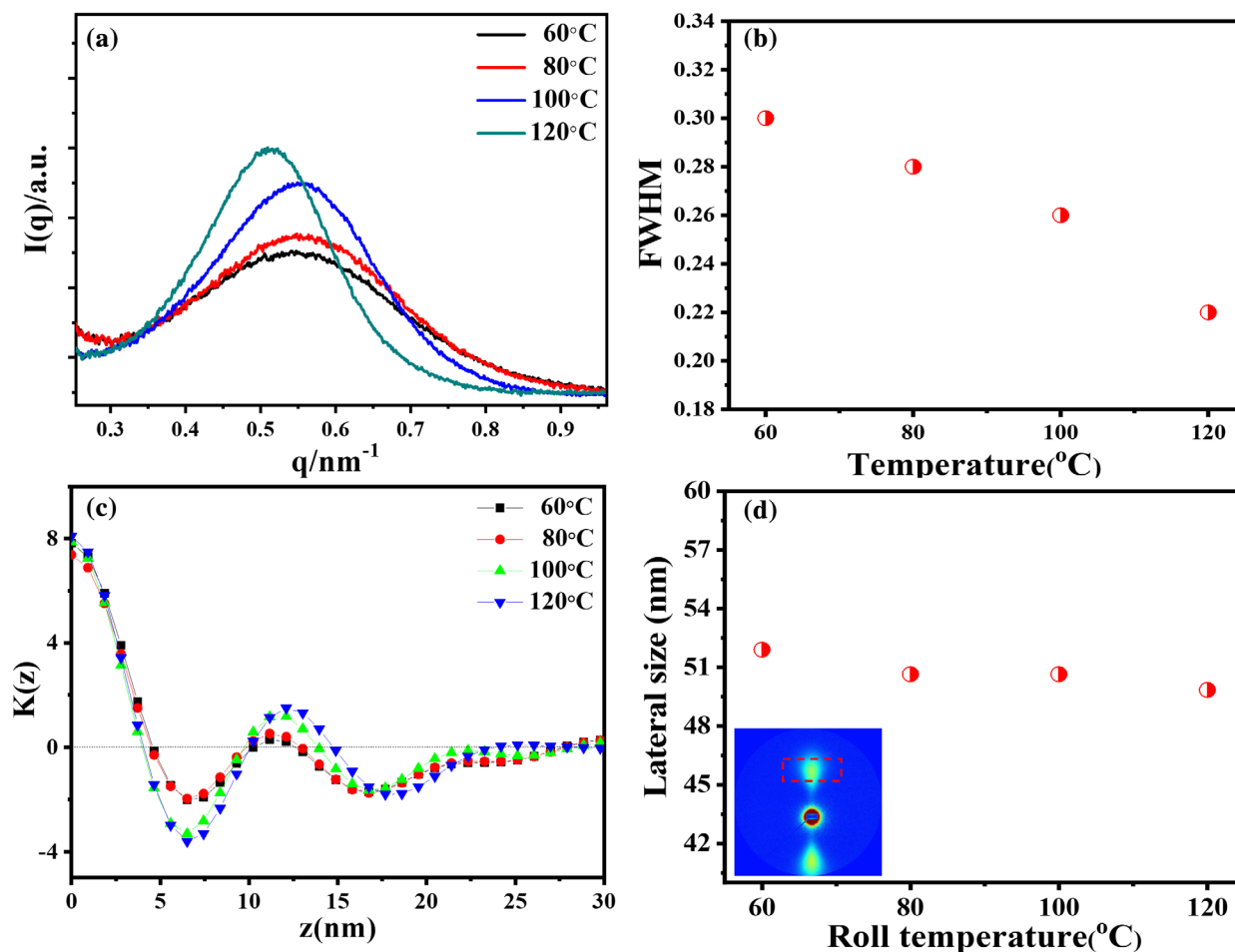


FIGURE 6 The $I(q)$ versus q cure (a), the full width at half maximum for the intensity curve (b), one-dimensional correlation function (c), the lamellar lateral size of the lamellar structure (d) of PP cast films prepared under different roll temperatures. [Color figure can be viewed at wileyonlinelibrary.com]

TABLE 2 Lamellae structure parameters of PP cast films prepared under different roll temperatures.

Roll temperature (°C)	L (nm)	L_c (nm)	L_a (nm)
60	11.51	5.31	6.20
80	11.55	5.44	6.11
100	12.10	5.50	6.60
120	12.13	5.48	6.65

structures, as the molecular chain at higher temperatures has a higher motivation ability and is easy to disorient.

3.3 | The effect of roll temperature on the properties of PP stretched microporous membrane

To investigate the effect of roll temperature on the properties of PP stretched microporous membrane, the

surface SEM images were collected and shown in Figure 8. And the detailed statistical values of SEM images were shown in Table 3. As shown in Figure 8, the typical separated lamellar clusters, micropores, and connecting bridges are found in all the samples. For the SEM image prepared under the roll temperature of 60°C, it is found that some lamellar clusters are not completely separated during stretching, and no open micropores are in these areas. With the increase of roll temperature from 60 to 120°C, the average thickness of lamellar clusters visibly decreases from 247 to 189 nm, the average length of connecting bridges increases obviously from 141 to 195 nm, and the area of micropore also increases with the roll temperatures. These changes represent that lamellar clusters of the stretched membrane prepared under a higher roll temperature could be separated more completely during stretching, the thickness of lamellar clusters becomes smaller, and the micropores become larger.

The Gurley values, porosity and thermal shrinkage of PP microporous membrane prepared under different

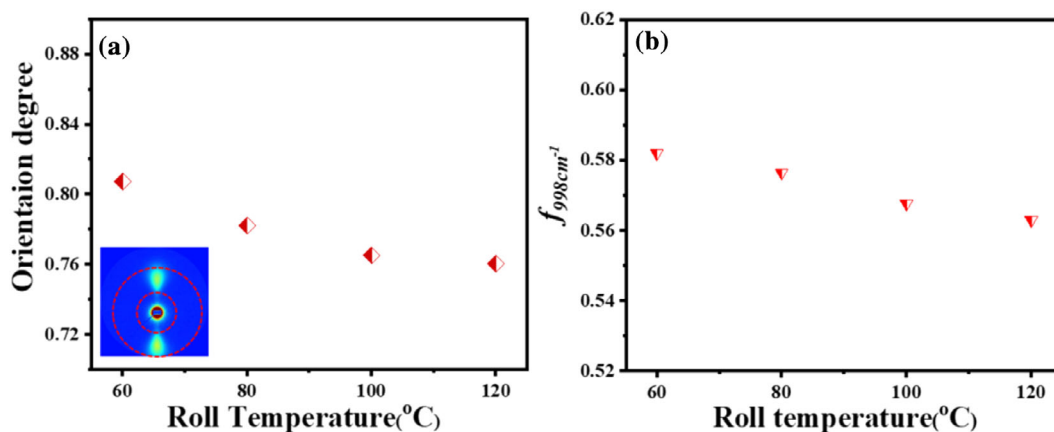


FIGURE 7 The orientation degree of the crystalline region calculated by SAXS (a) and calculated by FTIR (b). [Color figure can be viewed at wileyonlinelibrary.com]

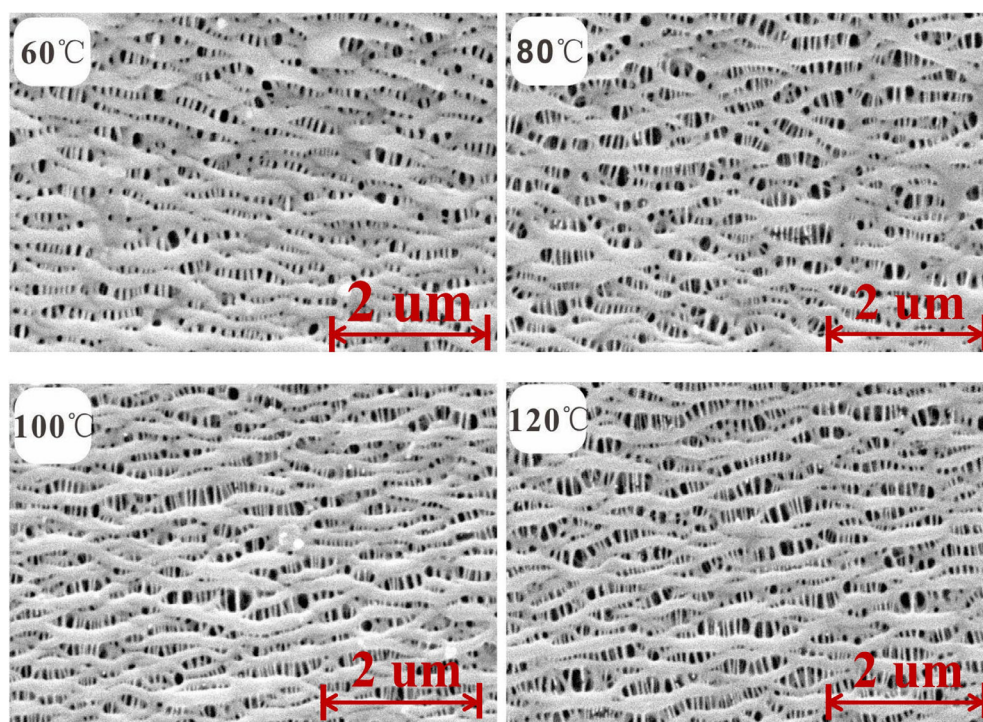


FIGURE 8 SEM images of PP stretched microporous membrane prepared under different roll temperatures. [Color figure can be viewed at wileyonlinelibrary.com]

TABLE 3 The average thickness of lamellar clusters (T_{lc}), the average length (L_b) of connecting bridges and the area of pore in a unit area of the stretched membrane prepared under different roll temperatures.

Sample	60°C	80°C	100°C	120°C
T_{lc} (nm)	247 ± 4	217 ± 5	204 ± 5	189 ± 5
L_b (nm)	141 ± 4	168 ± 5	181 ± 5	195 ± 6
Area (%)	17	18	20	21

roll temperatures were further tested and listed in Table 4. The Gurley value, porosity and thermal shrinkage are 258 s, 49.5% and 7.6% for the roll temperature of 60°C. When the roll temperature increases

TABLE 4 Air permeability, porosity and thermal-shrinkage of stretched microporous membrane prepared under different roll temperatures.

Roll temperature (°C)	Gurley value (s/100 mL)	Porosity (%)	Thermal-shrinkage (%)
60	258	49.5	7.6
80	246	50.5	6.4
100	242	50.5	6.0
120	240	49.5	6.3

to 120°C, the Gurley value, porosity and thermal shrinkage are improved to 240 s, 50.5% and 6.4%, respectively. And the air permeability and thermal

shrinkage resistance are improved compared with the roll temperature of 60°C. These results verify that the higher roll temperature is beneficial to the perfection of the lamellar structure to obtain higher-performance microporous membranes.

4 | CONCLUSION

In summary, the effect of roll temperature from 60 to 120°C on the microstructure and properties of oriented PP cast films and the stretching microporous membrane was studied. With the increasing roll temperature, the long period of the lamellar structure is increased from 11.5 to 12.1 nm, the crystalline phase thickness and the amorphous phase thickness are also increased, and the regularity of the lamellar structure improves. In comparison, the lamellae lateral dimension is nearly unchanged at 50 nm. The orientation of the lamellar structure slightly decreases from 0.81 to 0.76 with increasing roll temperature. The increase in the long period and the improvement in the regularity of the lamellar structure lead to the increase of the elastic recovery value of PP cast film. For the stretched microporous membranes prepared under a higher roll temperature, the lamellar clusters could be separated more completely, showing a smaller thickness of lamellar clusters and larger micropores. The air permeability and thermal shrinkage resistance are also improved with increasing roll temperature. The higher roll temperature is beneficial to the perfection of the lamellar structure, obtaining the higher-performance microporous membrane.

AUTHOR CONTRIBUTIONS

Dahua Chen: Writing – original draft (lead). **Xiande Chen:** Data curation (lead); investigation (lead). **Liangdong Yin:** Data curation (supporting). **Ruijie Xu:** Conceptualization (lead); funding acquisition (supporting); writing – review and editing (supporting). **Caihong Lei:** Funding acquisition (lead). **Jiayi Xie:** Conceptualization (lead); funding acquisition (supporting); writing – review and editing (supporting).

ACKNOWLEDGMENTS

The authors also would like to thank the Project of the National Science Foundation of China under Grant (52173033), Guangzhou Science and Technology Plan Project (202102020952), Project of Science Foundation of Guangdong Province (2021A1515011914), The Youth Fund Project of Regional Joint Foundation-Fundamental and Applied Basic Research Foundation of Guangdong Province (2021A1515110648), and Foshan Science and Technology Innovation Project (No. FS0AA-KJ919-4402-0145).

CONFLICT OF INTEREST STATEMENT

The authors declare no conflicts of interest.

DATA AVAILABILITY STATEMENT

The data in this article is repeatable and the data sources are available.

ORCID

Caihong Lei  <https://orcid.org/0000-0002-3660-7715>

REFERENCES

- [1] A. J. McHugh, *J. Controll. Release* **2005**, *109*, 211.
- [2] G. Venugopal, J. Moore, J. Howard, S. Pandalwar, *J. Power Sources* **1999**, *77*, 34.
- [3] S. S. Zhang, *J. Power Sources* **2007**, *164*, 351.
- [4] T. Wu, K. Wang, M. Xiang, Q. Fu, *Chinese J. Chem.* **2019**, *37*, 1207.
- [5] V. Etacheri, R. Marom, R. Elazari, G. Salitra, D. Aurbach, *Energy Environ. Sci.* **2011**, *4*, 3243.
- [6] J. Xie, Y. Wu, Z. Yin, L. Yin, R. Xu, C. Lei, *Chinese J. Polym. Sci.* **2022**, *40*, 403.
- [7] Y. Lin, X. Li, X. Chen, M. An, Q. Zhang, D. Wang, L. Li, *Polymer* **2019**, *178*, 121579.
- [8] F. Sadeghi, A. Ajji, P. J. Carreau, *J. Membr. Sci.* **2007**, *292*, 62.
- [9] F. Zeng, R. Xu, L. Ye, *Ind. Eng. Chem. Res.* **2019**, *58*, 2217.
- [10] S. H. Tabatabaei, P. J. Carreau, A. Ajji, *J. Membr. Sci.* **2009**, *345*, 148.
- [11] S.-Y. Lee, S.-Y. Park, H.-S. Song, *Polymer* **2006**, *47*, 3540.
- [12] F. Sadeghi, A. Ajji, P. Carreau, *J. Plast. Film. Sheet.* **2005**, *21*, 199.
- [13] F. Sadeghi, A. Ajji, P. J. Carreau, *Polym. Eng. Sci.* **2007**, *47*, 1170.
- [14] J. Xie, L. Yin, Y. Wu, R. Xu, C. Lei, *Polym. Test.* **2021**, *104*, 107394.
- [15] S. Y. Lee, S. Y. Park, H. S. Song, *J. Appl. Polym. Sci.* **2007**, *103*, 3326.
- [16] B. Hu, C. Lei, R. Xu, W. Shi, Q. Cai, H. Mo, C. Chen, *J. Plast. Film. Sheet.* **2014**, *30*, 300.
- [17] R. Xu, X. Chen, J. Xie, Q. Cai, C. Lei, *Ind. Eng. Chem. Res.* **2015**, *54*, 2991.
- [18] D. M. Freitas, A. D. Oliveira, A. M. Alves, S. N. Cavalcanti, P. Agrawal, T. J. Melo, *J. Appl. Polym. Sci.* **2021**, *138*, 49910.
- [19] S. H. Tabatabaei, P. J. Carreau, A. Ajji, *Polymer* **2009**, *50*, 4228.
- [20] J. Liu, Z. T. Ding, Z. Y. Liu, J. M. Feng, W. Yang, M. B. Yang, *Acta Polym. Sin.* **2011**, *11*, 1278.
- [21] A. P. Gray, *Thermochim. Acta* **1970**, *1*, 563.
- [22] G. R. Strobl, M. J. Schneider, I. G. J. Voigt-Martin, *Polym. Sci. Polym. Phys.* **1980**, *18*, 1361.
- [23] M. Houska, M. Brummell, *Polym. Eng. Sci.* **1987**, *27*, 917.
- [24] C. Chen, C. Lei, Q. Cai, H. Mo, R. Xu, *J. Plast. Film. Sheet.* **2015**, *31*, 78.
- [25] A. Saffar, A. Ajji, P. J. Carreau, M. R. Kamal, *Polymer* **2014**, *55*, 3156.
- [26] S. Cannon, G. McKenna, W. Statton, *J. Polym. Sci. Macromol. Rev.* **1976**, *11*, 209.
- [27] C. Lei, R. Xu, Z. Tian, H. Huang, J. Xie, X. Zhu, *Macromolecules* **2018**, *51*, 3433.
- [28] Z. Ding, R. Bao, B. Zhao, J. Yan, Z. Liu, M. Yang, *J. Appl. Polym. Sci.* **2013**, *130*, 1659.

- [29] C. Xiande, X. Ruijie, X. Jiayi, L. Yuanfei, L. Caihong, L. Liangbin, *Polymer* **2016**, *94*, 31.
- [30] G. Elyashevich, I. Kuryndin, V. Lavrentyev, E. Popova, V. Bukošek, *Phys. Solid State* **2018**, *60*, 2019.
- [31] B. Crist, *J. Appl. Crystallogr.* **1979**, *12*, 27.
- [32] Y. Tang, Z. Jiang, Y. Men, L. An, H.-F. Enderle, D. Lilge, S. V. Roth, R. Gehrke, J. Rieger, *Polymer* **2007**, *48*, 5125.
- [33] Y. Lin, X. Li, L. Meng, X. Chen, F. Lv, Q. Zhang, R. Zhang, L. Li, *Macromolecules* **2018**, *51*, 2690.
- [34] J. Z. Xu, L. Xu, Y. Y. Liang, G. J. Zhong, J. Lei, Z. M. Li, *J. Polym. Sci. Polym. Phys.* **2015**, *53*, 673.

How to cite this article: D. Chen, X. Chen, L. Yin, J. Xie, R. Xu, C. Lei, *J. Appl. Polym. Sci.* **2023**, *140*(30), e54080. <https://doi.org/10.1002/app.54080>

检索证明

报告编号: 20230926CS01

受广东轻工职业技术学院 冯爱娟 的委托,中国科学院广州分院、广东省科学院信息中心通过 **Web of Science** 数据库,对冯爱娟作为文章第一作者,发表的论文“A new chromone derivative from an endophytic *Aspergillus* sp. GXNU-B1”被 **SCI** 收录的情况进行联机检索,结果如下:

该篇论文被 **SCI** 收录。

1. Title: A new chromone derivative from an endophytic *Aspergillus* sp. GXNU-B1

Author(s): **Feng, AJ (Feng, Aijuan)**; Zhang, WX (Zhang, Wenxiu); Wang, LX (Wang, Lixia); Zhou, JQ (Zhou, Junqiang); Chen, JW (Chen, Jinwei); Xu, XY (Xu, Xiaoyun); Huang, XS (Huang, Xishan); Huang, JG (Huang, Jiguo)

Source: NATURAL PRODUCT RESEARCH DOI: 10.1080/14786419.2023.2181805 Early Access Date: FEB 2023

Accession Number: WOS:000937660200001

PubMed ID: 36815551

Document Type: Article; Early Access

Addresses: [Feng, Aijuan; Wang, Lixia; Zhou, Junqiang; Chen, Jinwei; Xu, Xiaoyun; Huang, Jiguo] Guangdong Engn Tech Res Ctr Green Household Chem, Sch Chem Engn & Technol, Guangdong Ind Polytech, Guangzhou, Peoples R China.

[Zhang, Wenxiu; Huang, Xishan] Guangxi Normal Univ, Coll Chem & Pharmaceut Sci, State Key Lab Chem & Mol Engn Med Resources, Guilin, Peoples R China.

Corresponding Address: Huang, JG (corresponding author), Guangdong Engn Tech Res Ctr Green Household Chem, Sch Chem Engn & Technol, Guangdong Ind Polytech, Guangzhou, Peoples R China.

E-mail Addresses: huangjiguo@126.com

ISSN: 1478-6419

eISSN: 1478-6427

特此证明



119 Views
0 CrossRef citations to date
0 Altmetric



Full access

Research Article

A new chromone derivative from an endophytic *Aspergillus* sp. GXNU-B1

Aijuan Feng, Wenxiu Zhang, Lixia Wang, Junqiang Zhou, Jinwei Chen, Xiaoyun Xu, ... show all

Received 22 Dec 2022; Accepted 14 Feb 2023; Published online: 23 Feb 2023

Cite this article | <https://doi.org/10.1080/14786419.2023.2181805> | Check for updates

Full Article | Figures & data | References | Supplemental | Citations | Metrics | Reprints & Permissions

View PDF | View Epub

In this article

Abstract

Graphical Abstract

1. Introduction

2. Results and discussion

3. Experimental

4. Conclusion

Supplemental material

Disclosure statement

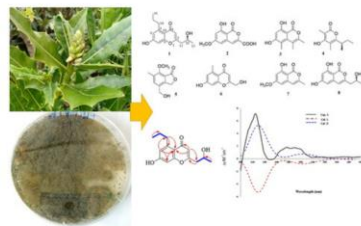
Additional information

References

Abstract

A new chromone derivative, aspergione A (**1**), along with seven known metabolites, was isolated from a mangrove endophytic fungus, *Aspergillus* sp. GXNU-B1, which was collected from mangrove *Acanthus ilicifolius* L. Their structures and the absolute configuration of **1** were elucidated based on the analysis of HR-ESI-MS, NMR, and ECD calculation. Compounds **1-8** were evaluated for their anti-inflammatory effects on the production of nitric oxide (NO). Compounds **1** and **8** have potent inhibitory effects

against NO production in activated macrophages with IC₅₀ values of 38.26 and 44.30 μM, respectively.



Q Keywords: *Aspergillus* sp., mangrove endophytic fungus, aspergione A, anti-inflammatory effect

Previous article

View latest articles

Next article

1. Introduction

Chromone derivatives, which represent a class of fungal metabolites with a core structure consisting of a chromone moiety, have been demonstrated to be an important source of structurally new and biologically active metabolites. Chromone derivatives have usually been obtained from more than ten genera, including *Aspergillus* (Tian et al. 2007), *Engyodontium album* (Yao et al. 2014), *Mycloptodiscus* (Siriwach et al. 2012), *Botryosphaeriaceae* (Isaka et al. 2018), *Xylomelasma* (Lai et al. 2021), *Xylaria nigripes* (Li et al. 2022), *Dryaria fortune* (Han et al. 2015), *Penicillium* (Huang et al. 2017),

Ilyonectriarabusta (Kuang et al. 2022), *Taeniolaella* (Intaraudom et al. 2021), *Bipolariseusines* (He et al. 2019), and so on. Among them, chromone derivatives from marine-derived fungi have attracted considerable attention for their diverse structural complexity and promising bioactivities (Carroll et al. 2022). For instance, a new chromone derivative was screened for cytotoxicity, which exhibited a 0.14 μM IC₅₀ against the P338 cell line (Tian et al. 2007). A new antibacterial chromone derivative showed antibacterial activity against *Salmonell* with a MIC value of 2.00 ± 0.02 μM (Huang et al. 2017).

During our on going search for biologically active metabolites from the mangrove endophytic fungi (Hao et al. 2022; Zhou et al. 2022; Qin et al. 2022; Zhang et al. 2021; Huang et al. 2022). In our chemical investigation on the fungus *Aspergillus* sp. GXNU-B1, a new chromone derivative **1**, together with seven known metabolites **2-8**, was obtained (see Figure S1 in the Supplementary Material). The structures of the isolated compounds were established by HR-ESI-MS, 1D, and 2D NMR data (see Figures S4–S23 in the Supplementary Material), as well as by comparison with literature data. Herein, the isolation, structure determination, and anti-inflammatory activity of these compounds **1-8** are described in detail.

2. Results and discussion

Compound **1** was obtained as a white powder with the molecular formula C₁₅H₁₀O₄ as determined from its HR-ESI-MS, of which a hydrogen adduct quasimolecular ion at *m/z* 263.1274 [M + H]⁺ (calcd 263.1278 for C₁₅H₁₀O₄)⁺ (7 degrees of unsaturation). The ¹H NMR data of **1** (see Table S1 in the Supplementary Material) displayed three phenyl protons at δ_H 6.67 (1H, d, *J* = 2.4 Hz), 6.64 (1H, d, *J* = 2.4 Hz) and 6.06 (1H, s), one methine group at δ_H 4.19 (1H, ddd, *J* = 8.0, 6.2, 4.8 Hz), three methylene groups at δ_H 3.13 (2H, dd, *J* = 9.1, 6.2 Hz), 2.72 (1H, dd, *J* = 14.3, 4.8 Hz)/2.65 (1H, dd, *J* = 14.3, 8.0 Hz), 1.59 (2H, m),

Related research

People also read | Recommended articles | Cited by

Desmoarycoumarin and episoyasapogenol B: two new compounds from *Desmodium salicifolium* (Poir.) DC (Fabaceae) >

People also read | Recommended articles | Cited by

Desmoarycoumarin and episoyasapogenol B: two new compounds from *Desmodium salicifolium* (Poir.) DC (Fabaceae) >

Aphalaine Pinchemell Tiombou Donkia et al. Natural Product Research Published online: 23 Feb 2023

A new lactone from mangrove endophytic fungus *Aspergillus* sp. GXNU-A9 >

Wenxiu Zhang et al. Natural Product Research Published online: 22 Dec 2021

A new depsidone derivative from mangrove endophytic fungus *Aspergillus* sp. GXNU-A9 >

Lili Hao et al. Natural Product Research Published online: 27 Aug 2020

View more

GDIP WEB Internet 访问

People also read | Recommended articles | Cited by

Desmoarycoumarin and episoyasapogenol B: two new compounds from *Desmodium salicifolium* (Poir.) DC (Fabaceae) >

Aphalaine Pinchemell Tiombou Donkia et al. Natural Product Research Published online: 23 Feb 2023

A new lactone from mangrove endophytic fungus *Aspergillus* sp. GXNU-A9 >

Wenxiu Zhang et al. Natural Product Research Published online: 22 Dec 2021

A new depsidone derivative from mangrove endophytic fungus *Aspergillus* sp. GXNU-A9 >

Lili Hao et al. Natural Product Research Published online: 27 Aug 2020

View more

Abstract
Graphical Abstract
1. Introduction
2. Results and discussion
3. Experimental
4. Conclusion
Supplemental material
Disclosure statement
Additional information
References

two methyl groups at δ_{H} 1.28 (3H, d, $J = 6.2$ Hz) and 0.98 (3H, t, $J = 14.7, 7.3$ Hz). The ^{13}C NMR and HSQC spectroscopic data showed the presence of 15 signals (see Figures S5, S6 in the Supplementary Material) for two methyl carbons (δ_{C} 14.4 and 23.5), three methylene carbons (δ_{C} 25.8, 38.3, and 44.2), one oxygen-bearing methine (δ_{C} 66.4), three aromatic carbons (δ_{C} 112.5, 117.7, and 101.9), and six quaternary carbons, including one ketone carbonyl (δ_{C} 181.5, 166.9, 163.2, 161.8, 148.3, and 115.2), accounting for six double-bond equivalents. The remaining degree of unsaturation was due to the presence of two rings in molecule **1**. The above data indicated that **1** might belong to a chromone-type derivative, whose structure usually consists of two rings (rings A and B) (Kashiwada et al. 1984). The spin systems 3.13 (H-14)/1.59 (H-15)/0.98 (H₃-16) (fragment A) and 2.72 or 2.65 (H₂-11)/4.19 (H-12)/1.28 (H₃-13) (fragment B) were successfully established and attributed to the ^1H - ^1H COSY correlations (see Figure S7 in the Supplementary Material). The HMBC correlations (see Figure S8 in the Supplementary Material) from δ_{H} 3.13 (H₂-14) to δ_{C} 148.3 (C-5), 117.7 (C-6), 115.2 (C-10), and from δ_{H} 6.64 (H-6) to δ_{C} 38.3 (C-14) suggested that the fragment A connected with C-5. The HMBC correlations (see Figure S8 in the Supplementary Material) from δ_{H} 2.72/2.65 (H₂-11) to δ_{C} 166.9 (C-2), and from δ_{H} 6.06 (H-3) to δ_{C} 44.2 (C-11), 181.5 (C-4), and 115.2 (C-10), suggested that the fragment B connected with C-2. Detailed analysis of the HSQC, COSY and HMBC spectra allowed the assignment of all protons and carbons resonances. Detailed analyses of the above NMR data showed that **1** had highly similar skeleton to those of 2-(2'-hydroxypropyl)-5-methyl-7-hydroxychromone (Kashiwada et al. 1984), except for the presence of a propyl group instead of a methyl group connected with C-2 (see Table S1, Figure S2 in the Supplementary Material). Based on these analyses, the planar structure of **1** was determined to be as shown in Figure S1 (see the Supplementary Material).

There is only one stereogenic carbon in **1**. To assign the absolute configuration of **1**, the structures 11S-**1** and 11R-**1** were subjected to quantum chemical TDDFT calculations of their ECD spectra. As shown in Figure S3 (see the Supplementary Material), the experimental ECD curves with Cotton at 225

and 280 nm matched well with the predicted ECD spectrum of **1**, suggesting that the absolute configurations of C-11 in **1** could be assigned as 11R. Thus, **1** was named aspergione A.

The remaining known compounds **2-8** were determined based on the analysis of their NMR data (see Figures S10-S23 in the Supplementary Material), along with a comparison with previously published data in the literature, and identified as 6-methoxy-8-hydroxyisocoumarin-3-carboxylic acid (**2**) (Wang et al. 2017), decarboxycitrinone (**3**) (Whyte et al. 1996), phomapyrone C (**4**) (Pedras et al. 1994), convolvulol (**5**) (Tsantrizos et al. 1992), 7-hydroxy-2-hydroxymethyl-5-methyl-4H-chromen-4-one (**6**) (Kimura et al. 1992), 3-methyl-6-methoxy-8-hydroxyisocoumarin (**7**) (Kumaga et al. 1994), and methyladioporthin (**8**) (Zhang et al. 2020), respectively.

Compounds **1-8** were evaluated for their anti-inflammatory effects on the production of nitric oxide (NO) in the RAW 264.7 macrophage cell line that was exposed to the inflammatory stimulus by lipopolysaccharide (LPS) (see Table S2 in the Supplementary Material). The results show that compounds **1** and **8** have potent inhibitory effects against the NO release (IC_{50} 38.26 and 44.30 μM), while compounds **2-4**, **6**, and **7** show weak inhibitory activities against the NO production. Compound **5** has no anti-inflammatory properties under its safe concentration.

3. Experimental

3.1. General experimental procedures

1D and 2D NMR spectra were obtained at 400 MHz for ^1H and 100 MHz for ^{13}C , respectively, on a Bruker Avance III HD 400 spectrometer (Bruker, Ettlingen, Germany) with residual solvent peaks as references. ESI-MS and HR-ESI-MS were obtained on a Bruker Esquire 3000 plus and a

Waters/Micromass Q-TOF-Ultima (Waters, Milford, MA, USA) mass spectrometers, respectively. Silica gel (300-400 mesh, Qingdao Haiyang Chemical Co. Ltd, Qingdao, China), Sephadex LH-20 (Pharmacia Biotech AB, Uppsala, Sweden), and ODS-A-HG reversed-phase silica gel (12 nm 5-50 μm , YMC Co., Ltd., Japan) were used for column chromatography (CC). Silica gel HSGF254 (Yantai Jiangyou Gujiao Kaifa Co., Yantai, China) was used for TLC. Semi-preparative HPLC was performed using an Agilent 1260 HPLC system, and samples were separated on a Waters Sun Fire-C₁₈ column (5 μm , i.d. 10 mm \times 250 mm).

3.2. Fungal material and fermentation

The fungus was isolated from the mangrove *Acanthus ilicifolius* L., which was collected at the seaside of Qin Zhou, Guangxi Province, China, October 2019. The fungus strain GXNU-B1 was determined as *Aspergillus* sp. by 18S rDNA analysis (GenBank accession number: MT626059). The strain was statically cultured at 28 °C for 30 days in 500-mL Erlenmeyer-flasks (400 \times 200 mL, a total of 80 L) each containing 200 mL of cultural media (glucose 20 g, yeast extract 2 g, $\text{MgSO}_4 \cdot 7\text{H}_2\text{O}$ 0.1 g, KH_2PO_4 0.2 g, sea salt 5 g in 1 L water).

3.3. Extraction and isolation

The culture solid (50 L) was filtered and extracted with EtOAc three times and concentrated under a vacuum to remove EtOAc obtain 18.8 g metabolite extract. The mycelium was extracted by methanol and then concentrated under a vacuum. The concentrate was extracted with EtOAc and then combined with broth extract. The total extract (11.4 g) was fractionated by silica gel CC eluted in a gradient from dichloromethane (D)-methanol (M) (D/M from 100:1 to 70:30) to yield eight fractions (Fr.s 1-4) based on TLC analysis. Fr.2 was subjected to repeated CC and then purified by semi-preparative HPLC (10 ID \times 250 mm, 4.0 mL/min, 60% Methanol in H₂O) to afford compounds **1** (5.3

People also read	Recommended articles	Cited by
Desmoaylcoumarin and episoyasapogenol B: two new compounds from <i>Desmodium salicifolium</i> (Poir.) DC (Fabaceae) >		
Aphalaine Pinchemell Tiombou Donkia et al. Natural Product Research Published online: 22 Feb 2023		
A new lactone from mangrove endophytic fungus <i>Aspergillus</i> sp. GXNU-A9 >		
Wenxiu Zhang et al. Natural Product Research Published online: 22 Dec 2021		
A new depsidone derivative from mangrove endophytic fungus <i>Aspergillus</i> sp. GXNU-A9 >		
Lili Hao et al. Natural Product Research Published online: 27 Aug 2020		
View more		

Abstract
Graphical Abstract
1. Introduction
2. Results and discussion
3. Experimental
4. Conclusion
Supplemental material
Disclosure statement
Additional information
References

and 280 nm matched well with the predicted ECD spectrum of **1**, suggesting that the absolute configurations of C-11 in **1** could be assigned as 11R. Thus, **1** was named aspergione A.

The remaining known compounds **2-8** were determined based on the analysis of their NMR data (see Figures S10-S23 in the Supplementary Material), along with a comparison with previously published data in the literature, and identified as 6-methoxy-8-hydroxyisocoumarin-3-carboxylic acid (**2**) (Wang et al. 2017), decarboxycitrinone (**3**) (Whyte et al. 1996), phomapyrone C (**4**) (Pedras et al. 1994), convolvulol (**5**) (Tsantrizos et al. 1992), 7-hydroxy-2-hydroxymethyl-5-methyl-4H-chromen-4-one (**6**) (Kimura et al. 1992), 3-methyl-6-methoxy-8-hydroxyisocoumarin (**7**) (Kumaga et al. 1994), and methyladioporthin (**8**) (Zhang et al. 2020), respectively.

Compounds **1-8** were evaluated for their anti-inflammatory effects on the production of nitric oxide (NO) in the RAW 264.7 macrophage cell line that was exposed to the inflammatory stimulus by lipopolysaccharide (LPS) (see Table S2 in the Supplementary Material). The results show that compounds **1** and **8** have potent inhibitory effects against the NO release (IC_{50} 38.26 and 44.30 μM), while compounds **2-4**, **6**, and **7** show weak inhibitory activities against the NO production. Compound **5** has no anti-inflammatory properties under its safe concentration.

3. Experimental

3.1. General experimental procedures

1D and 2D NMR spectra were obtained at 400 MHz for ^1H and 100 MHz for ^{13}C , respectively, on a Bruker Avance III HD 400 spectrometer (Bruker, Ettlingen, Germany) with residual solvent peaks as references. ESI-MS and HR-ESI-MS were obtained on a Bruker Esquire 3000 plus and a

Waters/Micromass Q-TOF-Ultima (Waters, Milford, MA, USA) mass spectrometers, respectively. Silica gel (300-400 mesh, Qingdao Haiyang Chemical Co. Ltd, Qingdao, China), Sephadex LH-20 (Pharmacia Biotech AB, Uppsala, Sweden), and ODS-A-HG reversed-phase silica gel (12 nm 5-50 μm , YMC Co., Ltd., Japan) were used for column chromatography (CC). Silica gel HSGF254 (Yantai Jiangyou Gujiao Kaifa Co., Yantai, China) was used for TLC. Semi-preparative HPLC was performed using an Agilent 1260 HPLC system, and samples were separated on a Waters Sun Fire-C₁₈ column (5 μm , i.d. 10 mm \times 250 mm).

3.2. Fungal material and fermentation

The fungus was isolated from the mangrove *Acanthus ilicifolius* L., which was collected at the seaside of Qin Zhou, Guangxi Province, China, October 2019. The fungus strain GXNU-B1 was determined as *Aspergillus* sp. by 18S rDNA analysis (GenBank accession number: MT626059). The strain was statically cultured at 28 °C for 30 days in 500-mL Erlenmeyer-flasks (400 \times 200 mL, a total of 80 L) each containing 200 mL of cultural media (glucose 20 g, yeast extract 2 g, $\text{MgSO}_4 \cdot 7\text{H}_2\text{O}$ 0.1 g, KH_2PO_4 0.2 g, sea salt 5 g in 1 L water).

3.3. Extraction and isolation

The culture solid (50 L) was filtered and extracted with EtOAc three times and concentrated under a vacuum to remove EtOAc obtain 18.8 g metabolite extract. The mycelium was extracted by methanol and then concentrated under a vacuum. The concentrate was extracted with EtOAc and then combined with broth extract. The total extract (11.4 g) was fractionated by silica gel CC eluted in a gradient from dichloromethane (D)-methanol (M) (D/M from 100:1 to 70:30) to yield eight fractions (Fr.s 1-4) based on TLC analysis. Fr.2 was subjected to repeated CC and then purified by semi-preparative HPLC (10 ID \times 250 mm, 4.0 mL/min, 60% Methanol in H₂O) to afford compounds **1** (5.3

People also read	Recommended articles	Cited by
Desmoaylcoumarin and episoyasapogenol B: two new compounds from <i>Desmodium salicifolium</i> (Poir.) DC (Fabaceae) >		
Aphalaine Pinchemell Tiombou Donkia et al. Natural Product Research Published online: 23 Feb 2023		
A new lactone from mangrove endophytic fungus <i>Aspergillus</i> sp. GXNU-A9 >		
Wenxiu Zhang et al. Natural Product Research Published online: 22 Dec 2021		
A new depsidone derivative from mangrove endophytic fungus <i>Aspergillus</i> sp. GXNU-A9 >		
Lili Hao et al. Natural Product Research Published online: 27 Aug 2020		
View more		

Abstract
Graphical Abstract
1. Introduction
2. Results and discussion
3. Experimental
4. Conclusion
Supplemental material
Disclosure statement
Additional information
References

Waters/Micromass Q-TOF-Ultima (Waters, Milford, MA, USA) mass spectrometers, respectively. Silica gel (300-400 mesh, Qingdao Haiyang Chemical Co. Ltd, Qingdao, China), Sephadex LH-20 (Pharmacia Biotech AB, Uppsala, Sweden), and ODS-A-HG reversed-phase silica gel (12 nm 5-50 μm , YMC Co., Ltd., Japan) were used for column chromatography (CC). Silica gel HSGF254 (Yantai Jiangyou Gujiao Kaifa Co., Yantai, China) was used for TLC. Semi-preparative HPLC was performed using an Agilent 1260 HPLC system, and samples were separated on a Waters Sun Fire-C₁₈ column (5 μm , i.d. 10 mm \times 250 mm).

3.2. Fungal material and fermentation

The fungus was isolated from the mangrove *Acanthus ilicifolius* L., which was collected at the seaside of Qin Zhou, Guangxi Province, China, October 2019. The fungus strain GXNU-B1 was determined as *Aspergillus* sp. by 18S rDNA analysis (GenBank accession number: MT626059). The strain was statically cultured at 28 °C for 30 days in 500-mL Erlenmeyer-flasks (400 \times 200 mL, a total of 80 L) each containing 200 mL of cultural media (glucose 20 g, yeast extract 2 g, $\text{MgSO}_4 \cdot 7\text{H}_2\text{O}$ 0.1 g, KH_2PO_4 0.2 g, sea salt 5 g in 1 L water).

3.3. Extraction and isolation

The culture solid (50 L) was filtered and extracted with EtOAc three times and concentrated under a vacuum to remove EtOAc obtain 18.8 g metabolite extract. The mycelium was extracted by methanol and then concentrated under a vacuum. The concentrate was extracted with EtOAc and then combined with broth extract. The total extract (11.4 g) was fractionated by silica gel CC eluted in a gradient from dichloromethane (D)-methanol (M) (D/M from 100:1 to 70:30) to yield eight fractions (Fr.s 1-4) based on TLC analysis. Fr.2 was subjected to repeated CC and then purified by semi-preparative HPLC (10 ID \times 250 mm, 4.0 mL/min, 60% Methanol in H₂O) to afford compounds **1** (5.3

People also read	Recommended articles	Cited by
Desmoaylcoumarin and episoyasapogenol B: two new compounds from <i>Desmodium salicifolium</i> (Poir.) DC (Fabaceae) >		
Aphalaine Pinchemell Tiombou Donkia et al. Natural Product Research Published online: 23 Feb 2023		
A new lactone from mangrove endophytic fungus <i>Aspergillus</i> sp. GXNU-A9 >		
Wenxiu Zhang et al. Natural Product Research Published online: 22 Dec 2021		
A new depsidone derivative from mangrove endophytic fungus <i>Aspergillus</i> sp. GXNU-A9 >		
Lili Hao et al. Natural Product Research Published online: 27 Aug 2020		
View more		

Abstract
Graphical Abstract
1. Introduction
2. Results and discussion
3. Experimental
4. Conclusion
Supplemental material
Disclosure statement
Additional information
References

preparative HPLC (10 ID × 250 mm, 4.0 mL/min, 60% Methanol in H₂O) to afford compounds **1** (5.3 mg), **3** (4.8 mg), **6** (7.5 mg) and **4** (15.2 mg). Fr.3 was further purified by CC and semi-preparative HPLC (70% Methanol in H₂O) to obtain compound **2** (4.9 mg), **5** (6.6 mg), **6** (7.5 mg), and **8** (22.2 mg). Fr.4 was further purified by CC and semi-preparative HPLC (70% Methanol in H₂O) to obtain compounds **6** (2.9 mg), **7** (3.4 mg), and **8** (6.2 mg).

3.5.1. Physicochemical and spectral data

Compound **1**: white powder; ¹H and ¹³C NMR data, see Table S1; (+)-HR-ESI-MS *m/z* 263.1274 [M + H]⁺ (calcd 263.1278 for C₁₅H₁₃O₄⁺), see Figure S9.

Compounds **2-8**: ¹H and ¹³C NMR data, see Figures S10–S23.

3.4. Anti-inflammatory assay

The anti-inflammatory effects of all compounds were examined on the production of nitric oxide (NO) in LPS-stimulated cells using a method according to our previously described method (Liu et al. 2020).

4. Conclusion

The chemical investigation of mangrove endophytic fungus *Aspergillus* sp. GXNU-B1 resulted in the isolation of a new chromone derivative, aspergione A (**1**), together with seven known metabolites **2-8**. Compounds **1-8** were evaluated for their anti-inflammatory effects on the production of NO. Compounds **1** and **8** showed reduced the production of NO in LPS-stimulated cells with IC₅₀ values of 38.26 and 44.30 μM, respectively.

Abstract
Graphical Abstract
1. Introduction
2. Results and discussion
3. Experimental
4. Conclusion
Supplemental material
Disclosure statement
Additional information
References

Supplemental material

A new chromone derivative from an endophytic *Aspergillus* sp. GXNU-B1

Showing 1/2: gnpl_a_2181805_sm2902.pdf 105 views 0 shares 29 downloads

SUPPLEMENTARY MATERIAL

A new chromone derivative from an endophytic *Aspergillus* sp. GXNU-B1

Aijuan Feng^a, Wenxiu Zhang^b, Lixia Wang^a, Junqiang Zhou^a, Jimwei Chen^a, Xiaoyun Xu^a, Xishan Huang^a, Jiguo Huang^{a*}

^aSchool of Chemical Engineering and Technology, Guangdong Industry Polytechnic, Guangdong Engineering Technical Research Center for Green Household Chemicals, Guangzhou, China
^bState Key Laboratory for Chemistry and Molecular Engineering of Medicinal Resources, College of Chemistry and Pharmaceutical Sciences, Guangxi Normal University, Guilin, P. R. China
*Correspondence: huangjiguo@126.com

1 / 2 Share Download

Disclosure statement

The authors declare no conflict of interest.

Additional information

Funding

The authors (J.G. Huang, and X.S. Huang) acknowledge the following agencies for funding this project: Department of Science and Technology of Guangzhou under grant number 202102020608/2021KTCX200. National Natural Science Foundation of China (42066005); the Natural Science Foundation of Guangxi Province (2020JJA150036); Guangxi Science and Technology Base Special Talents (2019AC20095).

[← Previous article](#)
[View latest articles](#)
[Next article →](#)

References

- Carroll A, Copp B, Davis R, Keyzers R, Prinsep M. 2022. Marine natural products. *Nat Prod Rep.* 39(6):1122–1171. [Crossref], [PubMed], [Web of Science ®], [Google Scholar]
- Han L, Zheng F, Zhang Y, Liu E, Li W, Xia M, Wang T, Gao X. 2015. Triglyceride accumulation inhibitory effects of new chromone glycosides from *Drynaria fortunei*. *Nat Prod Res.* 29(18):1703–1710. [Taylor & Francis Online], [Web of Science ®], [Google Scholar]

People also read	Recommended articles	Cited by
<p>Desmoarycoumarin and episoyasapogenol B: two new compounds from <i>Desmodium salicifolium</i> (Poir.) DC (Fabaceae) ➤</p>		
<p>Aphalaine Pinchemell Tiombou Donkia et al. <i>Natural Product Research</i> Published online: 23 Feb 2023</p>		
<p>A new lactone from mangrove endophytic fungus <i>Aspergillus</i> sp. GXNU-A9 ➤</p>		
<p>Wenxiu Zhang et al. <i>Natural Product Research</i> Published online: 22 Dec 2021</p>		
<p>A new depsidone derivative from mangrove endophytic fungus <i>Aspergillus</i> sp. GXNU-A9 ➤</p>		
<p>Lili Hao et al. <i>Natural Product Research</i> Published online: 27 Aug 2020</p>		

View more

read	articles
<p>Desmoarycoumarin and episoyasapogenol B: two new compounds from <i>Desmodium salicifolium</i> (Poir.) DC (Fabaceae) ➤</p>	
<p>Aphalaine Pinchemell Tiombou Donkia et al. <i>Natural Product Research</i> Published online: 23 Feb 2023</p>	
<p>A new lactone from mangrove endophytic fungus <i>Aspergillus</i> sp. GXNU-A9 ➤</p>	
<p>Wenxiu Zhang et al. <i>Natural Product Research</i> Published online: 22 Dec 2021</p>	
<p>A new depsidone derivative from mangrove endophytic fungus <i>Aspergillus</i> sp. GXNU-A9 ➤</p>	
<p>Lili Hao et al. <i>Natural Product Research</i> Published online: 27 Aug 2020</p>	

View more

Abstract
Graphical Abstract
1. Introduction
2. Results and discussion
3. Experimental
4. Conclusion
Supplemental material
Disclosure statement
Additional information
References

People also read	Recommended articles	Cited by
<p>Desmoarycoumarin and episoyasapogenol B: two new compounds from <i>Desmodium salicifolium</i> (Poir.) DC (Fabaceae) ➤</p>		
<p>Aphalaine Pinchemell Tiombou Donkia et al. <i>Natural Product Research</i> Published online: 23 Feb 2023</p>		
<p>A new lactone from mangrove endophytic fungus <i>Aspergillus</i> sp. GXNU-A9 ➤</p>		
<p>Wenxiu Zhang et al. <i>Natural Product Research</i> Published online: 22 Dec 2021</p>		
<p>A new depsidone derivative from mangrove endophytic fungus <i>Aspergillus</i> sp. GXNU-A9 ➤</p>		
<p>Lili Hao et al. <i>Natural Product Research</i> Published online: 27 Aug 2020</p>		

View more

Abstract
Graphical Abstract
1. Introduction
2. Results and discussion
3. Experimental
4. Conclusion
Supplemental material
Disclosure statement
Additional information
References

- Hao L, Zhou D, Qin X, Zhang W, Yang R, Li J, Huang X. 2022. A new depsidone derivative from mangrove endophytic fungus *Aspergillus* sp. GXNU-A9. *Nat Prod Res.* 36(7):1878-1882. [Taylor & Francis Online], [Web of Science ®], [Google Scholar]
- He J, Li Z, Ai H, Feng T, Liu J. 2019. Anti-bacterial chromones from cultures of the endophytic fungus *Bipolariselesines*. *Nat Prod Res.* 33(24):3515-3520. [Taylor & Francis Online], [Web of Science ®], [Google Scholar]
- Huang J, Bo X, Wu F, Tan M, Wei Y, Wang L, Zhou J, Wu G, Huang X. 2022. Asperphenyltones A and B: new phenylfuropyridinones keleton from an endophytic *Aspergillus* sp. GXNU-A1. *Molecules.* 27(23):8160-8166. [Crossref], [PubMed], [Web of Science ®], [Google Scholar]
- Huang H, Liu T, Wu X, Guo J, Lan X, Zhu Q, Zhang X, Zhang K. 2017. A new antibacterial chromone derivative from mangrove-derived fungus *Penicillium aculeatum* (No. 9EB). *Nat Prod Res.* 31(22):2593-2598. [Taylor & Francis Online], [Web of Science ®], [Google Scholar]
- Intaradom C, Bunbamrung N, Drama A, Boonyuen N, Choowong W, Rachtawee P, Pittayakhajonwut P. 2021. Chromone derivatives, R- and S-taeniolin, from the marine-derived fungus *Taeniolaella* sp. BCC31839. *Nat Prod Res.* 35(3):392-398. [Taylor & Francis Online], [Web of Science ®], [Google Scholar]
- Isaka M, Palasarn S, Sommai S, Laksanacharoen P, Srichomthong K. 2018. Maleic anhydride and chromone derivatives from the endophytic fungus BCC 54265 (*Botryosphaeriaceae*). *Nat Prod Res.* 32(13):1506-1511. [Taylor & Francis Online], [Web of Science ®], [Google Scholar]
- Kashiwada Y, Nonaka G, Nishioka I. 1984. Studies on Rhubarb (RheiRhizoma) V. isolation & characterization of chromone & chromanone derivatives. *Chem Pharm Bull.* 32:3493-3500. [Crossref], [Web of Science ®], [Google Scholar]
- Kimura Y, Shiojima K, Nakajima H, Hamasaki T. 1992. Structure and biological activity of plant growth regulators produced by *Penicillium* sp. No. 31f. *Biosci Biotechnol Biochem.* 56(7):1138-1139. [Taylor & Francis Online], [Web of Science ®], [Google Scholar]
- Kuang M, Peng W, Huang Y, Li M, Qin S, Zheng Y, Xu L, Huang Q, Zou Z. 2022. Two new chromone derivatives from the rhizosphere soil fungus *Ilyonectriarobusta*. *Nat Prod Res.* DOI: 10.1080/14786419.2022.2147169. [Taylor & Francis Online], [Web of Science ®], [Google Scholar]
- Kumaga H, Amemiya M, Naganawa H, Sawa T, Ishizuka M, Takeuchi T. 1994. Biosynthesis of antitumor antibiotic, cytogenin. *J Antibiot (Tokyo).* 47(4):440-446. [Crossref], [PubMed], [Web of Science ®], [Google Scholar]
- Lai D, Li J, Zhao S, Gu G, Gong X, Proksch P, Zhou L. 2021. Chromone and isocoumarin derivatives from the endophytic fungus *Xylomelasma* sp. Samif07, and their antibacterial and antioxidant activities. *Nat Prod Res.* 35(22):4616-4620. [Taylor & Francis Online], [Web of Science ®], [Google Scholar]
- Li J, Jiang Y, Li L, Long H, Liu H, Yang R, Liu S, Wang W, Liu J. 2022. A pair of new chromone enantiomers from *Xylaria nigripes*. *Nat Prod Res.* DOI: 10.1080/14786419.2022.2110097. [Taylor & Francis Online], [Web of Science ®], [Google Scholar]
- Liu W, Deng S, Zhou D, Huang Y, Li C, Hao L, Zhang G, Su S, Xu X, Yang R, et al. 2020. 3,4-seco-dammarane triterpenoid saponins with anti-inflammatory activity isolated from the leaves of *Cyclocarya paliurus*. *J Agric Food Chem.* 68(7):2041-2053. [Crossref], [PubMed], [Web of Science ®], [Google Scholar]
- Pedras M, Morales V, Taylor J. 1994. Phomapyromes: three metabolites from the blackleg fungus. *Phytochem Lett.* 36(5):1315-1318. [Crossref], [Google Scholar]
- Qin X, Huang J, Zhou D, Zhang W, Zhang Y, Li J, Yang R, Huang X. 2022. Polyketide derivatives, guhyoxyionols A-D from a mangrove endophytic fungus *Aspergillus* sp. GXNU-Y45 that inhibit nitric oxide production. *Mar Drugs.* 20(1):5-16. [Crossref], [Web of Science ®], [Google Scholar]
- Siriwach R, Kinoshita H, Kitani S, Igarashi Y, Pansuksan K, Panbangred W, Nihira T. 2012. Mycoleptione, a new chromone derivative isolated from the endophytic fungus *Mycoleptodiscus* sp. MU41. *J Antibiot (Tokyo).* 65(12):627-629. [Crossref], [PubMed], [Web of Science ®], [Google Scholar]
- Tian L, Cai S, Li D, Lin Z, Zhu T, Fang Y, Liu P, Gu Q, Zhu W. 2007. Two new metabolites with cytotoxicities from deep-sea fungus, *Aspergillus sydowii* YH11-2. *Arch Pharm Res.* 30(9):1051-1054. [Crossref], [PubMed], [Web of Science ®], [Google Scholar]
- Tsantrizos Y, Ogilvie K, Watson K. 1992. Phytotoxic metabolites of *Phomopsis convolvulus*, a host-specific pathogen of field bindweed. *Can J Chem.* 70(8):2276-2284. [Crossref], [Web of Science ®], [Google Scholar]
- Wang H, Umeokoli BO, Eze P, Heering C, Janiak C, Müller WE, Orfali RS, Hartmann R, Dai H, Lin W, et al. 2017. Secondary metabolites of the lichen-associated fungus *Aplospora montagne*. *Tetrahedron Lett.* 58(17):1702-1705. [Crossref], [Web of Science ®], [Google Scholar]
- Whyte A, Gloer J, Scott J, Malloch D. 1996. Cercophorins A-C: novel antifungal and cytotoxic metabolites from the coprophilous fungus *Cercophora areolate*. *J Nat Prod.* 59(8):765-769. [Crossref], [PubMed], [Web of Science ®], [Google Scholar]
- Yao Q, Wang J, Zhang X, Nong X, Xu X, Qi S. 2014. Cytotoxic polyketides from the deep-sea-derived fungus *Engyodontium album* DF5CS021. *Mar Drugs.* 12(12):5902-5915. [Crossref], [PubMed], [Web of Science ®], [Google Scholar]

People also read	Recommended articles	Cited by
Desmoarylcoumarin and episoyasapogenol B: two new compounds from <i>Desmodium salicifolium</i> (Poir.) DC (Fabaceae) >		
Aphalaine Pinchemell Tiombou Donkia et al. Natural Product Research Published online: 23 Feb 2023		
A new lactone from mangrove endophytic fungus <i>Aspergillus</i> sp. GXNU-A9 >		
Wenxiu Zhang et al. Natural Product Research Published online: 22 Dec 2021		
A new depsidone derivative from mangrove endophytic fungus <i>Aspergillus</i> sp. GXNU-A9 >		
Lili Hao et al. Natural Product Research Published online: 27 Aug 2020		

[View more](#)

People also read	Recommended articles	Cited by
Desmoarylcoumarin and episoyasapogenol B: two new compounds from <i>Desmodium salicifolium</i> (Poir.) DC (Fabaceae) >		
Aphalaine Pinchemell Tiombou Donkia et al. Natural Product Research Published online: 23 Feb 2023		
A new lactone from mangrove endophytic fungus <i>Aspergillus</i> sp. GXNU-A9 >		
Wenxiu Zhang et al. Natural Product Research Published online: 22 Dec 2021		
A new depsidone derivative from mangrove endophytic fungus <i>Aspergillus</i> sp. GXNU-A9 >		
Lili Hao et al. Natural Product Research Published online: 27 Aug 2020		

[View more](#)

People also read	Recommended articles	Cited by
Desmoarylcoumarin and episoyasapogenol B: two new compounds from <i>Desmodium salicifolium</i> (Poir.) DC (Fabaceae) >		
Aphalaine Pinchemell Tiombou Donkia et al. Natural Product Research Published online: 23 Feb 2023		
A new lactone from mangrove endophytic fungus <i>Aspergillus</i> sp. GXNU-A9 >		
Wenxiu Zhang et al. Natural Product Research Published online: 22 Dec 2021		
A new depsidone derivative from mangrove endophytic fungus <i>Aspergillus</i> sp. GXNU-A9 >		
Lili Hao et al. Natural Product Research Published online: 27 Aug 2020		

[View more](#)

Abstract
Graphical Abstract
1. Introduction
2. Results and discussion
3. Experimental
4. Conclusion
Supplemental material
Disclosure statement
Additional information
References

Abstract
Graphical Abstract
1. Introduction
2. Results and discussion
3. Experimental
4. Conclusion
Supplemental material
Disclosure statement
Additional information

24. Zhang W, Hao L, Qin X, Huang J, Yang R, Li J, Huang X. 2021. A new lactone from mangrove endophytic fungus *Aspergillus* sp. GXNU-A9. *Nat Prod Res*, DOI: 10.1080/14786419.2021.1977298. [Taylor & Francis Online], [Web of Science ®], [Google Scholar]
25. Zhang X, Qu H, Bao S, Deng Z, Guo Z. 2020. Secondary metabolites from the endophytic fungus *Xylariales* sp. and their antimicrobial activity. *Chem Nat Compd*. 56(3):530–532. [Crossref], [Web of Science ®], [Google Scholar]
26. Zhou D, Zhang W, Hao L, Qin X, Yang R, Li J, Huang X. 2022. A new sesquiterpene from mangrove endophytic fungus *Aspergillus* sp. GXNU-MA1. *Nat Prod Res*. 36(7):1857–1863. [Taylor & Francis Online], [Web of Science ®], [Google Scholar]

[Download PDF](#)

Natural Product Research
Published online: 23 Feb 2023

A new lactone from mangrove endophytic fungus *Aspergillus* sp. GXNU-A9 >

Wenxiu Zhang et al.
Natural Product Research
Published online: 22 Dec 2021

A new depsidone derivative from mangrove endophytic fungus *Aspergillus* sp. GXNU-A9 >

Lili Hao et al.
Natural Product Research
Published online: 27 Aug 2020

[View more](#)



检索 > Research on the weighting... > Research on the Weighting Values of Community Aging-Friendly Constructi...

出版商处的免费全文

全文链接

导出

添加到标记结果列表

Research on the Weighting Values of Community Aging-Friendly Construction Indexes With Different Expert Groups

作者: Mei, WB (Mei, Wen-Bing) [1]; Li, K (Li, Kun) [2]; Huang, YZ (Huang, Yi-Zhe) [1]

查看 Web of Science ResearcherID 和 ORCID (由 Clarivate 提供)

INQUIRY-THE JOURNAL OF HEALTH CARE ORGANIZATION PROVISION AND FINANCING

卷: 60

文献号: 00469580231167984

DOI: 10.1177/00469580231167984

出版时间: APR 2023

已索引: 2023-05-06

文献类型: Article

跳转至

被引参考文献深度分析

摘要:

The construction of weight values for the indicators of community aging-friendly construction is helpful to guide the formulation of strategies for allocating elderly resources in community aging-friendly constructions, and to reflect the shortcomings of community aging-friendly constructions and propose improvement strategies when evaluating the effectiveness of the existing community aging-friendly constructions. The paper uses the Fuzzy Analytic Hierarchy Process (FAHP) to calculate the weighting values of each indicator, consulting the government, industry, and academic experts. The research results show that the weighting-value order is "public environment (W = 0.364)," "health care (W = 0.342)," "humanistic care (W = 0.204)" and "social economy (W = 0.090)." Accordingly, the article proposes specific suggestions to improve the effectiveness of community aging-friendly constructions, including the need to find consensus among all parties involved in the aging industry, the need to focus on improving the public environment of the community, and the need to improve the socio-economic policies as soon as possible.

关键词

作者关键词: community; aging-friendly construction; expert group; index; weighting value

作者信息

通讯作者地址: Li, Kun (通讯作者)

Guangzhou Univ, 230 Outer Ring West Rd, Guangzhou 510006, Guangdong, Peoples R China

地址:

1 Guangdong Ind Polytech, Guangzhou, Guangdong, Peoples R China

2 Guangzhou Univ, 230 Outer Ring West Rd, Guangzhou 510006, Guangdong, Peoples R China

电子邮件地址: 289201238@qq.com

类别/分类

研究方向: Health Care Sciences & Services

引文主题: 6 Social Sciences > 6.294 Operations Research & Management Science > 6.294.1807 Foresight

可持续发展目标: 09 Industry, Innovation and Infrastructure

Web of Science 类别: Health Care Sciences & Services; Health Policy & Services

MeSH 词表 来自 MEDLINE®

基金资助

基金资助机构

授权号

2021 Guangdong Philosophy and Social Science Planning Project

GD21CYS28

查看资金资助信息

文献信息

语种: English

入藏号: WOS:000969199400001

PubMed ID: 37042210

ISSN: 0046-9580

eISSN: 1945-7243

其他信息

IDS 号: D5NM3

来自 MEDLINE® 的分主题子库: Index Medicus

查看较少数据字段

引文网络

来自 Web of Science 核心合集

0

被引频次

创建引文跟踪

49

篇引用的参考文献

查看相关记录

Web of Science 中的使用情况

Web of Science 使用次数

0

0

最近 180 天

2013 年至今

进一步了解

此记录来自:

Web of Science 核心合集

- Science Citation Index Expanded (SCI-Expanded)
- Social Sciences Citation Index (SSCI)

建议修正

如果您要改进此记录中的数据质量, 请建议修正



INQUIRY-THE JOURNAL OF HEALTH CARE ORGANIZATION PROVISION
AND FINANCING

出版商名称: SAGE PUBLICATIONS INC

期刊影响因子™

2021 五年
2.099 2.57

JCR 学科类别	类别排序	类别分区
HEALTH CARE SCIENCES & SERVICES 其中 SCIE 版本	84/109	Q4
HEALTH POLICY & SERVICES 其中 SSCI 版本	65/88	Q3

来源: Journal Citation Reports 2021. 进一步了解



Research on the Weighting Values of Community Aging-Friendly Construction Indexes With Different Expert Groups

INQUIRY: The Journal of Health Care Organization, Provision, and Financing
Volume 60: 1–13
© The Author(s) 2023
Article reuse guidelines:
sagepub.com/journals-permissions
DOI: 10.1177/00469580231167984
journals.sagepub.com/home/inq



Wen-Bing Mei, PhD¹ , Kun Li, PhD², and Yi-Zhe Huang, PhD¹

Abstract

The construction of weight values for the indicators of community aging-friendly construction is helpful to guide the formulation of strategies for allocating elderly resources in community aging-friendly constructions, and to reflect the shortcomings of community aging-friendly constructions and propose improvement strategies when evaluating the effectiveness of the existing community aging-friendly constructions. The paper uses the Fuzzy Analytic Hierarchy Process (FAHP) to calculate the weighting values of each indicator, consulting the government, industry, and academic experts. The research results show that the weighting-value order is “public environment ($W = 0.364$),” “health care ($W = 0.342$),” “humanistic care ($W = 0.204$)” and “social economy ($W = 0.090$).” Accordingly, the article proposes specific suggestions to improve the effectiveness of community aging-friendly constructions, including the need to find consensus among all parties involved in the aging industry, the need to focus on improving the public environment of the community, and the need to improve the socio-economic policies as soon as possible.

Keywords

community, aging-friendly construction, expert group, index, weighting value

What do we already know about this topic?

The weighting values of the indicators in the 4 sub-levels of the community’s aging-friendly construction are “public environment ($W=0.364$)> health care ($W=0.342$)> humanistic care ($W=0.204$).>social economy ($W=0.090$).”

How does your research contribute to the field?

The research results show that the public environment is the core element of a community’s aging-friendly construction, and social economy is an effective supplement, and we learned that some differences exist in the government, industry, and academia’s perceptions. Hence, it is necessary to find consensus among all parties to make the aging-friendly construction comprehensive and sustainable.

What are your research’s implications toward theory, practice, or policy?

The results of our study have practical implications for the precise investment of senior care resources, the development of strategies to prioritize older adults’ needs, the objective evaluation of the effectiveness of the community’s aging-friendly construction, and proposing targeted improvement strategies.

Research Background and Objectives

With the development of its economy and the rise of its real estate industry, China’s community’s function is becoming more and more powerful. Therefore, in the 13th 5-year Plan for developing China’s aging cause, it is proposed to build a “home-based, supported by community and institutions” social older-adult care service system as soon as possible. The community home-based older-adult care model has

¹Guangdong Industry Polytechnic, Guangzhou, Guangdong, China

²Guangzhou University, Guangzhou, Guangdong, China

Received 1 December 2022; revised 24 February 2023; revised manuscript accepted 20 March 2023

Corresponding Author:

Kun Li, GuangZhou University, NO.230 Outer Ring West Road, University Town, Guangzhou, GuangDong 510006, China.
Email: 289201238@qq.com



gradually sprung up and developed into China's most crucial older-adult care model.¹ Statistics show that China's older-adult care is based mainly on the "9073" model, 90% of the older adults rely on community home-based for older-adult care.² Since 2011, led by the Ministry of Civil Affairs and the National Development and Reform Commission, the "Community's Home-based Older-adult Care Service Plan" has been implemented all over the country, and many community older-adult care service facilities and older-adult activity centers have been established. Social security systems such as pension and medical insurance have gradually improved. The daily care services for the older adults have been significantly improved.³ As an essential part of the older adults' pension, the ultimate goal of a community's home-based older-adult care service is to comprehensively improve the service supply at the levels of community humanistic care, public environment, health care, and social economy, therefore improving the quality of life and older-adult care satisfaction of the older adults.⁴ Whether the community older-adult care services and the aging-friendly constructions match the older adults' needs, and whether the older adults' diversified care needs are effectively met, are the essential factors affecting the development of the community's home-based older-adult care industry.⁵ Although economic growth and the improvement of community service levels make it possible to meet older-adult care needs, the heterogeneous characteristics of older-adult groups will produce a diversified demand focus, and increase the complexity of demand identification. At the same time, the social background of rapid aging and "getting old before getting rich" also determines that due to the limitation of social pension resources, the pension needs of the older adults can not be fully met. The development of the community's home-based older-adult care industry depends on the recognition and acceptance of the older-adult care model by the older adults. The current community home-based older-adult care service model generally has structural contradictions, such as a high supply rate versus a low utilization rate, single content versus diversified demand, and insufficient accuracy of demand identification versus repeated investment of resources.⁶ Therefore, in order to completely distinguish the index factors for community's aging-friendly construction, to determine the construction sequence's priority according to the "importance" of different factors, and to accurately match the limited social pension resources with diversified pension services, whether in practical or academic level, it is necessary to study the index elements of China's community's aging-friendly construction and the importance of each index element under the community's home-based older-adult care model.

The research objectives of this thesis are as follows:

1. By applying the FAHP method, complete the weighting allocation of each community's aging index

under the home-based older-adult care model. Construct the all-factor indexes that affect community's aging-friendly construction into a progressive relationship, and evaluate the complex evaluation indexes and research objects. The stratified division clarifies the micro-level structure, which is conducive to guiding the input of community's aging-friendly construction resources at the macro level and formulating priority strategies at the micro level.

2. Construct a complete set of evaluation weighting systems covering all elements of community's aging-friendly construction that effectively assess the current status of community's aging-friendly construction in existing communities or after renovation. Make qualitative and quantitative judgments on the community's aging-friendly construction, and reflect on the current situation of aging communities or the shortcomings in their construction, creating effective contrast and promotion.

Research Theory and Literature Review

Research on the Construction of Aging-Friendly Construction Index System

In April 2002, the "Active Aging Index (AAI)," a policy framework to deal with aging in the 21st century, was officially put forward at the United Nations' second world assembly on Aging. Active aging refers to prolonging the healthy life span and improving the quality of life of the older adults by optimizing the level of health, social participation, and security of the older adults,⁷ This new policy theory has attracted attention worldwide and raised extensive discussions. In recent years, scholars in related fields in different regions of the world have started exploring indicators for the level of active aging based on the socioeconomic and cultural background of each area, and suggested many theories, such as the Healthy Aging Index (HAI), Productive Aging Index (PAI) and Successful Aging Index (SAI). Thailand is the first country to release the research and development results of quantitative measurement tools for active aging after the World Health Organization introduced the concept of "active aging." Thanakwang believes that in addition to physical, cognitive, psychological, social and environmental factors and economic resources, positive aging is also affected by cultural factors, He developed an active aging index evaluation tool adapted to Thailand's socioeconomic culture based on the World Health Organization (WHO)'s conceptual framework.⁸ Bowling and Stafford surveyed the older adults over 65 on active aging and evaluated the influencing factors using an analytic hierarchy process, The results show that "maintaining good health and working", "leisure and social activities", "functions

and activities”, and “social relations and contacts” are the most critical factors affecting the older adults’ active aging.⁹ Lim and Thompson added the spiritual happiness index to the active aging index, and used a multiple regression model to test 120 Singaporeans of Chinese, Malay and Indian origin aged 55 to 64 and over 65. The results show that the AAI evaluation model cannot significantly predict the activity level of the older adults only by controlling age; but the accuracy is significantly improved by implanting spiritual happiness. Significant differences exist in the final evaluation of the AAI index among different ages and races.¹⁰ Based on health, participation, and security, China’s active aging mainly includes development, harmony, and sharing. It can therefore build an all-round policy system including economy, culture, politics, social development, family relations, and social resources.¹¹ Liu and Yang used Charls and CGSS databases and learned from the EU active aging measurement framework. They used the analytic hierarchy process and DEA method to design China’s active aging index, measured the active aging index of China’s 28 provinces, and studied the development level of active aging at the regional, urban and rural, provincial and gender levels.¹²

However, it is important to point out that, with the deepening research on gerontology and aging, the connotation of the concept of “older adults” has become the focus of academic research. Academics usually understand “older adults” in the context of “Aging,” and there are mainly 2 perspectives: “natural aging” and “social aging.” On the one hand, as biological individuals, older adults are “human beings” and have a biological continuum of natural aging¹³; on the other hand, as a socially interacting entity, older adults will gradually be marginalized by society as their physical functions decline.^{14,15} “In this study, we follow the scholars mentioned above” opinions and consider people starting to enter the aging state as older adults by combining many factors such as living states, health condition, and living ability in addition to their ages.

Study on Indicators of Community’s Aging-Friendly Construction

Setting the family as the core and relying on the community and professional services as the foundation, the community’s home-based older-adult care makes full use of the community’s resources, which include community health service institutions, various older-adult care institutions, and community public service institutions. It provides social services to help solve older-adult care needs, including life care, medical care, spiritual care, and social pension services of one or more services such as culture, sports, and emergency assistance.¹⁶ The community’s aging-friendly construction is the supportive and instrumental service obtained by the

older adults from the community to ensure their care. The *International Consensus on Establishing Long-Term Care Policies for the Older Adults* issued by the WHO in 2000 pointed out: “based on the community, provide extensive preventive, remedial and developmental services for the older adults, and take independence, participation, care, and self-enrichment as the main objectives of long-term care policies for the older adults.”¹⁷ In addition, the *Global Report on Aging and Health* proposed: “focusing on the health security, social attributes, economic rights and human rights development of the older adults, and the older adults should receive care, services and protection from the community.”¹⁸ In foreign studies, a community’s aging-friendly construction is generally summarized as “1e3m”: environment, money, medical, and mental. It refers to the public environmental security at the “environment” level, material and economic security at the “money” level, health care security at the “medical” level and psychological care at the “mental” level.¹⁹ Forder summarized the community’s older-adult care needs into 4 aspects: health, economy, residence, and society, and extended to multiple sub-items such as chronic disease management, health maintenance, economic resources, living environment, and psychological comfort.²⁰ Harrison et al divided the community’s aging-friendly construction in Australia from the general service needs of the community’s older adults, which includes 76 indicators such as house-keeping, care, personal affairs and mental health.²¹ The pension system proposed by China’s academics since 1982, which includes “the older adults having a sense of security, medical care, learning, achievement, and happiness,” is the earliest standard used in China’s older-adult care policy and research field.²² With the progress of the times and the development of society, especially the continuous improvement of the social pension security system and community environment, 4 primary and 9 secondary criteria have been developed based on the original pension system. The 4 primary ones are humanistic care, living environment, health care, and social economy. A community’s aging-friendly construction, with a total of 48 indicators, has become a common and recognized division method in academic circles in line with China’s current conditions.²³ The ultimate goal of the development of community home-based aging services is to improve the service supply in humanistic care, public environment, health care and socio-economic aspects of the community in a comprehensive manner, thus enhancing the quality of life and satisfaction of the older adults.^{24,25} Therefore, using “humanistic care, public environment, health care and social economy” as the dimensions of community aging construction is consistent with all the elements of community aging-friendly construction under the community home-based aging service model. It can meet the diversified needs of older adults living in communities.²⁶

Research on Related Theory and Application of FAHP

The Analytic Hierarchy Process (AHP) is a systematic evaluation method for multiple judgment bases and comprehensive decision-making under uncertainty, which was founded by Thomas Saaty, a famous American scholar, in 1971. It mathematizes the evaluator's complex thinking process.²⁷ The AHP requires that the judgment matrix among all levels must conform to the consistency test. To achieve matrix consistency, the matrix value needs to be adjusted and tested several times, affecting decision-making quality. The Fuzzy Analytic Hierarchy Process (FAHP) is an evaluation method developed based on the combination of fuzzy comprehensive evaluation and AHP. It helps to reduce or avoid the impact caused by the evaluator's subjectivity, fuzziness, and uncertainty. It has been widely used in economic progress prediction, national industrial structure research, national defense and military research, energy policy analysis, scientific and technological achievement evaluation, and development strategy formulation.²⁸ When making decisions with the FAHP method, the following steps are mainly used:

The first step is to combine the multi-level evaluation model. When using FAHP to solve various evaluation problems, we should first decompose the complex system problems into several levels, and then classify the different influencing factors to build a multi-level evaluation model.

The second step is to construct the paired comparison matrix. After the hierarchical structure is built, the paired comparison between the indicators at each level must be carried out. Numbers 1 to 9 and their reciprocals are used as scales, to assign the relative importance between the indicators and construct the paired comparison matrix, as shown in formula (1).

$$R = \begin{bmatrix} r_{11} & r_{12} & \cdots & r_{1n} \\ r_{21} & r_{22} & \cdots & r_{2n} \\ \vdots & \vdots & \vdots & \vdots \\ r_{n1} & r_{n2} & \cdots & r_{nn} \end{bmatrix} \quad (1)$$

When using the FAHP method for group decision-making, Saaty suggests using "geometric average" to obtain group opinions²⁹: if n experts participate in scoring, and their scoring values are $x_1, x_2, x_3 \dots x_n$ respectively, the average value is calculated as formula (2):

$$X = \sqrt[n]{X_1 \times X_2 \times X_3 \times \cdots \times X_n} \quad (2)$$

The third step is to obtain the feature vector and check its consistency. According to the pairwise comparison matrix,

the maximum feature vector of each index at the same level can be calculated as ω , which meet $\sum_{i=1}^n w_i = 1$. Then, it is normalized, which can be used as relative weight. When the eigenvalue is no longer equal to n , the difference between λ_{max} and n can be used as the consistency standard to measure the consistency before and after expert judgment. This process is called consistency verification. Saaty suggests that when the consistency index $CR \leq 0.1$, the error is within the acceptable range.

Research Methods and Processes

This study aims to determine the weighting value of various indicators of a community's aging-friendly construction under the community home-based older-adult care model, thus building a complete evaluation system of the community's aging-friendly construction indicators. The research is divided into 2 stages. The first stage is the investigation of the FAHP expert questionnaire. Experts from 3 decision-making groups: professional academia, government management and community industry, will then score the relative importance of various indicators. It reflects the cognitive contrasts of different decision-making groups on the importance of a community's aging-friendly construction indicators. The second stage is calculating the weight of the community's aging-friendly construction indicators. A super decisions software is used to summarize and calculate the experts' evaluation, reducing the subjective understanding of evaluators from different decision-making groups, and therefore building a comprehensive and appropriate weighting system for indicators.

The Super Decisions software was developed by Saaty and his research team, Creative Decisions Foundation. It is used to compute models with dependencies and provide decision feedback. It can run the FAHP.³⁰ The Super Decisions software allows decision-makers to quickly analyze the problem by comparing 2 factors to find the relative weightage of each factor in the overall structure, which saves more computing time and makes the decision-making process more efficient.³¹

The First Stage: FAHP Expert Questionnaire Survey

Construction of evaluation system of community's aging-friendly construction index. This study considers the critical elements of community's aging-friendly construction from humanistic care, public environment, health care, and social economy. It is divided into 4 criteria levels, 9 sub-criteria levels, and 48 indicator levels, to build a complete *CAFCIS*.³² See Table 1:

Table 1. Index System of Community's Aging-Friendly Construction.

Criterion	Sub-criterion	Indicator
Humanistic Care	Community care	Exchanging community information, organizing community activities, improving neighborhood relations, organizing cultural and sports performances, cultivating community identity, improving community services, providing spiritual comfort, providing cultural education, promoting relevant policies
	Social care	Providing legal assistance, managing older-adult articles, handling related affairs, providing psychological guidance
Public environment	Physical environment	Improving the physical environment of buildings, improving the road condition of communities, managing community vehicles orderly, beautifying public environment, separating the static and dynamic activity spaces, ensuring the accessibility of environmental spaces, developing community safety and control measures, renovating the buildings' aging facilities
	Facility environment	Ensuring road accessibility, providing leisure seats, improving lighting facilities, improving public health facilities, improving fitness facilities
	Related environment	Ensuring public transportation, providing living and commercial facilities
Health care	Health management	Providing chronic disease care, providing in-home medical service, providing accompanying medical services, providing regular medical checkups, providing medicine delivery services, providing rehabilitation care guidance, installing emergency assistance systems
	Medical treatment	Providing community clinics, building community day care centers, providing healthcare lectures
Social economy	Public Security	Publicizing service information, providing service consultation, establishing older-adult information files, providing internet older-adult care information, providing online clinic services, building older-adult safety monitoring systems, providing social security services
	Daily life	Constructing older-adult canteens, providing housekeeping services, providing day care services

Table 2. Instruction Sheet for Filling Out the Fuzzy Hierarchy Analysis Expert Questionnaire.

Questionnaire Content	Survey Objective
1. Completion instructions: Explain in detail how to fill out the questionnaire and use examples to explain	Use simple instructions to make it easier for respondents to fill out the questionnaire and save time.
2. Aging-friendly community evaluation index framework: 4 factors, 24 indexes	Let the interviewees understand the structural relationship of each factor of the "Aging-Friendly Community Evaluation Index System."
3. Fill in the questionnaire and explain the indicators: Respondents checked the "relative importance value," "the maximum acceptable value," and "the minimum acceptable value" by comparing the pairwise factors according to their importance (Table 3)	<p>1. Ordering of factors: There are four factors: 1. facilities; 2. road system; 3. environmental functions; 4. landscape greening. If you think its order of importance is "1. facilities" > "3. environmental functions" > "2. road system" > "4. landscape greening," then please record (1) > (3) > (2) > (4).</p> <p>2. Relative importance of indicators: If you think that (i) the "relative importance" ratio of "public health facilities" to "Daily health care" is 5:1, (ii) the maximum acceptable value is 7:1, and (iii) the minimum acceptable value is 2:1, please separately tick (7:1), (5:1), (2:1) (Table 2)</p>

Fuzzy analytic hierarchy process questionnaire design. This stage aimed to understand the relationship between the evaluation indicators of the community public environment and aging. The evaluation index weighting of the aging-friendly community was calculated using a fuzzy hierarchy analysis expert questionnaire. With this evaluation method, a relative weight ratio was used, and "relatively important values," "the maximum acceptable value," and "the minimum acceptable value" were selected. The collected data were sorted, compared, and checked according to the relative importance of the indicators. The ratio was then subjectively determined based on the experts' professional and academic experience.

The instructions for filling out the fuzzy-level analysis expert questionnaire are listed in Table 2.

Selection of expert groups and distribution of questionnaires. In the part of expert group selection, this study believes that the scope of the index evaluation system is broad and complex. If only a particular category of experts was selected, the data obtained might be too biased and less credible. Therefore, this study believes that it is necessary to include the opinions of multiple expert groups. Based on the technical indicators of selecting experts based on "politics" and "analysis,"³³ Relevant experts and scholars from the community pension

Table 3. Example of Fuzzy Level Expert Analysis Questionnaire.

Impact indicator	Strong Relative									Importance Weak									Impact indicator
	9:1	8:1	7:1	6:1	5:1	4:1	3:1	2:1	1:1	1:2	1:3	1:4	1:5	1:6	1:7	1:8	1:9		
Public health facilities			✓		✓			✓										Daily health care	

Table 4. Expert Fuzzy Interval Value Conversion Rules.

Original	17	16	15	14	13	12	11	10	9	8	7	6	5	4	3	2	1
Conversion	9:1	8:1	7:1	6:1	5:1	4:1	3:1	2:1	1:1	1:2	1:3	1:4	1:5	1:6	1:7	1:8	1:9

industry management, community pension research academia, and community planning and construction officials put forward valuable opinions on the expert scoring stage of this study to achieve accuracy. Dalkey believes that when the number of people is at least 10, the group error can be minimized, and the reliability is the highest.³⁴ Therefore, the research committee invited 16 experts and scholars to participate in the questionnaire group. The number of experts interviewed is 10 males and 6 females. Among them, there are 7 bachelors, 6 masters and 3 PhDs. The interviewees include professional academic research experts above the associate professor level, community industry workers with more than 15 years of employment, and experts from the Civil Affairs and Medical Insurance System departments with more than 20 years of experience. The questionnaire was distributed by e-mail and WeChat files on October 17, 2021. During the survey, online video communication was carried out through Tencent meetings and enterprise WeChat. A total of 16 questionnaires were distributed. The deadline was November 27, 2021. All questionnaires were recovered with a recovery rate of 100%.

The Second Stage: Calculation of the Community’s Aging-Friendly Construction Indicators’ Weighting Value

Expert fuzzy evaluation conversion. In this study, the expert fuzzy interval value conversion rule (Table 4) is used

to calculate the geometric average of 16 experts through Microsoft Excel 2019 software. The vague average of each scale is calculated for expert fuzzy evaluation conversion. Then the Super Decision software is used to compare the total target layer, criterion layer, sub-criterion layer, and each index factor. Saaty and its research team jointly develop this Super Decisions software. With the software, decision-makers can quickly analyze problems, leaving more computing time. The decision-maker only needs to construct the relationship diagram of the problem, and does not need to clarify the type of matrix formed by the graph, making it more effective in calculation and selection. After comparing the importance of each factor, the relative weighting value of each factor in the whole structure can be obtained.

Construct pairwise comparison matrix. This study calculates the weight value of the target layer, criterion layer, sub-criterion layer, and each index of the *CAFCIS* under the community home-based older-adult care model. It uses the Super Decisions software to check and solve it. Due to limited space and consistent operation, the following only takes the criterion layer of one of the expert questionnaires as an example to illustrate how to establish the results and paired comparison matrix. Under the general objective level of the *CAFCIS*, the experts check the “relative importance” of the 4 criteria level of humanistic care, public environment, health care, and social economy, as shown in Table 5 below:

Table 5. Checklist of Relative Importance of Community’s Aging-Friendly Construction Index Level.

Impact indicators	Experts tick the specific weighting value																	Impact indicators
	9	8	7	6	5	4	3	2	1	1/2	1/3	1/4	1/5	1/6	1/7	1/8	1/9	
Humanistic concern					5				2									Public environment Health care
Public environment							3											Social economy Health care
Health care								2			1/3							Social economy Social economy

Input the “relative importance value” in Table 3 into super decisions software to get the questionnaire results, as shown in Figure 1:

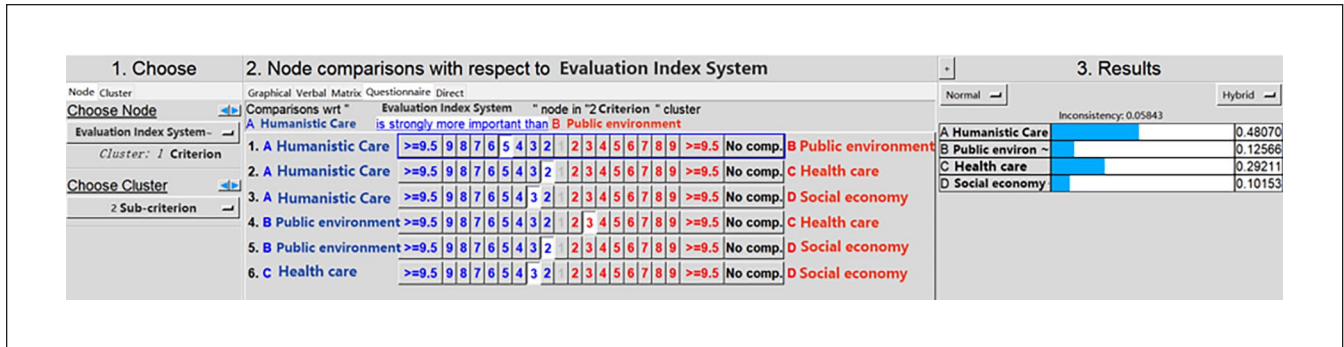


Figure 1. Results of questionnaires at each criterion level.

The pairwise comparison matrix between the layers of the criteria under the overall objective is shown in Table 6

Calculation of eigenvectors and consistency verification. After completing all the paired comparison matrices of a questionnaire, the verification of the characteristic vector and consistency of each paired comparison matrix in the “CAFCIS under the community home-based older-adult care mode” can be obtained by using super decisions software. The consistency ratio Cr is obtained by dividing the consistency index CI by the random consistency index RI, and its calculation formula is as follows:

$$CR = \frac{CI}{RI} \tag{3}$$

As long as the consistency calculation result is less than or equal to 0.1, it is within the allowable error range. Otherwise, it will be regarded as an invalid questionnaire, or experts will adjust it again. With the help of Tencent conference and other network video methods, this study uses super decisions

software to verify the data in real-time. When the consistency verification fails, experts will be informed to make corrections and adjustments. Therefore, the consistency ratio of the final 16 points questionnaire ($CR \leq 0.1$) is within the acceptable range.

Research Results and Discussion

The CAFCIS constructed by this research emphasizes its construction effect evaluation ability and expresses its guiding value for the accurate construction of community aging. Therefore, based on indicators such as scientific, comprehensiveness, comparability, practicability, feasibility, and the opinions of experts from various fields, we can understand the criteria at all levels of community’s aging-friendly construction indicators and their relative weighting. Officials, industry and academia can thus use them to guide community construction and evaluate its effectiveness.

Research Results

Since the evaluation of the index system of community’s aging-friendly construction involves many disciplines, to ensure that the data obtained are complete, fair, and incorporate multiple expert opinions, the experts are divided into 3 types: professional academic, government management, and community industrial. The weighting values of various criteria and indicators of community’s aging-friendly construction are shown in Table 7:

Table 6. Pairwise comparison matrix table between benchmark layers.

	Humanistic concern	Public environment	Health care	Social economy
Humanistic concern	1	5	2	3
Public environment	1/5	1	1/3	2
Health care	1/2	3	1	3
Social economy	1/3	1/2	1/3	1

Table 7. Statistics of Weight Values of Community's Aging-Friendly Construction Indicators.

Criterion					Sub-criterion					Indicator				
Name	Gp	Gg	Gc	Go	Name	Gp	Gg	Gc	Go	Name	Gp	Gg	Gc	Go
Humanistic Care	0.147	0.412	0.245	0.204	Community care	0.117	0.309	0.184	0.153	Exchanging community information	0.018	0.026	0.025	0.020
										Organizing community activities	0.027	0.092	0.044	0.039
										Improving neighborhood relations	0.004	0.017	0.008	0.007
										Organizing cultural and sports performances	0.012	0.025	0.013	0.014
										Cultivating community identity	0.004	0.021	0.012	0.007
										Improving community services	0.041	0.102	0.063	0.054
					Social care	0.029	0.103	0.061	0.051	Providing spiritual comfort	0.004	0.017	0.012	0.007
										Providing cultural education	0.007	0.009	0.007	0.006
										Promoting relevant policies	0.010	0.019	0.015	0.013
										Providing legal assistance	0.002	0.017	0.009	0.006
										Managing older-adult articles	0.004	0.011	0.007	0.006
										Handling related affairs	0.011	0.050	0.026	0.022
										Providing psychological guidance	0.002	0.005	0.004	0.003
Public environment	0.423	0.291	0.374	0.364	Physical environment	0.264	0.129	0.202	0.196	Improving the physical environment of buildings	0.051	0.028	0.041	0.034
										Improving the road condition of communities	0.032	0.020	0.030	0.031
										Managing community vehicles orderly	0.009	0.005	0.009	0.008
										Beautifying public environment	0.011	0.005	0.010	0.008
										Separating the static and dynamic activity spaces	0.014	0.007	0.013	0.011
										Ensuring the accessibility of environmental spaces	0.008	0.006	0.010	0.008
										Developing community safety and control measures	0.031	0.010	0.030	0.022
										Renovating the buildings' aging facilities	0.107	0.048	0.059	0.074
					Facility environment	0.101	0.113	0.111	0.108	Ensuring road accessibility	0.046	0.049	0.047	0.047
										Providing leisure seats	0.027	0.025	0.030	0.028
										Improving lighting facilities	0.014	0.015	0.017	0.016
										Improving public health facilities	0.007	0.011	0.006	0.007
										Improving fitness facilities	0.006	0.013	0.012	0.010
Aligned environment	0.058	0.049	0.061	0.060	Ensuring public transportation	0.043	0.025	0.031	0.040					
					Providing living and commercial facilities	0.014	0.025	0.031	0.020					
Health care	0.346	0.200	0.291	0.342	Health management	0.231	0.160	0.219	0.256	Providing chronic disease care	0.019	0.023	0.019	0.024
										Providing in-home medical service	0.021	0.010	0.013	0.019
										Providing accompanying medical services	0.018	0.006	0.017	0.015
										Providing regular medical checkups	0.065	0.031	0.054	0.063
										Providing medicine delivery services	0.011	0.011	0.013	0.013
										Providing rehabilitation care guidance	0.018	0.023	0.029	0.032
										Installing emergency assistance systems	0.080	0.056	0.075	0.090
										Providing community clinics	0.077	0.020	0.046	0.054
					Medical treatment	0.115	0.040	0.073	0.085	Building community day care centers	0.019	0.010	0.017	0.016
										Providing healthcare lectures	0.019	0.010	0.010	0.015
										Publicizing service information	0.001	0.006	0.003	0.002
										Providing service consultation	0.001	0.002	0.002	0.002
										Establishing older-adult information files	0.002	0.007	0.004	0.004
Social economy	0.085	0.097	0.089	0.090	Public Security	0.028	0.048	0.060	0.045	Providing internet older-adult care information	0.001	0.003	0.004	0.002
										Providing online clinic services	0.004	0.003	0.006	0.004
										Building older-adult safety monitoring systems	0.010	0.007	0.016	0.012
										Providing social security services	0.009	0.020	0.024	0.017
					Daily life	0.056	0.048	0.030	0.045	Constructing older-adult canteens	0.033	0.010	0.008	0.015
										Providing housekeeping services	0.009	0.019	0.010	0.015
										Providing day care services	0.014	0.019	0.012	0.015

Gp=Group of professional academic; Gg=Group of government management; Gc=Group of community industry; Go=Group of Overall opinion.

Research Discussion

First level (criterion level) evaluation facet analysis. The overall opinion (all samples) analysis results show that the “public environment ($W = 0.364$)” project is the most important, followed by the “health care ($W = 0.342$)” project. There is little difference between the weighting values of the 2 criteria. The results of this study verified He and Wei Ling-Hua and other scholars' conclusions: improving the aging-friendly community environment, creating more and better leisure and

interaction spaces, and creating a positive community atmosphere are the core priorities of a community's aging-friendly construction.³⁵ In terms of the professional academic group, the “public environment ($W = 0.423$)” project is the most important, followed by the “health care ($W = 0.346$)” project. The government management group believes that the “humanistic care ($W = 0.412$)” project is the most important, followed by the “public environment ($W = 0.291$)” and “health care ($W = 0.200$)” projects. Community industry groups also believe that the “public environment ($W = 0.374$)” project is

the most important, followed by “health care ($W=0.291$)” and “humanistic care ($W=0.245$).” Overall, “public environment” is the most crucial criterion considered by all 3 decision-making groups, and “social economy” is the least important. It shows that the social economy portion under the current community home-based older-adult care mode still needs to be strengthened.³⁶ The importance of the “humanistic care” project has a considerable cognitive difference among the 3 expert groups. Its importance is particularly affirmed by the government management group, which shows that strengthening the community’s aging-friendly construction can best obtain support from the local government management department. In organizing and guiding the construction of aging-friendly communities, government departments should include more “people-oriented” ideas, avoid utilitarianism, and reflect the warmth of social care.³⁷

The second level (sub-criterion level) evaluation facet analysis. In the aspect assessment of the second level, the overall opinion indicates that the more critical assessment items are “health management ($W=0.256$),” “physical environment ($W=0.196$),” and “community care ($W=0.153$).” The 3 decision-making groups have a relatively consistent understanding of the importance of each evaluation item at the standard level. Professional and academic groups believe that the “physical environment ($W=0.264$)” project is the most important, followed by “health management ($W=0.231$)” and “community care ($W=0.117$).” The government management group believes that the “community care ($W=0.309$)” project is the most important, followed by the “health management ($W=0.160$)” and “physical environment ($W=0.129$)” projects. The community industry group believes that the “health management ($W=0.219$)” project is the most important, followed by the “physical environment ($W=0.202$)” and “community care ($W=0.184$)” projects. Thus, it is clear that the community environment is the primary place for daily leisure, communication, interaction, and exercise activities of older adults, and that the community’s physical environment is one of the most critical factors influencing older adults’ activities and prosperous aging in place.^{38,39} Notably, the “daily life” project’s weightage is not high among the 3, indicating that the concept of emphasizing daily older-adult care service in community home-based older-adult care has not been paid attention to.⁴⁰ It is urgent to further promote the concept of older-adult daily care service and develop an appropriate supply model. At the same time, it is also worth noting that although the government management group pays more attention to the “social care” project, the weighting value given to the “social care” project by professional academic and industrial community groups is relatively low. It shows that while the government management department vigorously promoted the concept of actively using social resources to improve the community’s aging-friendly construction, it has not been recognized by academic and industrial circles. This also shows that the community’s function as a social resource platform still needs strengthening.⁴¹

The third level (index level) evaluation facet analysis. The 3 expert groups have differences in the importance of each evaluation item in this dimension. The overall opinion shows that “installing emergency assistance systems ($W=0.090$),” “renovating the buildings’ aging facilities ($W=0.074$),” and “providing regular medical checkups ($W=0.063$)” are more critical at these levels. Professional and academic groups believe that “renovating the buildings’ aging facilities ($W=0.107$)” is the most important, followed by “installing emergency assistance system ($w = 0.080$)” and “Providing community clinics ($W=0.077$).” The government management group believes that “improving community services ($W=0.102$)” is the most important, followed by “organizing community activities ($W=0.092$)” and “installing emergency assistance systems ($W=0.056$).” Community industry groups believe that “installing emergency assistance systems ($W=0.075$)” is the most important, followed by “improving community services ($W=0.063$)” and “renovating the buildings’ aging facilities ($W=0.059$).” To conclude, “installing emergency assistance systems” and “renovating the buildings’ aging facilities” are unanimously recognized by the 3 decision-making groups. It shows that the core concepts of “safety” and “convenience” emphasized in the community’s aging-friendly construction have been jointly recognized by all in the community home-based older-adult care industry.⁴² Similarly, when evaluating the importance of “improving community services,” there are significantly different results obtained from the 3 groups. It indicates that government and industry groups hope to prioritize improving the soft needs of community service, which is not recognized by the academic community due to the lack of connotation and evaluation standards.⁴³ Thus, it can be seen that in order to develop the home-based community older-adult service industry and build aging-friendly medical institutions, the government needs to accelerate the construction of barrier-free facilities to enhance the community environment through policy guidance and support,^{44,45} while also emphasize responsive, rational and standardized older-adult service provision.^{46,47}

Through the above analysis, we can conclude the following. Government participants in community’s aging-friendly construction pay more attention to policy formulation and plan implementation. Professional and academic circles emphasize the importance of the public environment in a community’s aging-friendly construction, and attend more to the considerations related to their professional background. The industrial community pays more attention to pension needs in their own interests. These differences in cognition and needs can enable all participants in the community’s aging-friendly construction to reflect and think about the places where consensus needs to be sought, and also remind community industry practitioners to strengthen interaction and communication with academia and government management departments based on the common interests of community older-adult care industry.

Research Conclusions and Suggestions

The weightage of the community aging-friendly construction evaluation indexes constructed in this study can screen the importance of different index elements, to accurately match the limited social older-adult resources with diversified older-adult services, thus enhancing the effectiveness of community home-based aging services. The evaluation system of the community home-based aging model covers a broad and complex scope, and this study incorporates multiple expert opinions to improve its objectivity and comprehensiveness through cross-validation of the opinions from government, industry and academia to ensure more thorough and objective research conclusions.

The development of the community home-based older-adult care model and the construction of the true meaning of community's aging-friendly construction should be a process established by the consensus of multiple groups. In order to improve the construction of aging-friendly communities and expand its coverage, establishing an effective and collaborative innovation mechanism should be encouraged from the levels of government, communities and individuals. The government should actively carry out top-level design, introduce related social resources, and provide policy guidance and financial support for the smooth implementation of community aging-friendly renovation. Communities should be a good platform, actively connecting with social older-adult care resources and providing diversified services. This study suggests that when counseling community aging-friendly constructions, the management departments and practitioners related to community home-based aging services should take the older-adult needs as the guide, and use the evaluation system constructed in this study to assist the government, society, community, and other relevant stakeholders to effectively screen and make decisions using the evaluation tools, to find the most relevant results. Through theoretical and empirical analysis, this study presents the following conclusions and suggestions:

Research Conclusion

The public environment is the core elements of community's aging-friendly construction. Through the opinion analysis and systematic practical operation of 3 decision-making groups: government directors, professional academics, and community pension industry experts, this study proposes a comprehensive weighting system of community's aging-friendly construction indicators. The results show that among the 4 criteria levels, the weighting value of "public environment ($W=0.364$)" is the highest, followed by "health care ($W=0.342$)," "humanistic care ($W=0.204$)" and "social economy ($W=0.090$)." It shows that the construction of the public environment and the improvement of the health and medical system are still the core content of community's aging-friendly construction under the development of the community home-based older-adult care model. At the same

time, from the weighting value of "humanistic care," it can be seen that the older adults' pension needs have gradually changed from "physical" to "spiritual," and from "survival" to "development," which has been widely recognized by the society.⁴⁸ The social economy's weighting value is relatively low, limited by the lack of social pension resources and pension funds. Currently, the community's social and economic pension services, such as housekeeping services, life care, intermediary assistance, and canteen for the older adults, are not free of charge. It leads to low recognition in the social and economic aspects. Therefore, enriching social pension resources and improving social pension security are urgent problems to be solved in the future development of community home-based older-adult care model and the community's aging-friendly construction.⁴⁹

Consensus of all parties must be required to build a comprehensively suitable community's aging-friendly construction. Through the analysis of 3 decision-making groups on the community's aging-friendly construction index weighting system, this study also finds similarities and differences in the groups' opinions. Regarding the first-level evaluation, "public environment" and "health care" are the critical dimensions jointly considered by the 3 groups. Still, there are significant cognitive differences among the 3 groups regarding the importance of "humanistic care." Regarding the second-level evaluation, the groups tend to be consistent. The importance of "social care" has been affirmed by the government management group. Still, it seems to be relatively ignored by the industrial community group, which shows that the community function advocated by the government, as a platform for older-adult care and social pension resources, still needs to be strengthened at the operation level. Regarding the third-level evaluation, "improving community service" has been valued by government management and community industry groups. Still, the academic community does not seem to agree, indicating that the government wants the community to provide community services and soft-need care for the older adults, which the academic community has not recognized due to the lack of construction standards and effect evaluation.⁵⁰ The cognitive differences of these decision-making groups show that there are still many areas to seek consensus in the construction of community aging adaptation.

Improving the social security level for older adults is the key to the construction of aging-friendly communities. The weightage of "social economy" is relatively low. It is caused by the lack of social older-adult resources and the shortage of older-adult funds. Current services provided by the community, such as home care, life care, intermediary help and older-adult canteen, are not free of charge, leading to the low recognition of the social economy component in the community aging-friendly construction. Therefore, enriching older adults' social resources and improving their social security level is critical in developing the community's

home-based aging model and improving the community's aging-friendly constructions.⁴

Research Recommendations

Review and suggestions on research methods. This study attempts to construct a comprehensive evaluation system of community's aging-friendly construction indicators. Yet, the research and formulation of any evaluation system will inevitably encounter generality and particularity. This study attempts to consider general and individual needs and hopes to construct a comprehensive evaluation system that can reflect the situation of community's aging-friendly construction through the FAHP expert questionnaire survey of government, school, industry and other community's aging-friendly construction participants. However, establishing a community's aging-friendly construction index evaluation system is a dynamic interactive process that needs to constantly rely on the joint participation of the community's aging-friendly construction's decision-makers and the community's older adults for feedback and correction. Limited by research resources, research methods and the survey sample number, this study is only a preliminary study. More detailed investigation and analysis are needed for feedback correction.

Recommendations for follow-up studies. This study has preliminarily constructed the evaluation weighting system of the community's aging-friendly construction index. Future research directions are based on this foundation. After that, we will score and quantify the index elements in the index system, construct a community's aging-friendly construction index evaluation scale, and select specific community examples for confirmatory analysis and quantitative evaluation of community's aging-friendly construction. On the one hand, it can provide a macro-level construction strategy and a micro-level priority satisfaction strategy for the community's aging-friendly construction that has not been upgraded. On the other hand, it can evaluate the construction effectiveness of the updated community's aging-friendly construction, identify the shortcomings of specific indicators' construction, and propose targeted rectification suggestions to bring in practical significance.

Research Limitations

The main limitations of this study are the following 2. The first is that it uses the FAHP method to construct an assessment system of community aging-friendly construction. It is objective and rational; however, the weightage of each overall assessment index is determined by the consensus among experts, and there are significant differences in the perceptions of the importance of each index by different expert groups. Due to the limitations of the research method and time, the results may be limited in terms of research scope

and general inference. Secondly, this paper focuses on exploring and grasping the needs of older adults in general. However, at the individual level, their situation has a great deal of complexity and variability. In particular, there are different levels of intersection between age, disability, and residential status, and the corresponding needs may change. This paper does not analyze the specific needs of older-adult groups.

Author Contributions

“Conceptualization, Wen-Bing Mei, Kun Li. and Yi-zhe Huang.; methodology, Wen-Bing Mei, Kun Li. and Yi-zhe Huang.; software, Kun Li, Wen-Bing Mei.; validation, Wen-Bing Mei, Kun Li. and Yi-zhe Huang.; formal analysis, Wen-Bing Mei, Yi-zhe Huang.; investigation, Kun Li, Wen-Bing Mei.; resources, Kun Li, Wen-Bing Mei.; data curation, Wen-Bing Mei, Kun Li. and Yi-zhe Huang.; writing—original draft preparation, Wen-Bing Mei, Kun Li.; writing—review and editing, Wen-Bing Mei. and Yi-zhe Huang.; funding acquisition, Kun Li, Wen-Bing Mei. All authors have read and agreed to the published version of the manuscript.”

Declaration of Conflicting Interests

The author(s) declared no potential conflicts of interest with respect to the research, authorship, and/or publication of this article.

Funding

The author(s) disclosed receipt of the following financial support for the research, authorship, and/or publication of this article: “This research was funded by 2021 Guangdong Philosophy and Social Science Planning Project, grant number GD21CYS28.”

Ethics and Consent statements

Our study does not require the approval of the ethics committee, because this study mainly focuses on the calculation of the weight of community aging construction indicators under the community home-based care model, and does not involve ethical issues.

Informed Consent Statement

Informed consent was obtained from all subjects involved in the study.

ORCID iD

Wen-Bing Mei  <https://orcid.org/0000-0002-3103-6407>

References

1. China Central and State Council. *Social Elderly Service System Construction Plan (2011-2015)*, 2011. http://www.gov.cn/zhengce/content/2011-12/27/content_6550.htm (accessed November 11, 2012).
2. China Development Research Foundation. *China Development Report 2020: Development Trends and Policies of China's Population Aging*. China Development Press; 2020.
3. Yang BQ, Gao XL, Yuan HH. A structural equation model of satisfaction for the elderly in urban communities. *Chin Gerontol.* 2015;35(21):6211-6215.

4. Mei W-B, Hsu C-Y, Ou S-J. Research on the Evaluation Index System of the construction of communities suitable for aging by the Fuzzy Delphi method. *Environments*. 2020;7(10):92. doi:10.3390/environments7100092
5. Yang ZX. Build a quality of life system for the elderly with Chinese characteristics. *J Shenzhen Univ*. 2002;01:60-66.
6. Zhu H. Elaborate index evaluation and realization mechanism of community home care service: A case study of Hangzhou City. *J Jiangsu Univ*. 2019;21(05):77-85.
7. WHO. (2002). *International Programme of Action on Ageing*. https://www.un.org/chinese/documents/decl-con/docs/aging_prog.pdf
8. Thanakwang K, Soonthorndhada K. Attributes of active ageing among older persons in Thailand: evidence from the 2002 survey. *Editor Advis Board*. 2007;21(3):113-135.
9. Bowling A, Stafford M. How do objective and subjective assessments of neighbourhood influence social and physical functioning in older age? Findings from a British survey of ageing. *Soc Sci Med*. 2007;64(12):2533-2549.
10. Lim EZK, Thompson CL. Measuring active ageing among older adults in Singapore. *Ageing Soc*. 2016;36(9):1853-1869.
11. Wu CP. Actively respond to the interpretation of the theory of population aging. *Scientific Res Aging*. 2013;1:4-13.
12. Liu W, Yang FP. Measurement of China's active aging development level—based on data research of Eastern, Central and Western Regions and 28 provinces and cities. *Demogr J*. 2019;41(2):100-112.
13. López-Otín C, Blasco MA, Partridge L, Serrano M, Kroemer G. The hallmarks of aging. *Aging Cell*. 2013;153(6):1194-1217.
14. Ferrucci L, Gonzalez-Freire M, Fabbri E, et al. Measuring biological aging in humans: a quest. *Aging Cell*. 2020;19(2):e13080.
15. He W, Goodkind D, Kowal PR. *An aging world: 2015*. United States Census Bureau; 2016.
16. Zhang XZ. Notes on the Law of the People's Republic of China on the protection of the rights and interests of the Elderly (Revised draft). Communiqué of the Standing Committee of the National People's Congress of the People's Republic of China; 2013:37-41.
17. WHO. *Establish an international consensus on long-term care policies for the elderly*. 2000. http://www.who.int/publications/list/WHO_HSC_AHE_00_1/zh/.
18. WHO. *A guide to the construction of global friendly cities for the elderly*. 2007. https://www.who.int/ageing/AFCGuide_Chinese.pdf?ua=1
19. He B. *Research on the demand level and satisfaction strategies of home-based care services for the urban elderly in communities*. PhD thesis, East China Normal University; 2018.
20. Forder A. *Concepts in Social Administration: A Framework for Analysis*. Routledge/Thoemms Press; 1974.
21. Harrison F, Low LF, Barnett A, Gresham M, Brodaty H. What do clients expect of community care and what are their needs? The community care for the elderly: needs and service use study (CENSUS). *Australas J Ageing*. 2014;33(3):206-213.
22. Liu LF. Problems and countermeasures in the development of the elderly community. *Macrocon Res*. 2012;1:29-32.
23. Mei W-B, Hsu C-Y, Ou S-J. Research on evaluation indexes and weights of the aging-friendly community public environment under the community home-based pension model. *Int J Environ Res Public Health*. 2020;17(8):2863. doi:10.3390/ijerph17082863
24. Zhao J. *Research on Residential Welfare under the Mode of Home Care in Urban Community*. PhD thesis, Shandong University; 2019.
25. Hou B. *Research on the demand levels and satisfaction strategies of home-based care services for the elderly in urban communities*. PhD thesis, East China Normal University; 2018.
26. Mei WB. Research on the construction of evaluation index system for community aging-friendly environment construction. *Chin Arts*. 2022;128(03):102-111.
27. Saaty T. *The Analytic Hierarchy Process*, Vol. 70. Mcgraw Hill; 1980.
28. Zhang JJ. Fuzzy analytic hierarchy process (fahp). *Fuzzy Syst Mathemat*. 2000;14(2):80-88.
29. Saaty TL. How to make a decision: The analytic decision processes. *Interfaces*. 1994;24(6):19-43.
30. Mu E, Pereyra-Rojas M. *Practical Decision Making Using Super Decisions v3: An Introduction to the Analytic Hierarchy Process*. Springer; 2017.
31. Saaty RW, Saaty TL. (2003). Super decisions. *Software for Decision Making with Dependence Feedback*. Tutorial.
32. Wen-Bing M. *Research on the Construction and Application of the Evaluation Index of the Aging Construction of the Community*. Chaoyang University of Technology; 2021.
33. Meltzer AJ. *Policy Analysts in the Bureaucracy*. Univ of California Press; 1976.
34. Dalkey NC. (1969). *The Delphi method: An experimental study of group opinion*.
35. He LH, Wei G. Built community environment renovation for senior people. *Planners*. 2015;31(11):23-28.
36. Sun LL, Wang QY. Research on the influencing factors of urban residents' Social Security Satisfaction—An empirical analysis based on the ordinal Logistic-ISM Model. *Surv World*. 2019;4:100-105.
37. Wang YF, Tian M, Liu F. Qualitative research on opinions and suggestions of experts in related fields on aging-friendly renovation of home environment. *Nurs J*. 2022;29(19):56-61.
38. Zhao XM, Guo WW, Shi JR. Aging-adaptive allocation model of community outdoor environment elements based on the type of daily activities of the elderly. *Architecture J*. 2017;581(02):48-52.
39. Wood GER, Pykett J, Daw P, et al. The role of urban environments in promoting active and healthy aging: A systematic scoping review of citizen science approaches. *J Urban Health*. 2022;99(3):427-456.
40. Li YY, Li JX, Zeng P. A preliminary study on the implementation path of community renewal based on the community support system for the elderly. *Mod Urban Stud*. 2022;01:15-23.
41. Tang D, Yu YJ, et al. A study on the satisfaction of the government's purchase of community elderly services—an empirical analysis based on Shanghai survey data. *Northwest Popul*. 2017;38(3):93-99.
42. Li M. Research on the influencing factors of the willingness to provide for the aged at home in the community—taking Beijing as an example. *Popul Develop*. 2014;2:102-106.
43. Zhong F, Liu X, Lian RR. From production to practice—see the practical connotation of social design from the perspective

- of aging transformation design. *Zhuangshi*. 2022;347(03): 44-49.
44. Liu B, Yang CX, Tian T. Research progress on aging barrier-free and its enlightenment to the construction of aging-friendly environment. *Chin J Gerontol*. 2021;41(20):4569-4574.
 45. Hu X, Wei Y, Tang J. Design strategy of friendly and healthy environment for Urban Aging Community. *IOP Conf Ser Earth Sci*. 2020;598.
 46. Wang XC. From concept to practice: community home-based elderly care gradually makes up for shortcomings. *Ind Build*. 2021;51(09):234.
 47. Benefield LE, Holtzclaw BJ. Aging in place: merging desire with reality. *Nurs Clin*. 2014;49(2):123-131.
 48. Zhao J. *Research on Residential Welfare under the Mode of Home-based Care in Urban Communities*. PhD thesis, Shan Dong University; 2019.
 49. Li X. Research on the issues of home care in urban communities from the perspective of social embeddedness theory. *Guangxi Soc Sci*. 2014;4:131-134.
 50. Han JJ, Liu C. The construction of multiple systems of community home care services. *Soc Sec Res*. 2012;6:36-40.

暨南大学 文献收录证明

检索课题：广东轻工职业技术学院陈大华发表的文献在 SCIE 数据库中的收录情况。

检索工具及年限：

Science Citation Index Expanded (SCI-EXPANDED) 2000-2023 年

检索结果：根据委托方提供的文献目录，经上述数据库及年限范围内检索，共计 1 篇论文被 SCIE 收录，结果如下：

序号	文献信息	作者顺序	影响因子	中科院 大类 分区
1	标题:Effect of molecular weight distribution on the structure and properties of polypropylene cast film and stretched microporous membrane 作者:Chen, Dahua;Yin, Liangdong;Su, Zhixiang;Xie, Jiayi;Xu, Ruijie;Lei, Caihong; 来源出版物:JOURNAL OF POLYMER ENGINEERING 卷:43 期:9 页 791-800 DOI:10.1515/polyeng-2023-0118 出版年:OCT 26 2023 Web of Science 核心合集中的 被引频次:0 入藏号:WOS:001074265500001 文献类型:Article ISSN:0334-6447	第一作者	2.0	4 区

声明：本证明的文献信息由委托人提供，检索结果已由委托人核实确认无误。如果由于委托人提供信息不实而造成任何后果，本查新站概不负责。

委托人（签名）：

检索员： 汤华清
教育部科技查新工作站(Z15)
暨南大学图书馆学科服务与咨询部

2023 年 11 月 29 日

Original Article

Dahua Chen, Liangdong Yin, Zhixiang Su, Jiayi Xie*, Ruijie Xu and Caihong Lei*

Effect of molecular weight distribution on the structure and properties of polypropylene cast film and stretched microporous membrane

<https://doi.org/10.1515/polyeng-2023-0118>

Received May 19, 2023; accepted August 27, 2023;

published online September 27, 2023

Abstract: Two isotactic polypropylene (iPP) resins with approximate weight-average molecular weight (M_w) and different molecular weight distribution (MWD) were chosen to prepare cast films by the melt-stretching method. The lamellar morphology and mechanical properties of the initial precursor films and stretched microporous membranes were characterized. It was found that PP1 resin with a broader MWD exhibits a higher relaxation time of around 5.5 s, a larger entanglement density of 24.7 mol/m^3 and fast crystalline ability. The lamellar lateral size, orientation degree and entanglement density of the corresponding cast film are significantly increasing, resulting in higher elastic recovery and more apparent strain-hardening behavior. The PP resin with broader MWD also benefits the pore formation, resulting in a larger pore size and better air permeability of the stretched microporous membrane.

Keywords: crystallization; polypropylene; molecular weight distribution

1 Introduction

Polypropylene microporous membrane is one of the most widely commercially available membrane products, mainly used in lithium batteries, pharmaceutical filtration, water treatment and other fields [1]. The melt stretching method is the primary method for preparing polypropylene microporous membranes, which is also widely used to prepare other polymer microporous membranes, such as PE, PVDF, and PMP [2–4]. Studying the melt stretching method would help to guide the preparation of high-performance microporous membranes.

Preparing polypropylene microporous membrane by melt stretching is generally divided into the four following steps: (1) The formation of highly oriented lamellar structures during the melt-stretching process; (2) Annealing to improve the lamellar structure, increasing the thickness and orientation of the lamellar structure; (3) stretching at room temperature and high temperature to form a regular pore structure; (4) heat-setting to stabilize the pore structure [5]. Among them, forming an oriented lamellar structure in the first process is the most critical step. During the melt-stretching process, the polymer melt is rapidly stretched and cooled at the exit of the extruder die. The polymer molecules are stretched and oriented along the flow direction, forming a shish-kebab structure (or an oriented layered kebab structure without shish). At this point, polymer chains compete between oriented-induced crystallization and chain relaxation. Therefore, polymer structural parameters and processing parameters that could affect polymer crystallization and relaxation are the main factors that control the formation of the initial oriented structure during the melt-stretching process [2, 5–10]. Previous works have suggested that high molecular weight resin with long chains is a good candidate to generate a proper row-nucleated lamella since they form long fibrils that act as sites for lateral lamellae crystallization [11]. Sadeghi et al. found that the resin with a higher molecular weight tended to form a planar crystalline morphology as the melt-drawing ratio increased [5]. Xu et al. figured out that higher molecular

*Corresponding authors: **Jiayi Xie**, School of Chemistry and Civil Engineering, Shaoguan University, Shaoguan 512005, P. R. China, E-mail: xiejy710@163.com; and **Caihong Lei**, Guangdong Provincial Key Laboratory of Functional Soft Condensed Matter, School of Materials and Energy, Guangdong University of Technology, Guangzhou 510006, P. R. China, E-mail: lch528@gdut.edu.cn. <https://orcid.org/0000-0002-3660-7715> (C. Lei)

Dahua Chen, School of Chemical Engineering and Technology, Guangdong Industry Polytechnic, Guangzhou 510300, P. R. China

Liangdong Yin, Zhixiang Su and Ruijie Xu, Guangdong Provincial Key Laboratory of Functional Soft Condensed Matter, School of Materials and Energy, Guangdong University of Technology, Guangzhou 510006, P. R. China

weight would enhance the orientation of lamellae but not change the thickness of lamellae [12]; they also found that the cast film containing higher molecular weight components had a larger elongation at break and yield stress but lower elastic recovery during the cycle stretching. Additionally, our previous work showed that low molecular weight tails resulted in higher lamellar thickness in the cast film and improved pore properties of the stretched microporous membrane [13]. Apparently, the structural parameters of polymer highly affect the lamellar structure and properties of cast film. However, there are few systematic studies on the effect of molecular weight distribution (*MWD*) on lamellar structure and properties of cast film. Some researchers have reported the effect of *MWD* on the formation of shear-induced oriented structures [14]. But compared with the shear field, the melt stretching process has a more complex crystallization environment with a high-speed stretching force field and rapid cooling temperature field; the process of oriented crystallization during melt stretching is different from that of shear-induced crystallization. The study on the effect of *MWD* on the lamellar structure and properties of cast film still needs to be clarified.

In this paper, the two polypropylene resins with similar molecular weights and different *MWD* were used to prepare the cast film and stretched membrane via an extrusion casting process. The rheological and crystalline properties of PP raw resins were characterized by Dynamic rheological measurements and Differential scanning calorimetry (DSC). The structure parameters and properties of PP extrusion cast film and stretched microporous membrane were characterized by SEM, FTIR, DSC, 2D-SAXS, and tensile test. The relationship between *MWD* and the structure and properties of the cast film and stretched microporous membrane was clarified.

2 Materials and methods

2.1 Materials

Two polypropylene resins PP1 (F401) and PP2(HP741H) were supplied by Huajin petrochemical company China and LyondellBasell Industries, respectively. The melt flow index for PP1 and PP2 are 2.7 and 3 g/10 min (230 °C, 2.16 kg load). The catalyst(s) used for two PP are Ziegler-Natta catalysts. The tacticity of PP1 and PP2 are 96.3 % and 97.5 %, respectively. The molecular weight and *MWD* were measured using a GPC (Viscotek model 350) at 135 °C and 1, 2, 4-trichlorobenzene (TCB) as the solvent. The universal calibration curve obtained with polystyrene (PS12000K, APSC) was used to calibrate the corresponding molecular weight. The GPC curves and the corresponding molecular weight values are shown in Figure 1. PP1 and PP2 had an approximate weight-average molecular weight (*M_w*), but the *MWD* of PP1 is larger

than PP2, indicating that PP1 has more content of lower molecular weight parts and higher molecular weight parts.

2.2 Preparation of precursor film and stretched microporous membrane

The precursor film was prepared by the melt-stretching process through an extrusion machine with a hot roll and air knife (PUTO, CHINA). During extrusion, the uniaxial stretching (machine direction, MD) was applied to the PP melt, which resulted in oriented crystalline structures. The die temperature was set at 210 °C, the extruding velocity of the PP melt was set at 0.5 mm/s and the melt-drawing ratio of 80 was applied. The melt-drawing ratio is a specific ratio between the line speed of the casting roll and the extruding velocity of the PP melt. The films were produced at a chill roll temperature of 80 °C. The thickness of the precursor film was controlled at 25 μm.

The prepared precursor film was annealed at a taut condition at 145 °C in a hot oven for 2 h. The stretched PP microporous membranes were prepared by the H&P Inspekt table blue machine equipped with a heating chamber. The prepared procedures were shown as follows: the annealed PP films were first stretched to 20 % with a drawing speed of 100 %/min under room temperature and then stretched to 120 % with a drawing speed of 100 %/min at 130 °C; then the stretched film was further heat-setting for 10 min at 145 °C.

2.3 Dynamic rheological measurements

Dynamic rheological measurements were carried out using an Anton Paar MCR 301 with parallel plate geometry of 25 mm diameter and a gap equal to 1 mm at the temperature of 210 °C. Before the frequency sweep tests, the time sweep tests at a frequency of 0.628 rad s⁻¹ were performed for 2 h to check the thermal stability of the specimens. No degradation (less than 3 % changes) was observed for the duration of the time sweep tests. The dynamic data were obtained in the linear regime.

2.4 Differential scanning calorimetry (DSC)

Differential scanning calorimetry (DSC) measurements were carried out via a DSC3 (Mettler-Toledo, Switzerland) using nitrogen as a purge gas. The temperature and heat flow were calibrated with indium. The DSC curves were obtained upon heating and cooling at a rate of 10 °C/min. The crystallinity (*X_c*) was calculated as follows:

$$X_c (\%) = \frac{\Delta H_m}{\Delta H_m^0} \times 100 \quad (1)$$

where ΔH_m is the endothermic heat of melting, and ΔH_m^0 is the endothermic heat of melting for perfectly crystalline. This value for PP is 209 J/g [15].

The lamellar thickness can be calculated by the Thomson equation,

$$L = 2 \frac{\sigma_e}{\Delta H_m} \frac{T_m^0}{T_m^0 - T_m} \times 10^9 \quad (2)$$

where T_m is the observed melting point of lamellae with thickness. T_m^0 is the equilibrium melting point of an infinite crystal ($T_m^0 = 457$ K for iPP), σ_e is the surface free energy of the basal plane ($\sigma_e = 49.6 \times 10^3$ J/m³ for iPP), ΔH_m is the enthalpy of fusion per unit volume ($\Delta H_m = 1.34 \times 10^8$ J/m³ for PP) [16].

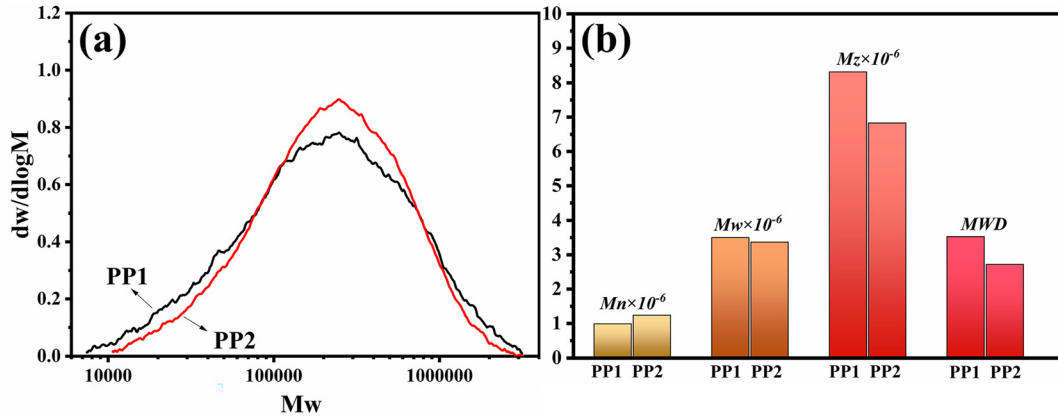


Figure 1: The GPC curves (a) and the material characteristics (b) of two PP resins.

Non-isothermal crystallization was performed as follows: the samples were first heated to 210 °C at a rate of 10 °C/min under a dry nitrogen atmosphere and held for 5 min. Then the samples were quenched to 25 °C at a rate of 30 °C/min.

2.5 SEM morphology

The surface morphology of the etched cast films was characterized using scanning electron microscopy (S3400, Hitachi, Japan). All the samples were sputtered with a platinum ion beam for 100 s before testing. To clearly observe the lamellar clusters of the cast films, an etching method was used to remove the amorphous part. The films were dissolved in a 0.7 % solution of potassium permanganate in a mixture of 35 vol% of orthophosphoric and 65 vol% of sulfuric acid. The average pore size was collected by the software ‘Nano Measurer’.

2.6 Small-angle X-ray scattering (SAXS) experiments

Small-angle X-ray scattering (SAXS) experiments were performed using synchrotron radiation with $\lambda = 0.154$ nm at Beamline 1W2A of the Beijing Synchrotron Radiation Facility (Beijing, China). Mar165-CCD was set at a 4970 mm sample-detector distance in the direction of the beam for small-angle X-ray scattering (SAXS) data collection.

2.7 Tensile test

The stress-strain curves and elastic recovery of the cast films were tested using an H&P Inspekt table blue machine. The stretching sample is 15 mm wide, and the gage length is 50 mm. The grip is the standard plate jaw face grip used for flat and thin specimens. A drawing speed of 50 mm/min was applied. The elastic recovery ratio was determined along the stretched direction of the film. The percent elastic recovery ratio (ER) was calculated using the following equation:

$$ER = \frac{L - L'}{L - L_0} \times 100 \% \quad (3)$$

where L_0 is the initial length of the film before the extension, L is the length when strained to 100 % and L' is the length at the end of the extension.

2.8 Air permeability and porosity

The air permeability of stretched microporous membranes was characterized by Gurley Densometer model No. 4150 (Gurley Precision Instruments, New York, USA) according to ASTM D726. The Gurley value was defined as the time required for a specific amount of air (100 mL) to pass through a specific area of the microporous membrane under a specific pressure (20 kgf/cm²). The porosity was measured using liquid absorption methods according to ASTM D2873. The paraffin oil was used and the porosity was calculated based on the weight difference before and after immersion in the liquid.

3 Results and discussion

3.1 The rheological properties of two PP resins

To prepare a microporous membrane based on the melt-stretching mechanism, the first step is preparing a cast film with a row-nucleated crystalline structure during the melt-stretching process. Here, the crystalline orientation and morphology strongly depend on the rheological properties of the raw materials. The rheological properties of two PP resins were first tested in a frequency range from 0.05 to 300 rad s⁻¹.

Figure 2a presents the storage modulus as a function of frequency. As a typical polymer melt, the storage and loss modulus of two PP resins decreases with the increasing angular frequency. The storage modulus and loss modulus of PP1 is higher than PP2, especially at the low angular

frequency range, due to more high molecular weight parts of PP1. Figure 2b also presents that the complex viscosity of PP1 at a low angular frequency range is higher than PP2, which is related to higher molecular weight parts of PP1.

To further explain the relaxation behavior of the PP raw materials, the relaxation spectrum ($H(\lambda)$) was calculated and shown in Figure 2c; here, λ means the relaxation time. $H(\lambda)$ is a useful method to explain the viscoelastic relaxation of different components, which can be determined through the Tschoegle approximation as revealed in Equation (4) [17, 18]:

$$H(\lambda) = G' \left[\frac{d \lg G'}{d \lg \omega} - \frac{1}{2} \left(\frac{d \lg G'}{d \lg \omega} \right)^2 - \frac{1}{4.606} \left(\frac{d^2 \lg G'}{d (\lg \omega)^2} \right) \right]_{1/\omega = \lambda/\sqrt{2}} \quad (4)$$

Then the relaxation time τ_e can be represented by the position of the maximum value in the resulting curve. The relaxation time of PP1 is 5.5 s, larger than that of PP2, about 0.97 s, due to the existence of the high molecular weight part of PP1. The longer relaxation time means that the molecular networks of polymer melt have more time to form the oriented lamellar structure during the melt-stretching process.

Except for the relaxation time, the entanglement molecular weight (M_e) is another important parameter affecting stress-induced crystallization [19]. The entanglement molecular weight reflects the molecular weight between adjacent temporary entanglement points, which is

usually calculated by the plateau modulus (G_N^0). For the semi-crystalline polymer with a broader MWD, the plateau modulus is difficult to measure by the minimum and maximum of G'' [20]. Here, an alternative calculated method of M_e based on the terminal crosspoint of G' and G'' ($G_x = G' = G''$ at angular frequency $\omega = \omega_x$) proposed by Nobile–Cocchini was used [21]. The plateau modulus can be defined by Equation (5) and shown in Figure 2d:

$$\log \left(\frac{G_x}{G_N^0} \right) = \frac{-0.524 + 0.431 \log \frac{M_w}{M_n} - 1.843 \log \frac{M_z}{M_w}}{1 - 0.559 \log \frac{M_w}{M_z} + 0.841 \log \frac{M_z}{M_w}} \quad (5)$$

It must be pointed out that the plateau modulus values obtained from the crossover methods are not absolute values, which are only used for qualitative comparisons. The entanglement molecular (M_e) and the entanglement density (N_e) could be further calculated by Equations (6) and (7):

$$G_N^0 = \frac{\rho RT}{M_e} \quad (6)$$

$$N_e = \frac{\rho}{M_e} \quad (7)$$

R is the gas constant, 8.314 J/mol k, and ρ is the density of the PP, 0.90 g/mol, at temperature T , 483 K, at which the plateau modulus was measured. The M_e and the entanglement density N_e are shown in Figure 2d. It can be seen that the entanglement molecular weight of PP1 is 96,418 g/mol,

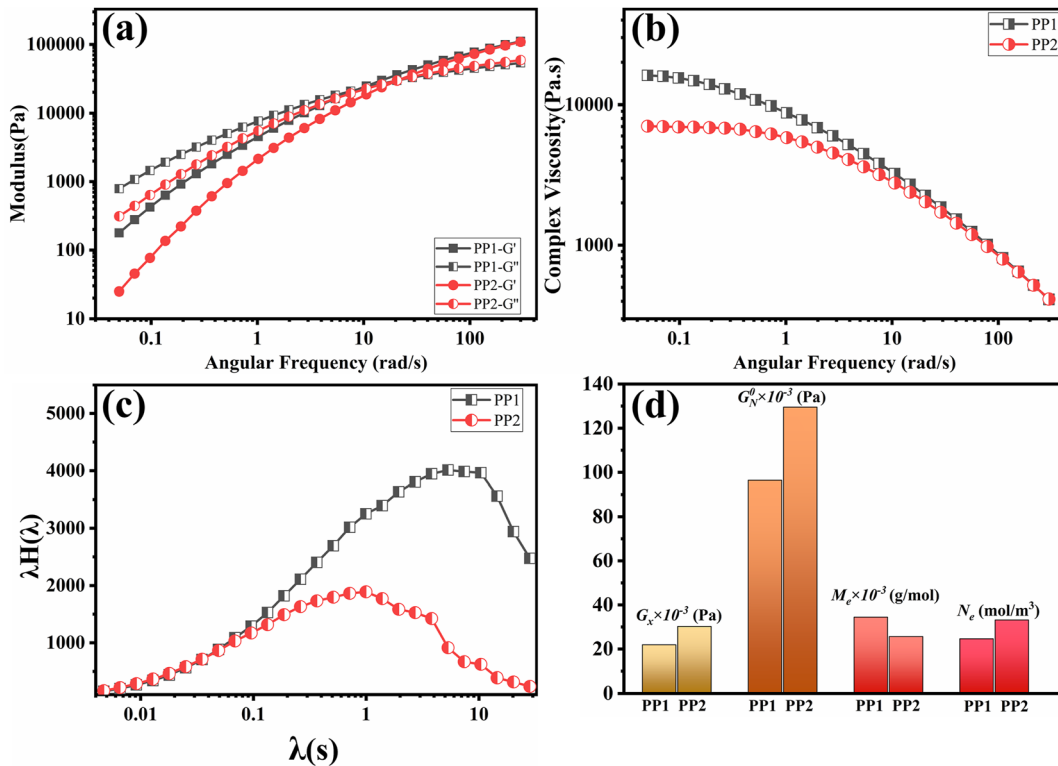


Figure 2: Storage modulus (a), complex viscosity (b), relaxation time spectrum (c) and entanglement parameter (d) of two PP resins.

which is smaller than the value of PP2, 129,527 g/mol. The entanglement density of PP1 is 24.7 mol/m³, which is smaller than the value of PP2, 33.2 mol/m³. The polymer with higher entanglement density is easier to orient the molecular chain and form the oriented crystalline structure during melt stretching.

3.2 Crystallization behavior of two PP resins

Figure 3 gives the related crystallization kinetic curves for two PP resins. It can be seen that the crystallization onset temperature of PP1 was 124.8 °C, which is higher than the crystallization onset temperature of PP2 at 122.8 °C. The maximum crystallization temperature of PP1 was 116.8 °C, which is also significantly higher than the maximum crystallization temperature of PP2 at 111.9 °C. These results indicated that PP1 has a higher crystallization ability. Figure 3b presented that the half crystallization of PP1 is 67.4 s, a little larger than 80.0 s of PP2, meaning that the crystallization rate of PP1 is faster than that of PP2. The existence of high molecular weight species in PP1 is beneficial for forming initial crystalline structures [22], and the content of low molecular weight chains also benefits the growth of crystalline structures [13]. The broader *MDW* of PP1 results in PP1 having a better crystallization ability. Figure 3c presents the melting curve of two PP resins that are similar. Although PP1 has a faster crystallization rate, these two polymers show a similar total crystallization degree. The different crystallization ability of the two PP resins seems to have little effect on their crystallization structure.

3.3 Microstructure and properties of the precursor films prepared by two PP resins

Figure 4 gives the etched surface morphology of cast films prepared by PP1 and PP2. It can be seen that row-nucleated

crystalline structures arranged perpendicular to the extrusion direction have been formed for all two samples. PP1 and PP2 showed approximate uniform lamellar crystalline and crystalline thickness. The difference in molecular weight does not affect the morphology of lamellar clusters. The detailed structure parameter should be further clarified.

Figure 5 gives the DSC curves of the cast films prepared with two PP resins. The melting peak of the two samples is very similar, which means that the two cast films have similar crystalline structural parameters. The lamellar thickness and the crystalline degree are further calculated by applying the DSC experimental results. As we can see from Figure 5, the melting peak temperature and the lamellar thickness of the PP1 cast film is a little higher than that of the PP2 film, while the crystalline degree of the PP1 cast film is slightly lower than that of the PP2 film. As mentioned in Figure 3, although the PP1 resin has a faster crystallization rate, these two polymer resins show a similar total crystallization degree. During the melt-stretching process, the polymer melt undergoes a stretching stress field, which is also a flow-induced crystallization behavior. Previous researchers suggested that flow-induced crystallization behavior in the melt stretching process could accelerate the crystallization rate but nearly not change the crystalline degrees [10, 23]. Hence, the cast films of these two resins also show similar crystalline thickness and crystalline degrees, consistent with the above SEM results. 2D-WAXS was also used to investigate the crystal information of precursor films. The 1D integrated curve for WAXS patterns (Figure S1) show that only α phase crystal are formed in our experiment. Hence, the phase transformation in the melt stretching process of PP film does not need to be considered.

2D-SAXS were further used to investigate the lamellar structure of precursor films. Figure 6a gives the 2D-SAXS pattern of PP cast films. Two spot scattering patterns of both samples are shown in the vertical direction, indicating the formation of an oriented crystalline structure during melt-stretching, in agreement with the above SEM and DSC results. The scattering intensity was further integrated along

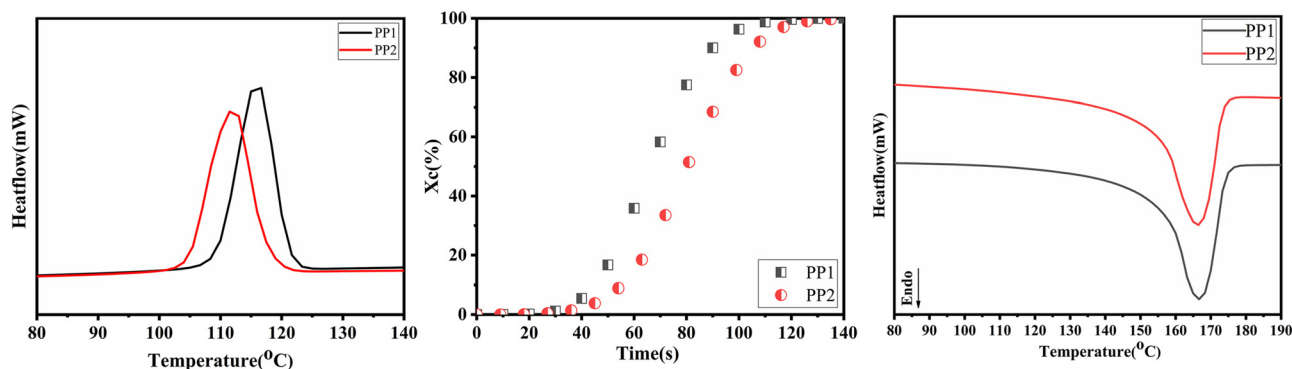


Figure 3: The crystallization curve (a) and the relative crystallization degree (b), the melting curve of two PP resins.

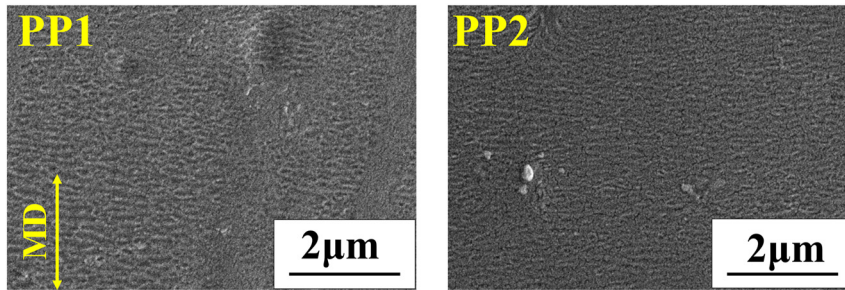


Figure 4: Surface SEM of cast films prepared by two PP resins.

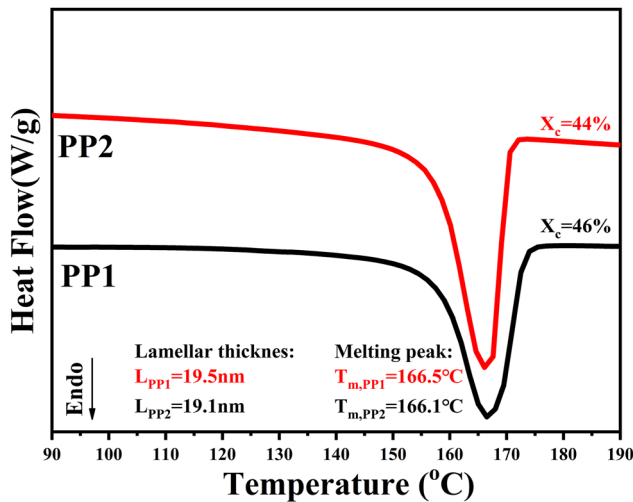


Figure 5: Melting curves of precursor films with two PP resins.

the vertical direction and analyzed by the one-dimensional correlation function. The detailed structural parameters, e.g., the long period (L_p), the crystal region thickness (L_c), and the amorphous region thickness (L_a), were calculated according to the well-known methodology proposed by Strobl et al. [24], as shown in Figure 6c and d. The L , L_c , and L_a of the PP1 sample are 14.5 nm, 5.8 nm and 8.7 nm, respectively, which are slightly larger than that of the PP2 sample. The approximated value of L_p , L_c and L_a of the two samples mainly attribute to their similar M_w , unaffected by the *MWD*.

We further calculated the lamellar lateral sizes from the width of the peaks at half-height along the horizontal direction. Figure 6e shows that the lateral size of PP1 is 47 nm, significantly large than the 32 nm of PP2. And the orientation of the lamella was further calculated from the intensity curves along the azimuthal direction. As shown in Figure 6e,

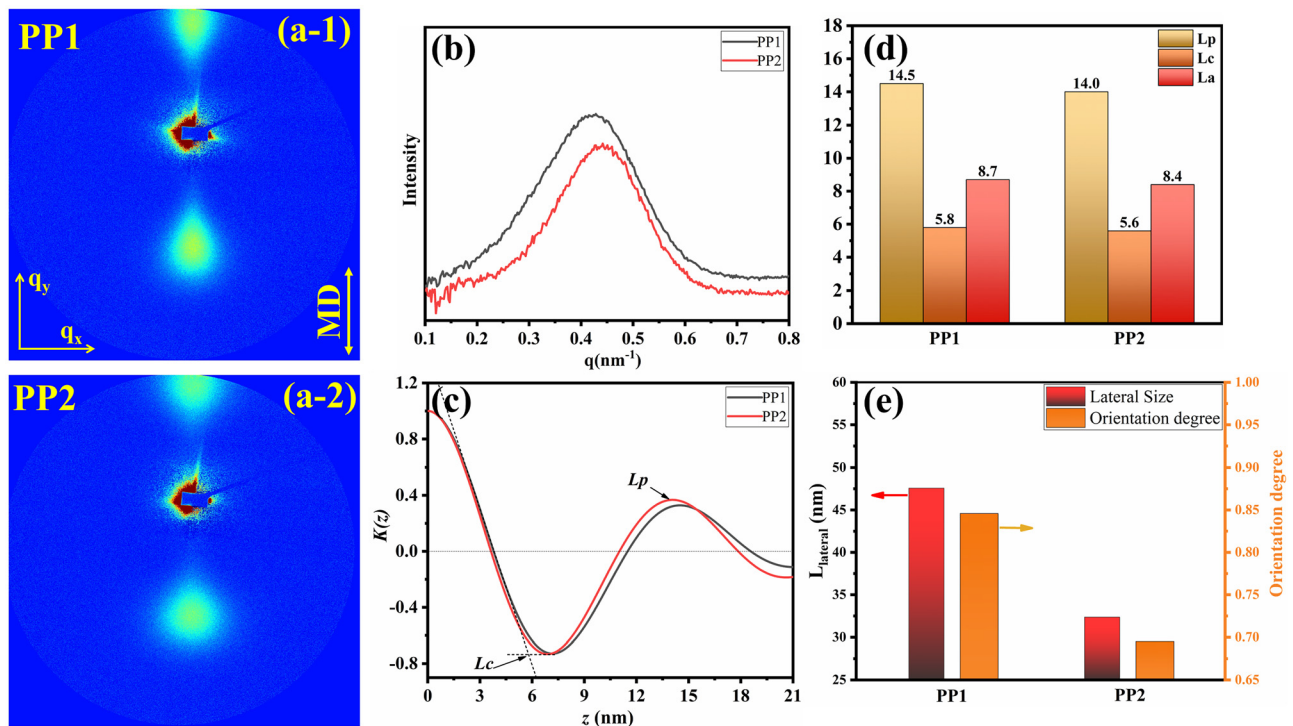


Figure 6: 2D SAXS patterns (a), corresponding one-dimensional scattering intensity distribution (b), one-dimensional correlation function (c), lamellar structure parameters (d) and lateral size and orientation degree (e) of PP precursor films.

the orientation degree of the PP1 cast film is 0.85, which is obviously higher than 0.69 of the PP2 cast film. The difference in the lateral sizes and orientation degree of the lamellar structure may be connected with the *MWD* in two PP resins.

By summarizing the above results, we can find that the effect of molecular parameters on the microstructure of PP cast film is understood. In the melt stretching process, the polymer melt undergoes a stretching force field and the cooling field, the molecular chains of high molecular weight are first stretched and oriented to form a highly oriented initial nuclei structure (ghost nuclei) along the flow direction [25]. The other molecular chain continues to form a lamellar structure surrounding the initial nuclei structure that aligns perpendicular to the flow direction. In our previous work on PE cast film [26], we found that higher molecular weight parts could increase the content of shish structure crystals under the same extrusion conditions. Somani et al. [27] also concluded that a slight increase in the concentration of high molecular weight chains led to a significant increase in the shish or nuclei site formation during the shear-induced crystallization of isotactic polypropylene. For the cast film of PP1 and PP2, no shish structure was formed during the melt stretching process. The higher molecule part mainly accelerates the crystallization nucleation and the total crystalline ability still depends on the *Mw*. Hence PP1 and PP2 show a similar crystalline degree and thickness of L_p , L_c , and L_a . On the other hand, as the existence of low molecules tail is beneficial to enhance the growing up of the lamellar structure, the PP1 shows a larger lateral size of lamellar structure than the PP2. Besides, the polymer molecular chains during the melt stretching process are in a dynamic balance between stretching to orientation and relaxation of the molecular chain. For PP1 with a larger relaxation time, it is easier to form a higher-oriented lamellar structure. In

contrast, for PP2 with a short relaxation time, which is easy to relax in the melt-stretching process, PP2 cast film shows a lower orientation degree.

3.4 The mechanical properties of PP cast films

Figure 7 gives the stress–strain curves of two PP cast films. For the two films, no apparent necking phenomenon was observed, showing a typical stress–strain curve of PP film with hard elastic behavior [25]. In the small strain region, the elastic modulus and yield strength of these two films are similar, as they have a similar thickness of the lamellar structure. But the ER of the PP1 cast film is 84.8 %, significantly higher than the PP2 cast film of 76.6 %. Because the PP1 cast film has a higher orientation, the irreversible damage of the lamellar structure is not prone to occur during stretching. At the large strain region, the PP2 shows apparent strain-hardening behavior. Men et al. [28] reported that the extension of the amorphous network would dominate the deformation process at a large strain region. A higher entanglement density implies higher stress generated at a large strain region. Haward et al. [29] proposed that the strain hardening modulus is determined by the sum of the restraints imposed by a mesh of uncrossable polymer chains. Here, the strain-hardening region behavior was analyzed based on the Gaussian network theory of rubber elasticity proposed by Haward and Thackray using the equation [30]:

$$\sigma = Y/\lambda + G_p(\lambda - 1/\lambda^2) \quad (8)$$

where σ is the true stress, G_p is the strain-hardening modulus, Y is the yield stress and λ is the stretching ratio. As shown in Figure 7, the slope of σ versus the Gaussian strain

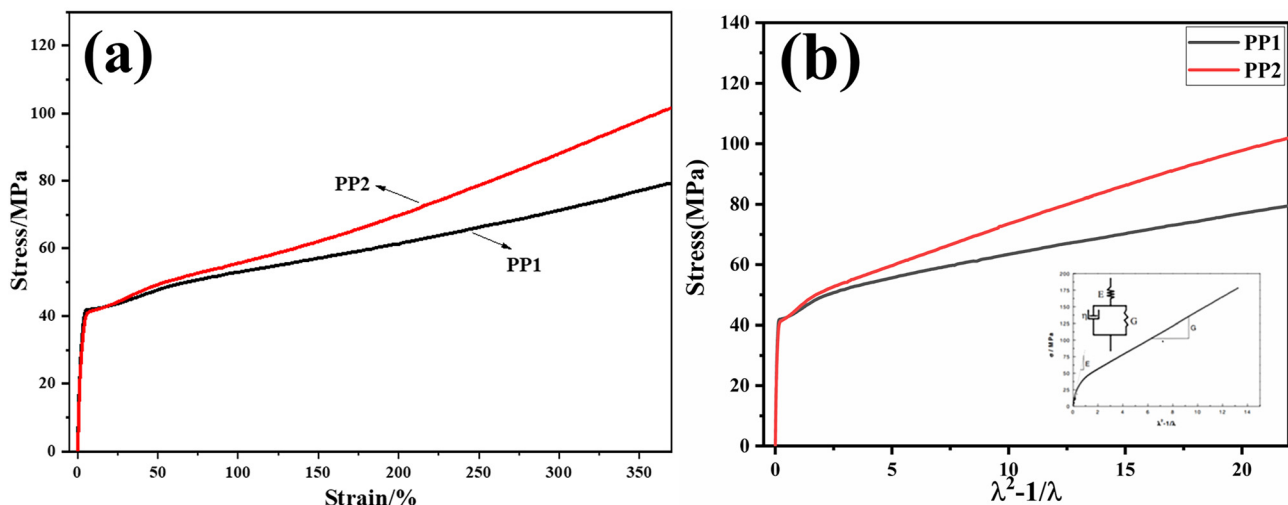


Figure 7: Stress-strain curves (a), stress versus the Gaussian strain (b) of PP cast films.

Table 1: The mechanical properties of two PP cast films.

Sample	E (GPa)	Yield strength (MPa)	ER (%)	G_p	v_e (nm) ⁻¹
PP1	15.51	41.8	84.8	1.37	0.33
PP2	15.73	41.4	76.6	2.50	0.607

yields the strain-hardening modulus G_p . The G_p of PP1 is apparently larger than that of PP2. According to Haward and Thackray, the value of G_p is related to the network density v_e by the equation [29, 30]:

$$G_p = v_e k_B T \quad (9)$$

where k_B is the Boltzmann constant and T is the temperature.

Table 1 lists the G_p and the network density (v_e) calculated by the G_p . The entanglement density of PP2 is larger than that of PP1. This result of network density v_e is consistent with the entanglement density (N_e) calculated by the

rheological test. As the N_e is a qualitative value, the ratio of v_e of two PP resins differs from that of N_e . But it is clear that the more apparent strain-hardening behavior in PP2 film is connected with its larger entanglement density.

3.5 The structure and properties of stretched microporous membranes

Figure 8 shows the SEM images of stretched microporous membranes with two PP resins. The typical separated lamellar clusters, pores, and connecting bridges are observed in all the samples. The SEM images of PP1 show more apparent separated lamellar clusters and larger pores. The pore sizes are calculated from the SEM image and shown in Table 2. The statistics pore value also proves that PP1 stretched microporous membrane has a larger pore size. To further give the air permeability and porosity of the stretched microporous membrane, it can be seen that PP1 has a smaller Gurley value and higher porosity, implying

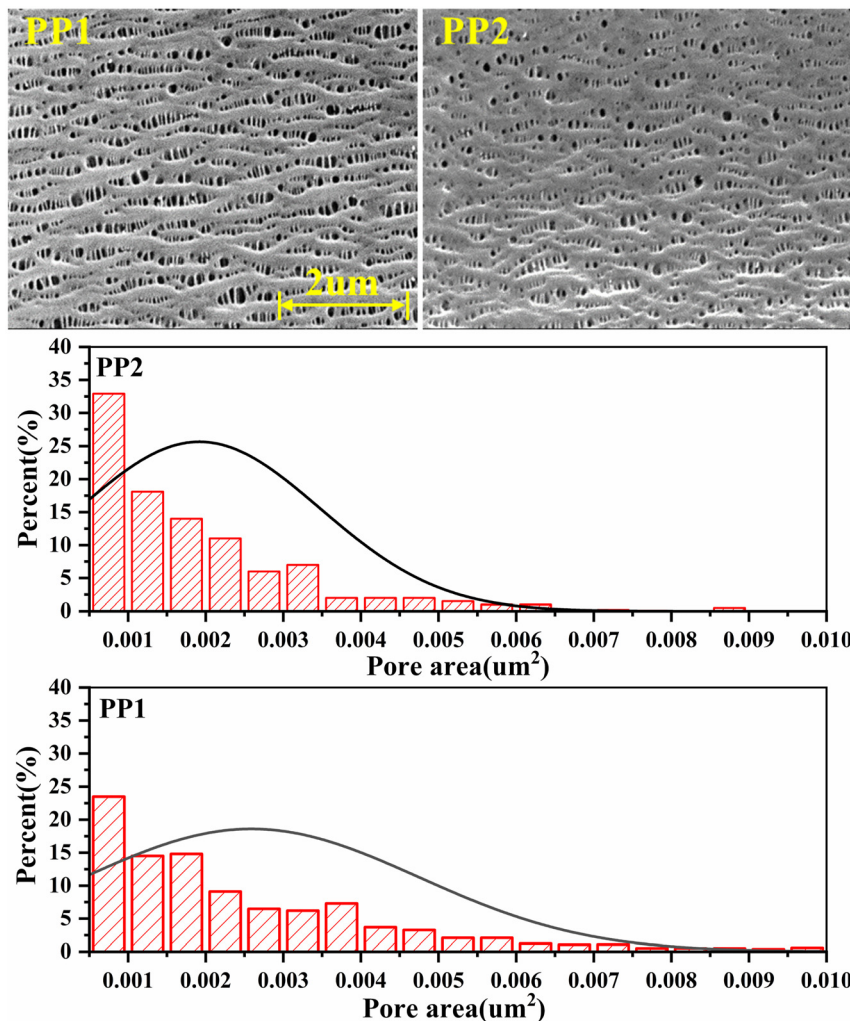
**Figure 8:** SEM images of stretched microporous membranes, and the pore area in the stretched microporous membranes.

Table 2: The porosity, Gurley value and pore area of stretched microporous membranes.

	Porosity (%)	Gurley value(s)	Pore area (μm^2)
PP1	46	210	0.0026
PP2	42	257	0.0019

that the PP1 stretched microporous membrane has better properties of air permeability. This result reflects that the PP1 resin with broader *MWD* could form the cast film with higher oriented lamellar structures, which is beneficial to the pore formation during stretching.

4 Conclusions

In this article, two PP resins with approximate M_w and different *MWD* were used to prepare cast films by the melt-stretching method. And the effect of *MWD* on the microstructure parameter and properties of cast film and stretched microporous membrane were investigated. Our findings can be summarized as follows:

- (1) PP1 resin has a broader *MWD* with high molecular weight species, exhibiting a higher relaxation time of around 5.5 s, a larger entanglement density of 24.7 mol/m^3 and fast crystallization ability.
- (2) Due to the longer relaxation time and the contribution of low molecules tail, the PP1 cast film has a higher orientation degree and a larger lamellar lateral size. The higher orientation degree and larger entanglement density result in higher elastic recovery and more apparent strain-hardening behavior.
- (3) Since the thickness and crystalline degree depend on the M_w , PP1 and PP2 cast film shows a similar L_p , L_c , L_a and crystalline degree, resulting in similar elastic modulus and yield strength of PP1 and PP2 cast film.
- (4) The PP resin with broader *MWD* could form the cast film with higher oriented lamellar structures, which benefits the pore formation, resulting in a larger pore size and better air permeability of PP1 stretched microporous membrane.

Research ethics: Not applicable.

Author contributions: All the authors have accepted responsibility for the entire content of this submitted manuscript and approved submission.

Competing interests: The authors declare no conflicts of interest regarding this article.

Research funding: The authors would like to thank the Project of the National Science Foundation of China under

grant 52173033, Guangzhou Science and Technology Plan Project (202102020952), Project of Science Foundation of Guangdong Province (2021A1515011914), The Youth Fund Project of Regional Joint Foundation- Fundamental and Applied Basic Research Foundation of Guangdong Province (2021A1515110648), Foshan Science and Technology Innovation Project (no. FS0AA-KJ919-4402-0145).

References

1. Mchugh A. The role of polymer membrane formation in sustained release drug delivery systems. *J. Control Release* 2005, 109, 211–221.
2. Lee S.-Y., Park S.-Y., Song H.-S. Lamellar crystalline structure of hard elastic HDPE films and its influence on microporous membrane formation. *Polymer* 2006, 47, 3540–3547.
3. Sadeghi F., Tabatabaei S. H., Aji A., Carreau P. J. Effect of PVDF characteristics on extruded film morphology and porous membranes feasibility by stretching. *J. Polym. Sci. Pol. Phys.* 2010, 47, 1219–1229.
4. Wang J., Xu Z., Xu Y. Preparation of poly(4-methyl-1-pentene) asymmetric or microporous hollow-fiber membranes by melt-spun and cold-stretch method. *J. Appl. Polym. Sci.* 2006, 100, 2131–2141.
5. Sadeghi F., Aji A., Carreau P. J. Analysis of microporous membranes obtained from polypropylene films by stretching. *J. Membrane Sci.* 2007, 292, 62–71.
6. Sadeghi F., Aji A., Carreau P. Study of polypropylene morphology obtained from blown and cast film processes: initial morphology requirements for making porous membrane by stretching. *J. Plast. Film. Sheet.* 2005, 21, 199–216.
7. Tabatabaei S. H., Carreau P. J., Aji A. Microporous membranes obtained from PP/HDPE multilayer films by stretching. *J. Membrane Sci.* 2009, 345, 148–159.
8. Mileva D., Gahleitner M., Gloger D., Tranchida D. Crystal structure: a way to control properties in cast films of polypropylene. *Polym. Bull.* 2018, 75, 5587–5598.
9. Di Sacco F., Gahleitner M., Wang J., Portale G. Systematic investigation on the structure-property relationship in isotactic polypropylene films processed via cast film extrusion. *Polymers* 2020, 12, 1636.
10. Sadeghi F., Aji A., Carreau P. J. Analysis of row nucleated lamellar morphology of polypropylene obtained from the cast film process: effect of melt rheology and process conditions. *Polym. Eng. Sci.* 2007, 47, 1170–1178.
11. Yu T.-H., Wilkes G. L. Orientation determination and morphological study of high density polyethylene (HDPE) extruded tubular films: effect of processing variables and molecular weight distribution. *Polymer* 1996, 37, 4675–4687.
12. Xu G., Ding L., Wu T., Xiang M., Yang F. Effect of high molecular weight on pore formation and various properties of microporous membrane used for lithium-ion battery separator. *J. Polym. Res.* 2018, 25, 1–11.
13. Caihong L., Shuqiu W., Ruijie X., Xinlong P., Wenqiang S., Bing H. Influence of low molecular weight tail of polypropylene resin on the pore structure by room-temperature stretching. *Polym. Eng. Sci.* 2013, 53, 2594–2602.
14. Nogales A., Hsiao B. S., Somani R. H., Srinivas S., Tsou A. H., Balta-Calleja F. J., Ezquerro T. A. Shear-induced crystallization of isotactic polypropylene with different molecular weight distributions: in situ small-and wide-angle X-ray scattering studies. *Polymer* 2001, 42, 5247–5256.

15. Gray A. P. Polymer crystallinity determinations by DSC. *Thermochim. Acta* 1970, 1, 563–579.
16. An Y., Holt J., Mitchell G., Vaughan A. Influence of molecular composition on the development of microstructure from sheared polyethylene melts: molecular and lamellar templating. *Polymer* 2006, 47, 5643–5656.
17. Gramespacher H., Meissner J. Interfacial tension between polymer melts measured by shear oscillations of their blends. *J. Rheol.* 1992, 36, 1127–1141.
18. Tschoegl N. W. *The Phenomenological Theory of Linear Viscoelastic Behavior: An Introduction*; Springer: London, 2012.
19. Kato S., Tanaka H., Yamanobe T., Uehara H. In situ analysis of melt-drawing behavior of ultrahigh molecular weight polyethylene films with different molecular weights: roles of entanglements on oriented crystallization. *J. Phys. Chem. B* 2015, 119, 5062–5070.
20. Liu C., He J., Van Ruymbeke E., Keunings R., Bailly C. Evaluation of different methods for the determination of the plateau modulus and the entanglement molecular weight. *Polymer* 2006, 47, 4461–4479.
21. Nobile M. R., Cocchini F. Evaluation of molecular weight distribution from dynamic moduli. *Rheol. Acta* 2001, 40, 111–119.
22. Parrini P., Corrieri G. The influence of molecular weight distribution on the primary crystallization kinetics of isotactic polypropylene. *Makromol. Chem.* 1963, 62, 83–96.
23. Xu R., Chen X., Xie J., Cai Q., Lei C. Influence of melt-draw ratio on the crystalline structure and properties of polypropylene cast film and stretched microporous membrane. *Ind. Eng. Chem. Res.* 2015, 54, 2991–2999.
24. Strobl G., Schneider M., Voigt-Martin I. Model of partial crystallization and melting derived from small-angle X-ray scattering and electron microscopic studies on low-density polyethylene. *J. Polym. Sci. Polym. Phys. Ed.* 1980, 18, 1361–1381.
25. Xu M., Zhang C., Zeng Z., Pu K. Semiconducting polymer nanoparticles as activatable nanomedicines for combinational phototherapy. *ACS Appl. Polym. Mater.* 2021, 3, 4375–4389.
26. Xie J., Xu R., Chen C., Chen X., Zhang F., Lei C., Lin Y., Li L. Influence of material characteristics on the structure and properties of high-density polyethylene microporous membranes. *RSC Adv.* 2016, 6, 62769–62777.
27. Somani R. H., Hsiao B. S., Nogales A., Srinivas S., Tsou A. H., Sics I., Balta-Calleja F. J., Ezquerro T. A. Structure development during shear flow-induced crystallization of i-PP: in-situ small-angle X-ray scattering study. *Macromolecules* 2000, 33, 9385–9394.
28. Men Y., Rieger J., Strobl G. Role of the entangled amorphous network in tensile deformation of semi-crystalline polymers. *Phys. Rev. Lett.* 2003, 91, 095502.
29. Haward R. Strain hardening of thermoplastics. *Macromolecules* 1993, 26, 5860–5869.
30. Haward R., Thackray G. The use of a mathematical model to describe isothermal stress-strain curves in glassy thermoplastics. *Proc. R. Soc. London, A* 1968, 302, 453–472.

Supplementary Material: This article contains supplementary material (<https://doi.org/10.1515/polyeng-2023-0118>).

检索证明

编号：20230406CS01

受广东轻工职业技术学院杨红玲的委托，中国科学院广州分院、广东省科学院信息服务中心通过 **Web of Science Core Collection** 数据库，对杨红玲作为文章第一作者发表的论文 “**Trait mindfulness and cell phone addiction in adolescents: A moderated mediation model**”，被 **SSCI** 收录的情况进行联机检索，结果如下：

序号	论文目录清单	数据库收录	影响因子 (2021)	JCR 分区	中科院分区 (2022 升级版)
1	Yang, HL; Huang, X; Zhao, XH; Lu, AT. Trait mindfulness and cell phone addiction in adolescents: A moderated mediation model. SOCIAL BEHAVIOR AND PERSONALITY . 2023, 51(2), e11984.	SSCI	1.183	该期刊在 PSYCHOLOGY, SOCIAL 领域中为 Q4. (SSCI 版本)	心理学 4 区

共计：被 **SSCI** 收录 1 篇。

特此证明

详情见附录

中国科学院广州分院
广东省科学院
信息服务中心
2023 年 4 月 4 日

附录

SSCI 论文题录信息

标题: Trait mindfulness and cell phone addiction in adolescents: A moderated mediation model

作者: Yang, HL (Yang, Hongling); Huang, X (Huang, Xin); Zhao, XH (Zhao, Xihe); Lu, AT (Lu, Aitao)

来源出版物: SOCIAL BEHAVIOR AND PERSONALITY 卷: 51 期: 2 文献号: e11984 DOI: 10.2224/sbp.11984 出版年: FEB 2023

入藏号: WOS:000925807600002

文献类型: Article

地址: [Yang, Hongling] Guangdong Ind Polytech, Sch Management, Guangzhou, Peoples R China.

[Huang, Xin; Zhao, Xihe; Lu, Aitao] South China Normal Univ, Philosophy & Social Sci Lab Reading & Dev Childre, Guangzhou, Peoples R China.

[Huang, Xin; Zhao, Xihe; Lu, Aitao] South China Normal Univ, Sch Psychol, Guangzhou, Peoples R China.

[Huang, Xin; Zhao, Xihe; Lu, Aitao] Minist Educ, Guangzhou, Peoples R China.

通讯作者地址: Lu, AT (通讯作者), South China Normal Univ, Ctr Studies Psychol Applicat, 55 Zhongshan Ave, Guangzhou, Peoples R China.

电子邮件地址: lu_yoyo@yealt.net

Web of Science Index: Social Science Citation Index (SSCI)

ISSN: 0301-2212

eISSN: 1179-6391

影响因子 (2021) : 1.183

JCR分区: 该期刊在 PSYCHOLOGY, SOCIAL 领域中为 Q4. (SSCI 版本)

中科院分区: 心理学 4 区. (2022升级版大类学科)





Trait mindfulness and cell phone addiction in adolescents: A moderated mediation model

Hongling Yang¹, Xin Huang², Xihe Zhao², Aitao Lu²

¹School of Management, Guangdong Industry Polytechnic, Guangzhou, People's Republic of China

²Philosophy and Social Science Laboratory of Reading and Development in Children and Adolescents, and School of Psychology, South China Normal University, and Ministry of Education, People's Republic of China

How to cite: Yang, H., Huang, X., Zhao, X., & Lu, A. (2023). Trait mindfulness and cell phone addiction in adolescents: A moderated mediation model. *Social Behavior and Personality: An international journal*, 51(2), e11984

We explored the moderating and mediating roles of self-concept and self-control on the relationship between trait mindfulness and cell phone addiction. A sample of 259 Chinese adolescents completed measures related to cell phone addiction, trait mindfulness, self-control, self-concept, and their background information. Results showed that (a) trait mindfulness is positively related to self-control and self-concept, while negatively related to cell phone addiction; (b) self-control plays a mediating role between trait mindfulness and cell phone addiction; (c) self-concept plays a moderating role on the mediation pathway of self-control on trait mindfulness and cell phone addiction. The results underscore the importance of identifying the mechanisms that moderate the mediated path between trait mindfulness and cell phone addiction. These findings point to the potential implications about how to reduce the overuse of cell phones among adolescents through improving their levels of trait mindfulness, self-control, and self-concept.

Keywords

trait mindfulness, cell phone addiction, self-control, self-concept

Article Highlights

- Pairwise relationships among cell phone addiction, trait mindfulness, self-control, self-concept were found.
- Self-control mediated the relationship between trait mindfulness and cell phone addiction.
- Self-concept moderated the mediation effect of self-control on the relationship between trait mindfulness and cell phone addiction.

Research has shown that addiction results in a variety of undesirable social outcomes, including a decrease in happiness and a rise in mistrust (e.g., Chi et al., 2019; Gros et al., 2020). Thus, scholarly attention is increasingly being paid to addiction in adolescents (e.g., Esposito et al., 2020; Veisani et al., 2020). Previous studies have considered mindfulness as a determinant of addiction. For instance, Spinella et al. (2013) reported that mindfulness has a negative effect on attitude toward compulsive buying behavior and alcohol addiction. Other research has suggested that interventions based on mindfulness can be effective in treating addiction (e.g., Johnson et al., 2016).

One specific concern about the effect of mindfulness on addiction is the impact of trait mindfulness on cell phone addiction (Chen et al., 2021; Karl & Fischer, 2022; Yang et al., 2019). According to previous research, *cell phone*



addiction (i.e., problematic cell phone use) manifests as a dependence on excessive use of cell phones, a strong physiological experience, and behavioral discomfort (Cho et al., 2017). It is regarded as a behavioral as opposed to substance addiction. *Trait mindfulness* refers to an individual's natural or innate mindfulness tendency, which has been perceived as a stable, permanent characteristic (Brown & Ryan, 2003). As a psychological treatment, mindfulness has been found to reduce symptoms of anxiety and depression (Yang et al., 2019), improve sleep quality (Liu et al., 2017), and be effective as a smartphone addiction intervention (Lan et al., 2018). However, how this addiction intervention interacts with an individual's intrinsic factors, such as self-control and self-concept, is still unknown.

Self-control refers to exercising control over the self by oneself (Flores et al., 2020), reflecting one's different quantities of self-control resources (Baumeister, 2016). Evidence has shown that self-control has buffering effects against the harmful consequences of adverse environments (see, e.g., J.-B. Li et al., 2020). For instance, it might be easier for people with high self-control to resist the temptation to use cell phones (e.g., Ding et al., 2021). Other studies have shown that addiction is an important part of one's *self-concept* (e.g., Pickard, 2021), which refers to the totality of how one thinks and feels about oneself (Rosenberg, 1979). When people think they are addicted, they create a feeling of being disempowered and lacking self-control. Thus, some researchers believe that an important step in the struggle to overcome addiction is attaining new forms of social identity (e.g., a high self-control image; Flanagan, 2018).

Although previous studies have primarily focused on the direct link between trait mindfulness and cell phone addiction, it is still unclear what factors indirectly moderate and/or mediate this association. To address these gaps, we examined the mediating effect of self-control and moderating effect of self-concept on cell phone addiction in Chinese adolescents. Our aim was to underline the effect of trait mindfulness on cell phone addiction by developing a moderated mediation model.

On the basis of previous findings and given the strong links between trait mindfulness, self-control, self-concept, and cell phone addiction suggested in previous studies (e.g., Ding et al., 2021; Hao & Jin, 2020; Kim et al., 2018; Pickard, 2021), we proposed the following hypotheses:

Hypothesis 1: Trait mindfulness will be positively related to self-control and self-concept, but negatively related to cell phone addiction in Chinese adolescents.

Hypothesis 2: Self-control will mediate the association between trait mindfulness and cell phone addiction in Chinese adolescents.

According to empirical evidence, a strong sense of self is a resilience asset (Bracken, 1996). People with high self-concept respect themselves and make others respect them, which allows them to adapt more quickly and engage in relationships with others. Moreover, cognitive vulnerability models (see, e.g., Abramson et al., 1978) suggest that cognitive styles (e.g., a negative or positive self-concept) moderate the development and maintenance of mental symptoms (e.g., depression and addiction). Additionally, self-concept theory indicates that adolescents tend to affect their motivations, attitudes, and behaviors by improving their self-concept (Kennis et al., 2020; Kong et al., 2020). Therefore, we formed the following hypothesis:

Hypothesis 3: Self-concept will moderate the effect of self-control in the relationship between trait mindfulness and adolescent cell phone addiction.

To sum up, we proposed a moderated mediation model (see Figure 1).

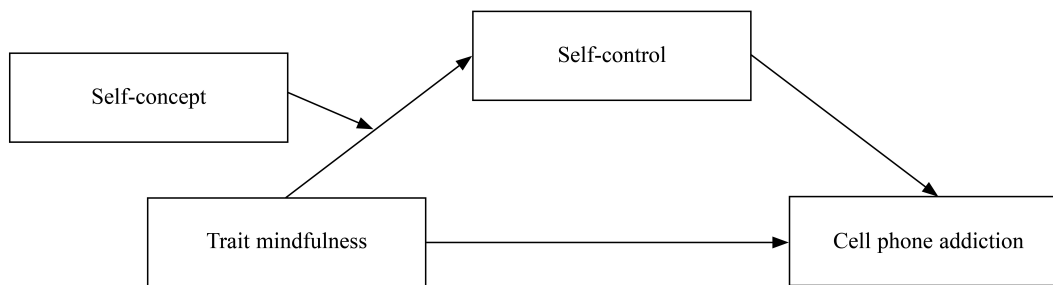


Figure 1. *Proposed Moderated Mediation Model*

Method

Participants and Procedure

We recruited 259 students (150 girls, 109 boys; $M_{\text{age}} = 15.58$ years, $SD = 0.73$, range = 14–18; Grade 7 = 120 students, Grade 8 = 90 students, Grade 9 = 49 students) from two high schools in Guangzhou, China, using convenience sampling. Written informed consent was obtained from each participant and their guardians, following the research protocol approved by the Institutional Review Board of the South China Normal University (SCNU-PSY-2020-3-078). This study was carried out in accordance with the Code of Ethics of the World Medical Association as set out in The Declaration of Helsinki.

Data were collected by trained psychology students. Respondents voluntarily participated in the study during school hours. They were given a complete description of the research and were instructed to fill in paper-and-pencil questionnaires. To encourage honest reporting, the responses were kept anonymous.

Measures

Cell Phone Addiction

Cell phone addiction was measured with the Mobile Phone Addiction Index Scale (Leung, 2008). The scale consists of 17 items that measure four dimensions of smartphone addiction: seven items for inability to control cravings (e.g., “You can never spend enough time on your cell phone”), five for anxiety and feeling lost (e.g., “You find it difficult to switch off your cell phone”), three for withdrawal and escape (e.g., “You have used your cell phone to talk to others when you were feeling lonely”), and two for productivity loss (e.g., “Your productivity has decreased as a direct result of the time you spend on your cell phone”). Each item was rated on a 5-point Likert scale ranging from 1 = *never* to 5 = *always*. The scale is reliable and valid for use in the adolescent population (Leung & Lee, 2012). In this study the Cronbach’s alpha coefficient was .89.

Trait Mindfulness

Trait mindfulness was measured using the 39-item Five-Facet Mindfulness Questionnaire (FFMQ; Baer et al., 2008), which comprises five dimensions: nonreactivity to inner experience (seven items; e.g., “I perceive my feelings and emotions without having to react to them”), observing (eight items; e.g., “I notice the smells and aromas of things”), acting with awareness (eight items; e.g., “I find myself doing things without paying attention”), describing (eight items; e.g., “I am good at finding words to describe my feelings”), and nonjudgment of inner experience (eight items; e.g., “I think some of my emotions are bad or inappropriate and I should not feel them”). Responses are made on a 5-point Likert scale ranging from 1 = *never* to 5 = *always*. The FFMQ is reliable and valid for use in adolescents (Gervais et al.,

2021). Cronbach’s alpha coefficient in this study was .68.

Self-Control

Self-control was measured with the 19-item Self-Control Scale (Tan & Guo, 2008), which was adapted from Tangney et al. (2004) and includes five dimensions: self-discipline (four items; e.g., “I am good at resisting temptation”), nonimpulsive action (six items; e.g., “I lose my temper too easily”), healthy habits (three items; e.g., “I am lazy”), work ethic (three items; e.g., “I have trouble concentrating”), and abstinence (three items; e.g., “I spend too much money”). Responses are made on a 5-point Likert scale ranging from 1 = *strongly disagree* to 5 = *strongly agree*. This is a reliable and valid instrument for use with adolescents (Zhang et al., 2021). Cronbach’s alpha coefficient in this study was .86.

Self-Concept

Self-concept was measured with the Adolescents’ Self-Concept Short Scale (Veiga & Leite, 2016), which includes 30 items that measure six dimensions (five items each): anxiety (e.g., “I cry easily”), physical appearance (e.g., “I am good-looking”), behavior (e.g., “I often get into trouble”), popularity (e.g., “I feel left out of things”), happiness (e.g., “I am cheerful”), and intellectual status (e.g., “I forget what I learn”). Responses are made on a 6-point Likert scale ranging from 1 = *completely disagree* to 6 = *completely agree*. The Chinese version is valid and reliable for use in the adolescent population (Adigun, 2020). In this study Cronbach’s alpha coefficient was .90.

We translated all measures except the Mobile Phone Addiction Index Scale into Chinese by the author, then a professor who is fluent in both Chinese and English backtranslated them into English. No further modifications were required.

Results

Common Method Bias Test

We used Harman’s single-factor test to check for common method bias. The amount of variance explained by the first factor was 17.22%, which is lower than the 40% threshold. Thus, common method variance did not substantially affect our findings.

Descriptive Analysis

The descriptive statistics and correlation analysis (see Table 1) showed that cell phone addiction was negatively correlated with trait mindfulness ($r = -.12, p < .05$), self-control ($r = -.50, p < .001$), and self-concept ($r = -.28, p < .001$). Additionally, trait mindfulness was positively correlated with self-control ($r = .46, p < .001$) and self-concept ($r = .57, p < .001$). Thus, Hypothesis 1 was supported.

Table 1. Means, Standard Deviations, and Bivariate Correlations of Study Variables

	<i>M ± SD</i>	1	2	3	4	5	6
1. Gender	0.42 ± 0.49	—					
2. Age	15.57 ± 0.73	.10	—				
3. Cell phone addiction	44.21 ± 12.23	-.06	.08	—			
4. Trait mindfulness	116.56 ± 9.93	-.04	-.13*	-.12*	—		
5. Self-control	56.28 ± 11.70	.01	.01	-.50***	.46***	—	
6. Self-concept	117.74 ± 19.35	-.04	-.10	-.28***	.57***	.61*	—

Note. Gender was dummy coded as 0 = girl, 1 = boy.

* $p < .05$. ** $p < .01$. *** $p < .001$.

Mediation Analysis

We used Model 4 of the PROCESS 3.0 macro for SPSS 26.0 to test the mediating effect of self-control in the relationship between trait mindfulness and cell phone addiction after controlling gender and age (see Table 2). The mediation analysis results showed that the direct and indirect effects were significant. That is, trait mindfulness and cell phone addiction were associated through self-control, $b = -0.27$, $SE = 0.04$, 95% CI $[-0.36, -0.19]$. Additionally, trait mindfulness was directly and positively related to cell phone addiction, $b = 0.15$, $SE = 0.06$, 95% CI $[0.03, 0.27]$. Thus, Hypothesis 2 was supported.

Table 2. Mediation Analysis of Self-Control

Mediating effect	Effects	Boot CI		
		SE	LL	UL
Total effect of X on Y	-0.12	0.06	-0.24	0.01
Direct effect of X on Y	0.15	0.06	0.03	0.27
Indirect effect of X on Y X → M → Y	-0.27	0.04	-0.36	-0.19

Note. X = trait mindfulness; M = self-control; Y = cell phone addiction; CI = confidence interval; LL = lower limit; UL = upper limit. Original scores were transformed into z scores.

Moderated Mediation Analysis

Table 3 presents the main results of testing the proposed moderated mediation model with self-concept as the moderator. The results indicated there was a significant moderated mediation effect, index of moderated mediation = -0.06 , $SE = 0.02$, 95% CI $[-0.11, -0.02]$. When self-concept was high ($M + 1 SD$), the conditional indirect effect of trait mindfulness on cell phone addiction through self-control was negative, $b = -0.16$, $SE = 0.04$, 95% CI $[-0.25, -0.08]$. For participants with a high self-concept, trait mindfulness reduced cell phone addiction by promoting self-control. When self-concept was low ($M - 1 SD$), there was no conditional indirect effect, $b = -0.05$, $SE = 0.03$, 95% CI $[-0.12, 0.01]$. For participants with a low self-concept, trait mindfulness did not help in reducing cell phone addiction by enhancing self-control. Thus, Hypothesis 3 was supported. Figure 2 illustrates the simple slopes of the conditional indirect effect at high and low levels of self-concept.

Table 3. Regression and Bootstrapping Analysis Results for the Moderated Mediation Model

Regression equations					Coefficients	
Dependent variables	Independent variables	R	R ²	F	β	t
Self-control		.65	.42	36.43***		
	Gender				.08	0.83
	Age				.11	1.61
	Trait mindfulness				.18	3.07**
	Self-concept				.53	8.95***
Cell phone addiction	Trait mindfulness × Self-concept				.11	3.18**
		.52	.28	24.07***		
	Gender				-.12	-1.13
	Age				.15	2.04*
	Trait mindfulness				.15	2.49*
	Self-control				-.57	-9.36***

Note. N = 259. Original scores were transformed into z scores.

* $p < .05$. ** $p < .01$. *** $p < .001$.

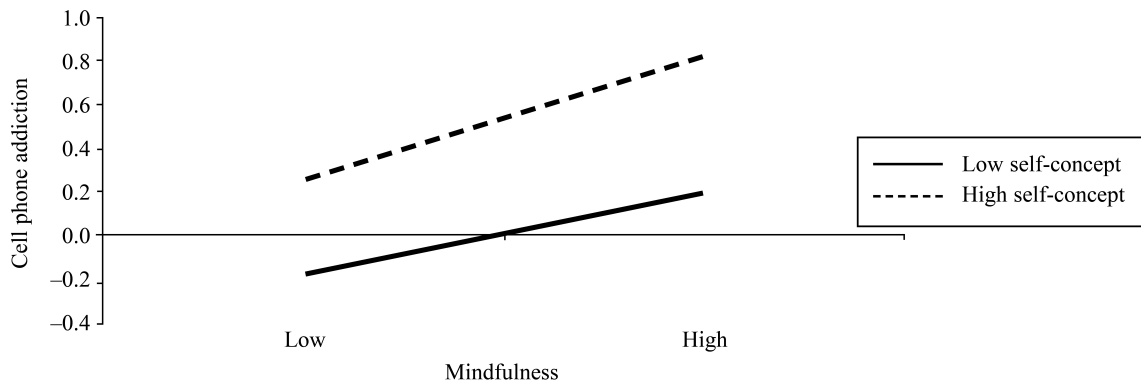


Figure 2. Moderating Effect of Self-Concept in the Relationship Between Trait Mindfulness and Cell Phone Addiction

Discussion

The results of our study showed that trait mindfulness is indirectly related to adolescent cell phone addiction through self-control, and this process is enhanced by self-concept. The moderated mediation model provides insights into developing preventive interventions for cell phone addiction among adolescents.

Our findings confirmed the hypothesis that the direct association is mediated by self-control. The result that mindfulness is negatively associated with problematic cell phone use is in line with previous study findings (e.g., Hao & Jin, 2020). It has been found that mindfulness can increase self-control by increasing the likelihood that individuals will acknowledge their own thoughts and feelings (Elkins-Brown et al., 2017). Adolescents who have experienced a high level of mindfulness have better executive functioning (Riggs & Brown, 2017). In addition, the second link in the mediation chain strengthens understanding of the previously supported relationship between self-control and adolescent cell phone addiction (Ding et al., 2021). Specifically, adolescents with higher self-control are less likely to be addicted to cell phone use as they may have stronger autonomy and efficiency or pursue goals with better outcomes, which, in turn, decreases their cell phone use (Q. Li et al., 2021).

In addition, our results support the hypothesis that self-concept moderates the impact of trait mindfulness on self-control. Thus, adolescents who have stronger feelings about their own abilities may have a growth mindset and take more ownership to manage their impulses, emotions, and behaviors to achieve long-term goals. However, when the adolescents experience a lower level of self-concept, the protective role of trait mindfulness is nonsignificant. One possible explanation is that trait mindfulness can increase self-control by allowing individuals to acknowledge their own thoughts and feelings (Elkins-Brown et al., 2017). When adolescents have a lower level of self-concept, the protective effect of mindfulness that enables them to supersede their thoughts, emotions, or behaviors becomes weaker. In summary, high self-control, following on from high trait mindfulness, is more likely to reduce the risk of cell phone addiction under a high self-concept level than under a low self-concept level.

There are limitations to this study. First, the causality between trait mindfulness and cell phone addiction could not be established using a cross-sectional research design. Longitudinal approaches will be needed in future to explore causality. Second, self-reported measures were used in our study and participant response bias is therefore unavoidable. Future studies could consider incorporating measures from multiple informants, such as teachers, parents, and peers, to reduce measurement error. Finally, the Cronbach's alpha coefficient of our FFMQ evaluation (.68) was low; thus, we

need to treat the findings regarding trait mindfulness with caution. Other populations have demonstrated similarly low Cronbach's alphas for FFMQ (e.g., .69 in the Philippines; Centeno & Fernandez, 2020), suggesting the varying internal consistency of FFMQ across cultures. Future studies could first adapt the FFMQ to ensure all the items are representatives of the domain of behavior in the target culture.

The current study revealed that the effect of trait mindfulness on reducing cell phone addiction does not function alone but comes into play via self-control in this process. Moreover, such an indirect effect may play a role only at a high self-concept level. On the basis of these findings, this study has considerable implications. For example, the results may be useful for guiding educational interventions for adolescents. Specifically, we recommend that self-control and self-concept should be considered when developing intervention programs and strategies intended to reduce adolescents' cell phone addiction, in particular under a low mindfulness condition.

Acknowledgments

This research was funded supported by the joint project of "14th Five-Year Plan" for Guangzhou Philosophy and Social Sciences in 2022 (2022GZGJ133) and by the 13th Five-Year Research Plan Project of Guangdong Province in 2020 (Moral Education Special Project, 2020JKDY018). The authors declare that they have no competing interests. The raw data supporting the conclusions of this article will be made available by the authors, without undue reservation (doi: 10.6084/m9.figshare.19759240). The authors declare that no code was used in this research.

References

- Abramson, L. Y., Seligman, M. E. P., & Teasdale, J. D. (1978). Learned helplessness in humans: Critique and reformulation. *Journal of Abnormal Psychology, 87*(1), 49–74.
<https://doi.org/10.1037/0021-843X.87.1.49>
- Adigun, O. T. (2020). Self-esteem, self-efficacy, self-concept and intimate image diffusion among deaf adolescents: A structural equation model analysis. *Heliyon, 6*(8), Article e04742.
<https://doi.org/10.1016/j.heliyon.2020.e04742>
- Baer, R. A., Smith, G. T., Lykins, E., Button, D., Krietemeyer, J., Sauer, S., ... Williams, J. M. G. (2008). Construct validity of the Five Facet Mindfulness Questionnaire in meditating and nonmeditating samples. *Assessment, 15*(3), 329–342.
<https://doi.org/10.1177/1073191107313003>
- Baumeister, R. F. (2016). Limited resources for self-regulation: A current overview of the strength model. In E. R. Hirt, J. J. Clarkson, & L. Jia (Eds.), *Self-regulation and ego control* (pp. 1–17). Springer.
<https://doi.org/10.1016/B978-0-12-801850-7.00001-9>
- Bracken, B. A. (1996). *Handbook of self-concept: Developmental, social, and clinical considerations*. Wiley Publications.
- Brown, K. W., & Ryan, R. M. (2003). The benefits of being present: Mindfulness and its role in psychological well-being. *Journal of Personality and Social Psychology, 84*(4), 822–848.
<https://doi.org/10.1037/0022-3514.84.4.822>
- Centeno, R. P. R., & Fernandez, K. T. G. (2020). Effect of mindfulness on empathy and self-compassion: An adapted MBCT program on Filipino college students. *Behavioral Sciences, 10*(3), Article 61.
<https://doi.org/10.3390/bs10030061>
- Chen, W.-Y., Yan, L., Yuan, Y.-R., Zhu, X.-W., Zhang, Y.-H., & Lian, S.-L. (2021). Preference for solitude and mobile phone addiction among Chinese college students: The mediating role of psychological distress and moderating role of mindfulness. *Frontiers in Psychology, 12*, Article 750511.
<https://doi.org/10.3389/fpsyg.2021.750511>

- Chi, X., Liu, X., Guo, T., Wu, M., & Chen, X. (2019). Internet addiction and depression in Chinese adolescents: A moderated mediation model. *Frontiers in Psychiatry, 10*, Article 816.
<https://doi.org/10.3389/fpsy.2019.00816>
- Cho, H.-Y., Kim, D. J., & Park, J. W. (2017). Stress and adult smartphone addiction: Mediation by self-control, neuroticism, and extraversion. *Stress and Health, 33*(5), 624–630.
<https://doi.org/10.1002/smi.2749>
- Ding, Z.-C., Yan, J., & Fu, J. (2021). Internet and mobile phone addiction self-control mediate physical exercise and subjective well-being in young adults using IoT. *Mobile Information Systems, 2021*, Article 9923833.
<https://doi.org/10.1155/2021/9923833>
- Elkins-Brown, N., Teper, R., & Inzlicht, M. (2017). How mindfulness enhances self-control. In J. C. Karremans & E. K. Papies (Eds.), *Mindfulness in social psychology* (pp. 65–78). Routledge.
<https://doi.org/10.4324/9781315627700-5>
- Esposito, M. R., Serra, N., Guillari, A., Simeone, S., Sarracino, F., Continisio, G. I., & Rea, T. (2020). An investigation into video game addiction in pre-adolescents and adolescents: A cross-sectional study. *Medicina, 56*(5), Article 221.
<https://doi.org/10.3390/medicina56050221>
- Flanagan, O. (2018). Identity and addiction. In H. Pickard & S. H. Ahmed (Eds.), *The Routledge handbook of philosophy and science of addiction* (pp. 77–89). Routledge.
<https://doi.org/10.4324/9781315689197-8>
- Flores, J., Caqueo-Úrizar, A., Ramírez, C., Arancio, G., & Cofré, J. P. (2020). Locus of control, self-control, and gender as predictors of internalizing and externalizing problems in children and adolescents in northern Chile. *Frontiers in Psychology, 11*, Article 2015.
<https://doi.org/10.3389/fpsyg.2020.02015>
- Gervais, C. L. M., & Johnston, M. S. (2021). Caregivers' considerations of remorse and responsibility among youth who sexually offend. *Journal of Interpersonal Violence, 37*(21–22), Article 8862605211042815.
<https://doi.org/10.1177/08862605211042815>
- Gros, L., Debue, N., Lete, J., & van de Leemput, C. (2020). Video game addiction and emotional states: Possible confusion between pleasure and happiness? *Frontiers in Psychology, 10*, Article 2894.
<https://doi.org/10.3389/fpsyg.2019.02894>
- Hao, Z., & Jin, L. (2020). Alexithymia and problematic mobile phone use: A moderated mediation model. *Frontiers in Psychology, 11*, Article 541507.
<https://doi.org/10.3389/fpsyg.2020.541507>
- Johnson, D., Mullen, D., Smith, I. D., & Wilson, A. (2016). Mindfulness in addictions. *BJPsych Advances, 22*(6), 412–419.
<https://doi.org/10.1192/apt.bp.114.014142>
- Karl, J. A., & Fischer, R. (2022). The state of dispositional mindfulness research. *Mindfulness, 13*, 1357–1372.
<https://doi.org/10.1007/s12671-022-01853-3>
- Kennis, M., Duecker, F., T'Sjoen, G., Sack, A. T., & Dewitte, M. (2022). Sexual self-concept discrepancies mediate the relation between gender dysphoria sexual esteem and sexual attitudes in binary transgender individuals. *The Journal of Sex Research, 59*(4), 524–536.
<https://doi.org/10.1080/00224499.2021.1951643>
- Kim, K., Milne, G. R., & Bahl, S. (2018). Smart phone addiction and mindfulness: An intergenerational comparison. *International Journal of Pharmaceutical and Healthcare Marketing, 12*(1), 25–43.
<https://doi.org/10.1108/IJPHM-08-2016-0044>
- Kong, F., Qin, J., Huang, B., Zhang, H., & Lei, L. (2020). The effect of social anxiety on mobile phone dependence among Chinese adolescents: A moderated mediation model. *Children and Youth Services Review, 108*, Article 104517.



<https://doi.org/10.1016/j.chilyouth.2019.104517>

Lan, Y., Ding, J.-E., Li, W., Li, J., Zhang, Y., Liu, M., & Fu, H. (2018). A pilot study of a group mindfulness-based cognitive-behavioral intervention for smartphone addiction among university students. *Journal of Behavioral Addictions*, 7(4), 1171–1176.

<https://doi.org/10.1556/2006.7.2018.103>

Leung, L. (2008). Linking psychological attributes to addiction and improper use of the mobile phone among adolescents in Hong Kong. *Journal of Children and Media*, 2(2), 93–113.

<https://doi.org/10.1080/17482790802078565>

Leung, L., & Lee, P. S. N. (2012). Impact of internet literacy, internet addiction symptoms, and internet activities on academic performance. *Social Science Computer Review*, 30(4), 403–418.

<https://doi.org/10.1177/0894439311435217>

Li, J.-B., Yang, A., Dou, K., & Cheung, R. Y. M. (2020). Self-control moderates the association between perceived severity of coronavirus disease 2019 (COVID-19) and mental health problems among the Chinese public. *International Journal of Environmental Research and Public Health*, 17(13), Article 4820.

<https://doi.org/10.3390/ijerph17134820>

Li, Q., Xiang, G., Song, S., Huang, X., & Chen, H. (2021). Examining the associations of trait self-control with hedonic and eudaimonic well-being. *Journal of Happiness Studies*, 23, 667–687.

<https://doi.org/10.1007/s10902-021-00418-w>

Liu, Q.-Q., Zhou, Z.-K., Yang, X.-J., Kong, F.-C., Niu, G.-F., & Fana, C.-Y. (2017). Mobile phone addiction and sleep quality among Chinese adolescents: A moderated mediation model. *Computers in Human Behavior*, 72, 108–114.

<https://doi.org/10.1016/j.chb.2017.02.042>

Pickard, H. (2021). Addiction and the self. *Noûs*, 55(4), 737–761.

<https://doi.org/10.1111/nous.12328>

Riggs, N. R., & Brown, S. M. (2017). Erratum to: Prospective associations between peer victimization and dispositional mindfulness in early adolescence. *Prevention Science*, 18(4), Article 490.

<https://doi.org/10.1007/s11121-017-0765-5>

Rosenberg, M. (1979). *Conceiving the self*. Basic Books.

Spinella, M., Martino, S., & Ferri, C. (2013). Mindfulness and addictive behaviors. *Journal of Behavioral Health*, 2(1), 1–7.

Tan, S.-H., & Guo, Y.-Y. (2008). Revision of a self-control scale for Chinese college students. *Chinese Journal of Clinical Psychology*, 16(5), 468–470.

Tangney, J. P., Baumeister, R. F., & Boone, A. L. (2004). High self-control predicts good adjustment, less pathology, better grades, and interpersonal success. *Journal of Personality*, 72(2), 271–324.

<https://doi.org/10.1111/j.0022-3506.2004.00263.x>

Veiga, F., & Leite, A. (2016). Adolescents' Self-Concept Short Scale: A version of PHCSCS. *Procedia – Social and Behavioral Sciences*, 217, 631–637.

<https://doi.org/10.1016/j.sbspro.2016.02.079>

Veisani, Y., Jalilian, Z., & Mohamadian, F. (2020). Relationship between internet addiction and mental health in adolescents. *Journal of Education and Health Promotion*, 9, Article 303.

https://doi.org/10.4103/jehp.jehp_362_20

Yang, X., Zhou, Z., Liu, Q., & Fan, C. (2019). Mobile phone addiction and adolescents' anxiety and depression: The moderating role of mindfulness. *Journal of Child and Family Studies*, 28(3), 822–830.

<https://doi.org/10.1007/s10826-018-01323-2>



Zhang, Z., Dang, J., Li, J., He, Y., Huang, S., Wang, Y., & Yang, X. (2021). Childhood trauma and self-control: The mediating role of depletion sensitivity. *Journal of Child and Family Studies*, 30(6), 1599–1606.
<https://doi.org/10.1007/s10826-021-01958-8>

证明编号：C2022-1467

论文收录引用 检索证明报告

深圳大学城图书馆
教育部科技查新工作站
二零二二年八月二十九日

作者单位：西安电子科技大学

作者姓名：赖金志（Lai, JZ; Lai, Jinzhi）

论文发表年限：2021-2022

检索数据库：

SCI-Expanded	2021-至今
Journal Citation Reports	2021
中科院分区	2021

检索结果：

(1) 《科学引文索引》（SCI-E）数据库收录情况：

共收录论文 2 篇，均为第一作者论文；

(2) 《期刊引证报告》JCR（论文发表当年）收录期刊分区和影响因子情况：

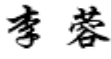
《中科院期刊分区表》（论文发表当年）升级版收录期刊分区情况：

详见《论文检索情况统计表》。

（详细结果见附件）

特此证明！

检索员：李杨 

审核员：李蓉 

深圳大学城图书馆

教育部科技查新工作站

2022 年 8 月 29 日

论文检索情况统计表

序号	文献	文献来源	作者类型	发表年份	SCI收录	JCR		中科院分区（升级版）		
						分区	期刊影响因子	大类	小类	TOP期刊
1	A Congestion-aware Hybrid SRAM and STT-RAM Buffer Design for Network-on-Chip Router	IEICE ELECTRONICS EXPRESS	第一	2022	√	Q4*	0.709*	4区*	4区*	/
2	Area and energy-efficient buffer designs for NoC based on domain-wall memory	IEICE ELECTRONICS EXPRESS	第一	2021	√	Q4	0.709	4区	4区	/
合计					2					

* 2022 年度 JCR 数据未出，此处为 2021 年期刊影响因子和 JCR 分区情况；

* 2022 年度中科院分区数据未出，此处为 2021 年期中科院分区情况。

论文收录情况附件目录

一、 SCI-Expanded 收录情况（2 篇）	5
---------------------------------	---

检测证明报告

一、SCI-Expanded 收录情况（2 篇）

Record 1 of 2

Title:A Congestion-aware Hybrid SRAM and STT-RAM Buffer Design for Network-on-Chip Router

Author(s):Lai, JZ(Lai, Jinzhi);Cai, JP(Cai, Jueping);Chu, J(Chu, Jie);

Source:IEICE ELECTRONICS EXPRESS **Volume:** **Issue:** **Pages:** **DOI:**10.1587/elex.19.20220078 **Early Access Date:**MAR 2022

Accession Number:WOS:000769565500001

Document Type:Article; Early Access

Addresses:[Lai, Jinzhi; Cai, Jueping; Chu, Jie] Xidian Univ, State Key Lab Wide Bandgap Semicond Technol Disci, Xian 710071, Peoples R China.;[Lai, Jinzhi] Guangdong Ind Polytech, Sch Informat Technol, Guangzhou 510300, Peoples R China.;

Reprint Address:Cai, JP (corresponding author), Xidian Univ, State Key Lab Wide Bandgap Semicond Technol Disci, Xian 710071, Peoples R China.

E-mail Addresses:jpcai@mail.xidian.edu.cn

Research Areas:Engineering, Electrical & Electronic

Record 2 of 2

Title:Area and energy-efficient buffer designs for NoC based on domain-wall memory

Author(s):Lai, JZ(Lai, Jinzhi);Cai, JP(Cai, Jueping);Xie, RL(Xie, Ruilian);Guan, J(Guan, Jiao);

Source:IEICE ELECTRONICS EXPRESS **Volume:**18 **Issue:**14 **Pages:** **DOI:**10.1587/elex.18.20210208

Published:JUL 25 2021

Accession Number:WOS:000684566800004

Document Type:Article

Addresses:[Lai, Jinzhi; Cai, Jueping; Guan, Jiao] Xidian Univ, State Key Lab Wide Bandgap Semicond Technol Disci, Xian 710071, Peoples R China.;[Lai, Jinzhi] Guangdong Ind Polytech, Sch Informat Technol, Guangzhou 510300, Peoples R China.;[Xie, Ruilian] Xian Univ Posts & Telecommun, Sch Comp Sci & Technol, Xian 710061, Peoples R China.;

Reprint Address:Cai, JP (corresponding author), Xidian Univ, State Key Lab Wide Bandgap Semicond Technol Disci, Xian 710071, Peoples R China.

E-mail Addresses:jpcai@mail.xidian.edu.cn

Research Areas:Engineering, Electrical & Electronic



声 明

我声明，本报告中所列本人发表的被收录、被引用文献，均经过本人逐篇核对，确认无误；如因本人原因造成报告内容不实，一切后果概由本人承担。

被检作者（签字）：

赖志

2022年08月30日

学位论文
检测证明

A congestion-aware hybrid SRAM and STT-RAM buffer design for network-on-chip router

Jinzhi Lai^{1, 2}, Jueping Cai^{1, a)}, and Jie Chu¹

Abstract Network-on-chip (NoC) offers a scalable and flexible communication infrastructure for many-cores systems. Buffers in router is used for fine-grain flow control and Quality of Service (QoS), yet it is the major contributor of area and power consumption. In this paper, we propose a hybrid buffer design with SRAM and Spin-Torque Transfer Magnetic RAM (STT-RAM) for NoC router leveraging a novel architecture combined Virtual Channel (VC) and Virtual Output Queuing (VOQ) to store congested and uncongested flow separately. Experiments demonstrates that the proposed scheme can achieve 11.8% network performance improvement and 32.9% power saving with only 8.2% area overhead degradation compared to conventional SRAM based buffer design.

Keywords: network-on-chip (NoC), router, STT-RAM, buffer, congestion-aware

Classification: Integrated circuits (memory, logic, analog, RF, sensor)

1. Introduction

Network-on-chip (NoC) has become the focus of recent multi-core research and the main development direction in the future. As the complexity of the business and function increases, NoC is reported to consume up to 33% of total chip power [1]. The buffer in NoC router is used to store and forward data for the purpose of more efficient flow control. However, the conventional SRAM buffer occupies up to 57.2% of dynamic power consumption and 81.5% of leakage power consumption [2]. Many studies, such as bufferless [3] and elastic buffer [4], attempt to reduce the use of memory to cut chip area and power consumption, but suffer the loss of performance, such as latency, quality-of-service (QoS) and protocol-level deadlock free. In order to retain the advantages of buffers, many studies strived to optimize the buffer structure in NoC by using emerging non-volatile memory (NVM), such as Phase Change Memory (PCM) [5], Spin-Transfer Torque Magnetic RAM (STT-RAM) [6, 7] and Domain-Wall Memory (DWM) [8], because of their properties of high-density, low leakage power and non-volatility. Compared with other emerging NVMs, STT-RAM can employ mature CMOS technology, and the commercial STT-RAM product had been launched [9, 10]. Hence, STT-RAM

is considered as the promising candidate to replace SRAM owing to its combination of fast read speed, high density and long endurance recently [11, 12]. But STT-RAM encounters long write latency and high write power consumption. In order to combine the advantageous characteristics in density, speed and power consumption of SRAM and STT-RAM, some hybrid memory buffer designs for NoC router buffer have been proposed [13, 14].

In this paper, we focus on the circuit-level approaches based on the congestion-aware flow control policy, and propose a performance-energy efficiency hybrid STT-RAM and SRAM NoC router buffer implementation. Then substantial evaluations on area, performance and power to evaluate the proposed scheme and reference implementations were performed.

2. Background and motivation

2.1 Basic of STT-RAM

As shown in Fig. 1, a basic structure of an STT-RAM cell is composed of an access transistor and a magnetic tunnel junction (MTJ) which consists of three layers: two ferromagnetic layers along with an MgO tunnel barrier layer in the middle. One of the ferromagnetic layers is designed as a free layer used for binary storage, and the other one is design as a reference layer. The reference layer retains a fixed magnetic direction, while the free layer can change its magnetic direction by applying a spin-polarized current. If the magnetization direction (in-plane or perpendicular) of the two layers are the same, indicating a “0” state and vice versa for a “1” state. By applying a MTJ for data storage instead of electric charges, STT-RAM exhibits a near-zero leakage power. Compared to the typical 6-transistor SRAM cells, STT-RAM achieves much smaller cell area by using 1T1J cells [15]. Several designs have been proposed to reduce the write energy by relaxing the retention time [16] and

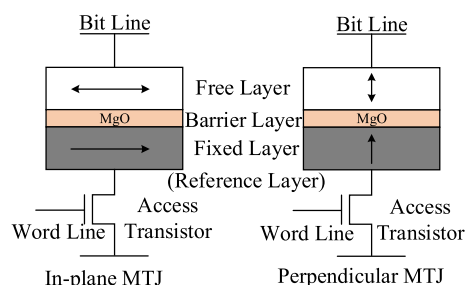


Fig. 1 STT-RAM bit-cell architecture.

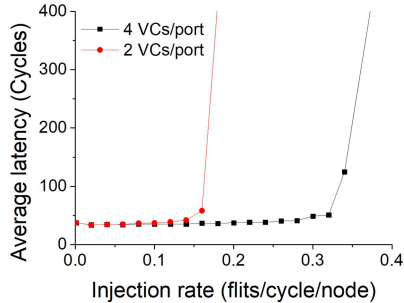
¹ State Key Laboratory of Wide Bandgap Semiconductor Technology Disciplines, Xidian University, Xi’an 710071, P.R. China

² School of Information Technology, Guangdong Industry Polytechnic, Guangzhou 510300, P.R. China

^{a)} jpcai@mail.xidian.edu.cn

Table I Parameters of SRAM and STT-RAM @ 32 nm [19].

Memory Types	Cell Size (F ²)	Latency (Cycle@1 GHz)		Access Energy/bit (pJ)		Leakage Power (mW)
		Read	Write	Read	Write	
SRAM	146	1	1	0.063	0.049	1.797
STT-RAM	45.6	1	2	0.082	0.286	0.044

**Fig. 2** Average latency of different VC organization.

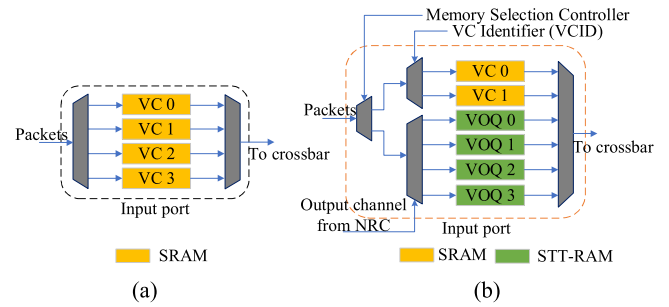
shorten the write latency to 2 ns [17], which corresponds to 2 cycles at 1 GHz clock frequency. Considering most hierarchical routers work under 1 GHz clock frequency [18], a 2-cycle write latency STT-RAM is adopted in our design accordingly. The parameters (footprint, speed, and power) of SRAM and STT-RAM are given in Table I [19].

2.2 Congestion aware implementation

The packet latency may increase tremendously and network throughput degrades dramatically when there occurs congestion in the network or a part of it. Congested packets prevent uncongested packets storing in the same queue from moving forward. This situation is referred as head-of-line (HoL) blocking. If congestion can be predicted as early as possible, the deterioration of congestion can be relieved. One of the most popular congestion aware methods is evaluating the occupancy of router input buffer [20]. The number of occupied VC serving as the congestion criterion is another common congestion aware method [21]. Perceiving the congestion state of the downstream before the current node entering congestion helps to relieve the spread of congestion and reduce the impact on network latency.

2.3 VC utilization test

In order to verify the performance of VC organization under different traffic load, we tested 4 VCs per input port (4-VC) and 4 flit buffers per VC and 2-VC scheme (The experimental setup is detailed in Section 4). As shown in Fig. 2, 2-VC buffer scheme performs almost identical to 4-VC at low traffic intensity. Network performance does not benefit from the increasing of VCs. But, as the injection rate rises, packets have to compete for storage source and bandwidth and 2-VC buffer scheme enters saturation quickly. It can be concluded that 4-VC buffer performs equivalent to 2-VC buffer under low traffic load with considerable underutilized buffer resource and has to withstand the high leakage power consumption of SRAM. Hence, it is necessary to take traffic condition into consideration in buffer design.

**Fig. 3** Logic view of (a) conventional SRAM buffer and (b) hybrid memory buffer.

3. Hybrid SRAM and STT-RAM buffer design

Inspired by the characteristics of STT-RAM, discussions on VC utilization and basic principle of congestion, we propose a congestion-aware hybrid SRAM/STT-RAM buffer design, which makes full use of the advantages of SRAM/STT-RAM memory technology without performance degradation.

3.1 Baseline NoC router architecture

A generic NoC router architecture depicted in [22] is adopted as a baseline router design. Route lookahead, which consists of next hop routing computation (NRC), virtual channel allocation (VA), switch allocation (SA) and switch traversal (ST), is used. NRC is performing in parallel with VA. The result of NRC is carried along with the head flit. Consequently, router can be aware of selected output channel of the incoming package.

3.2 Hybrid memory buffer with mixed queue (HMMQ)

In particular, the router is connected with 4 adjacent nodes. Different from the baseline router buffer with 4 pure SRAM VCs (SRAM-VCs) (Fig. 3(a)), the proposed HMMQ designates 2 SRAM VCs to conduct low workload situation. As mentioned above, buffer with only 2 VCs will encounter congestion and performance degradation in high workload. HMMQ adopts STT-RAM to enlarge buffer queues which will not consume extra leakage power owing to STT-RAM's near-zero leakage power in unoccupied state. At high workload, the congested flow stalls the progress of normal traffic because of HoL blocking. VOQ [23], where each VC corresponds to a single output channel connecting to the adjacent node, can eliminate HoL with high power and hardware complexity and is hard to be used in NoCs [24]. Packets enter corresponding VOQ according to the output channel selection from NRC. As shown in Fig. 3(b), HMMQ merges SRAM-VCs and STT-RAM based VOQs (STT-VOQs) together to store packets under different conditions. SRAM-VCs work all the time, while STT-VOQs start working once there occurs congestion in the corresponding adjacent node and be used to accept congested traffic particularly. Congested traffic stores in STT-VOQs while uncongested traffic can go through SRAM-VCs. Uncongested traffic flows are separated from the congested ones consequently.

According to the parameters in Table I, STT-RAM takes 2 cycles to complete write operation at 1 GHz clock frequency.

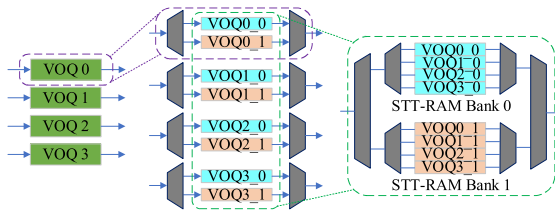


Fig. 4 Logic view of dual-bank STT-RAM VOQ.

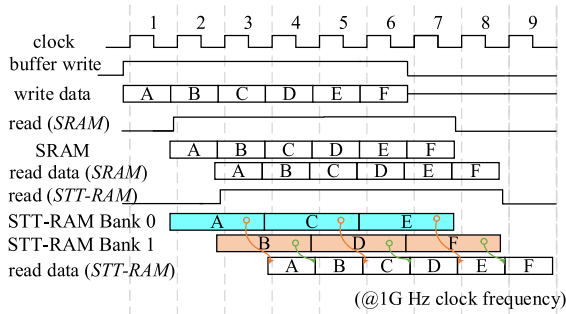


Fig. 5 Timing diagram of a dual-bank buffer access.

A single STT-RAM memory is not able to accomplish consecutive writes, which is not mentioned in most of the previous studies. Consecutive flits are written into dual banks in an alternate fashion in HMMQ, and 2-cycle latency of write operation is absorbed accordingly, as shown in Fig. 4. Flit stays in buffer and bids for grant to dequeue in SA stage which takes on less than 1 cycle. Read operation is triggered by grant and falls behind write operation by 1 cycle or more. As depicted in Fig. 5, dual STT-RAM scheme is used to meet the access timing. As a result, the read and write of STT-RAM in HMMQ perform the same as SRAM.

In non-uniform traffic, the traffic towards a certain node is heavier than other nodes, resulting in congestion of a certain VOQ while other VOQs are not full, which leads to a low overall buffer utilization. In order to improve the utilization of buffer, linked list structure is used to manage STT-VOQ buffer slots. The whole STT-RAM memory bank is shared among VOQs. Every slot in the buffer contains two fields which are used to store flit data and address pointing to the next slot respectively. With the help of linked list structure, each VOQ is of variable length rather than fixed length, which improves buffer utilization greatly in the cost of increased complexity and additional overhead. Nevertheless, the actual overhead is small [25].

3.3 Congestion management and flow control

If congestion occurs in downstream node, the traffic heading to that node is likely to be stalled at the current node and block the advance of the traffic to other nodes. The proposed design observes the usage of input buffer of downstream node by counting the credit of the input VC of the corresponding downstream node maintained by the output port. When the occupation of input buffer of downstream node exceeds a certain predefined threshold, a congestion sign is activated to indicate that the downstream node is congested. According the output channel information generated by NRC at last hop, packets heading to congested node will be put into the corresponding VOQ until the congestion of the ap-

pointed node relieves. At the same time, a credit is returned to the upstream node. Therefore, uncongested traffic can use credit to keep the flow advancing. On the other hand, packets of uncongested traffic flow enter VC according to the VC identifier (VCID) in head flit. Bandwidth is retained to serve uncongested traffic. In consequence, it mitigates the upward spread of congestion. Congestion management is implemented in Memory Selection Controller (MSC). Owing to the near-zero leakage power, packets waiting in STT-RAM consumes much less static power than SRAM.

ON/OFF flow control mechanism is used to avoid STT-RAM buffer overflow. When available slot of STT-VOQ buffer is less than a certain threshold, an X_{off} signal is asserted and sent to upstream node. The upstream node stops sending any flit once receiving an X_{off} signal until the X_{off} is released. The VOQ of corresponding congestion node quit to make any request for grants. Once the corresponding congestion disappears, VOQ raises requests immediately to prevent starvation.

4. Experiments and results

4.1 Experimental setup

In order to verify the effectiveness of the proposed buffer design, we have performed extensive evaluations for buffer designs as listed in Table II in terms of area, performance and power consumption. NVsim [26] was used for area and power consumption evaluation with different memory technologies using data as listed in Table I. A parametrized router RTL implementation [27] was applied in each buffer design, and then synthesized using Synopsys Design Compiler (DC) under 32-nm process design kit at 1 GHz clock frequency for area and timing examinations. BookSim2.0 [28], a cycle-accurate simulator, was used for VC designs and modified versions were used for VOQ designs, BB and HMMQ for performance examinations with both synthetic traffic and application traffic patterns. Orion2.0 [29] library was integrated in BookSim2.0 combined statistics as listed in Table I to estimate the power consumption of different designs. Application traces were generated by a full-system simulator M5 [30] running PARSEC [31] benchmark suite with the system configurations illustrated in Table III and fetched by Netrace [32] and then used in the simulations.

4.2 Experimental results and discussions

1) Area

We collected the area dissipations of memory from NVSim and non-memory components from DC. As mentioned in Section 2, cell size of SRAM is more than three times that of STT-RAM. All STT-RAM designs can get benefit from high density of STT-RAM memory. Fig. 6(a) shows the memory area overhead normalized to SRAM_VC. As expect, the memory in SRAM based designs dominate the largest area and the STT-RAM designs are minimum on the contrary. Since HMMQ applies both SRAM and STT-RAM, it consumes more area, about 30% augment over STTRAM_VOQ, but still gains nearly 9% improvement over SRAM based designs.

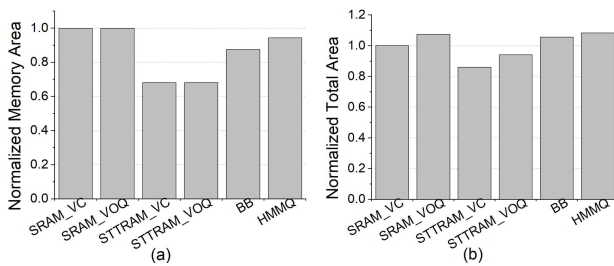
However, the total area is diverse owing to different con-

Table II Configurations of buffer designs.

Buffer design	Configuration
SRAM_VC	Baseline router buffer with SRAM based VC
SRAM_VOQ	Router buffer with SRAM based VOQ
STTRAM_VC	Router buffer with STT-RAM based VC
STTRAM_VOQ	Router buffer with STT-RAM based VOQ
BB	Hybrid SRAM and STT-RAM banked buffer design [14]
HMMQ	The proposed hybrid SRAM and STT-RAM buffer design

Table III System configuration.

core count	64	topology	8×8 2D mesh
L1 I & D cache	private, 32 KB	router pipeline	3-stage
L2 cache	shared, 32 banks 512 KB/bank	queue count	HMMQ: 2 VCs and 4 VOQs others: 4 VCs (VOQs)/port
cache line size	64 B	queue depth	4 flits/VC (VOQ)
frequency	1 GHz	packet length	5 flits, 16 B/flit

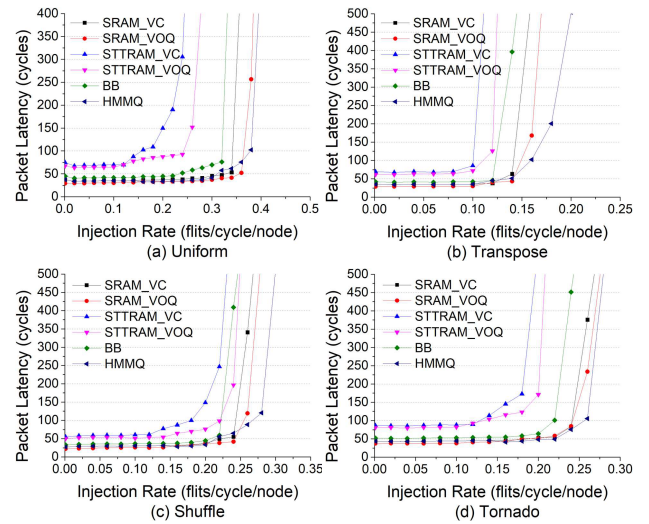
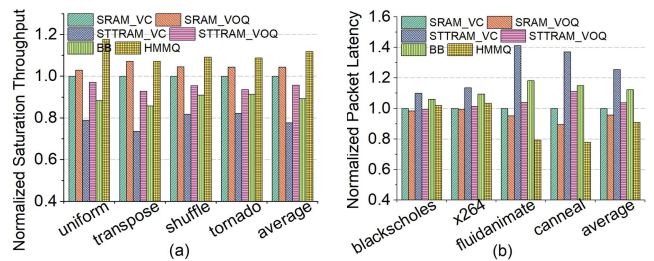
**Fig. 6** (a) Memory area and (b) total area of all designs normalized to baseline SRAM design.

trol logic. As shown in Fig. 6(b), STT-RAM designs had to impose complex control logic for queue scheduling and to overcome the high write latency of STT-RAM to adapt the router pipeline which erodes the superiority of memory size. HMMQ augments extra control circuits for congestion aware and flow control to achieve better performance and energy efficiency, leading to a reasonable 18% increase over STTRAM_VC, and only 8.2% increase over SRAM_VC in total area. The advantage of high density of STT-RAM retains and area consumption is constrained in an acceptable range. Moreover, synthesized result of router with HMMQ from DC demonstrated that timing constraint was met.

2) Performance

a) Synthetic traffic patterns

In order to evaluate the performance of different designs, we employed BookSim2.0 to run different synthetic traffic patterns, such as *uniform*, *transpose*, *shuffle*, and *tornado* traffic. Fig. 7 shows the average packet latency of all the designs. Unsurprisingly, due to the longer write latency, STT-RAM based designs perform worse in network latency. Because BB applies power-gating in individual VC to achieve energy saving, addition latency is introduced by wake-up operations unavoidably, and network latency increase consequently. Hence, BB slides into saturation faster than SRAM based designs. In low injection rate, all flits pass through router without stall and all designs are running fluently. As the injection rate increasing, competitions for output channel among flits rise. Not all the flits can get grants to leave in time and accumulation of flits in the VC emerges. When the occupation of buffer reaches a certain degree, the node is getting into congestion. Congestion will

**Fig. 7** Average packet latency of different designs for synthetic workloads. (a) Uniform, (b) Transpose, (c) Shuffle, (d) Tornado.**Fig. 8** (a) Saturation throughput under synthetic traffic and (b) average packet latency under application traffic normalized to baseline SRAM design.

spread upward to form a congestion tree if the congestion is not alleviated in time, which worsen the network latency further. Since VC does not handle HoL blocking, the packet latency of SRAM_VC and STTRAM_VC degrade quickly as the injection rising. VOQ schemes can effectively eliminate HoL blocking at low traffic and work better than VC schemes, but they cannot perceive and process congestion when encountering high traffic workload which worsen the performance. In contrast to the counter designs, HMMQ launches STT-VOQ when there appears congestion and congested traffic is isolated in STT-VOQ to release bandwidth for non-congested traffic, avoiding aggravation of congestion and keeping traffic flow continuous. Hence, HMMQ helps to cut down the latency of packets and slow down network stepping into saturation.

Fig. 8(a) depicts the saturation throughput normalized to baseline SRAM_VC. HMMQ exhibits the best performance and achieves improvement by 17.6%, 7.1%, 9%, 8.6% and 11.8% for *uniform*, *transpose*, *shuffle* and *tornado* traffic and on average respectively over baseline SRAM_VC and is even superior to the runner-up SRAM_VOQ by 20.5% on average.

b) Application traffic patterns

We also conduct experiments with application traffic patterns for more extensive performance verification. Fig. 8(b) demonstrates the packet latency of the proposed design and counter parts normalized to SRAM_VC. In low contented traffic, such as *blacksholes* and *x264*, STT-RAM based de-

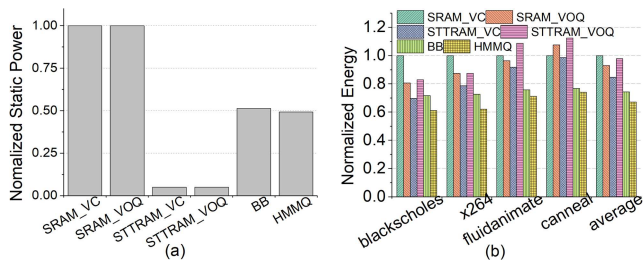


Fig. 9 (a) Memory static power dissipation and (b) total power dissipation normalized to baseline SRAM design.

signs obtain a degeneration as expected. BB also causes performance losses due to power-gating in drowsy SRAM of each VC. HMMQ achieves nearly the same performance with SRAM, the same as mentioned in synthetic traffic experiments. In high contented traffic, such as *fluidanimate* and *canneal*, as traffic rising, network congestion occurs frequently. STT-RAM based designs declines significantly. Combination of VC and VOQ helps HMMQ to accommodate more congested traffic, and slows down the saturation of node. Eventually, HMMQ gains 11%, 9% and 34% improvement over baseline SRAM design, the runner-up SRAM_VOQ and BB on average respectively.

3) Power consumption

We first ran simulations with NVSim for power dissipation of memory only. And then, Orion2.0 power library was integrated in Booksim2.0 to obtain the router power consumption including static and dynamic power consumption.

a) Memory static power consumption

With the great prospect of low leakage power, as shown in Fig. 9(a), compared to SRAM based designs, the use of STT-RAM reduces the static power consumption of memory significantly, where STT-RAM designs, BB and HMMQ achieve static power reduction by 95%, 48% and 46% over SRAM respectively.

b) Total power consumption

Fig. 9(b) illustrates the normalized total power consumption of buffer designs involved with different application traffic patterns to baseline SRAM design. As aforementioned, STT-RAM designs obtain gratifying reduction in memory static power consumption. However, according to Table I, the write energy of STT-RAM is near six times over SRAM which will hurt the memory power superiority. As traffic increasing, whether in low injection rate or high injection rate, the write/read operations of STT-RAM are implemented frequently and the backward of high dynamic energy comes out and total power consumption climbs up. Alternatively, HMMQ employs the STT-RAM VOQs according to congestion status which avoids frequent write/read operations of STT-RAM. Taking both low write/read access energy of SRAM and low leakage power of STT-RAM into account, HMMQ acquires an outstanding power saving by 32.9% and 9% over baseline SRAM design and BB on average.

Conclusion can be drawn that STT-RAM based buffer designs consume much more dynamic power which offsets the benefits of memory static power consumption and area overhead and it is not realistic to replace SRAM with STT-RAM directly in buffer design.

5. Conclusion

In this paper, we propose HMMQ, a hybrid memory NoC router buffer design with SRAM and STT-RAM with the combinative structure of VC and VOQ, which leverages the high density and extreme low leakage power of STT-RAM and develops the ability to perceive node congestion and alleviate congestion by isolating congested flow from uncongested flow. The experimental result showed that HMMQ improves the throughput, network latency and power dissipation by 11.8%, 11% and 32.9% on average respectively over baseline SRAM based design, while the area overhead is only increased by 8.2%.

Acknowledgments

This work was supported by Natural Science Basic Research Plan in Shaanxi Province of China (2021ZDLGY02-01), and the National 111 Center (B12026).

References

- [1] J. Wu, *et al.*: “Energy-efficient NoC with multi-granularity power optimization,” *The Journal of Supercomputing* **73** (2016) 1654 (DOI: [10.1007/s11227-016-1859-8](https://doi.org/10.1007/s11227-016-1859-8)).
- [2] H.-Y. Cheng, *et al.*: “Core vs. uncore: The heart of darkness,” 2015 52nd ACM/EDAC/IEEE Design Automation Conference (DAC) (2015) 1 (DOI: [10.1145/2744769.2647916](https://doi.org/10.1145/2744769.2647916)).
- [3] Y.-H. Kao and H.J. Chao: “Design of a bufferless photonic crosstalk network-on-chip architecture,” *IEEE Trans. Comput.* **63** (2014) 764 (DOI: [10.1109/TC.2012.250](https://doi.org/10.1109/TC.2012.250)).
- [4] G. Micheliogiannakis and W.J. Dally: “Elastic buffer flow control for on-chip networks,” *IEEE Trans. Comput.* **62** (2013) 295 (DOI: [10.1109/TC.2011.237](https://doi.org/10.1109/TC.2011.237)).
- [5] P. Zhou, *et al.*: “A durable and energy efficient main memory using phase change memory technology,” *ISCA '09* (2009) (DOI: [10.1145/1555754.1555759](https://doi.org/10.1145/1555754.1555759)).
- [6] Z. Sun, *et al.*: “Multi retention level STT-RAM cache designs with a dynamic refresh scheme,” 2011 44th Annual IEEE/ACM International Symposium on Microarchitecture (MICRO) (2011) 329 (DOI: [10.1145/2155620.2155659](https://doi.org/10.1145/2155620.2155659)).
- [7] C.W. Smullen, IV, *et al.*: “Relaxing non-volatility for fast and energy-efficient STT-RAM caches,” 2011 IEEE 17th International Symposium on High Performance Computer Architecture (2011) 50 (DOI: [10.1109/HPCA.2011.5749716](https://doi.org/10.1109/HPCA.2011.5749716)).
- [8] D. Kline, *et al.*: “Racetrack queues for extremely low-energy FIFOs,” *IEEE Trans. Very Large Scale Integr. (VLSI) Syst.* **26** (2018) 1531 (DOI: [10.1109/TVLSI.2018.2819945](https://doi.org/10.1109/TVLSI.2018.2819945)).
- [9] J.M. Slaughter, *et al.*: “High density ST-MRAM technology,” 2012 International Electron Devices Meeting (2012) 29.3.1 (DOI: [10.1109/IEDM.2012.6479128](https://doi.org/10.1109/IEDM.2012.6479128)).
- [10] N.D. Rizzo, *et al.*: “A fully functional 64 Mb DDR3 ST-MRAM built on 90 nm CMOS technology,” *IEEE Trans. Magn.* **49** (2013) 4441 (DOI: [10.1109/TMAG.2013.2243133](https://doi.org/10.1109/TMAG.2013.2243133)).
- [11] S. Ikegawa, *et al.*: “Magnetoresistive random access memory: present and future,” *IEEE Trans. Electron Devices* **67** (2020) 1407 (DOI: [10.1109/TEDE.2020.2965403](https://doi.org/10.1109/TEDE.2020.2965403)).
- [12] R. Bläsing, *et al.*: “Magnetic racetrack memory: from physics to the cusp of applications within a decade,” *Proc. IEEE* **108** (2020) 1303 (DOI: [10.1109/JPROC.2020.2975719](https://doi.org/10.1109/JPROC.2020.2975719)).
- [13] H. Jang, *et al.*: “A hybrid buffer design with STT-MRAM for on-chip interconnects,” *Proc. IEEE/ACM 6th Int. Symp. Network-on-Chip* (2012) 193 (DOI: [10.1109/NOCS.2012.30](https://doi.org/10.1109/NOCS.2012.30)).
- [14] J. Zhan, *et al.*: “Hybrid drowsy SRAM and STT-RAM buffer designs for dark-silicon-aware NoC,” *IEEE Trans. Very Large Scale Integr. (VLSI) Syst.* **24** (2016) 3041 (DOI: [10.1109/TVLSI.2016.2536747](https://doi.org/10.1109/TVLSI.2016.2536747)).

- [15] M.-T. Chang, *et al.*: “Technology comparison for large last-level caches (L3Cs): Low-leakage SRAM, low write-energy STT-RAM, and refresh-optimized eDRAM,” 2013 IEEE 19th International Symposium on High Performance Computer Architecture (HPCA) (2013) 143 (DOI: [10.1109/HPCA.2013.6522314](https://doi.org/10.1109/HPCA.2013.6522314)).
- [16] A. Jog, *et al.*: “Cache revive: architecting volatile STT-RAM caches for enhanced performance in CMPs,” DAC Design Automation Conference 2012 (2012) 243 (DOI: [10.1145/2228360.2228406](https://doi.org/10.1145/2228360.2228406)).
- [17] K.C. Chun, *et al.*: “A scaling roadmap and performance evaluation of in-plane and perpendicular MTJ based STT-MRAMs for high-density cache memory,” IEEE J. Solid-State Circuits **48** (2013) 598 (DOI: [10.1109/JSSC.2012.2224256](https://doi.org/10.1109/JSSC.2012.2224256)).
- [18] C. Li, *et al.*: “Hybrid memory buffer microarchitecture for high-radix routers,” IEEE Trans. Comput. (2021) 1 (DOI: [10.1109/TC.2021.3076431](https://doi.org/10.1109/TC.2021.3076431)).
- [19] L. Yang, *et al.*: “Optimal application mapping and scheduling for network-on-chips with computation in STT-RAM based router,” IEEE Trans. Comput. **68** (2019) 1174 (DOI: [10.1109/TC.2018.2864749](https://doi.org/10.1109/TC.2018.2864749)).
- [20] G. Ascia, *et al.*: “Implementation and analysis of a new selection strategy for adaptive routing in networks-on-chip,” IEEE Trans. Comput. **57** (2008) 809 (DOI: [10.1109/TC.2008.38](https://doi.org/10.1109/TC.2008.38)).
- [21] J. van den Brand, *et al.*: “Congestion-controlled best-effort communication for networks-on-chip,” 2007 Design, Automation & Test in Europe Conference & Exhibition (2007) 1 (DOI: [10.1109/date.2007.364415](https://doi.org/10.1109/date.2007.364415)).
- [22] W. Dally and B. Towles: *Principles and Practices of Interconnection Networks* (Morgan Kaufmann, 2003) 305.
- [23] M.J. Karol, *et al.*: “Improving the performance of input-queued ATM packet switches,” IEEE INFOCOM '92: The Conference on Computer Communications **1** (1992) 110 (DOI: [10.1109/INFCOM.1992.263574](https://doi.org/10.1109/INFCOM.1992.263574)).
- [24] C. Li, *et al.*: “RoB-router: a reorder buffer enabled low latency network-on-chip router,” IEEE Trans. Parallel Distrib. Syst., **29** (2018) 2090 (DOI: [10.1109/TPDS.2018.2817552](https://doi.org/10.1109/TPDS.2018.2817552)).
- [25] W. Dally and B. Towles: *Principles and Practices of Interconnection Networks* (Morgan Kaufmann, 2003) 332.
- [26] X. Dong, *et al.*: “NVSim: a circuit-level performance, energy, and area model for emerging nonvolatile memory,” IEEE Trans. Comput.-Aided Design Integr. Circuits Syst. **31** (2012) 994 (DOI: [10.1109/TCAD.2012.2185930](https://doi.org/10.1109/TCAD.2012.2185930)).
- [27] D.U. Becker: “Efficient microarchitecture for network-on-chip routers,” Ph.D Dissertation, Stanford University, Stanford, CA, USA (2012).
- [28] N. Jiang, *et al.*: “A detailed and flexible cycle-accurate network-on-chip simulator,” 2013 IEEE International Symposium on Performance Analysis of Systems and Software (ISPASS) (2013) 86 (DOI: [10.1109/ISPASS.2013.6557149](https://doi.org/10.1109/ISPASS.2013.6557149)).
- [29] A.B. Kahng, *et al.*: “ORION 2.0: a fast and accurate NoC power and area model for early-stage design space exploration,” 2009 Design, Automation & Test in Europe Conference & Exhibition (2009) 423 (DOI: [10.1109/DATE.2009.5090700](https://doi.org/10.1109/DATE.2009.5090700)).
- [30] N.L. Binkert, *et al.*: “The M5 simulator: modeling networked systems,” IEEE Micro **26** (2006) 52 (DOI: [10.1109/MM.2006.82](https://doi.org/10.1109/MM.2006.82)).
- [31] C. Bienia, *et al.*: “The PARSEC benchmark suite: characterization and architectural implications,” 2008 International Conference on Parallel Architectures and Compilation Techniques (PACT) (2008) 72 (DOI: [10.1145/1454115.1454128](https://doi.org/10.1145/1454115.1454128)).
- [32] J. Hestness, *et al.*: “Netrace: dependency-driven, trace-based network-on-chip simulation,” Proceedings of the 3rd International Workshop on Network on Chip Architectures (NoCArc) (2010) 31 (DOI: [10.1145/1921249.1921258](https://doi.org/10.1145/1921249.1921258)).